



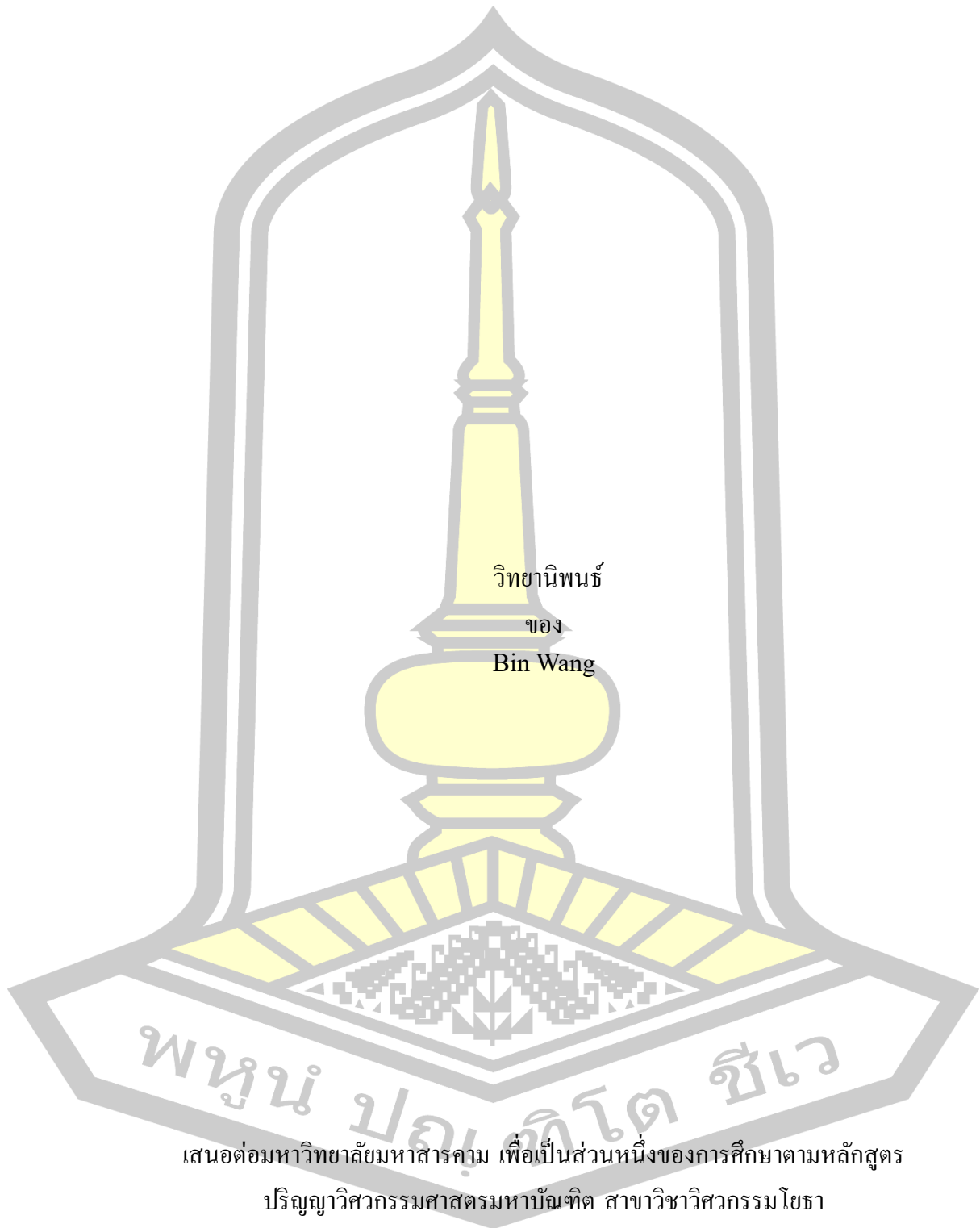
Numerical Study on Structural Behavior of RPC Deep Beams

Bin Wang

A Thesis Submitted in Partial Fulfillment of Requirements for
degree of Master of Engineering in Civil Engineering
November 2023

Copyright of Maharakham University

Numerical Study on Structural Behavior of RPC Deep Beams



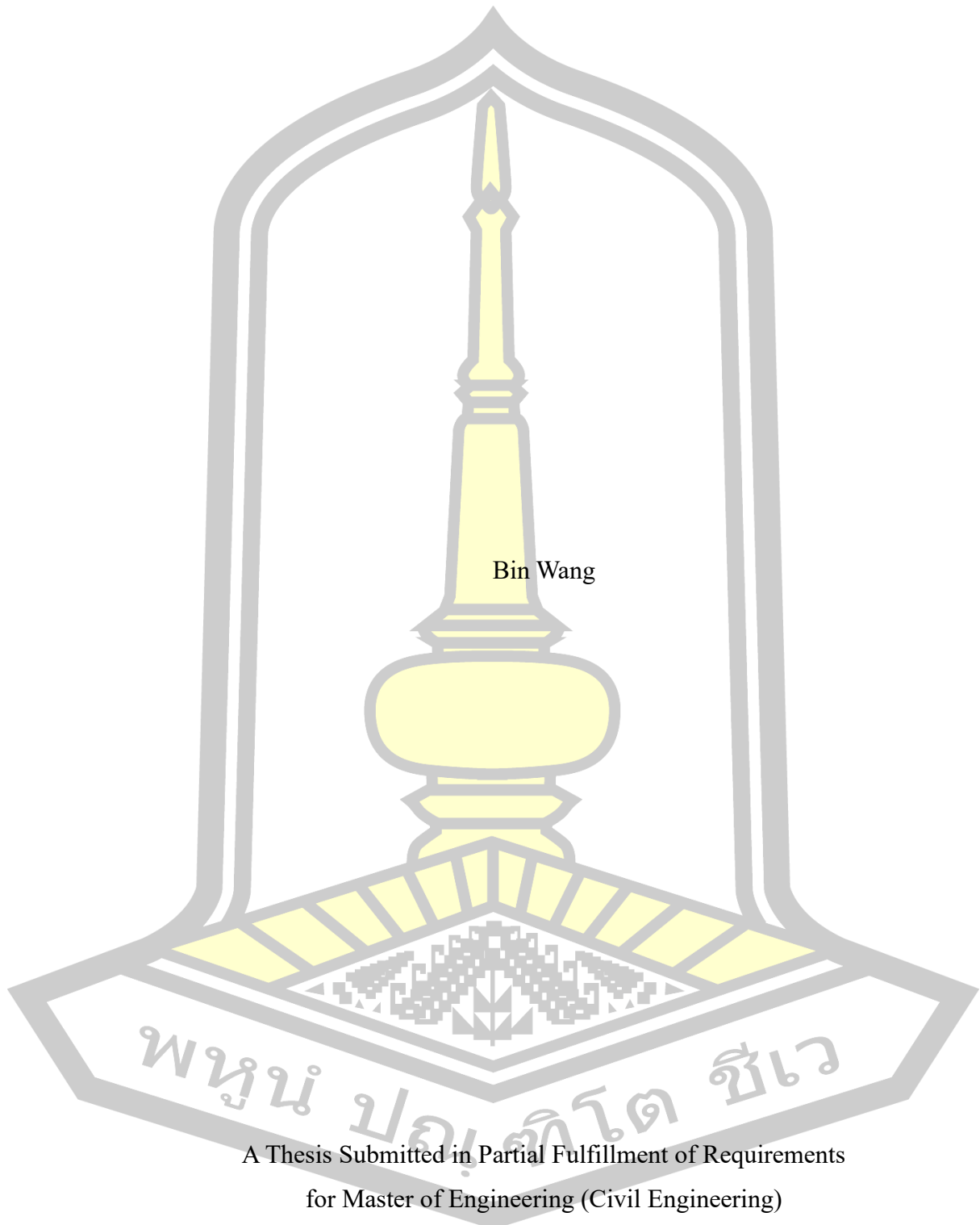
เสนอต่อมหาวิทยาลัยมหาสารคาม เพื่อเป็นส่วนหนึ่งของการศึกษาตามหลักสูตร

ปริญญาวิศวกรรมศาสตรมหาบัณฑิต สาขาวิชาวิศวกรรมโยธา

พฤศจิกายน 2566

ลิขสิทธิ์เป็นของมหาวิทยาลัยมหาสารคาม

Numerical Study on Structural Behavior of RPC Deep Beams



Bin Wang

A Thesis Submitted in Partial Fulfillment of Requirements
for Master of Engineering (Civil Engineering)

November 2023

Copyright of Mahasarakham University



The examining committee has unanimously approved this Thesis, submitted by Mr. Bin Wang , as a partial fulfillment of the requirements for the Master of Engineering Civil Engineering at Maharakham University

Examining Committee

- | | |
|--|------------|
| (Asst. Prof. Watwong Greepala ,
Ph.D.) | Chairman |
| (Assoc. Prof. Krit Chaimoon ,
Ph.D.) | Advisor |
| (Assoc. Prof. Nantawat Khomwan ,
Ph.D.) | Co-advisor |
| (Assoc. Prof. Raungrut Cheerarot ,
Ph.D.) | Committee |
| (Assoc. Prof. Sahalaph
Homwouttiwong , Ph.D.) | Committee |

Maharakham University has granted approval to accept this Thesis as a partial fulfillment of the requirements for the Master of Engineering Civil Engineering

(Assoc. Prof. Keartisak Sriprateep , Ph.D.)	(Assoc. Prof. Krit Chaimoon , Ph.D.)
Dean of The Faculty of Engineering	Dean of Graduate School

พญม ปญ ทิโต ชโร

TITLE Numerical Study on Structural Behavior of RPC Deep Beams
AUTHOR Bin Wang
ADVISORS Associate Professor Krit Chaimoon , Ph.D.
Associate Professor Nantawat Khomwan , Ph.D.
DEGREE Master of Engineering **MAJOR** Civil Engineering
UNIVERSITY Maharakham **YEAR** 2023
University

ABSTRACT

Reactive powder concrete (RPC) is a modern and advanced type of concrete categorized as ultra-high performance fiber-reinforced concrete with exceptional mechanical properties and durability. RPC exhibits immense potential for various applications in reinforced concrete members. However, limited attention has been devoted to numerically investigating the structural behavior of RPC deep beams, where stress-strain models are crucial.

This research deals with the assessment of stress-strain models outlined in the *fib* 2010, NF P 18-710 2016 (AFGC), and CECS 2020 standard codes to comprehend their efficacy in capturing the structural response of RPC deep beams using finite element analysis (FEA). Experimental data from the literature, which explored the influence of concrete compressive strength, shear span-to-effective depth ratio, and main reinforcement ratio, was employed for validation purposes. The FEA findings indicate that the *fib* 2010 code tends to yield conservative estimations, while the AFGC and CECS codes gave more accurate predictions. Additionally, this study employed strut-and-tie models (STMs) based on the ACI 318-11, EN 1992-1-1, and AFGC codes to forecast the shear strength of RPC deep beams.

Keyword : Reactive Powder Concrete, Finite Element Analysis, Stress-Strain Model, Strut-and-Tie Model, Deep Beam

พหุ ประถมศึกษา

ACKNOWLEDGEMENTS

The authors would like to express their gratitude and acknowledge the Faculty of Engineering, Maharakham University and SOFiSTiK for their support in conducting all the numerical work for this research. Their contributions have been instrumental in the successful completion of this study.

Bin Wang

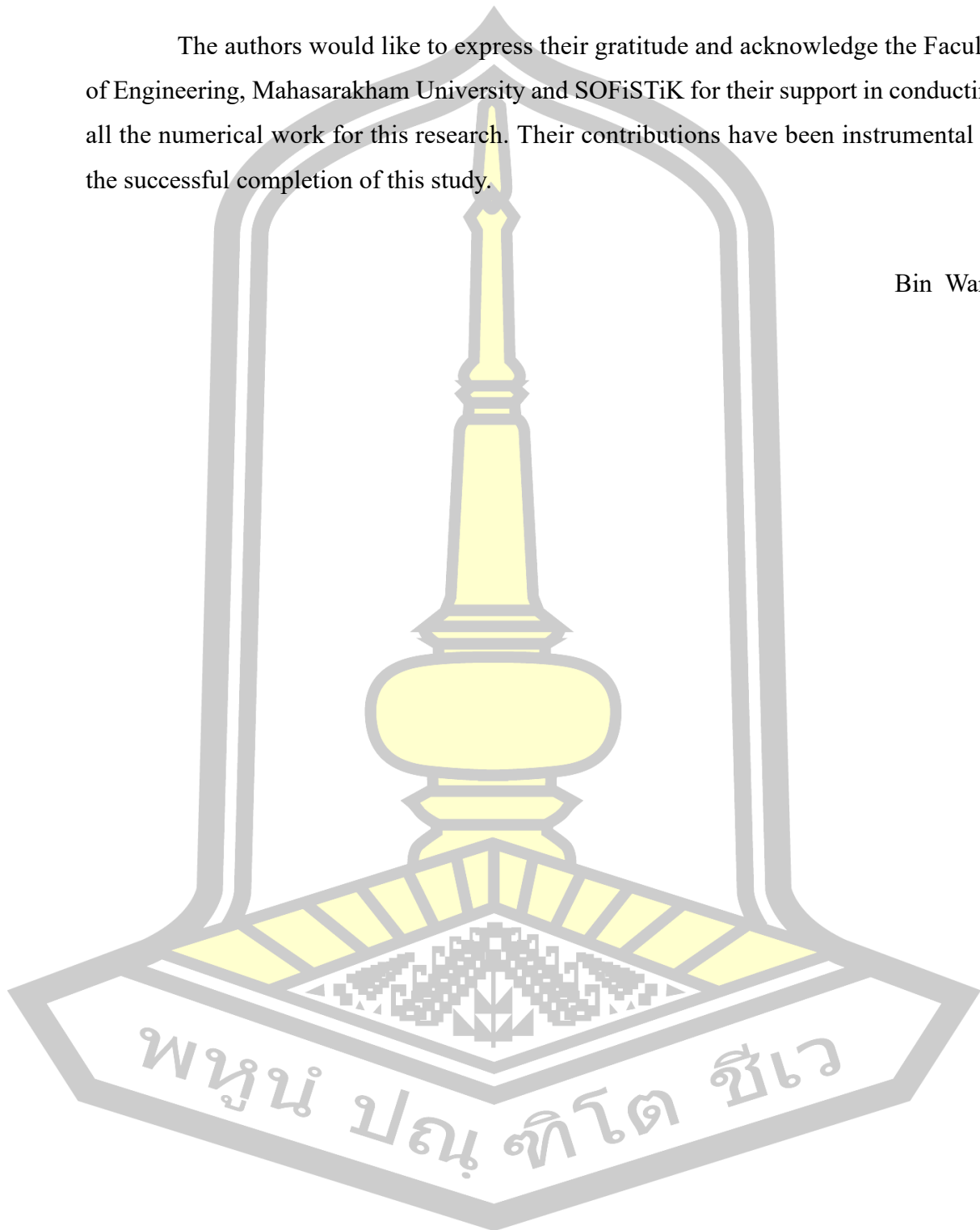


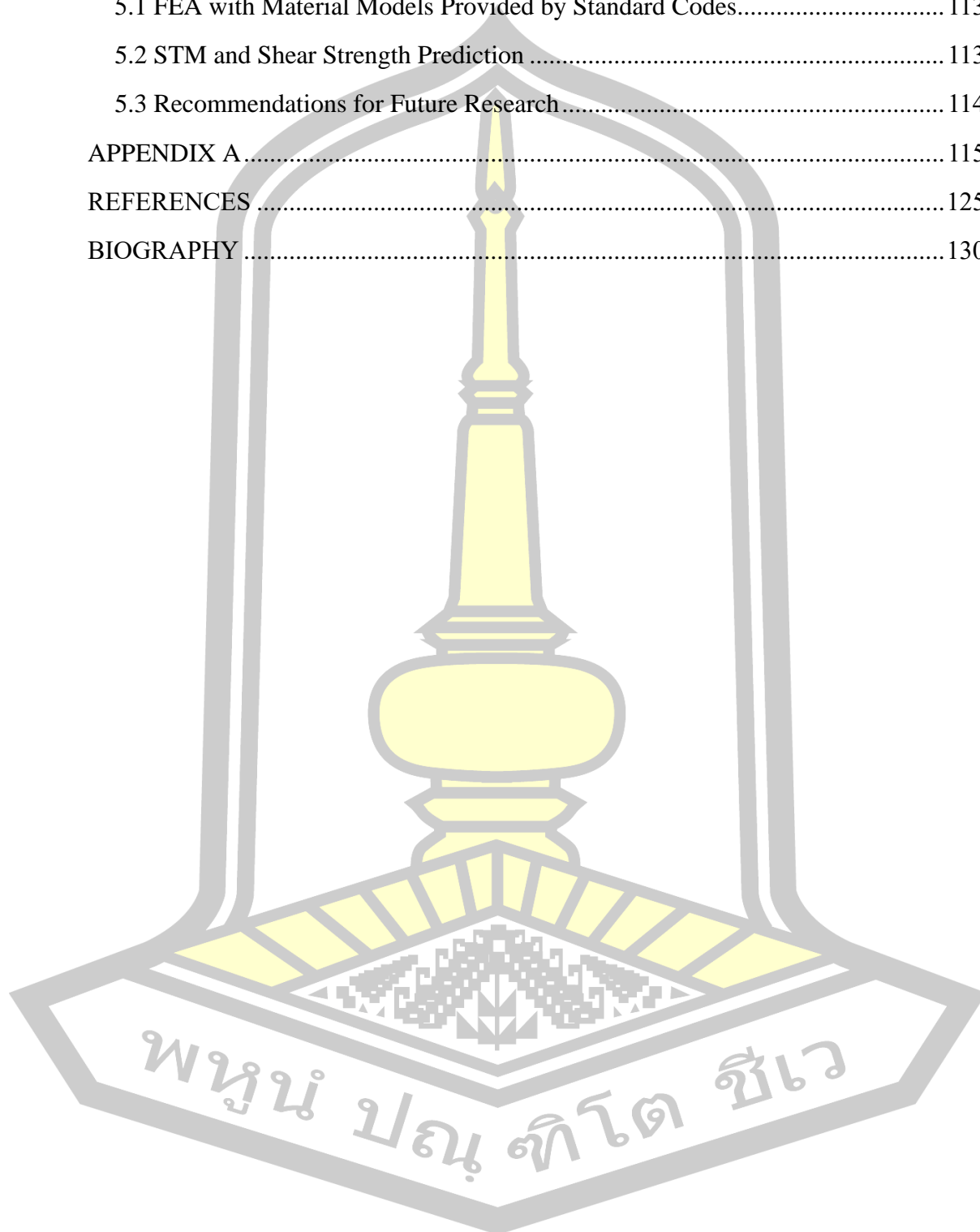
TABLE OF CONTENTS

	Page
ABSTRACT.....	D
ACKNOWLEDGEMENTS.....	E
TABLE OF CONTENTS.....	F
LIST OF TABLES.....	J
LIST OF FIGURES.....	L
Chapter 1 Introduction.....	1
1.1 Problem Statement.....	1
1.2 Research Objectives.....	2
1.3 Research Scope.....	2
1.4 Expected Advantages.....	3
Chapter 2 Literature Review.....	4
2.1 Deep Beams.....	4
2.1.1 Definition of Deep Beams.....	4
2.1.2 Design of Deep Beams.....	4
2.2 Reactive Powder Concrete.....	5
2.2.1 Introduction.....	5
2.2.2 Composition of RPC.....	6
2.2.3 Ingredients of RPC and Their Functions.....	6
2.2.3.1 Cement.....	6
2.2.3.2 Sand.....	7
2.2.3.3 Quartz Powder.....	7
2.2.3.4 Silica Fume.....	7
2.2.3.5 Steel Fibers.....	7
2.2.3.6 Super Plasticizer.....	7
2.2.4 Advantages of RPC.....	8

2.2.5 Limitations of RPC.....	8
2.3 Finite Element Analysis.....	8
2.3.1 Introduction.....	8
2.3.2 Basic Concepts of FEA.....	8
2.3.3 SOFiSTiK FEA Software.....	9
2.4 Strut-and-Tie Model.....	10
2.4.1 Introduction.....	10
2.4.2 Components of STM.....	11
2.4.2.1 Strut.....	11
2.4.2.2 Tension tie.....	12
2.4.2.3 Nodes.....	12
2.4.2.4 Nodal Zones.....	13
2.4.3 STM Methodology.....	14
2.4.4 Design strength.....	14
2.4.4.1 Strength of struts.....	14
2.4.3.3 Strength of Nodal Zones.....	17
2.5 Related Research.....	18
Chapter 3 Research Methods.....	22
3.1 Finite Element Analysis using SOFiSTiK.....	22
3.1.1 Constitutive Models: The <i>fib</i> Model Code 2010.....	23
3.1.1.1 The <i>fib</i> Model Code 2010: Compressive Stress-Strain Model.....	23
3.1.1.2 The <i>fib</i> Model Code 2010: Tensile Stress-Strain Model.....	25
3.1.2 Constitutive Models: NF P 18-710 (AFGC).....	26
3.1.2.1 NF P 18-710 (AFGC): Compressive Stress-Strain Model.....	26
3.1.2.2 NF P 18-710 (AFGC): Tensile Stress-Strain Model.....	27
3.1.3 Constitutive Models: CECS 2020.....	28
3.1.3.1 CECS 2020: Compressive Stress-Strain Model.....	28
3.1.3.2 CECS 2020: Tensile Stress-Strain Model.....	29
3.1.4 Constitutive Models for Rebar.....	32

3.2 Shear Strength Analysis using Strut-and-Tie Model	33
3.2.1 STM: ACI 318-11	33
3.2.2 STM: EN 1992-1-1	37
3.2.3 STM: NF P 18-710 (AFGC).....	38
Chapter 4 Study Results.....	40
4.1 FEA Results	40
4.1.1 RPC Deep Beams Tested by Yaseen [36]	40
4.1.1.1 Stress-Strain Curves of Rebar	40
4.1.1.2 Stress-Strain Curves of Concrete.....	41
4.1.1.3 Structural Model.....	52
4.1.1.4 Numerical Results	54
4.1.1.5 Conclusions	80
4.1.2 RPC Deep Beams Tested by Yousef et al. [37]	81
4.1.2.1 Stress-Strain Curves of Rebar	81
4.1.2.1 Stress-strain curves of concrete	82
4.1.2.2 Structural Model.....	84
4.1.2.3 Numerical Results	86
4.1.2.4 Conclusions	88
4.1.3 RPC Deep Beams Tested by Li et al. [38]	89
4.1.3.1 Stress-strain curves of concrete.....	89
4.1.3.2 Structural Model.....	92
4.1.3.3 Numerical Results	94
4.1.3.4 Conclusions	106
4.1.4 Main Parameter Effects on FEA Load-Deflection Curve.....	106
4.2 Shear Strength Prediction Using Strut-and-Tie Model.....	108
4.2.1 Parameters of Deep Beams for STM.....	109
4.2.2 Calculated and Experimental Shear Strengths	110
4.2.3 Conclusions for Shear Strength Predictions.....	110
4.3 Comparison of the FEA and STMs Peak Loads	111

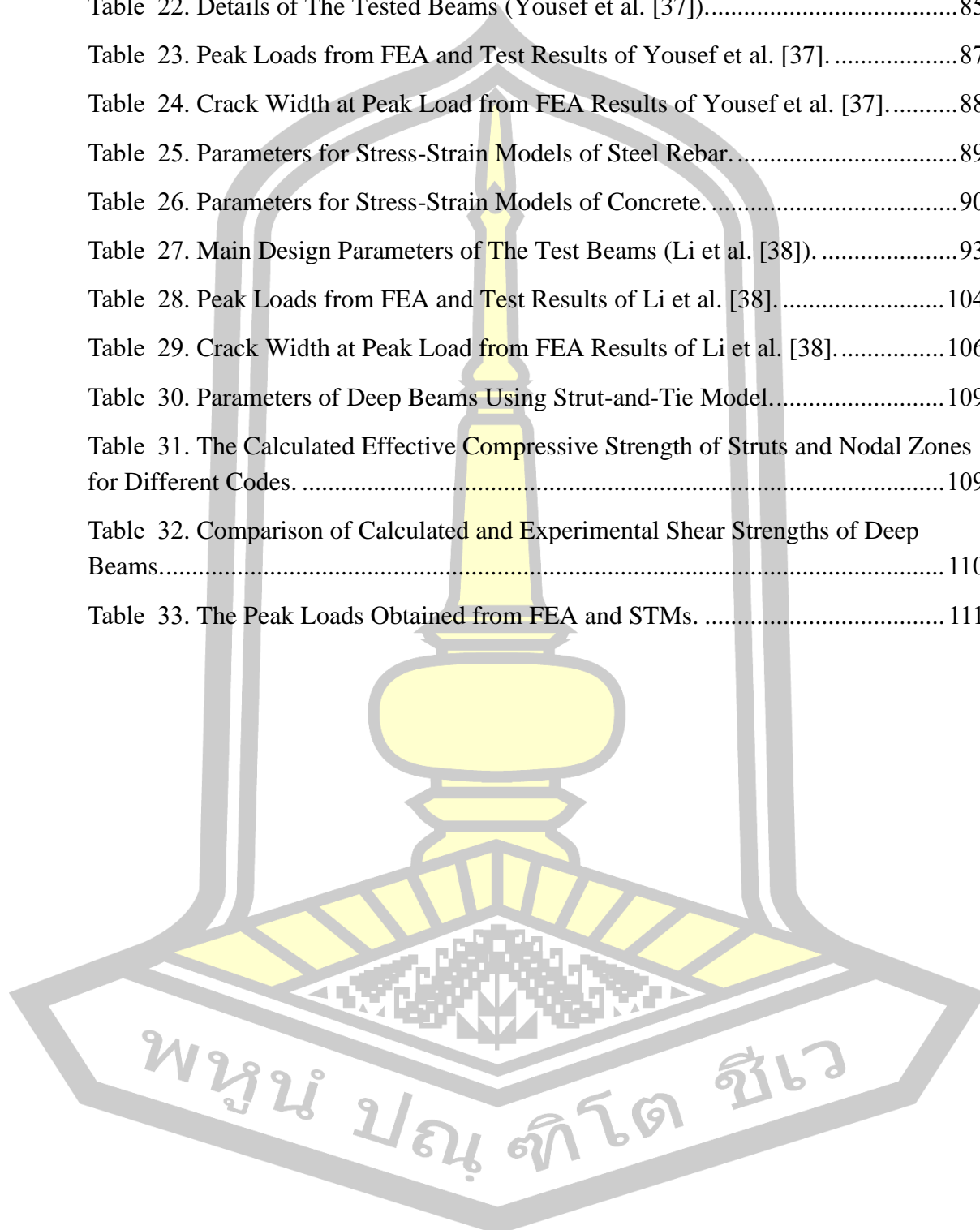
Chapter 5 Conclusions and Recommendations.....	113
5.1 FEA with Material Models Provided by Standard Codes.....	113
5.2 STM and Shear Strength Prediction	113
5.3 Recommendations for Future Research.....	114
APPENDIX A.....	115
REFERENCES	125
BIOGRAPHY	130



LIST OF TABLES

	Page
Table 1. Original RPC Compositions by Weight [11].	6
Table 2. Optimum Percentage of Principle Minerals of Cement [12].	7
Table 3. Strut Coefficient β_s [3].	15
Table 4. Nodal Zone Coefficient β_n [3].	17
Table 5. Strain $\varepsilon_{c,lim}$ and Plasticity Number k for Normal Weight Concrete [32]....	24
Table 6. Input Parameters and Calculated Parameters of Constitutive Model for RPC Following The fib Model Code 2010.....	25
Table 7. Input Parameters and Calculated Parameters of Constitutive Model for RPC Following AFGC Code.	28
Table 8. Modulus of Elasticity of RPC ($\times 10^4$ MPa) [34].	31
Table 9. Tensile Strength of RPC f_t Under Typical Parameters (MPa, $l_f / d_f = 65$) [34].	31
Table 10. Input Parameters and Calculated Parameters of Constitutive Model for RPC Following CECS Code.	32
Table 11. Input Parameters and Calculated Parameters of Constitutive Model for Rebar Following EN 1992-1-1.	33
Table 12. Test References and Values of Main Parameters Investigated in This Study.	40
Table 13. Parameters for Stress-Strain Models of Steel Rebar.	41
Table 14. Parameters for Stress-Strain Models of Concrete (fib Model Code 2010). 41	41
Table 15. Parameters for Stress-Strain Models of Concrete (AFGC code).	43
Table 16. Parameters for Stress-Strain Models of Concrete (CECS Code).	45
Table 17. Details of The Tested Beams (Yaseen [36]).	53
Table 18. Peak Loads from FEA and Test Results of Yaseen [36].	77
Table 19. Crack Width at Peak Load from FEA Results of Yaseen [36].	80
Table 20. Parameters for Stress-Strain Models of Steel Rebar.	81

Table 21. Parameters for Stress-Strain Models of Concrete.	82
Table 22. Details of The Tested Beams (Yousef et al. [37]).....	85
Table 23. Peak Loads from FEA and Test Results of Yousef et al. [37].	87
Table 24. Crack Width at Peak Load from FEA Results of Yousef et al. [37].	88
Table 25. Parameters for Stress-Strain Models of Steel Rebar.	89
Table 26. Parameters for Stress-Strain Models of Concrete.	90
Table 27. Main Design Parameters of The Test Beams (Li et al. [38]).	93
Table 28. Peak Loads from FEA and Test Results of Li et al. [38].	104
Table 29. Crack Width at Peak Load from FEA Results of Li et al. [38].	106
Table 30. Parameters of Deep Beams Using Strut-and-Tie Model.....	109
Table 31. The Calculated Effective Compressive Strength of Struts and Nodal Zones for Different Codes.	109
Table 32. Comparison of Calculated and Experimental Shear Strengths of Deep Beams.....	110
Table 33. The Peak Loads Obtained from FEA and STMs.	111

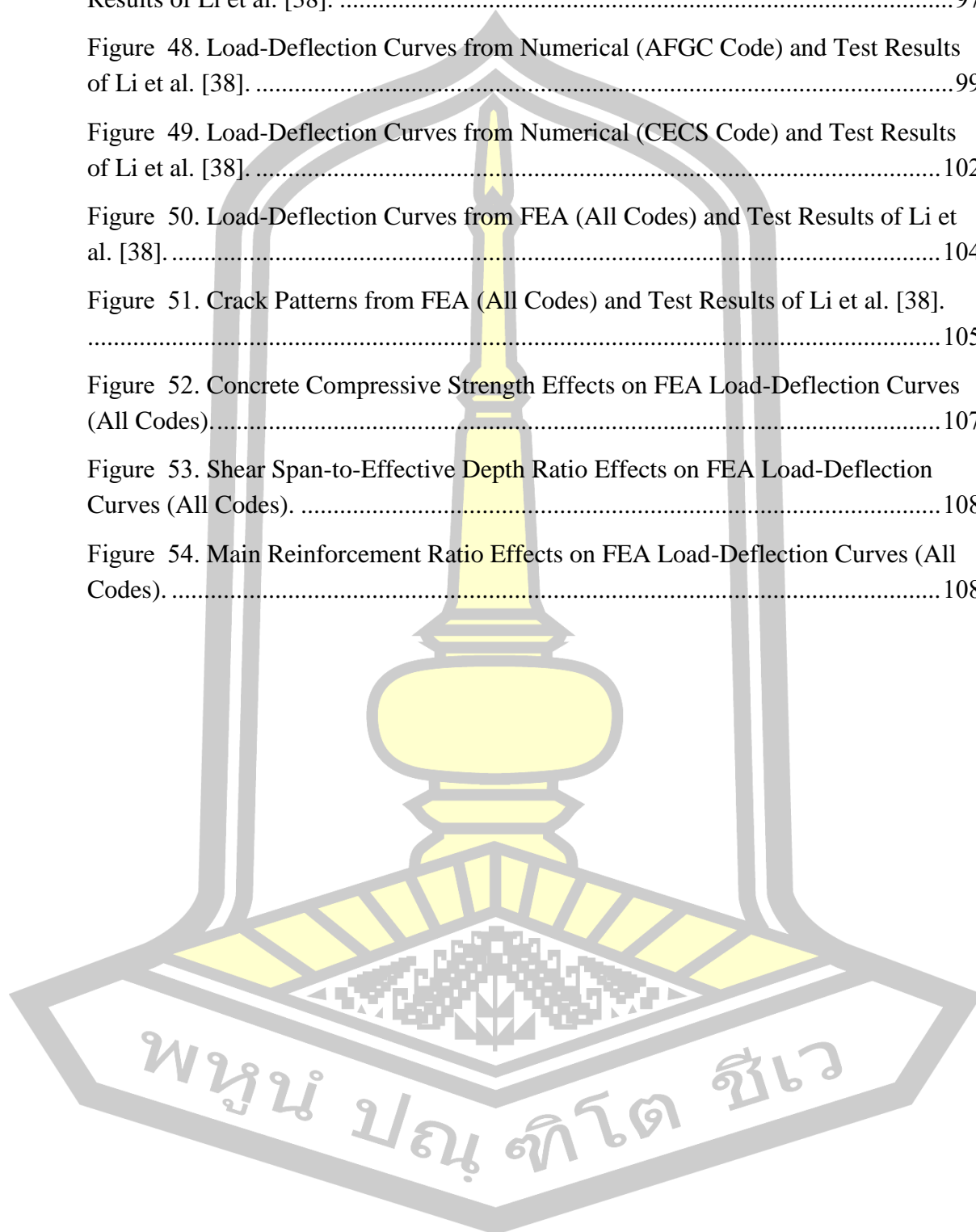


LIST OF FIGURES

	Page
Figure 1. Deep Beam Damage in A Bridge Structure [2].	2
Figure 2. Load Transferring in Deep Beam [10].	4
Figure 3. An Example of FE Mesh Created by Using FE Software [13].	9
Figure 4. FEA Results of Nonlinear Analysis of RC Beam by SOFiSTiK [16].	10
Figure 5. An Example of B-regions and D-regions in A Beam [17].	11
Figure 6. Components of A Strut-and-Tie Model in Deep Beam [17].	11
Figure 7. Effective Width of Ties (AASHTO and Eurocode) [17].	12
Figure 8. Types of Strut-and-Tie Model Nodes [17].	13
Figure 9. Types of Strut-and-Tie Model Nodal Zones [17].	13
Figure 10. Bottle-Shaped Strut: (a) Cracking of A bottle-Shaped Strut ; (b) A Model to Determine Transverse Tension [3].	16
Figure 11. Reinforcement Crossing A Strut [3].	16
Figure 12. Shell Element in Local Coordinate System [30].	22
Figure 13. An Example of Layer Material Model in SOFiSTiK [31].	22
Figure 14. Schematic Representation of The Stress-Strain Relation for Uniaxial Compression (According to fib Code 2010) [32].	24
Figure 15. Schematic Representation of The Stress-Strain and Stress-Crack Opening Relation for Uniaxial Tension (According to fib Code 2010) [32].	25
Figure 16. Diagrams for The ULS Regarding AFGC [33].	26
Figure 17. Constitutive Law of RPC in Compression Regarding CECS 2020 [34].	29
Figure 18. Constitutive Law of RPC in Tension Regarding CECS 2020 [34].	30
Figure 19. Constitutive Law of Rebar Following EN 1992-1-1 [35].	32
Figure 20. The STM Used in This Study.	33
Figure 21. Strut-and-Tie Model for Simply Supported Deep Beam.	34
Figure 22. Detail Calculating Diagram of Node B.	35
Figure 23. Detail Calculating Diagram of w_t and w_c .	36

Figure 24. Stress-Strain Curves for Rebar Used in FEA.	41
Figure 25. Stress-Strain Curves for Concrete Used in FEA (fib Model Code 2010). 43	
Figure 26. Stress-Strain Curves for Concrete Used in FEA (AFGC Code).....	44
Figure 27. Stress-Strain Curves for Concrete Used in FEA (CECS Code).	46
Figure 28. Stress-Strain Curves for Concrete in Compression (All Codes).	49
Figure 29. Stress-Strain Curves for Concrete in Tension (All Codes).	52
Figure 30. Details and Typical Cross Section of The Tested Beams (Yaseen [36]). .	53
Figure 31. Typical FE Model of The Beams.	53
Figure 32. Load-Deflection Curves from Numerical (fib Model Code 2010) and Test Results of Yaseen [36].	60
Figure 33. Load-Deflection Curves from Numerical (AFGC Code) and Test Results of Yaseen [36].	65
Figure 34. Load-Deflection Curves from Numerical (CECS Code) and Test Results of Yaseen [36].	71
Figure 35. Load-Deflection Curves from FEA (All Codes) and Test Results of Yaseen [36].	77
Figure 36. Crack Patterns from FEA (All Codes) and Test Results of Yaseen [36]. .	80
Figure 37. Stress-Strain Curves for Rebar Used in FEA.	81
Figure 38. Stress-Strain Curves for Concrete Used in FEA (All Codes).....	84
Figure 39. Details and Typical Cross Section of The Tested Beams (Yousef et al. [37]).....	85
Figure 40. Typical FE Model of The Beams.	85
Figure 41. Load-Deflection Curves from FEA (All Codes) and Test Results of Yousef et al. [37].....	87
Figure 42. Crack Patterns from FEA (All Codes) and Test Results of Yousef et al. [37].	88
Figure 43. Stress-Strain Curves for Rebar Used in FEA.	89
Figure 44. Stress-Strain Curves for Concrete Used in FEA (All Codes).....	92
Figure 45. Loading Device Diagram (Li et al. [38]).....	93
Figure 46. Typical FE Model of The Beams.	93

Figure 47. Load-Deflection Curves from Numerical (fib Model Code 2010) and Test Results of Li et al. [38].	97
Figure 48. Load-Deflection Curves from Numerical (AFGC Code) and Test Results of Li et al. [38].	99
Figure 49. Load-Deflection Curves from Numerical (CECS Code) and Test Results of Li et al. [38].	102
Figure 50. Load-Deflection Curves from FEA (All Codes) and Test Results of Li et al. [38].	104
Figure 51. Crack Patterns from FEA (All Codes) and Test Results of Li et al. [38].	105
Figure 52. Concrete Compressive Strength Effects on FEA Load-Deflection Curves (All Codes).	107
Figure 53. Shear Span-to-Effective Depth Ratio Effects on FEA Load-Deflection Curves (All Codes).	108
Figure 54. Main Reinforcement Ratio Effects on FEA Load-Deflection Curves (All Codes).	108



Chapter 1

Introduction

1.1 Problem Statement

Infrastructure is the lifeblood of any country's economic development and an important supporting force to ensure social stability and fast transportation. Since the 21st century, World's infrastructure industry has developed rapidly. However, with the continuous development of World's economy, due to the early design standards are relatively low, the quality of the project is not high, and there is no timely maintenance, making the phenomenon of disease in concrete structures. Improving the properties of concrete has become an urgent problem to be solved.

The tensile strength of the traditional ordinary concrete structures is low, and they are easy to crack under the action of external loads. In the actual projects, the durability of the concrete structures is more prominent, and a lot of money is needed to maintain the structures in the later stage of use. At present, the development of civil engineering industry is increasingly demanding sustainable development, so it is urgent to study a new type of civil engineering material with high strength, good durability, and environmental protection.

A new type of cement-based composite material developed in the past thirty years is ultra-high-performance concrete (UHPC), also known as reactive powder concrete (RPC). Compared with ordinary concrete, RPC has made significant progress in compressive strength, tensile strength, elastic modulus, and creep performance, especially in compressive performance. Using the excellent performance of RPC, the size of the structural elements and the weight of the structures can be reduced, and the seismic performance of the structures can be strengthened. RPC has also outstanding performance in impermeability, fire resistance, wear resistance and deformation performance. Its application in concrete structures can therefore reduce maintenance costs, prolong the service life of concrete structures, and reduce the overall cost of the project [1].

Deep beam is a type of structural elements that prefers a material with high performance like RPC as it normally contains congested reinforcement to be able to carry design loads safely. It is a special reinforced concrete (RC) element needed a specific analysis and design as it exhibits a complex behavior. And shear failure is its major concern. Birrcher [2] reported that the RC cover beams of some bridges in Texas, the United States, had diagonal cracks due to shear failure under normal use loads, and the two beams with excessively wide cracks required expensive reinforcement. The diagonal cracks and reinforcement measures of one of the beams are shown in [Figure 1](#). These beams are the deep beams according to ACI 318-11 [3] as they had concentrated load from I-girder acting within a distance two times of the beam depth from the face of the support.

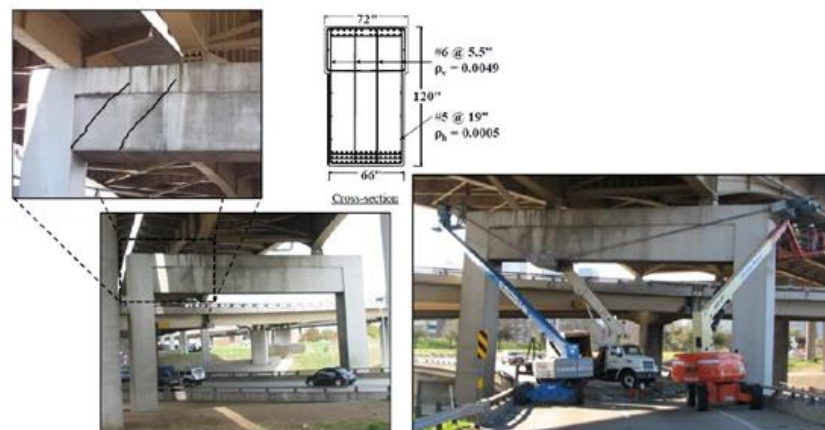


Figure 1. Deep Beam Damage in A Bridge Structure [2].

Application of RPC to deep beams is, therefore, of interest to civil engineers and researchers [4-8]. However, research work on RPC deep beams is still limited both in experimental and numerical study. At present, there is no general design specification in the industry, which greatly affects the application of RPC in practical engineering. An insight into the structural behavior of RPC deep beam is still needed. Alternative to experimental testing which can provide fundamental understanding on structural behavior but can be both expensive and time consuming is numerical study using finite element analysis (FEA). To be able to conduct realistic analyses of deep beams, reliable stress-strain models that accurately describe the material's behavior under compression and tension are essential.

To be able to implement numerical study, in this study, the stress-strain models provided by some standard codes were adopted and assessed their ability to capture the structural behavior of RPC deep beams. Some strut-and-tie models are also investigated and used to predict shear strength of RPC deep beams.

1.2 Research Objectives

The objectives of this research are:

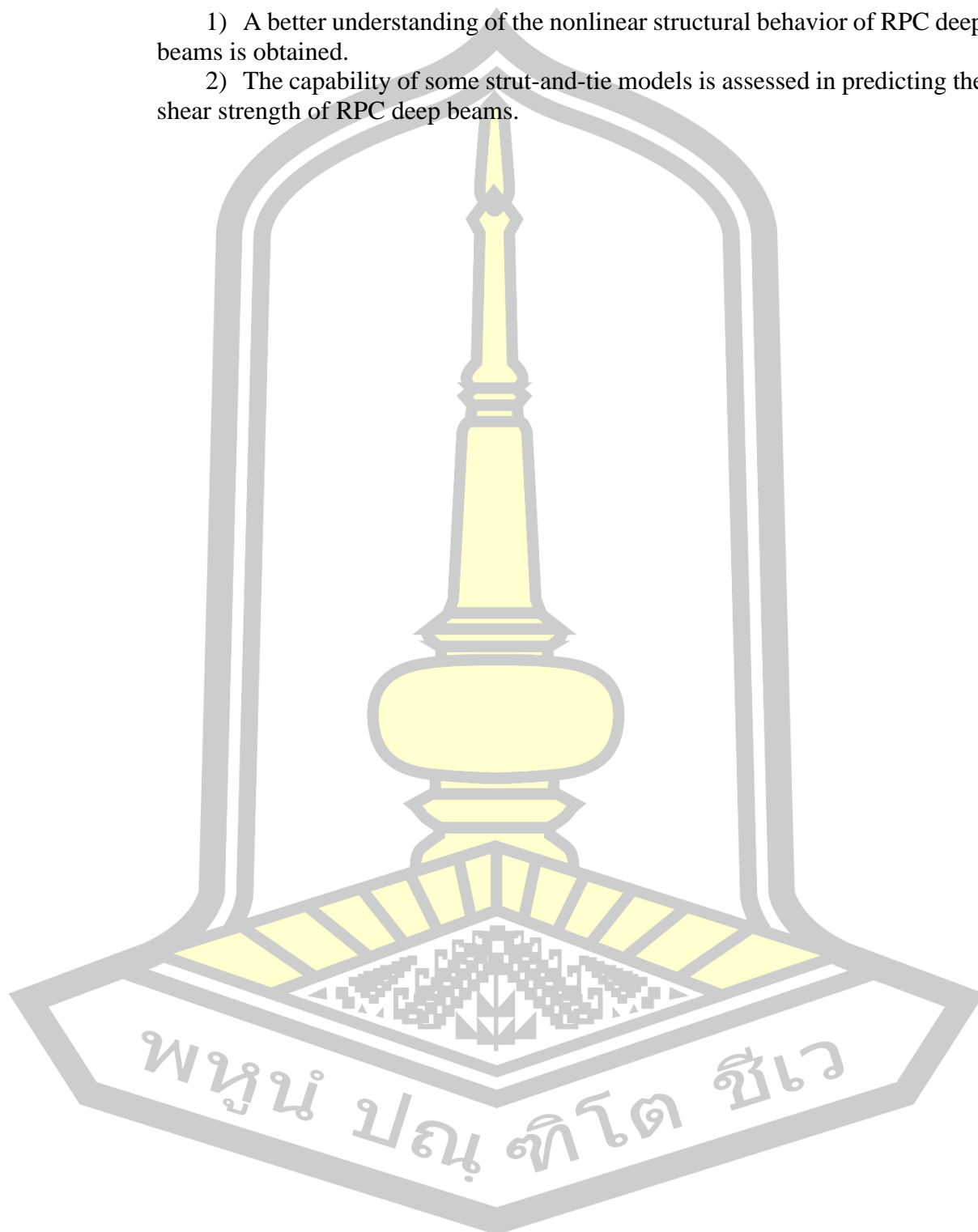
- 1) To investigate the effectiveness of stress-strain models provided by some standard codes in capturing structural behavior of RPC deep beams using finite element analysis
- 2) To assess the capability of some strut-and-tie models in predicting the shear strength of RPC deep beams

1.3 Research Scope

- 1) The stress-strain models provided by the *fib* model code 2010, NF P 18-710 (AFGC), and CECS 2020 are adopted.
- 2) SOFiSTiK finite element code is adopted.
- 3) The strut-and-tie models according to ACI 318-11, EN 1992-1-1, and NF P 18-710 (AFGC) codes are considered & the deep beams have the shear span-to-depth ratio $a/d \leq 2.0$.

1.4 Expected Advantages

- 1) A better understanding of the nonlinear structural behavior of RPC deep beams is obtained.
- 2) The capability of some strut-and-tie models is assessed in predicting the shear strength of RPC deep beams.



Chapter 2

Literature Review

2.1 Deep Beams

Deep beams are structural elements loaded as simple beams in which a significant amount of the load is carried to the supports by a compression force combining the load and the reaction as depicted in Figure 2. As a result, the strain distribution is no longer considered linear, and the shear deformations become significant when compared to pure flexure [9].

In view of ample shear strength, deep beams are primarily recommended as transfer girders. These members transfer loads through-loading face to supports in the transverse direction. The deep horizontal members predominantly fail in shear rather than flexure. These beams are characterized with small span-to-depth ratio. Pile caps, corbel, brackets, foundation walls and off-shore structures are few examples of RC deep beams.

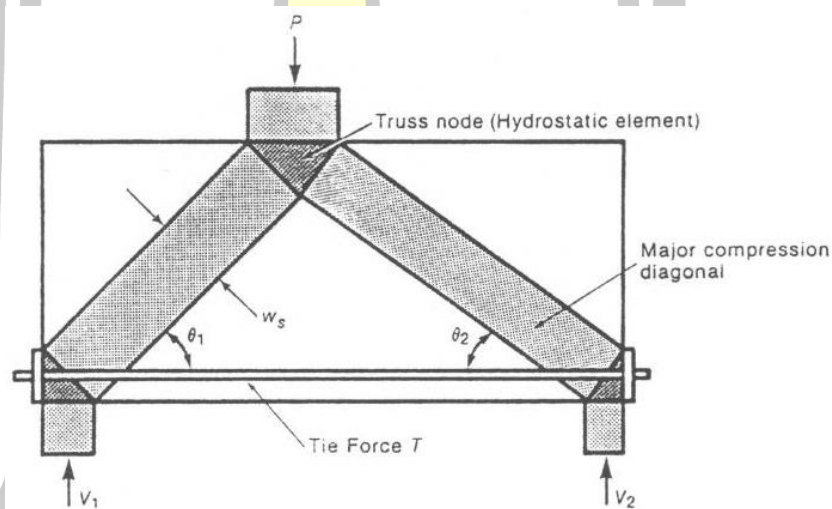


Figure 2. Load Transferring in Deep Beam [10].

2.1.1 Definition of Deep Beams

Though different codes define deep beams in different clear span-to-depth ratios, as a general rule deep beams are recognized by their relatively small span-to-depth ratio. In accordance with ACI 318-11 [3], deep beams are defined as members that are loaded on one face and supported on the opposite face such that strut-like compression elements can develop between the loads and supports and that satisfy (a) or (b):

- a) Clear span does not exceed four times the overall member depth h .
- b) Concentrated loads exist within a distance $2h$ from the face of the support.

2.1.2 Design of Deep Beams

According to the ACI 318-11 [3], deep beams shall be designed taking into account nonlinear distribution of longitudinal strain over the depth of the beam and

strut-and-tie models are deemed to satisfy this requirement. The provisions for design of deep beams are as follows. Note that the unit of stress is in MPa.

- (1) Dimensional limits: deep beam dimensions shall be selected such that:

$$V_n \leq 0.83\sqrt{f'_c}b_wd \quad (1)$$

- (2) Reinforcement limits: distributed reinforcement along the side faces of deep beams shall be at least that required in (a) and (b):

- a) The area of distributed reinforcement perpendicular to the longitudinal axis of the beam, A_v , shall be at least $0.0025b_ws$, where s is the spacing of the distributed transverse reinforcement.
- b) The area of distributed reinforcement parallel to the longitudinal axis of the beam, A_{vh} , shall be at least $0.0025b_ws_2$, where s_2 is the spacing of the distributed longitudinal reinforcement.

- (3) The minimum area of flexural tension reinforcement, $A_{s,min}$, shall be the greater of (a) and (b):

$$(a) \quad 0.25 \frac{\sqrt{f'_c}}{f_y} b_w d \quad (2)$$

$$(b) \quad 1.375 \frac{b_w d}{f_y} \quad (3)$$

- (4) Reinforcement detailing: spacing of distributed reinforcement required in Item (2) shall not exceed the lesser of $d/5$ and 300 mm.

2.2 Reactive Powder Concrete

2.2.1 Introduction

Reactive powder concrete (RPC) is one type of high-strength concrete (HSC) and ultra-high-performance concrete (UHPC). It was evolved from the researchers finding that the typical concrete breakdown is caused by the junction between the coarse aggregate and the mortar. Therefore, coarse aggregate is not used for mixing. And to improve ductility of concrete, researchers add some short steel fibers into concrete mix. RPC is a cement-based material as a binder to various aggregates. Its outstanding properties are achieved by using knowledge of microstructure of concrete together with knowledge of chemistry of cement and concrete. The principles of RPC are as follows [11].

- 1) Make the concrete as homogeneous as possible without coarse aggregate.
- 2) Improve the density by arranging the mix as tight as possible using a new concrete design method.

- 3) Improve microstructure to increase long-term durability by heat curing after initial setting which helps to reduce shrinkage.
- 4) Improve toughness by mixing with small steel fibers.

2.2.2 Composition of RPC

RPC is composed of very fine powders (cement, sand, quartz powder and silica fume), steel fibers (optional) and superplasticizer. The superplasticizer, used at its optimal dosage, decreases the water to cement ratio (w/c) while improving the workability of the concrete. A very dense matrix is achieved by optimizing the granular packing of the dry fine powders. This compactness gives RPC ultra-high strength and durability. RPC has compressive strengths ranging from 200 MPa to 800 MPa. The original RPC compositions, RPC200 and RPC800, are provided by Richard and Cheyrezy [11] as listed in Table 1.

Table 1. Original RPC Compositions by Weight [11].

Item	RPC 200				RPC 800	
	Non fibered		Fibered		Silica aggregates	Steel aggregates
Portland cement						
Silica fume	1	1	1	1	1	1
Sand 150 - 600 μm	0.25	0.23	0.25	0.23	0.23	0.23
Crushed quartz $d_{50}=10 \mu\text{m}$	1.1	1.1	1.1	1.1	0.5	-
	-	0.39	-	0.39	0.39	0.39
Superplasticizer (Polyacrylate)	0.016	0.019	0.016	0.019	0.019	0.019
Steel fiber L=12 mm	-	-	0.175	0.175	-	-
Steel fiber L=3 mm	-	-	-	-	0.63	0.63
Steel aggregates <800 μm	-	-	-	-	-	1.49
Water	0.15	0.17	0.17	0.19	0.19	0.19
Compaction pressure	-	-	-	-	50 MPa	50 MPa
Heat treatment temperature	20°C	90°C	20°C	90°C	250-400°C	250-400°C

2.2.3 Ingredients of RPC and Their Functions

Each ingredient of RPC has its own functions and selection parameters as discussed in [12] and listed below:

2.2.3.1 Cement

- 1) Ordinary Portland cement of medium fineness is suitable for making RPC. The cement particle size should be 1 micron to 100 microns.

- 2) The function of cement is to act as binding material and also to generate primary hydrants of concrete.
- 3) Optimum percentage of principle minerals or Bogues Compounds required to make RPC are in [Table 2](#).

Table 2. Optimum Percentage of Principle Minerals of Cement [12].

Mineral	Percentage
Tricalcium Silicate (C ₃ S)	60%
Dicalcium Silicate (C ₂ S)	22%
Tricalcium Aluminate (C ₃ A)	3.8%
Tetra-calcium Alumino Ferrite (C ₄ AF)	7.4%

2.2.3.2 Sand

- 1) Natural river bed or crushed sand of particle size 150 to 600 micron is recommended.
- 2) It should be of good hardness and readily available at low cost.
- 3) In reactive powder concrete, sand particles are highest sized particle hence, their function is to give strength to the concrete mix.

2.2.3.3 Quartz Powder

- 1) Generally, quartz powder is available in crystalline form. It is selected based on its fineness.
- 2) The particle size should be 5 microns to 25 microns.
- 3) The main function of quartz is to give maximum resistance to the concrete against heat.

2.2.3.4 Silica Fume

- 1) Silica fume is generally obtained from ferrosilicon industries. It should be selected in such a way that it should contain less quantity of impurities in it.
- 2) The particle size of silica fume is about 0.1 micron to 1 micron.
- 3) Its function is to fill the small voids and also to enhance flow properties of concrete.
- 4) It also helps to generate secondary hydrates in the concrete.

2.2.3.5 Steel Fibers

- 1) Steel fibers of length 13 to 25 mm and 0.15 to 0.2 mm diameter are selected to prepare reactive powder concrete.
- 2) It improves ductility of the concrete.

2.2.3.6 Super Plasticizer

- 1) Polyacrylate is used as super plasticizer in RPC.

- 2) The main function of polyacrylate is to decrease the water cement ratio and also to improve the workability of concrete.

2.2.4 Advantages of RPC

RPC has many advantages compared to other types of concretes as follows [12].

- 1) Due to its High ductility property, it always competes with steel.
- 2) Fine ingredients make the concrete void proof and no leakage of gas or liquid occurs.
- 3) There is a reduction of dead load of structure due to higher shear capacity along with superior strength.
- 4) RPC members have great resistance against seismic forces.

2.2.5 Limitations of RPC

RPC also has some limitations as follows [12]:

- 1) Aggregate replacing materials used in RPC are slightly expensive which increases the project cost.
- 2) Optimization of principle minerals in concrete also increase the cost of concrete.
- 3) Long term properties of reactive powder concrete are not known since it is still in developing stage.
- 4) There is no official code provided for Reactive powder concrete mix design.

2.3 Finite Element Analysis

2.3.1 Introduction

The finite element method (FEM) is a popular method for numerically solving differential equations arising in engineering and mathematical modeling. Typical problem areas of interest include the traditional fields of structural analysis, heat transfer, fluid flow, mass transport, and electromagnetic potential [13].

The FEM is a general numerical method for solving partial differential equations in two or three space variables (i.e., some boundary value problems). To solve a problem, the FEM subdivides a large system into smaller, simpler parts that are called finite elements. This is achieved by a particular space discretization in the space dimensions, which is implemented by the construction of a mesh of the object: the numerical domain for the solution, which has a finite number of points. The FEM formulation of a boundary value problem finally results in a system of algebraic equations. The method approximates the unknown function over the domain. The simple equations that model these finite elements are then assembled into a larger system of equations that models the entire problem. The FEM then approximates a solution by minimizing an associated error function via the calculus of variations. Studying or analyzing a phenomenon with FEM is often referred to as finite element analysis (FEA).

2.3.2 Basic Concepts of FEA

Typical work out of the FEA in stress analysis involves [14]:

- 1) Divide the structure or continuum into finite elements – Mesh generation programs, called preprocessors, help the user in doing this work (see [Figure 3](#)).
- 2) Formulate the properties (stiffness) of each element.
- 3) Assemble elements to obtain the finite element model of the structure.
- 4) Apply the known loads: nodal forces and/or moments.
- 5) Specify how the structure is supported. This step involves setting several nodal displacements to known values.
- 6) Solve simultaneous linear algebraic equations to determine nodal degree of freedoms (nodal displacement).
- 7) Calculate element strains from the nodal degree of freedoms (nodal displacement) and finally calculate stresses from strains. Output interpretation programs, called postprocessors, help the user sort the output and display it in graphical form.

Steps 1, 4, and 5 require decisions by the user and provide input data for the computer program. The data controls the selection of problem type, geometry, boundary conditions, element selection, and so on. Steps 2, 3, 6, and 7 are carried out automatically by the computer program.

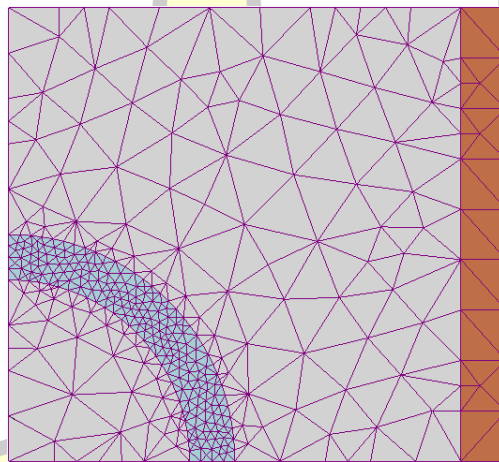


Figure 3. An Example of FE Mesh Created by Using FE Software [13].

2.3.3 SOFiSTiK FEA Software

The SOFiSTiK FEM packages [15] are customized solutions that build upon the proven SOFiSTiK finite element technology for structural analysis according to the finite element method. Based on an open system architecture, the powerful FE programs offer seamless workflows for all needs of modern civil engineering. The application area of the finite element solutions ranges from simple 2D slab design to 3D building and bridge design, from open, native and integrated BIM to big and small BIM.

All FEM packages include suitable code check modules for Eurocodes and many other standards, as well as complete and interactive post-processing and high-performance 64-bit solvers. Versatile input options, from parametric input via the AutoCAD® add-on SOFiPLUS to BIM planning with Autodesk® Revit®, round off

the FEM packages and provide civil engineers with the appropriate tools to successfully implement construction projects of any scale. More details will be given in Chapter 3. Figure 4 presents an example of the FEA results of nonlinear analysis of RC beam by the SOFiSTiK program using beam elements, beam elements including tension stiffening effect, and shell elements.

Material Nonlinear Analysis of Reinforced Concrete Beam SOFiSTiK

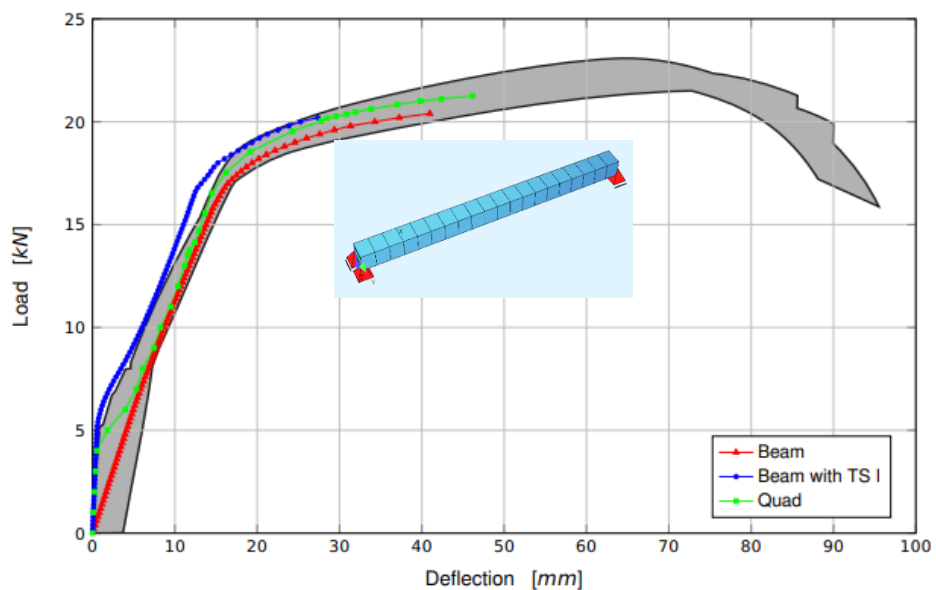


Figure 4. FEA Results of Nonlinear Analysis of RC Beam by SOFiSTiK [16].

2.4 Strut-and-Tie Model

2.4.1 Introduction

The strut-and-tie model (STM) is a generalization of the truss analogy, a concept used in shear design applied to all parts of the structure. The basic concept of the generalized truss analogy states that the flow of the force within a reinforced concrete structure is the same as the flow of the force within a truss model. Furthermore, this truss model comprises a compressive stress field and a tension tie, which connects the compressive stress field. Structural members can be divided into B-regions (Beam or Bernoulli) and D-regions (Discontinuity or Disturbed) as can be seen in Figure 5 for an example. Unlike the B-region, which undergoes beam action, the strain in the D-region undergoes arch action and has a nonlinear distribution. Moreover, because the arch action significantly increases the shear strength, it cannot be evaluated in the same way as the B-region. For this reason, the STM presents a generalized design method for the D-region in situations where the evaluation for the design of the D-region is not correctly performed, and it is inevitable to rely on the designer's experience. General structural members can be divided into B-region, where linear strain and beam theory are applied, and D-region where beam theory is not applied due to applied concentrated loads or discontinuous cross-sections [17].

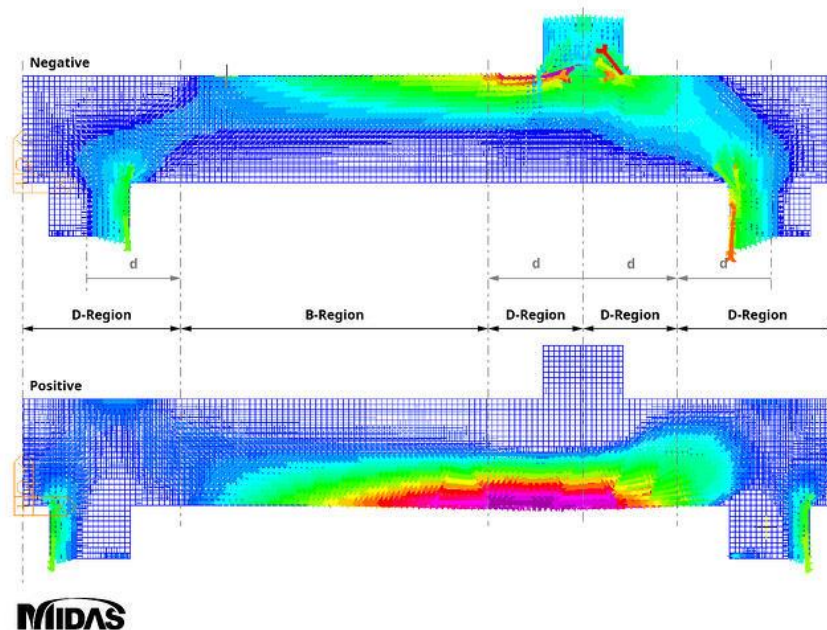


Figure 5. An Example of B-regions and D-regions in A Beam [17].

2.4.2 Components of STM

As shown in Figure 6, the flow of forces after concrete cracking can be expressed as a STM composed of compression strut, tension tie, and nodal zones. A description of each component is as follows [17]:

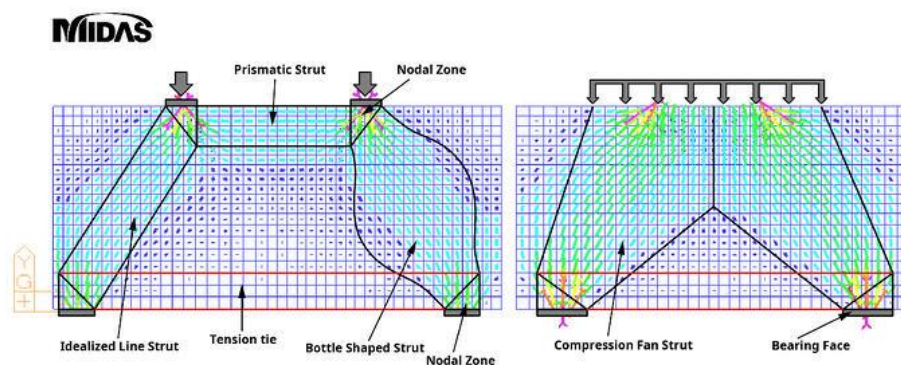


Figure 6. Components of A Strut-and-Tie Model in Deep Beam [17].

2.4.2.1 Strut

Strut is a STM member that expresses a compressive stress field under compressive forces. The strut's shape generally expressed as a prismatic strut or fan-shaped strut, as shown in Figure 6. However, it can also be expressed as a bottle-shaped strut. When bottle-shaped struts are applied to the design, longitudinal cracks may occur due to tensile forces acting perpendicular to the struts, so confining reinforcement should be placed in the direction perpendicular to the strut axis. For simplification of design, bottle-shaped struts are typically idealized as straight struts.

Strut capacity is a function of the effective compressive strength of concrete and is affected by concrete's strength, load duration effect, transverse tensile strain, and cracking. The nominal strength of the struts applied to the strut design shall be determined by the design criteria, and the smaller of the values calculated at both ends shall be applied to the design.

2.4.2.2 Tension tie

Tie is a tensile member subjected to tensile forces in STM. Ties placed in the center of the tensile rebar. The location at which the struts and ties meet is expressed as a triangular nodal zone. The width of this nodal zone is determined by the ties and is referred to as the effective width of the tie. When more than one row of tensile reinforcing bars is arranged, the effective width of ties proposed in the design criteria is followed, as shown in Figure 7.

Tie settlement should be reviewed from the location where the extended nodal zone and the center of the ties meet. The extended nodal zone refers to the area where each effective width overlaps at the location where the struts and ties meet.

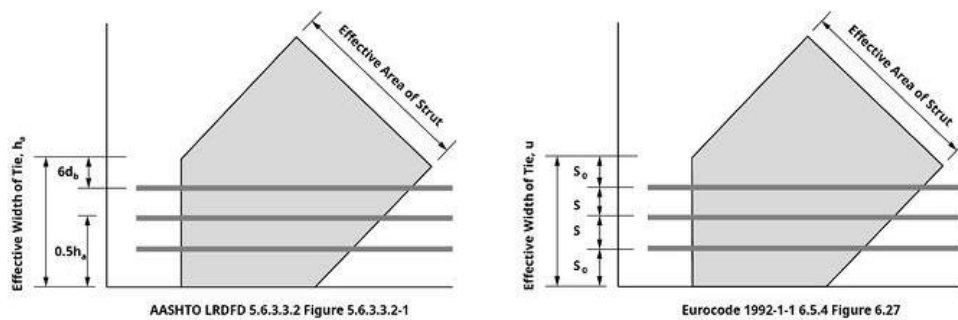
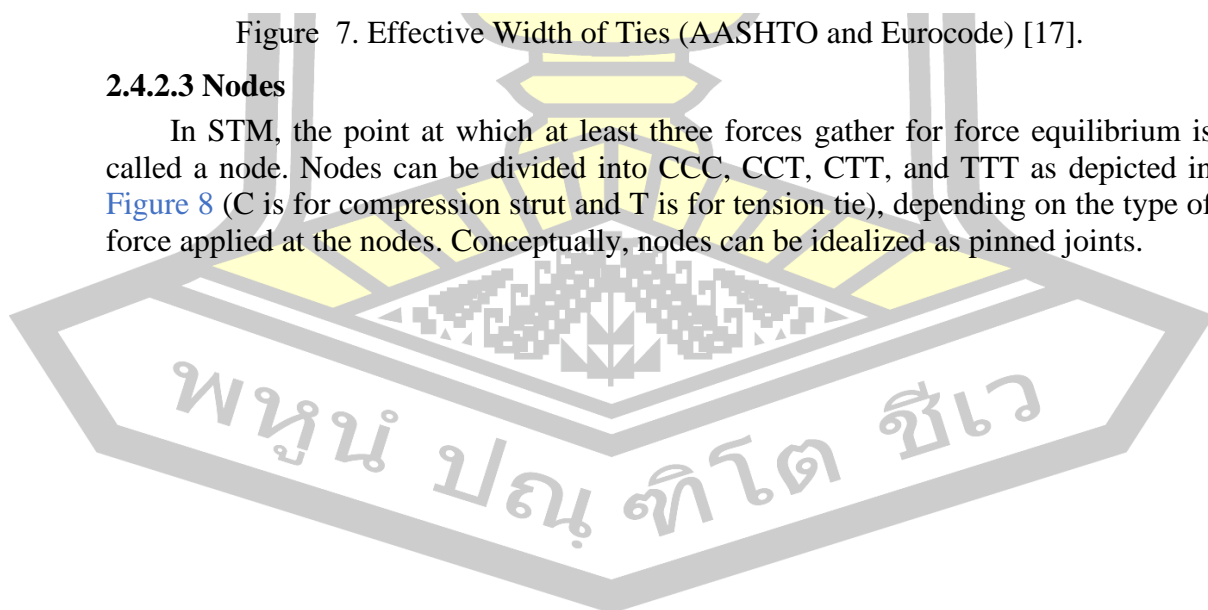


Figure 7. Effective Width of Ties (AASHTO and Eurocode) [17].

2.4.2.3 Nodes

In STM, the point at which at least three forces gather for force equilibrium is called a node. Nodes can be divided into CCC, CCT, CTT, and TTT as depicted in Figure 8 (C is for compression strut and T is for tension tie), depending on the type of force applied at the nodes. Conceptually, nodes can be idealized as pinned joints.



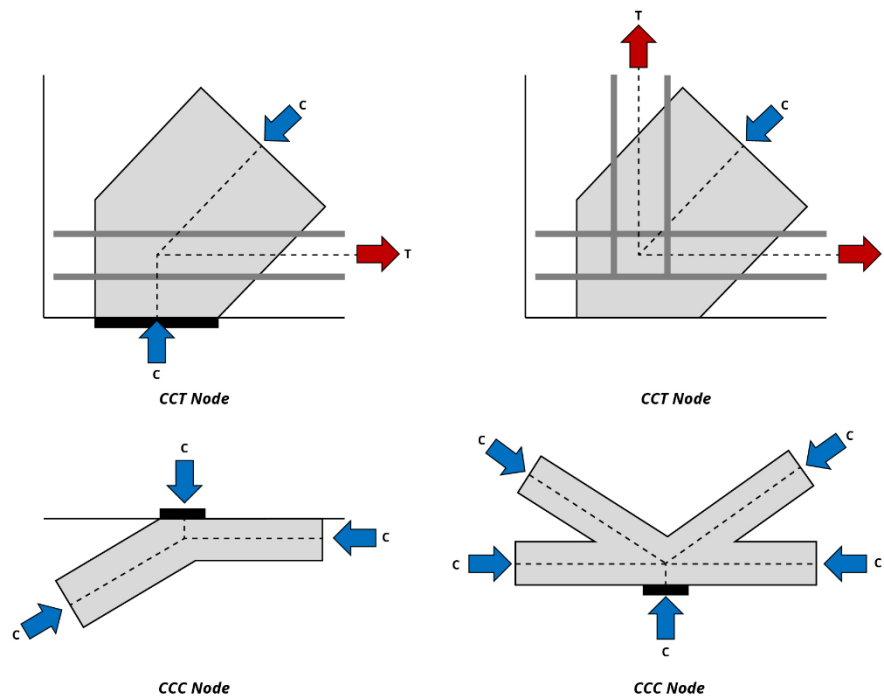


Figure 8. Types of Strut-and-Tie Model Nodes [17].

2.4.2.4 Nodal Zones

The concrete area at the node position that allows the strut and tie forces to be transmitted through the node is called the nodal zone. Hydrostatic nodal zones are zones where the sides of the nodes are placed perpendicular to the strut and ties so that all sides of the nodes have the same stress. When nodes are arranged in the Hydrostatic nodal zones, the ratio of the width of each node ($w_1 : w_2 : w_3$) is equal to the ratio of the three compressive forces ($C_1 : C_2 : C_3$), which can be used to calculate the strut's width.

Extended nodal zones consider nodes and struts, bearing faces, and even areas where the ties are extended. This method works advantageously in the settlement of rebar, considering that reaction forces or compressive forces by struts improve the adhesion of concrete and rebar.

Subdivision of nodal zones is a method that considers the reaction forces acting on the nodal zone. As shown in Figure 9, R can be subdivided into R_1 and R_2 by the bearing area ratio, and these values are the vertical components of C_1 and C_2 , respectively. This equilibrium relationship is useful for calculating the width of the inclined strut.

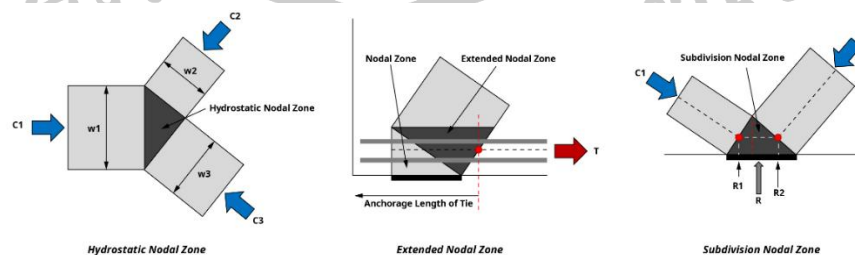


Figure 9. Types of Strut-and-Tie Model Nodal Zones [17].

2.4.3 STM Methodology

The following STM procedure proposed by MacGregor [18] can be summarized as follows:

- 1) Define and isolate the D-regions.
- 2) Compute the internal stress on the boundaries of the element.
- 3) Subdivide the boundary and compute the force resultants on each sub-length.
- 4) Draw a truss to transmit forces from boundary to boundary of the D-region.
- 5) Check the stresses in the individual members of the truss.
- 6)

2.4.4 Design strength

ACI 318-11 [3] provides the provisions for calculation of the design strength for STM as follows.

For each applicable factored load combination, design strength of each strut, tie, and nodal zone in a STM shall satisfy $\phi S_n \geq U$, including (a) through (c):

- a) Struts:

$$\phi F_{ns} \geq F_{us} \quad (4)$$

- b) Ties:

$$\phi F_{nt} \geq F_{ut} \quad (5)$$

- c) Nodal zones:

$$\phi F_{mn} \geq F_{un} \quad (6)$$

where ϕ for struts, ties, nodal zones, and bearing areas designed in accordance with strut-and-tie method shall be 0.75.

2.4.4.1 Strength of struts

2.4.4.1.1 The nominal compressive strength of a strut, F_{ns} , shall be calculated by (a) or (b):

- a) Strut without longitudinal reinforcement

$$F_{ns} = F_{ce} A_{cs} \quad (7)$$

- b) Strut with longitudinal reinforcement

$$F_{ns} = F_{ce} A_{cs} + A'_s f'_s \quad (8)$$

where F_{ns} shall be evaluated at each end of the strut and taken as the lesser value; A_{cs} is the cross-sectional area at the end of the strut under consideration; f_{ce} is given in Eq.(9); A'_s is the area of compression reinforcement along the length of the strut; and f'_s is the stress in the compression reinforcement at the nominal axial strength of the

strut. It shall be permitted to take f'_s equal to f_y for Grade 40 or 60 reinforcement according to ASTM A615.

2.4.4.1.2 Effective compressive strength of concrete in a strut, f_{ce} , shall be calculated in accordance with 2.4.5.3 or 2.4.5.4.

2.4.4.1.3 Effective compressive strength of concrete in a strut, f_{ce} , shall be calculated by:

$$f_{ce} = 0.85\beta_s f'_c \quad (9)$$

where β_s , in accordance with Table 3, accounts for the effect of cracking and crack-control reinforcement on the effective compressive strength of the concrete.

Table 3. Strut Coefficient β_s [3].

Strut geometry and location	Reinforcement crossing a strut	β_s	
Struts with uniform cross-sectional area along length	NA	1.0	(a)
Struts located in a region of a member where the width of the compressed concrete at midlength of the strut can spread laterally (bottle-shaped struts)	Satisfying 2.4.5.5	0.75	(b)
	Not Satisfying 2.4.5.5	0.60λ	(c)
Struts located in tension members or the tension zones of members	NA	0.40	(d)
All other cases	NA	0.60λ	(e)

2.4.4.1.4 If confining reinforcement is provided along the length of a strut and its effect is documented by tests and analyses, it shall be permitted to use an increased value of f_{ce} when calculating F_{ns} .

2.4.4.1.5 Reinforcement Crossing Bottle-Shaped Struts

2.4.4.1.5.1 For bottle-shaped struts designed using $\beta_s = 0.75$, reinforcement to resist transverse tension resulting from spreading of the compressive force in the strut shall cross the strut axis. It shall be permitted to determine the transverse tension by assuming that the compressive force in a bottle-shaped strut spreads at a slope of 2 parallel to 1 perpendicular to the axis of the strut as shown in Figure 10.

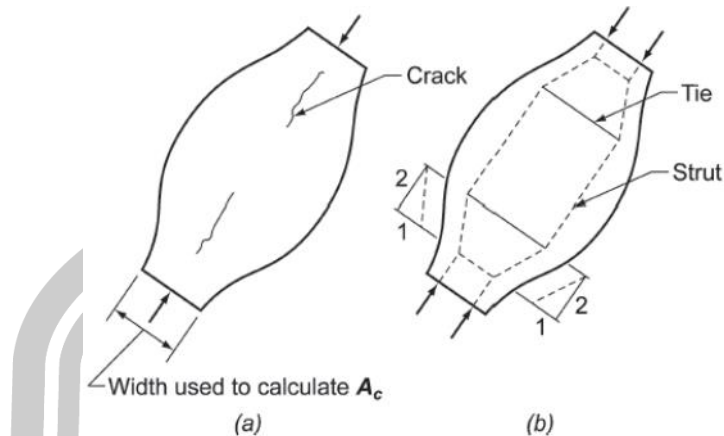


Figure 10. Bottle-Shaped Strut: (a) Cracking of A bottle-Shaped Strut ; (b) A Model to Determine Transverse Tension [3].

2.4.4.1.5.2 Distributed reinforcement calculated in accordance with Eq.(10) and crossing the strut axis shall be deemed to satisfy 2.4.5.5.1, if $f'_c \leq 41.37$ MPa (6,000 psi).

$$\sum \frac{A_{s_i}}{b_s s_i} \sin \alpha_i \geq 0.003 \quad (10)$$

where A_{s_i} is the total area of distributed reinforcement at spacing s_i in the i -th direction of reinforcement crossing a strut at an angle α_i to the axis of a strut, and b_s is the width of the strut. Distributed reinforcement required shall be placed orthogonally at angles α_1 and α_2 to the axis of the strut, or in one direction at an angle α_1 to the axis of the strut, see Figure 11. Where the reinforcement is placed in only one direction, α_1 shall be at least 40 degrees.

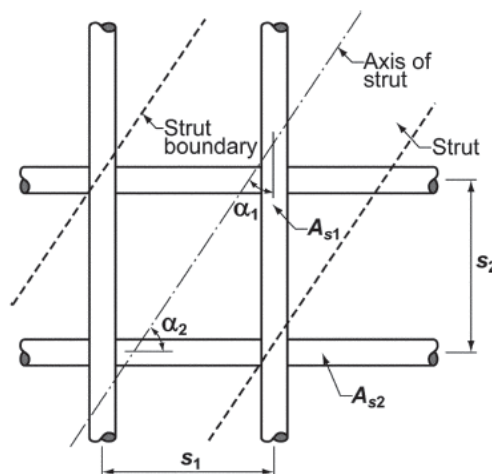


Figure 11. Reinforcement Crossing A Strut [3].

2.4.4.2 Strength of Ties

Tie reinforcement shall be non-prestressed or prestressed. The nominal tensile strength of a tie, F_{nt} , shall be calculated by:

$$F_{nt} = A_{ts}f_y + A_{tp}(f_{se} + \Delta f_p) \quad (11)$$

where $(f_{se} + \Delta f_p)$ shall not exceed f_{py} , and A_{tp} is zero for non-prestressed members. In Eq. (11), it shall be permitted to take Δf_p equal to 413.7 MPa (60,000 psi) for bonded prestressed reinforcement and 68.95 MPa (10,000 psi) for unbonded prestressed reinforcement. Higher values of Δf_p shall be permitted if justified by analysis.

2.4.3.3 Strength of Nodal Zones

2.4.3.3.1 The nominal compressive strength of a nodal zone, F_{mn} , shall be calculated by:

$$F_{mn} = f_{ce}A_{nz} \quad (12)$$

where f_{ce} is defined in 2.4.7.2 or 2.4.7.3 and A_{nz} is given 2.4.7.4 or 2.4.7.5.

2.4.3.3.2 The effective compressive strength of concrete at a face of a nodal zone, f_{ce} , shall be calculated by:

$$f_{ce} = 0.85\beta_n f'_c \quad (13)$$

where β_n shall be in accordance with Table 4.

Table 4. Nodal Zone Coefficient β_n [3].

Configuration of nodal zone	β_n	
Nodal zone bounded by struts, bearing areas, or both	1.0	(a)
Nodal zone anchoring one tie	0.80	(b)
Nodal zone anchoring two or more ties	0.60	(c)

2.4.3.3.3 If confining reinforcement is provided within the nodal zone and its effect is documented by tests and analyses, it shall be permitted to use an increased value of f_{ce} when calculating F_{mn} .

2.4.3.3.4 The area of each face of a nodal zone, A_{nz} , shall be taken as the smaller of (a) and (b):

- (a) Area of the face of the nodal zone perpendicular to the line of action of F_{us}
- (b) Area of a section through the nodal zone perpendicular to the line of action of the resultant force on the section

2.4.3.3.4 In a three-dimensional strut-and-tie model, the area of each face of a nodal zone shall be at least that given in 2.4.7.5, and the shape of each face of the nodal zone shall be similar to the shape of the projection of the end of the strut onto the corresponding face of the nodal zone.

2.5 Related Research

Fatehi et al. [4] reported an experimental study of the behavior of RPC deep beams with openings externally bonded by carbon fiber-reinforced polymer (CFRP) strips. The beam specimens were classified into three categories. The first category contains two RPC deep beams without strengthening. The second category has six RPC deep beams strengthened with different schemes of CFRP strips without mechanical anchorage. The last category includes four RPC deep beams strengthened with CFRP strips and using mechanical anchorage (bolts). The results showed that using a CFRP system as an external strengthening technique has an important effect on the overall response of the tested beam specimens. The ultimate strength of the deep beams with openings increased by 11%–94% compared to non-strengthened specimens.

Fahmi et al. [5] studied the behavior and shear strength characteristics of RPC deep beams subjected to concentrated loads. Seven reinforced deep beams made with RPC were cast and tested. The test variables included the shear span to effective depth ratio, and percentage of silica fume in the concrete. The effect of these parameters on the behavior of the test beams included deflection, concrete strains, failure mode, and ultimate loads were investigated. The experimental results are compared with analytical results using the strut and tie model of ACI 318M-11 Code and found both results to be, in general, in good agreement.

Makki et al. [6] used ANSYS, a FEA software, to make nonlinear analysis of RPC deep beams. The models simulating the test process were established, the calculation results of ANSYS are compared with the experimental results. Data of eight RPC deep beams tested by researchers were used for comparison with ANSYS models. Furthermore, three parametric studies were carried out by changing the size of opening, location of openings and CFRP systems configuration. The comparison showed that ANSYS analysis results are similar to experimental results (the maximum difference in the ultimate load was less than 7.5%), which indicated ANSYS analysis software can be used to simulate the mechanical property of RPC structures.

Hassan [7] presented an experimental investigation consisting of casting and testing twelve rectangular simply supported reinforced concrete deep beams. Three of the tested beams were made with conventional concrete (CC), three with ultra-high-performance concrete (UHPC) and six as hybrid beams of the two concretes (UHPC & CC). UHPC was used in compression in the hybrid beams. The effect of these parameters on the behavior of the test beams included deflection, failure mode, and ultimate loads was investigated. Experimental results generally showed that stiffer load

deflection behavior was obtained with the increase of UHPC layer thickness and steel fibers volumetric ratio for hybrid beams with UHPC in compression.

Hasan and Al-Shamaa [8] studied an implementation of bubbles in RPC deep beams in order to reduce their weight. An experimental work was carried out to test the effect of bubbles on the behavior of the beams. Six simply supported deep beams had the same rectangular cross section, flexural and shear reinforcement. They were cast with overall height (h) of 340 mm, width (b) of 120 mm and they were classified into two major groups (A and B) because of their total length (L) of (1000 mm and 1400 mm), respectively. The main parameters in this study were existing bubbles, flexural behavior and shear span-to-depth ratio. The results showed that increasing layer of bubbles caused a decreasing in first load cracking and ultimate loads and increasing in mid span deflection for all beams. Also, the result showed the existence of bubbles was caused reducing the weight of deep beam and ultimate load. For deep beams with shear span-to-depth ratio of 1.11 and with one and two layers the reduction in weight was 9.35% and 18.7%, respectively, while in other hand, there were reduction in ultimate load with 7.31% and 11.7%, respectively. Moreover, the reduction in weight of deep beam with shear span-to-depth ratio of 1.67 and with one and two layers were 13.09% and 26.18%, respectively resulting reduction in ultimate load of 12.5% and 21.8%, respectively. Therefore, the effect of bubbles for deep beam with shear span-to-depth ratio of 1.11 more useful than deep beam with shear span-to-depth ratio of 1.67.

Muhaison et al. [19] reported the experimental behavior of six simply supported RPC deep beams designed to be failed in shear loaded under two symmetrical point loads and subjected to monotonic and repeated load. All RPC mixes had a same aspect ratio of steel fiber, but different value of the volume fraction which was either 1% or 2%. The tested deep beams had the same overall span of 1200 mm, constant cross section; 115 mm wide and 400 mm overall depth, and reinforced with the same amount of main tension bars ($3\phi 20$), and a same amount of shear reinforcement ($\phi 4\text{mm} @ 100\text{ mm c/c}$). Each deep beam had two typical square opening. There were two different sizes of the opening; 40 mm and 80 mm. All deep beams had the same; water/cement ratio. Throughout the test operation, the crack patterns were drawn and identified the mode of failure of the tested deep beams. And the load deflection curves were plotted. It was found from observations of this study; a large opening often interrupted the load transfer by concrete struts in deep beams and caused a sharp decrease in strength and serviceability. Also, the presence of the opening in the deep beams decayed the ultimate load of the RPC specimens with volume fraction 1% under repeated load by 2.27 times. In particular, it was shown that the presence of steel fiber, along with the RPC, played a crucial role in the transition from flexural to shear dominated failure modes of the beam.

Yang et al. [20] conducted a bending test of UHPC beams. A total of 14 UHPC reinforced beams were designed in the test. The main test variables were the reinforcement ratio of the longitudinal main reinforcement of the beam and the pouring method of the test beam. The test results showed that when the reinforcement ratio is between 2% - 4%, there were many fine cracks in the pure bending section of the beam. When the beam reached the ultimate bearing capacity, there were many main cracks, and the beam showed good bending resistance. The test results also showed that the bearing capacity of test beams with different pouring methods was different, because the pouring method affected the arrangement of steel fiber inside the beam. It was also

suggested that the beam should be poured from one end to the other end to make the fiber distribution more uniform.

Adeline et al. [21] conducted a bending test of UHPC beams. In the test, two UHPC beams with a length of 15 m were designed. The two beams were equipped with 8 or 4 longitudinal tensile steel bars with a diameter of 15.2 mm. The test results showed that the failure mode of UHPC beams with four longitudinal tensile reinforcements was that the longitudinal reinforcements are broken, while the failure mode of UHPC beams with eight reinforcements was that the concrete in the compression zone was crushed.

Yoo and Yoon [22] conducted an experimental study on the bending performance of UHPC beams. The main variable in the test was the type of steel fiber mixed in UHPC. A total of 10 UHPC beams were fabricated in the test, and the same beam size was selected to maintain the single variable principle. The length of the designed test beam was 2.5m, and the cross section of the beam was a rectangular section of 150×220 mm. The test results showed that the incorporation of steel fiber did not affect the cracking load of the beam, but the steel fiber can effectively improve the post-cracking stiffness and ultimate bearing capacity of the beam. Using different length of steel fiber and twisted steel fiber, there was no significant difference in the performance and ductility of cracked beams. The failure mode of UHPC beam without steel fiber was crushing of concrete in compression zone, and the failure mode of UHPC beam with steel fiber was tensile failure of steel bar.

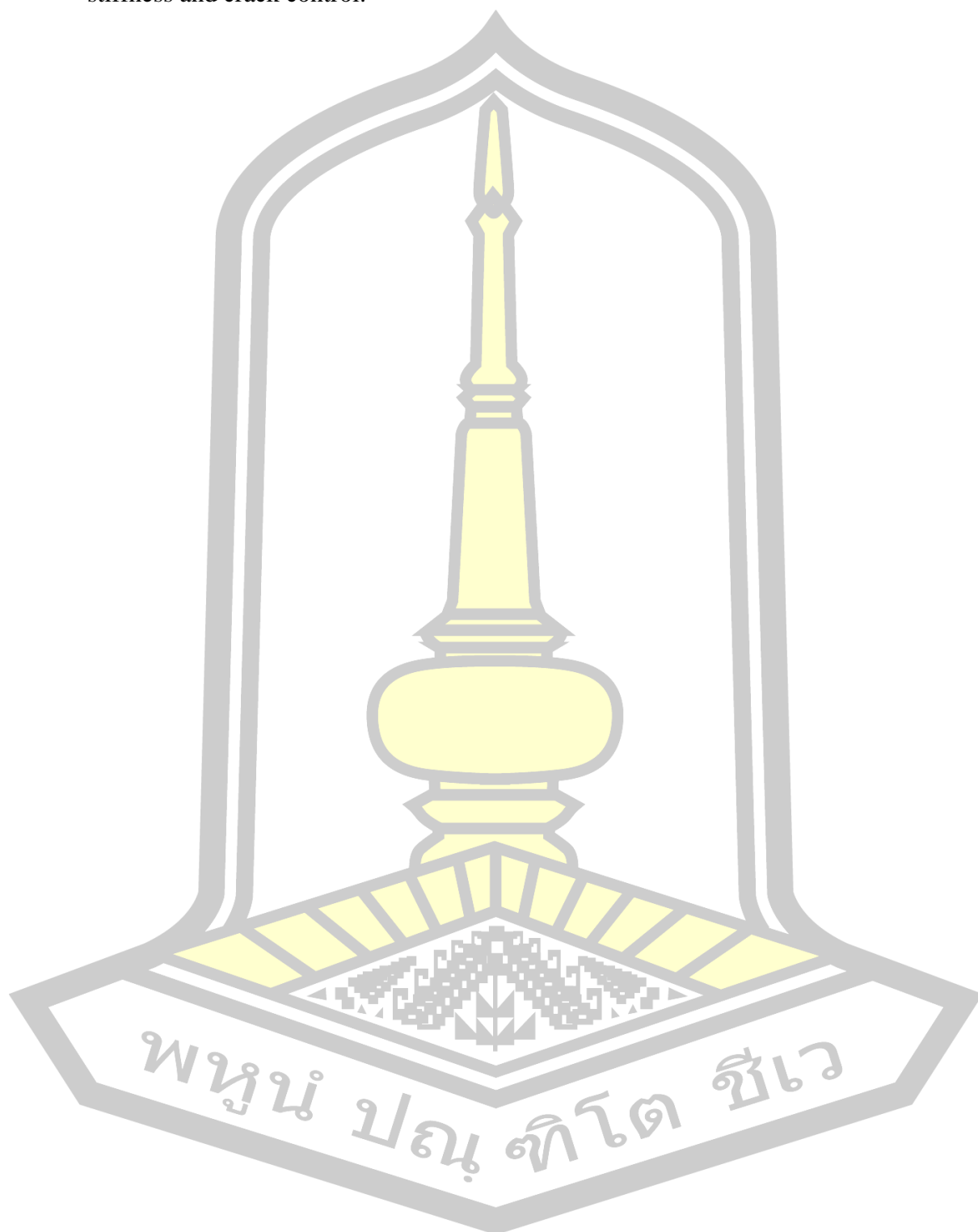
Spasojevic et al. [23] studied the influence of beam width (25-75mm) and beam height (25-500mm) on the flexural performance of ultra-high performance fiber reinforced concrete beams. The test results showed that the width of the concrete beam had little effect on the flexural strength of the beam. Height only increased the plastic deformation capacity of concrete by 2-3%.

Bărbos [24] analyzed the mechanical properties of ultra-high-strength concrete beams reinforced with different proportions of steel fibers, it was found that each type of ultra-high-strength concrete beam showed good durability in terms of strain, deflection and cracks. It was also recommended to use a volume percentage of 0.50% steel fiber to ensure good mechanical performance of the beam.

Alkaysi and El-Tawil [25] conducted pull-out tests on several groups of UHPC specimens. The main parameters of the specimens were the diameter of the steel bar, the amount of steel fiber in UHPC, the embedding length of the steel bar in UHPC, the pouring direction of the specimen and the curing time of the specimen. The pull-out test results showed that the bond strength between steel bar and concrete decreased with the increase of embedded length because the bond force was not evenly distributed along the length direction of steel bar. When using 1% fiber and 2% fiber, the difference of bond strength between steel and concrete was 36%. In the early stage of specimen curing, the bond strength of steel bar increased with the increase of curing time. The bond strength and compressive strength of UHPC and steel bar cured for 7 days reached 75% of the ultimate strength.

Hasgul et al. [26] studied the flexural performance of UHPC beams with different reinforcement ratios through experiments. The test results showed that compared with the non-fiber beam, the increase of steel fiber increased the flexural capacity of the test beam by 23-50%; the flexural stiffness increased by an average of 27% with the increase of fiber content, but the reinforcement ratio had no significant effect on the flexural stiffness. The use of UHPC can change the failure mode of beam. UHPC with

high reinforcement ratio had significant advantages in ductility, flexural capacity, stiffness and crack control.



Chapter 3

Research Methods

3.1 Finite Element Analysis using SOFiSTiK

In this study, SOFiSTiK FEM code [27] will be adopted for nonlinear analysis of deep beam behavior.

The deep beams will be modeled using four-node plane elements called QUAD or shell element, as shown in Figure 12, with the plate structural behavior based on Reissner-Mindlin theory. Using plate/shell elements, the contribution of the concrete between cracks (tension stiffening) is included in the element. Moreover, the program offers a layer material model, as depicted in Figure 13, for cracked concrete analysis having an advantage as the numerical stability and robustness exist with a simple 2D element by introducing a number of material layers for the element stiffness calculation in the Gauss points and a general quadrilateral element with four nodes is sufficient [28, 29].

To include the nonlinear behavior of the materials, the 2D stress-strain curves in tension and compression zone based on some standard codes and some simple assumptions will be input into the program.

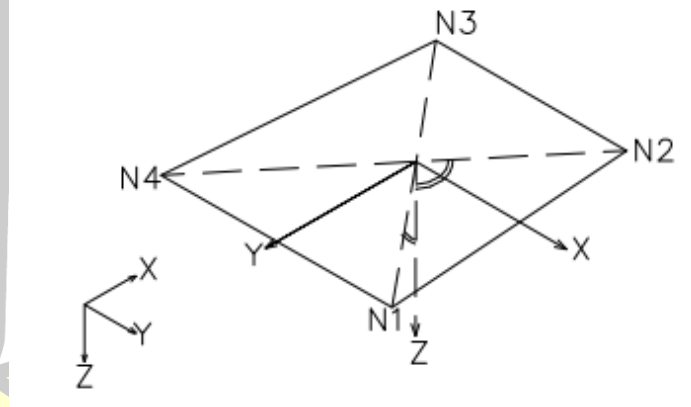


Figure 12. Shell Element in Local Coordinate System [30].

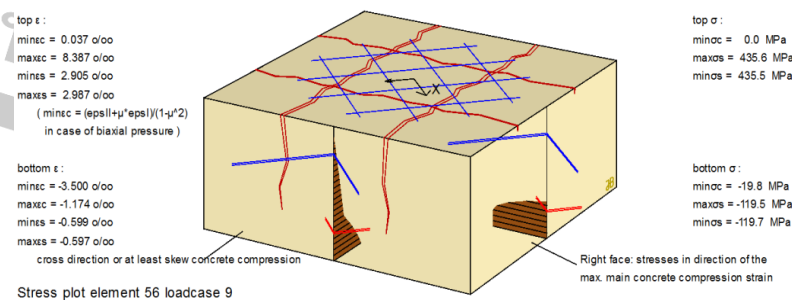


Figure 13. An Example of Layer Material Model in SOFiSTiK [31].

The finite element analysis method is one of the important methods to analyze the stress process of the structure. It digitizes the size, material properties and stress characteristics of the actual components, and uses the computer to carry out simulation operations to simulate the stress of the components. However, the accuracy of the finite element results is affected by the material constitutive model. Therefore, it is necessary to verify the selected constitutive model by comparing with the experimental results before the finite element analysis to ensure the accuracy of the finite element simulation results.

This chapter will introduce the constitutive model of normal strength concrete (NSC), high strength concrete (HSC) and RPC and re-bar according to the following standard codes.

3.1.1 Constitutive Models: The *fib* Model Code 2010

The *fib* model code 2010 [32] provides constitutive models of NSC and HSC. The International Federation for Structural Concrete (*fib*) is a pre-normative organization. 'Pre-normative' implies pioneering work in codification. This work has now been realized with the *fib* Model Code 2010. The *fib* Model Code 2010 is the most comprehensive code on concrete structures and the objectives of the *fib* Model Code 2010 are to serve as a basis for future codes for concrete structures.

3.1.1.1 The *fib* Model Code 2010: Compressive Stress-Strain Model

In analysis the compressive strength of concrete f'_c at an age of 28 days is applied. Values for the modulus of elasticity for normal weight concrete with natural sand and gravel can be estimated from the specified characteristic strength. If the actual compressive strength of concrete f'_c at an age of 28 days is known, E_{ci} can be estimated from Eq. (14):

$$E_{ci} = E_{c0} \cdot \alpha_E \cdot \left(\frac{f'_c}{10} \right)^{1/3} \quad (14)$$

where:

E_{ci} : the modulus of elasticity of concrete in [MPa] at concrete age of 28 days

f'_c : the compressive strength of concrete at an age of 28 days

$E_{c0} = 21.5 \cdot 10^3 \text{ MPa}$

α_E : 1.0 for quartzite aggregates (assumed)

According to the *fib* model code 2010, the stress-strain relationship in compression for concrete can be simulated using Eqs. (15) to (17).

$$f_c = \left(\frac{k \cdot \eta - \eta^2}{1 + (k - 2) \cdot \eta} \right) f'_c \quad (15)$$

$$\eta = \varepsilon_c / \varepsilon_{c1} \quad (16)$$

$$k = E_c / E_{c1} \quad (17)$$

where:

f_c : the compressive stress corresponding to compressive strain ($\varepsilon_c \leq \varepsilon_{c,lim}$)

$\varepsilon_{c,lim}$: the maximum compressive strain

f'_c : the maximum compressive stress

ε_{c1} : the strain at maximum compressive stress

k : the plasticity number

E_c : the initial elastic modulus

E_{c1} : the secant modulus from origin to peak compressive stress

The plasticity number k and the limit strain $\varepsilon_{c,lim}$ can according to Table 5. The relation between stress and strain for uniaxial compression is shown in Figure 14.

Table 5. Strain $\varepsilon_{c,lim}$ and Plasticity Number k for Normal Weight Concrete [32].

Concrete grade	f'_c [MPa]	$\varepsilon_{c,lim}$ [‰]	k
C12	12	-3.5	2.44
C20	20	-3.5	2.28
C30	30	-3.5	2.04
C40	40	-3.5	1.82
C50	50	-3.4	1.66
C60	60	-3.3	1.55
C70	70	-3.2	1.47
C80	80	-3.1	1.41
C90	90	-3	1.36
C100	100	-3	1.35
C110	110	-3	1.24
C120	120	-3	1.18

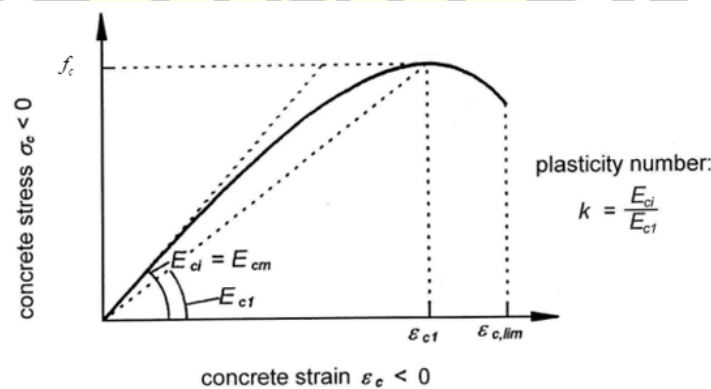


Figure 14. Schematic Representation of The Stress-Strain Relation for Uniaxial Compression (According to *fib* Code 2010) [32].

3.1.1.2 The *fib* Model Code 2010: Tensile Stress-Strain Model

The stress-strain relationship in tension can be obtained following the concept shown in Figure 15 along with using Eqs. (18) to (20).

$$f_t = 2.12 \cdot \ln(1 + 0.1 f'_c) \text{ MPa} \quad (18)$$

$$\varepsilon_{t1} = 0.15 + \frac{w_1}{l_c} \text{ mm/m} \quad (19)$$

$$w_1 = \frac{G_f}{f_t}; \quad G_f = 0.073 (f'_c)^{0.18} \text{ N/mm} \quad (20)$$

where:

f_t : the peak tensile stress

ε_{t1} : the tensile strain corresponding to crack opening w_1

w_1 : the crack opening when tensile stress = $0.2f_t$

l_c : the characteristic length taken as total height of section (h)

G_f : the fracture energy

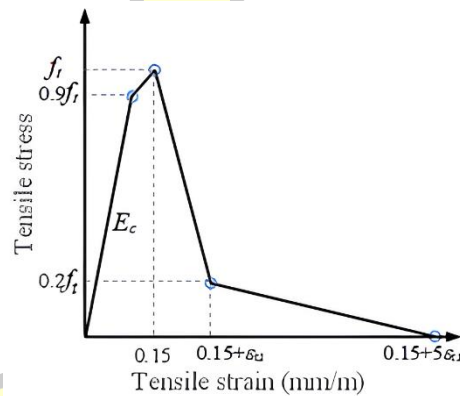


Figure 15. Schematic Representation of The Stress-Strain and Stress-Crack Opening Relation for Uniaxial Tension (According to *fib* Code 2010) [32].

The input parameters and calculated parameters (*fib* Code 2010) as Table 6 shows.

Table 6. Input Parameters and Calculated Parameters of Constitutive Model for RPC Following The *fib* Model Code 2010.

Input Parameters	Calculated Parameters
ν	E_{ci}
f'_c	E_{c1}
k	ε_{c1}
$\varepsilon_{c,lim}$	f_t
h	G_F

Input Parameters	Calculated Parameters
-	W_1
-	W_c
-	ϵ_c

3.1.2 Constitutive Models: NF P 18-710 (AFGC)

The NF P 18-710 (AFGC) [33] provides constitutive models of RPC. In April 2016, the French Association of Civil Engineering (AFGC) officially promulgated the UHPC design specification "National addition to Eurocode 2 - Design of Concrete structures: specific rules for NF P 18-710" as a supplementary specification to the European concrete structure design specification. In AFGC supplies application for ultimate limits of load-bearing capacity (ULS). The application is shown in Figure 16.

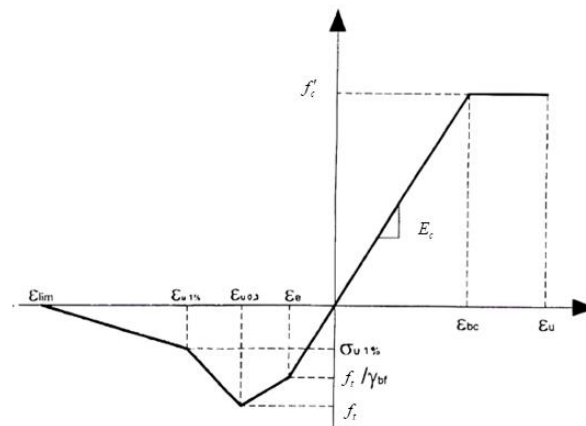


Figure 16. Diagrams for The ULS Regarding AFGC [33].

In the AFGC standard the area of tension in ULS is equally considered. Regarding the ULS solely the concrete tensile strength is divided by the load factor γ (1.3 for RPC) in the elastic area.

In this study will take the ULS, and the important behavior of concrete in compression and tension is modelled via the following several control points.

3.1.2.1 NF P 18-710 (AFGC): Compressive Stress-Strain Model

The strain ϵ_{bc} is defined by the following relationship:

$$\epsilon_{bc} = \frac{f'_c}{E_c} \quad (21)$$

where:

f'_c : the compressive strength of concrete at an age of 28 days

E_c : Young's modulus

Assuming the ultimate strain $\varepsilon_u = 0.0052$ to be taken into account at ULS and the Poisson's ratio of RPC $\nu = 0.19$

3.1.2.2 NF P 18-710 (AFGC): Tensile Stress-Strain Model

ε_{lim} : limit strain

$$\varepsilon_{lim} = \frac{l_f}{4 \cdot l_c} \quad (22)$$

where:

l_f : fiber length

l_c : characteristically length $l_c = \frac{2}{3}h$

h : height of the section

$\varepsilon_{u1\%}$: ultimate strain where the crack width equals 1% of the height of the specimen

$$\varepsilon_{u1\%} = \frac{w_{1\%}}{l_c} + \frac{f_t}{E_c} = \frac{0.01h}{l_c} + \frac{f_t}{E_c} \quad (23)$$

where:

h : height of the section

l_c : characteristically length $l_c = \frac{2}{3}h$

f_t : maximum tensile stress

E_c : Young's modulus

$\varepsilon_{u0.3}$: ultimate strain where a 0.3mm crack width is obtained

$$\varepsilon_{u0.3} = \frac{w_{0.3}}{l_c} + \frac{f_t}{E_c} = \frac{0.3}{l_c} + \frac{f_t}{E_c} \quad (24)$$

where:

l_c : characteristically length $l_c = \frac{2}{3}h$

f_t : maximum tensile stress

E_c : Young's modulus

ε_e : ultimate elastic tensile strain at the ultimate limit state

$$\varepsilon_e = \frac{f_t}{\gamma_{bf} E_c} = \frac{f_t}{1.3 E_c} \quad (25)$$

where:

γ_{bf} : load factor for RPC under tension $\gamma_{bf} = 1.3$

f_t : maximum tensile stress

E_c : Young's modulus

The input parameters and calculated parameters (AFGC Code) as [Table 7](#) shows.

Table 7. Input Parameters and Calculated Parameters of Constitutive Model for RPC Following AFGC Code.

Input Parameters	Calculated Parameters
f'_c	ε_{lim}
f_t	$\varepsilon_{u1\%}$
E_c	$\sigma_{u1\%}$
ε_u	$\varepsilon_{u0.3}$
ν	$\sigma_{u0.3}$
h	ε_e
l_f	σ_e
γ_{bf}	ε_{bc}

3.1.3 Constitutive Models: CECS 2020

The CECS 2020 [34] provides constitutive models of RPC.

3.1.3.1 CECS 2020: Compressive Stress-Strain Model

Constitutive law for RPC according China Association for Engineering Construction Standardization: Technical Specification for Ultra-High Performance Concrete Structures (CECS 2020) is as [Figure 17](#) shows:

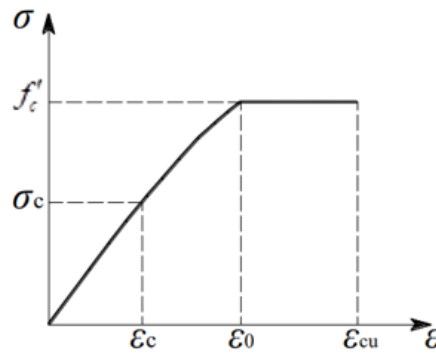


Figure 17. Constitutive Law of RPC in Compression Regarding CECS 2020 [34].

$$\sigma_c = f'_c \left[1 - \left(1 - \frac{\varepsilon_c}{\varepsilon_0} \right)^n \right] \quad (\varepsilon_c < \varepsilon_0) \quad (26)$$

$$\sigma_c = f'_c \quad (\varepsilon_0 \leq \varepsilon_c \leq \varepsilon_{cu}) \quad (27)$$

$$n = 1.2 - 0.001(f'_c - 100) \quad (28)$$

$$\varepsilon_0 = 0.0025 + 0.5 \times (f'_c - 100) \times 10^{-5} \quad (29)$$

$$\varepsilon_{cu} = 0.0042 - 0.3 \times (f'_c - 100) \times 10^{-5} \quad (30)$$

where:

σ_c : the stress in RPC at a compressive strain of ε_c

f'_c : the compressive strength of concrete at an age of 28 days

ε_0 : the compressive strain corresponding to peak stress f'_c in RPC

ε_{cu} : the ultimate compressive strain of RPC

3.1.3.2 CECS 2020: Tensile Stress-Strain Model

According to the CECS 2020, the tensile stress-strain model can be obtained following Figure 18 and using Eqs. (31) to (36).

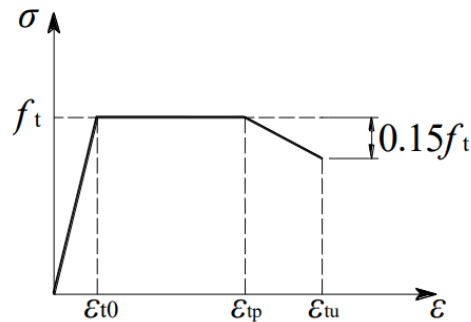


Figure 18. Constitutive Law of RPC in Tension Regarding CECS 2020 [34].

$$\sigma_t = E_c \varepsilon_t \quad (\varepsilon_t \leq \varepsilon_{t0}) \quad (31)$$

$$\sigma_t = f_t \quad (\varepsilon_{t0} < \varepsilon_t < \varepsilon_{tp}) \quad (32)$$

$$\sigma_t = f_t + 0.15 f_t \left(\frac{\varepsilon_{tp} - \varepsilon_t}{\varepsilon_{tu} - \varepsilon_{tp}} \right) \quad (\varepsilon_{tp} < \varepsilon_t \leq \varepsilon_{tu}) \quad (33)$$

where:

σ_t : the tensile stress in RPC with tensile strain ε_t

f_t : the peak tensile stress

ε_{tp} : the tensile strain of RPC when the tensile stress begins to decrease with increasing strain. It is advisable to determine this from tests, and when no test data are available, it is to be taken as:

$$\varepsilon_{tp} = 0.001 \alpha_s (-1.27 \lambda_f^2 + 5.61 \lambda_f - 3.26) \quad (34)$$

ε_{tu} : the ultimate tensile strain of RPC. It is advisable to determine this from tests, and when no test data are available, it is to be taken as

$$\varepsilon_{tu} = 0.003 (-0.49 \lambda_f^2 + 2.24 \lambda_f - 0.79) \quad (35)$$

α_s : the end type of fiber influence factor (1.30 for end-hooked fiber and 1.0 for straight steel fiber).

λ_f : the steel fiber characteristic parameter.

$$\lambda_f = \frac{\rho_f l_f}{d_f} \quad (36)$$

where:

ρ_f : the steel fiber volume ratio

l_f : the length of steel fiber

d_f : the equivalent diameter of steel fiber

And the Poisson's ratio of RPC ν adopted at 0.20 as suggested by the code.

Modulus of elasticity of RPC E_c shall be adopted from [Table 8](#) or calculated from Eq. (37).

Table 8. Modulus of Elasticity of RPC ($\times 10^4$ MPa) [34].

Elastic modulus	Concrete Grade				
	C120	C140	C160	C180	C200
E_c	4.29	4.52	4.71	4.86	5.00

$$E_c = \frac{10^5}{1.5 + \frac{100}{f'_c}} \quad (37)$$

where:

f'_c : the compressive strength of concrete at an age of 28 days

Tensile strength of RPC f_t can be adopted from [Table 9](#) or calculated from Eq. (38).

Table 9. Tensile Strength of RPC f_t Under Typical Parameters (MPa, $l_f / d_f = 65$) [34].

Steel fiber volume ratio	Concrete Grade				
	C120	C140	C160	C180	C200
1.5	6.5	7.5	8.6	9.7	10.8
2.0	6.7	7.9	9.0	10.1	11.2
3.0	7.3	8.5	9.7	10.9	12.1
4.0	7.8	9.1	10.5	11.8	13.1

$$f_t = 0.047 f'_c (1 + 0.15 \lambda_f) \quad (38)$$

where:

λ_f : the steel fiber characteristic parameter.

The input parameters and calculated parameters (CECS Code) as [Table 10](#) shows.

Table 10. Input Parameters and Calculated Parameters of Constitutive Model for RPC Following CECS Code.

Input Parameters	Calculated Parameters
f'_c	σ_c
E_c	n
ν	ε_0
ρ_f	ε_{cu}
l_f	ε_{t0}
d_f	ε_{tp}
α_s	ε_{tu}
f_t	-

3.1.4 Constitutive Models for Rebar

As an isotropic metallic material, the intrinsic model of steel reinforcement is relatively well developed, so in this study all the steel is modeled by an ideal elastic-plastic model. It should be noted that all codes investigated in this study also use this simple model, for example, Figure 19 shows the rebar model according to the EN 1992-1-1 [35].

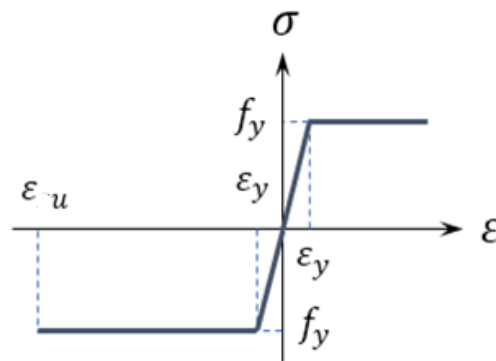


Figure 19. Constitutive Law of Rebar Following EN 1992-1-1 [35].

where:

f_y : yield strength of the rebar

E_s : modulus of elasticity for re-bar

ε_y : the strain when the stress is f_y , $\varepsilon_y = f_y/E_s$

ε_u : the ultimate limit strain of re-bar, assuming $\varepsilon_u = 0.0045$

The input parameters and calculated parameters (Rebar) as Table 11 shows.

Table 11. Input Parameters and Calculated Parameters of Constitutive Model for Rebar Following EN 1992-1-1.

Input Parameters	Calculated Parameters
f_y	f_y/E_s
ε_u	-
E_s	-

3.2 Shear Strength Analysis using Strut-and-Tie Model

3.2.1 STM: ACI 318-11

According to ACI 318-11 [3], deep beams shall be designed taking into account nonlinear distribution of longitudinal strain over the depth of the beam and strut-and-tie models (STM) are deemed to satisfy the requirement. In this study, the STM will be checked how accurate the STM can predict the shear strength (V_u) of RPC deep beams.

Using STM, the deep beam will be converted into an equivalent truss with a simple model where the tension and compression zones were transformed into equivalent ties and struts connected at the nodes as shown in Figure 20. The maximum value of V_u can be determined using the equations detailed in Chapter 2.

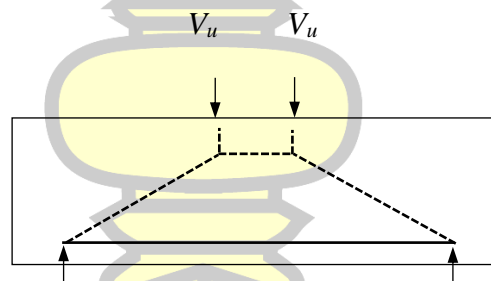


Figure 20. The STM Used in This Study.

In Chapter 2, the Code ACI 318-11 only introduces the design method of deep beam's strut and tie model, and there is no formula for calculating the shear bearing capacity of deep beams based on this design method. The following figure shows the strut and tie model calculation diagram of the simply supported deep beam with two points of symmetric concentrated load. Based on this diagram, the method of calculating the shear load capacity of deep beams with the American Standard strut and tie model is discussed.

When the deep beam is calculated by the strut and tie model, if the deep beam is bending failure, its bearing capacity depends on the tension tie bearing capacity; if the deep beam failure is shear failure, its bearing capacity depends on the compression strut bearing capacity.

The effective compressive strength of struts and nodal zones in Code ACI 318-11 has already shown in Chapter 2.

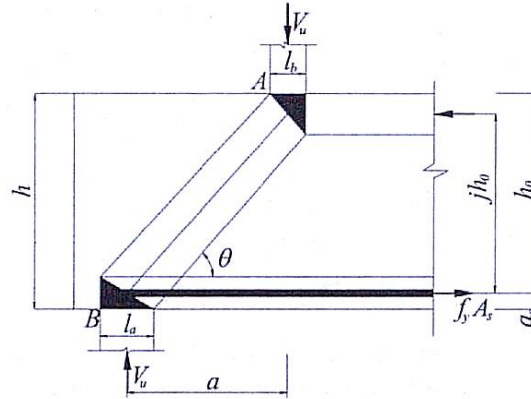


Figure 21. Strut-and-Tie Model for Simply Supported Deep Beam.

where:

V_u : shear strength of deep beam

a : shear span

h_0 : effective depth of deep beam

h : total depth of deep beam

θ : angle of strut with respect to x-axis

l_b : width of top bearing plate

l_a : width of bottom bearing plate

α_s : distance from the centerline of the bottom tensile longitudinal reinforcement to the bottom of deep beam

jh_0 : distance between the center of the upper compression strut and the lower tension tie

In general, it may be difficult to determine the true geometry of the struts accurately. However, it can be assumed that the struts have a uniform cross-section over their length, which is called the “prismatic struts.” as Figure 21 shows.

Obviously, that:

$$jh_0 = h - \alpha_s - \alpha_s \frac{l_b}{l_a} \quad (39)$$

If the bending failure occurs in the deep beam, it means that the tension tie in the deep beam is damaged before the compression strut, and the bearing capacity is determined by the tension tie bearing capacity. Then, according to the static limit equilibrium condition, the moment of the node at the applied load can be obtained:

$$V_u a = f_y A_s j h_0 \quad (40)$$

Then the bearing capacity of deep beam is:

$$V_u = \frac{f_y A_s j h_0}{a} \quad (41)$$

where:

f_y : the test value of tensile strength of re-bar

A_s : the area of tensile reinforcement re-bar

If shear failure occurs in the deep beam, it means that the compression bar in the deep beam is damaged before the tension bar, and the bearing capacity is determined by the compression bar bearing capacity. The load bearing capacity is determined by the node (take node B as an example, see Figure 22), the vertical force equilibrium can be obtained from the deep beam load bearing capacity force is:

$$V_u = f_{ce} A_{cs} \sin \theta \quad (42)$$

And obviously that:

$$\tan \theta = \frac{j h_0}{a} \quad (43)$$

$$\sin \theta = \frac{j h_0}{\sqrt{a^2 + (j h_0)^2}} \quad (44)$$

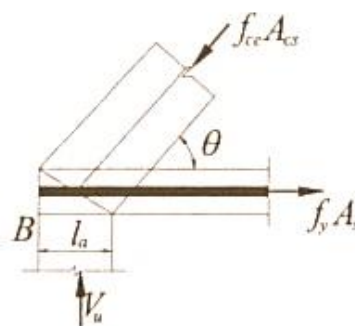


Figure 22. Detail Calculating Diagram of Node B.

f_{ce} is the effective compressive strength of struts and nodal zones, From the previous article, it is clear that:

$$f_{ce} = \min(0.85 \beta_n f'_c, 0.85 \beta_s f'_c) \quad (45)$$

A_{cs} is the smaller end cross-section area of the compression strut, calculated as follows:

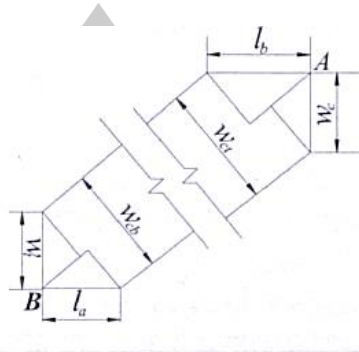


Figure 23. Detail Calculating Diagram of w_t and w_c .

where:

l_b : width of top bearing plate

l_a : width of bottom bearing plate

w_c : eight of the node at the load

w_t : height of the node at the support

w_{ct} : width of the top compression strut

w_{cb} : width of the bottom compression strut

In order to calculate w_{ct} and w_{cb} as shown in Figure 23, we should first define w_t and w_c .

According ACI 318:

$$w_t = 2(h - h_0) = 2\alpha_s \quad (46)$$

$$w_c = 0.8w_t \quad (47)$$

From the geometric condition:

The width of the top compression strut:

$$w_{ct} = l_b \sin \theta + w_c \cos \theta \quad (48)$$

The width of the bottom compression strut:

$$w_{cb} = l_a \sin \theta + w_t \cos \theta \quad (49)$$

Then the cross-section area of the compression strut:

$$A_{cs} = \min(w_{ct}b, w_{cb}b) \quad (50)$$

Finally, the deep beam bearing capacity is:

$$V_u = \min \left\{ \frac{f_y A_s h_0}{a}, f_{ce} A_{cs} \sin \theta \right\} \quad (51)$$

3.2.2 STM: EN 1992-1-1

For reinforced concrete deep beams, the Eurocode EN1992-1-1 [35] also adopts the strut and tie model method and the model used in the European code EN1992-1-1 and the American code ACI318-11 [3] is basically the same, only in some details, such as the struts and nodal zones compressive strength values are different.

The effective compressive strength of struts and nodal zones according to Eurocode EN1992-1-1 as the follows:

For struts:

1.If the concrete struts without transverse tension, the effective compressive strength:

$$f_{ce} = f'_c \quad (52)$$

2.If the concrete struts with transverse tension, the effective compressive strength:

$$f_{ce} = 0.6\nu' f'_c \quad (53)$$

For nodal zones:

1.If in compression nodes where no ties are anchored at the node, the effective compressive strength:

$$f_{ce} = k_1 \nu' f'_c \quad (54)$$

2.If in compression - tension nodes with anchored ties provided in one direction, the effective compressive strength:

$$f_{ce} = k_2 \nu' f'_c \quad (55)$$

3.If in compression - tension nodes with anchored ties provided in more than one direction, the effective compressive strength:

$$f_{ce} = k_3 \nu' f'_c \quad (56)$$

Under the conditions listed below, the effective compressive stress values given in above may be increased by up to 10% where at least one of the following applies:

(1) Triaxial compression is assured.

(2) All angles between struts and ties are $\geq 55^\circ$.

(3) The stresses applied at supports or at point loads are uniform, and the node is confined by stirrups

(4) The reinforcement is arranged in multiple layers.

(5) The node is reliably confined by means of bearing arrangement or friction.

4.If for all three directions of the struts the distribution of load is known, the triaxially compressed nodes may be checked according:

$$f_{ce} = k_4 v' f'_c \quad (57)$$

where:

f'_c : the compressive strength of concrete at an age of 28 days

v' : the compressive strength reduction factor of concrete and is given by equation:

$$v' = 1 - \frac{f'_c}{250} \quad (58)$$

k_n : the factor. $k_1 = 1, k_2 = 0.85, k_3 = 0.75, k_4 = 3$.

Therefore, the effective compressive strength of struts in Eurocode EN1992-1:

$$f_{ce} = \min(K f'_c, k_n v' f'_c) \quad (59)$$

Due to the different forms of internal forces, K is taken as 1 or $0.6v'$

Due to the different constraints, k_n is taken as 1, 0.85, 0.75 or 3

Then from the static limit equilibrium condition, the bearing capacity of the deep beam based on the struts and nodal zones compressive strength can calculated using Eq. (42) and the deep beam bearing capacity can calculated using Eq. (51).

3.2.3 STM: NF P 18-710 (AFGC)

The French code NF P 18-710 (AFGC) [33] further describes the RPC deep beams using the compression tie model based on the Eurocode EN1992-1-1. The effective compressive strength of struts and nodal zones according to NF P 18-710 that the present standard fully replaces the part of Eurocode EN 1992-1-1. And in Eurocode EN 1992-1-1 a non-linear strain distribution exists (e.g., supports, near concentrated loads or planar stress) strut-and-tie models may be used. The strut and tie method can be used if it is demonstrated that the forces path in the strut and tie model relates to forces path in an elastic analysis. Details as the follows:

For struts:

1.If the struts are subject to a positive or null transverse stress, the effective compressive strength in a compressed strut is:

$$f_{ce} = Kf'_c \quad (60)$$

2.If the struts are subject to a negative transverse stress (tensile) for consistency with the term f_{ce} using in verifying shear, the effective compressive strength in a compressed strut is:

$$f_{ce} = K\sqrt{2.3}(f'_c)^{\frac{2}{3}} \quad (61)$$

For nodal zones:

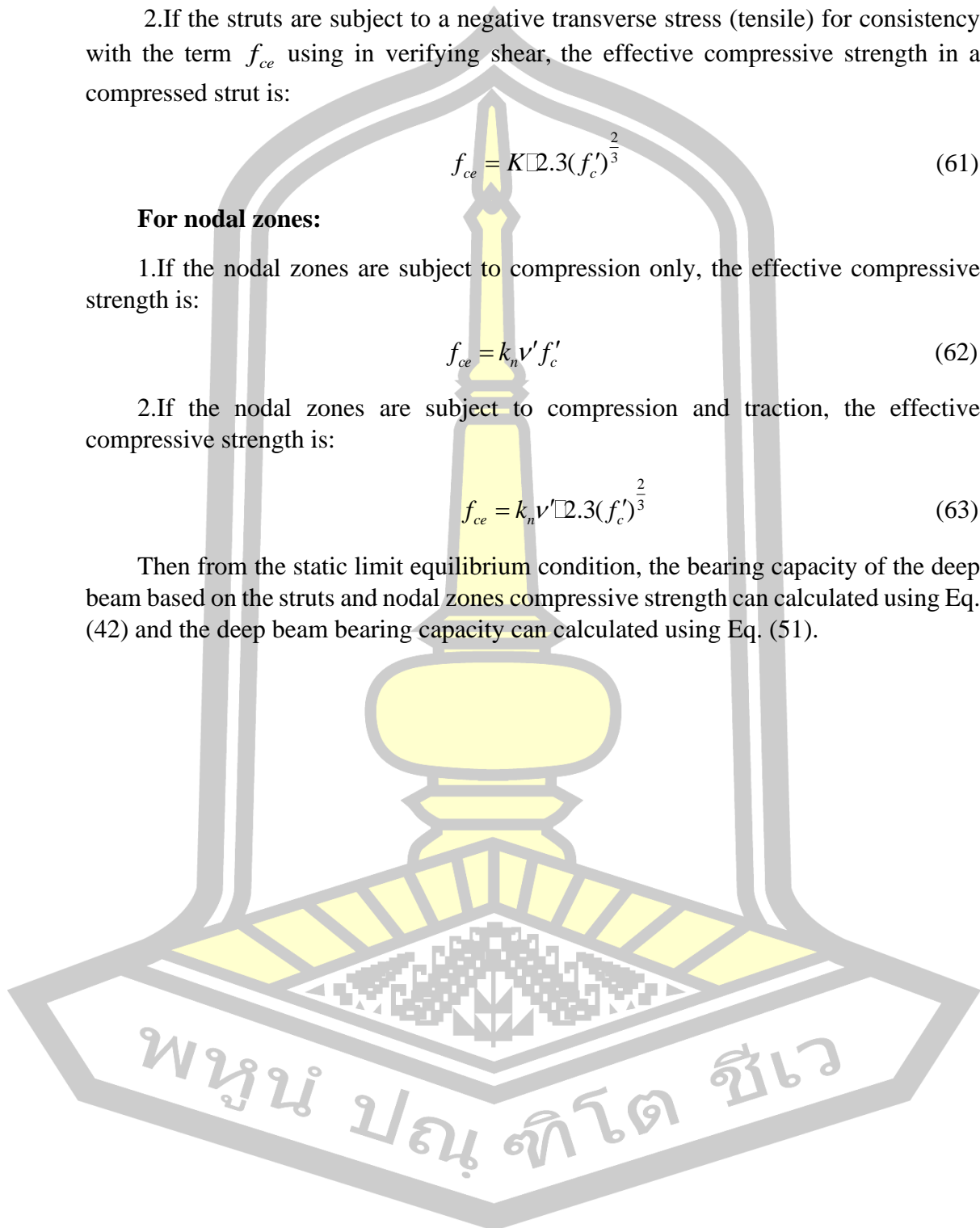
1.If the nodal zones are subject to compression only, the effective compressive strength is:

$$f_{ce} = k_n v' f'_c \quad (62)$$

2.If the nodal zones are subject to compression and traction, the effective compressive strength is:

$$f_{ce} = k_n v' \sqrt{2.3}(f'_c)^{\frac{2}{3}} \quad (63)$$

Then from the static limit equilibrium condition, the bearing capacity of the deep beam based on the struts and nodal zones compressive strength can calculated using Eq. (42) and the deep beam bearing capacity can calculated using Eq. (51).



Chapter 4

Study Results

In order to implement the stress-stress models, the *fib* 2010 [32], the NF P 18-710 (AFGC) [33], and the CECS [34] codes, described in Chapter 3, the nonlinear finite element program SOFiSTiK [27] was adopted. The test results of RPC deep beams carried out by Yaseen [36] and Yousef et al. [37] and Li et al. [38] were selected for investigating of capability of each stress-strain model in capturing the structural behavior of the RPC deep beams. In those tests, different main parameters affecting deep beam behavior were investigated and varied including concrete compressive strength (f'_c), shear span-to-effective depth ratio (a/d), main reinforcement ratio (ρ) as listed in Table 12. Moreover, the Strut-and-Tie models according to ACI 318-11 [3], EN 1992-1-1 [35], and NF P 18-710 (AFGC) [33] detailed in Chapter 3 were also examined to predict the shear strength of the RPC deep beams.

Table 12. Test References and Values of Main Parameters Investigated in This Study.

Ref.	Parameter and Ref. Beam					
	f'_c (MPa)	Beam	a/d	Beam	$\rho\%$	Beam
Yaseen [36]	43	G11	1.0	G21	1.35	G41
	79	G13	1.5	G22	2.40	G42
	100	G14	2.0	G14	3.76	G43
	-	-	2.5	G23	6.11	G15
	-	-	3.0	G24	-	-
Yousef et al. [37]	-	-	0.79	DBSU2	-	-
	-	-	0.94	DBSU4	-	-
Li et al. [38]	-	-	1.51	L1-1	4.43	L2-1
	-	-	2.26	L1-2	6.58	L1-2
	-	-	3.02	L1-3	8.04	L2-2

4.1 FEA Results

4.1.1 RPC Deep Beams Tested by Yaseen [36]

4.1.1.1 Stress-Strain Curves of Rebar

All RPC deep beams tested by Yaseen [36] that were investigated in this study used the same type of rebar with the properties listed in Table 13. The stress-strain points were calculated using the concept described in Section 3.1.4. Figure 24 shows the obtained curve. The model incorporated the Poisson's ratio values of 0.3 for steel rebar.

Table 13. Parameters for Stress-Strain Models of Steel Rebar.

Parameter	Value
f_y (MPa)	416
E_s (GPa)	200

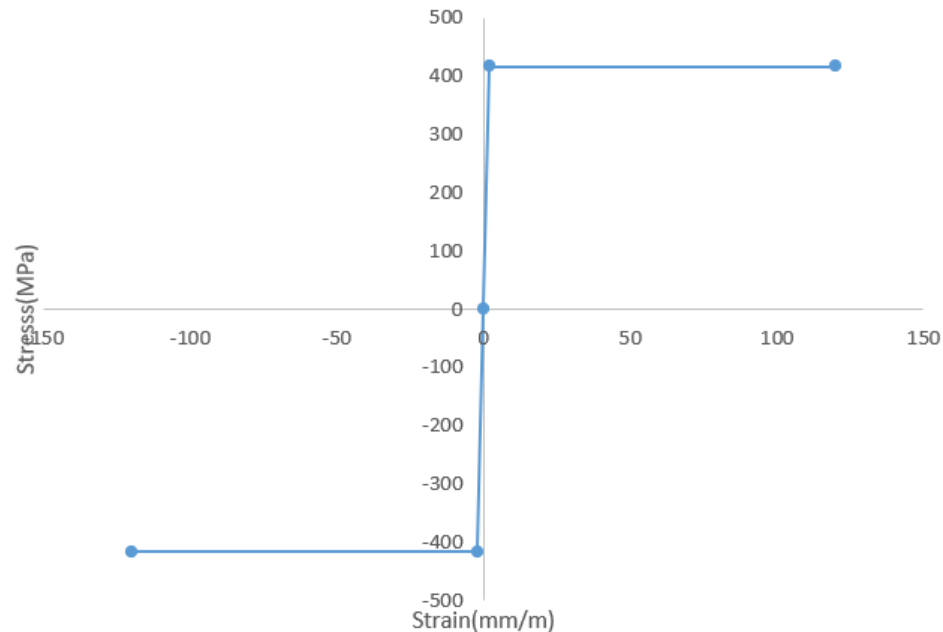


Figure 24. Stress-Strain Curves for Rebar Used in FEA.

4.1.1.2 Stress-Strain Curves of Concrete

The concrete properties provide by Yaseen [36] are only compressive strength. To be able to obtain the stress-strain curve some properties were determined using the equations provided by the code which are generally based on the compressive strength.

fib 2010 code

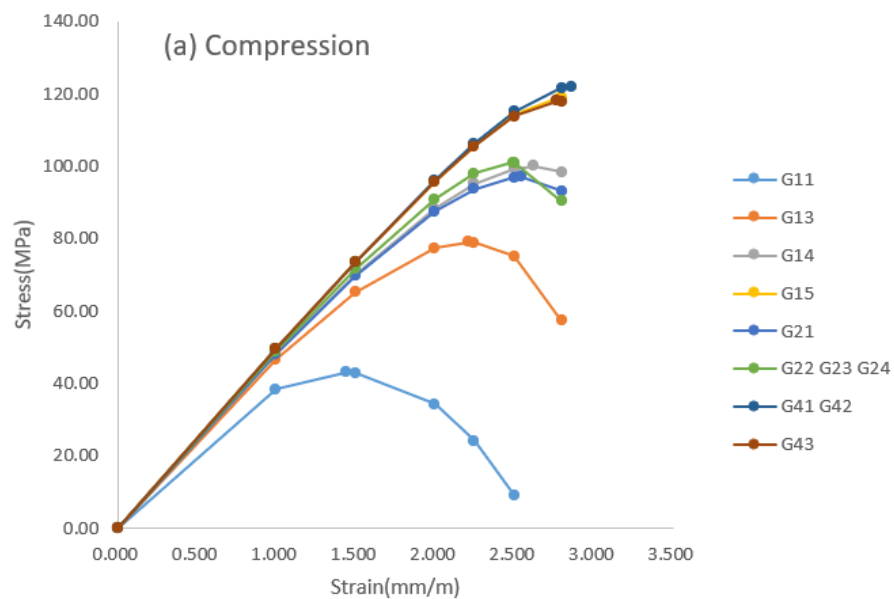
The stress-strain points for concrete in compression and tension zones were calculated using the parameters listed in Table 14 and the concept described in Section 3.1.1. It should be noted that all concrete parameters are dependent on the concrete grade, therefore, the concrete grades are also given in Table 14. It is worth noting that the input required by the *fib* 2010 code is only the test value of compressive strength.

Table 14. Parameters for Stress-Strain Models of Concrete (*fib* Model Code 2010).

Parameters	Beam							
	G11	G13	G14	G15	G21	G22& G23&G24	G41& G42	G43
<i>Compression</i>								
f'_c (MPa)	43	79	100	119	97	101	122	118
Concrete Grade	C40	C80	C100	C120	C100	C100	C120	C120
E_c (GPa)	35.0	42.8	46.3	49.1	45.9	46.5	49.5	48.9

Parameters	Beam							
	G11	G13	G14	G15	G21	G22& G23&G24	G41& G42	G43
k	1.82	1.41	1.32	1.18	1.32	1.32	1.18	1.18
$\varepsilon_{c,lim}$ (mm/m)	3.5	3.1	3.0	3.0	3.0	3.0	3.0	3.0
ε_{cl} (mm/m)	1.440	2.215	2.625	2.792	2.546	2.490	2.863	2.769
Tension								
f_t (MPa)	3.63	4.63	5.08	5.44	5.03	5.10	5.47	5.41
ε_{tl} (mm/m)	0.345	0.323	0.314	0.309	0.315	0.314	0.308	0.309

The obtained stress-strain curves in compression and tension for concrete are illustrated in Figure 25. The stress-strain points were directly inputted into the program. The model incorporated the Poisson's ratio values of 0.2 for concrete as suggested by the code.



พหุบัณฑิต ชีวะ

The obtained stress-strain curves in compression and tension for concrete are illustrated in Figure 26. The stress-strain points were directly inputted into the program.

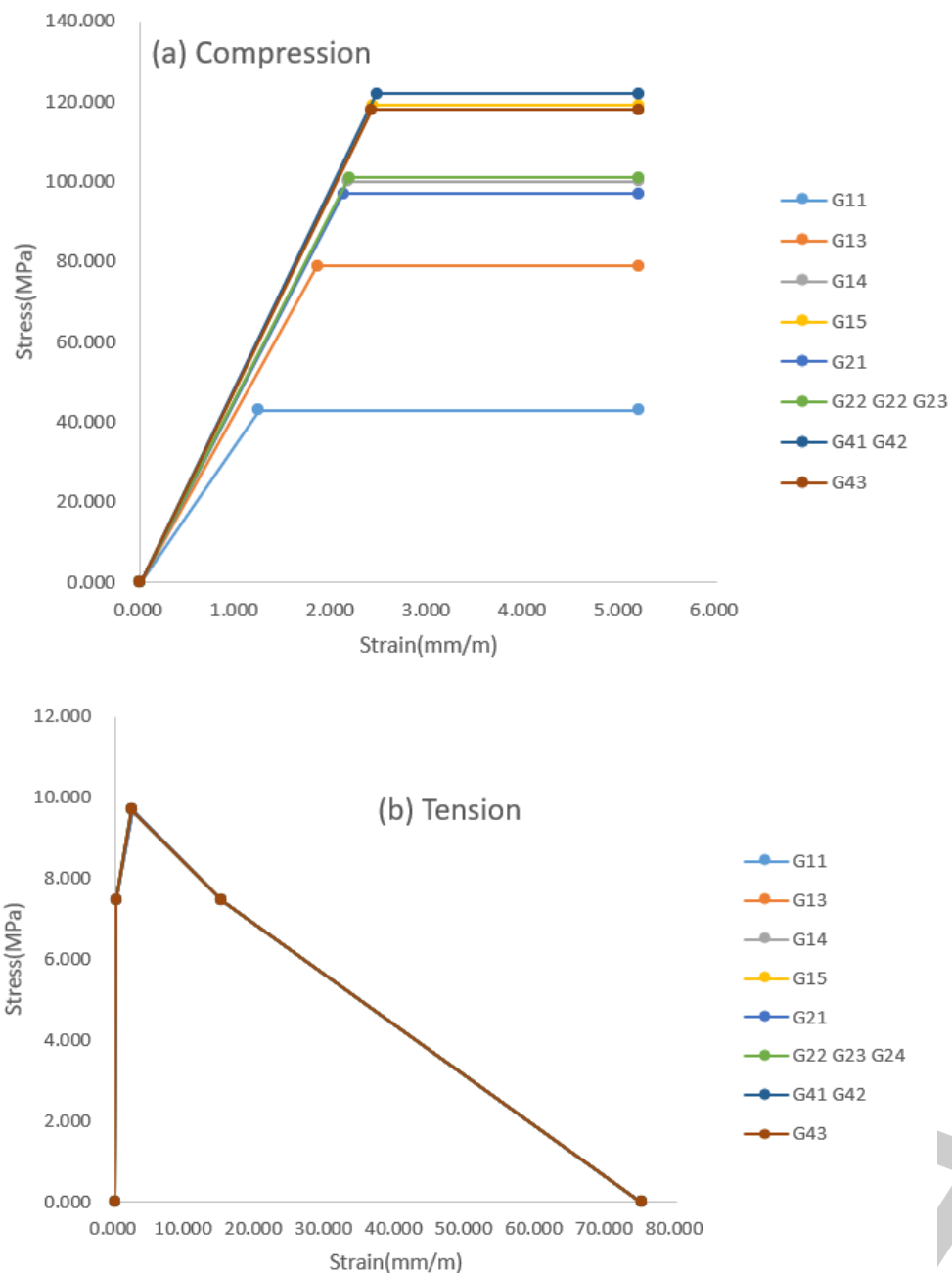


Figure 26. Stress-Strain Curves for Concrete Used in FEA (AFGC Code).

CECS Code

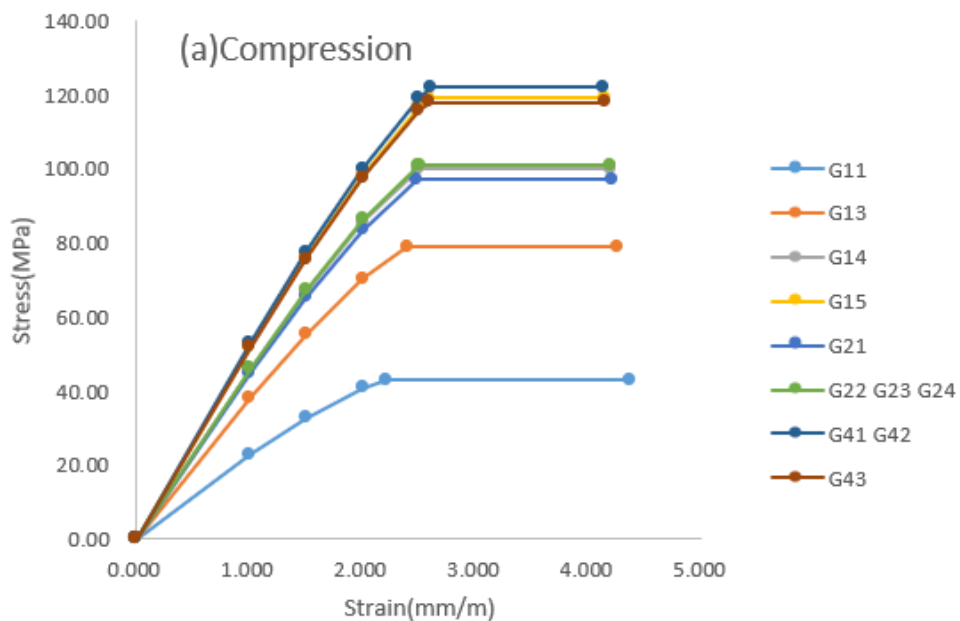
The stress-strain points for concrete in compression and tension zones were calculated using the parameters listed in Table 16 and the concept described in Section 3.1.3. In CECS code, the key parameters needed are the concrete compressive strength, the steel fiber volume ratio, the steel fiber length, and the equivalent diameter of steel

fiber. The Poisson's ratio ν take 0.2 as suggested by the code. It should be noted that the rest parameters can be determined from the compressive strength using the equations or the values in the table provided by the code, anyway, the obtained values are very close to each other. The values in [Table 16](#) are obtained from the table provided by the code.

Table 16. Parameters for Stress-Strain Models of Concrete (CECS Code).

Parameters	Beam							
	G11	G13	G14	G15	G21	G22& G23&G24	G41& G42	G43
<i>Compression</i>								
f'_c (MPa)	43	79	100	119	97	101	122	118
Concrete Grade	C40	C80	C100	C120	C100	C100	C120	C120
ε_0 (mm/m)	2.22	2.40	2.50	2.60	2.50	2.51	2.61	2.60
ε_{cu} (mm/m)	4.37	4.26	4.20	4.14	4.20	4.20	4.13	4.15
<i>Tension</i>								
λ	3.6	3.6	3.6	3.6	3.6	3.6	3.6	3.6
f_t (MPa)	3.02	5.66	7.19	8.58	6.97	7.26	8.80	8.51
E_c (GPa)	2.61	3.62	4.00	4.27	3.95	4.02	4.31	4.23
ε_{t0} (mm/m)	0.116	0.156	0.180	0.201	0.176	0.181	0.204	0.200
ε_{tp} (mm/m)	0.477	0.477	0.477	0.477	0.477	0.477	0.477	0.477
ε_{tu} (mm/m)	2.771	2.771	2.771	2.771	2.771	2.771	2.771	2.771

The obtained stress-strain curves in compression and tension for concrete are illustrated in [Figure 27](#). The stress-strain points were directly inputted into the program.



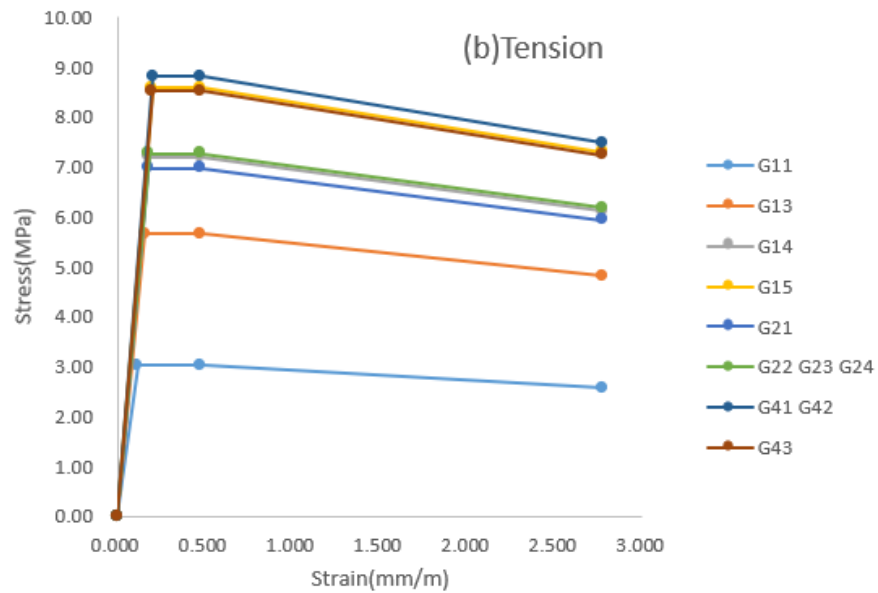
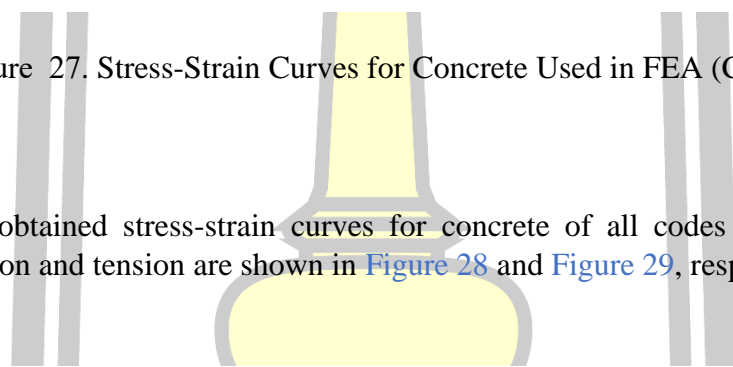
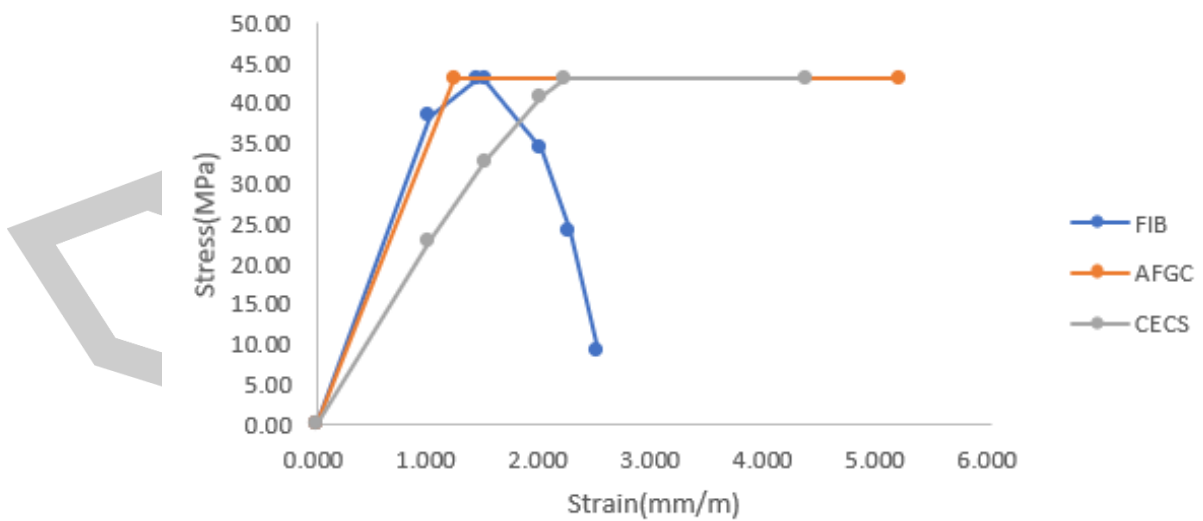


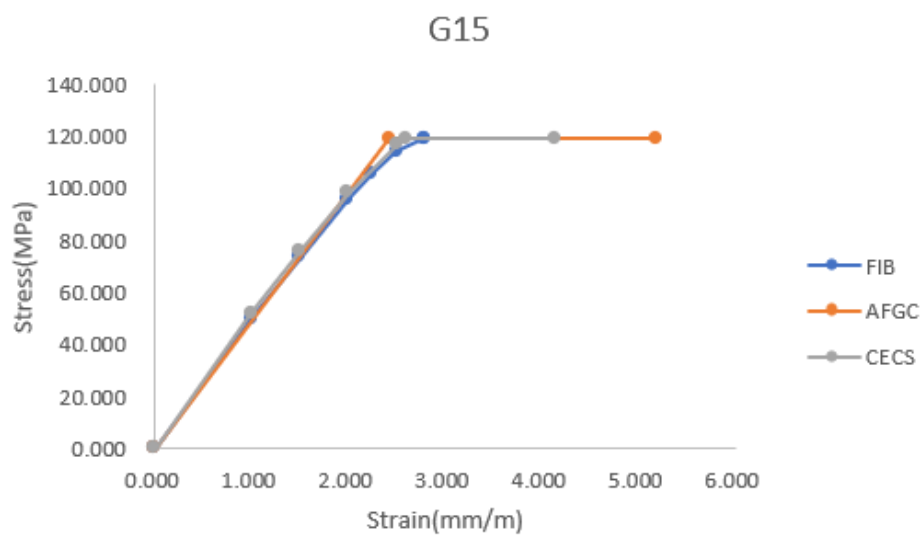
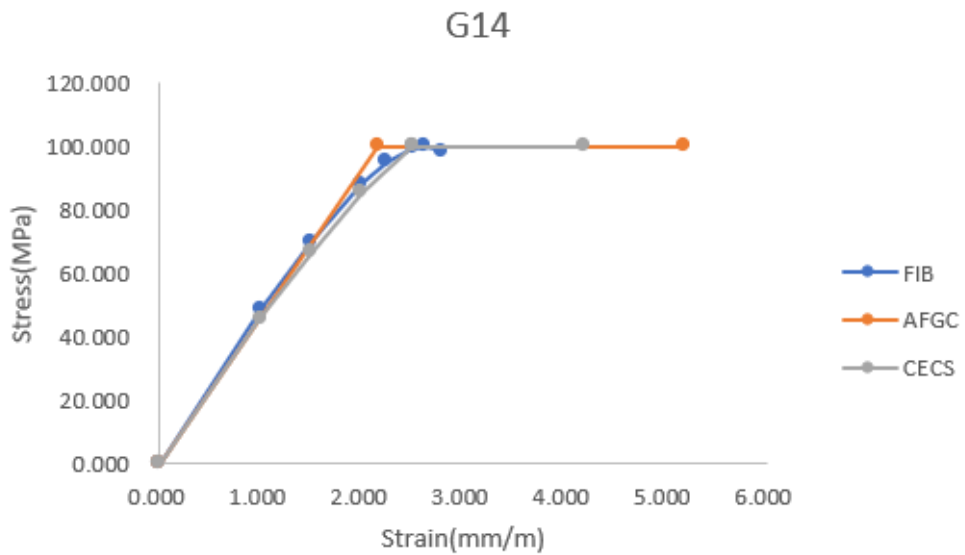
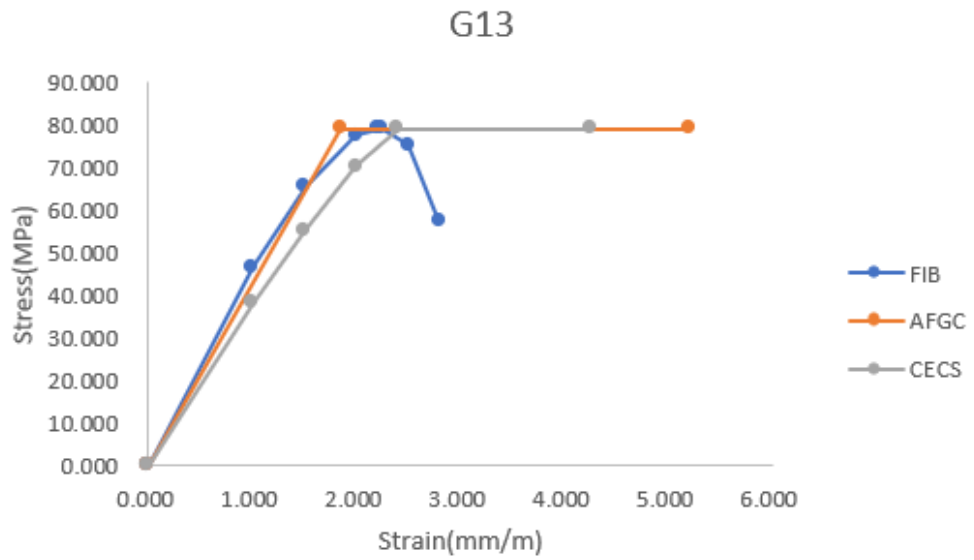
Figure 27. Stress-Strain Curves for Concrete Used in FEA (CECS Code).

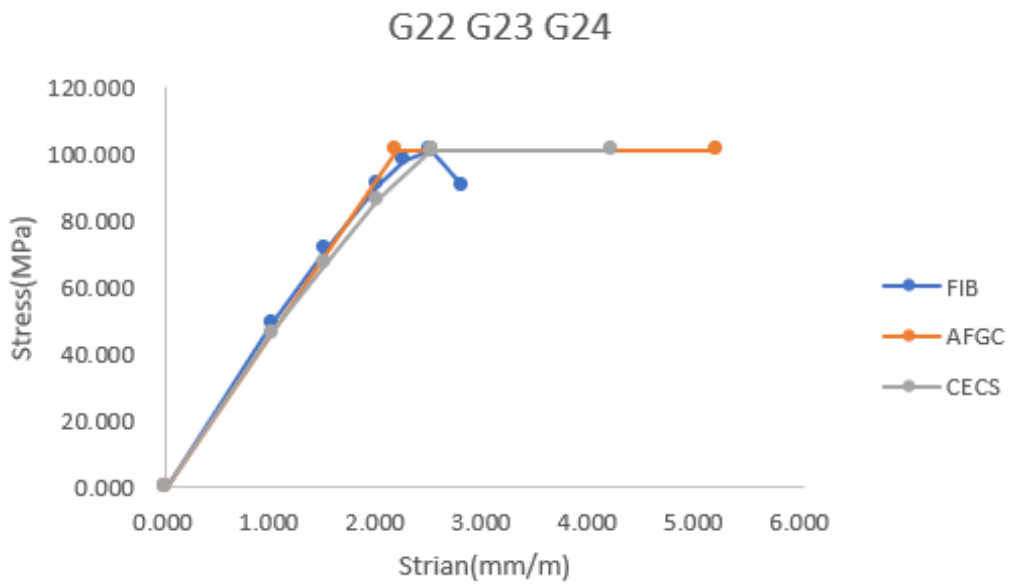
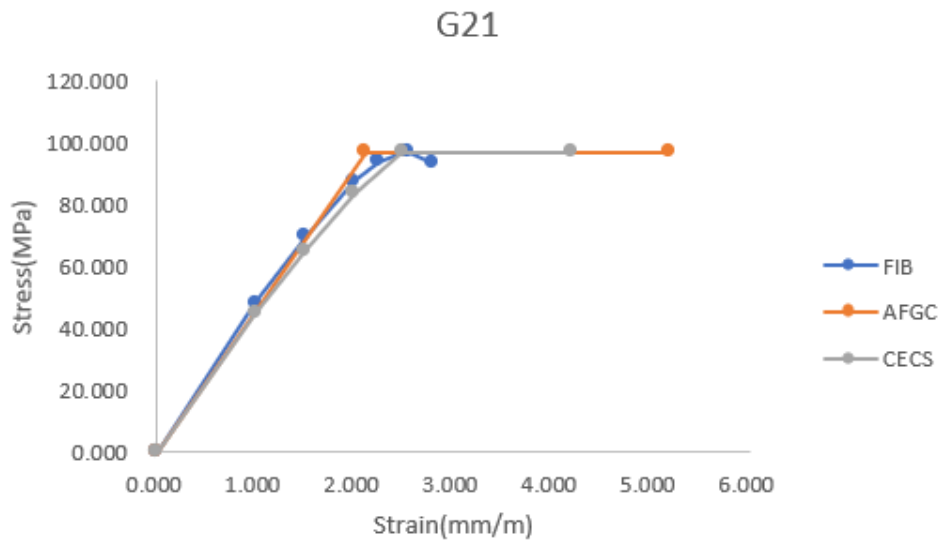
The obtained stress-strain curves for concrete of all codes for each beam in compression and tension are shown in Figure 28 and Figure 29, respectively.



G11







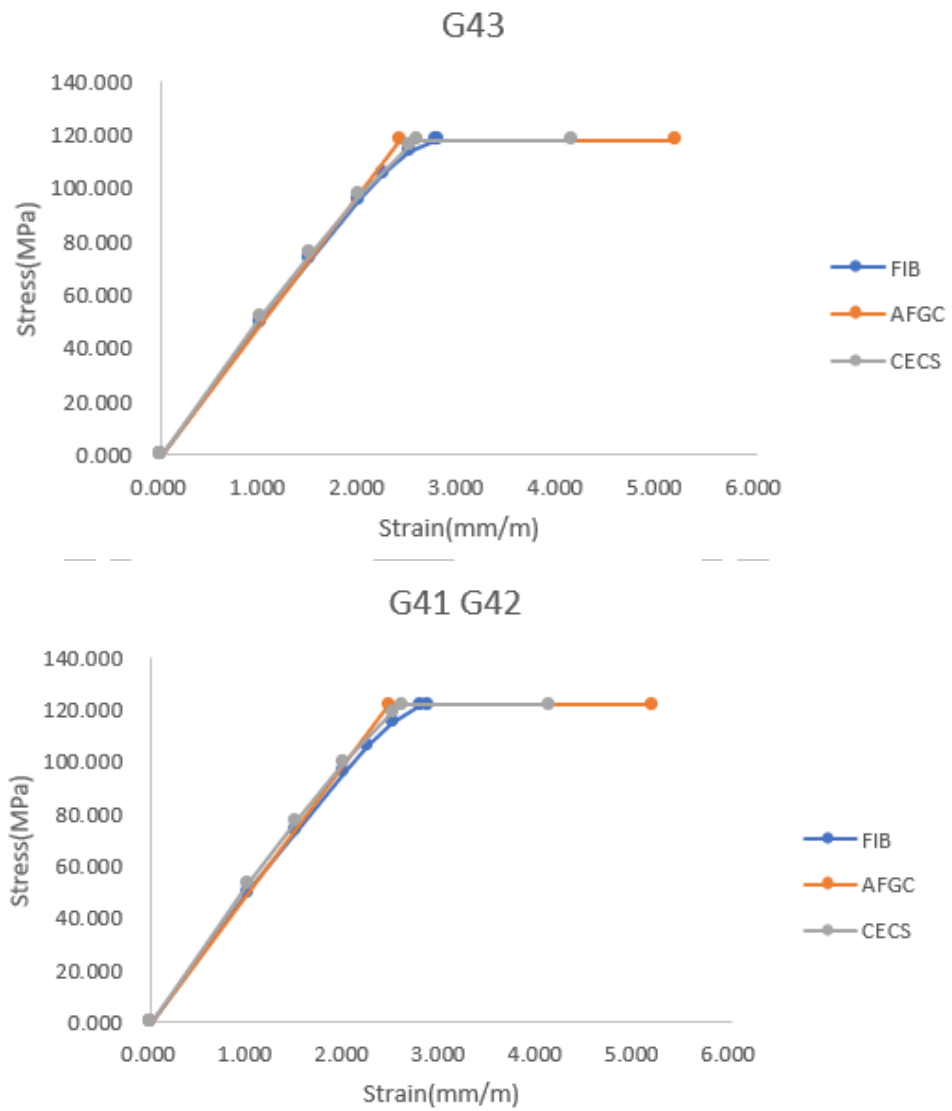
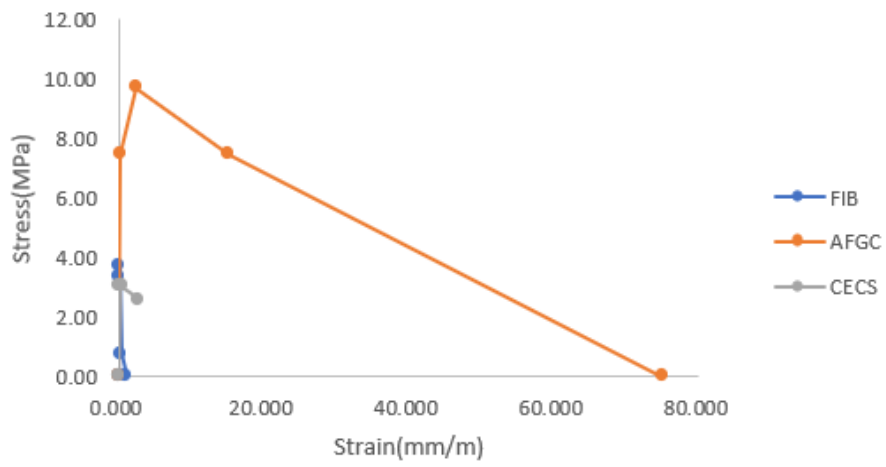


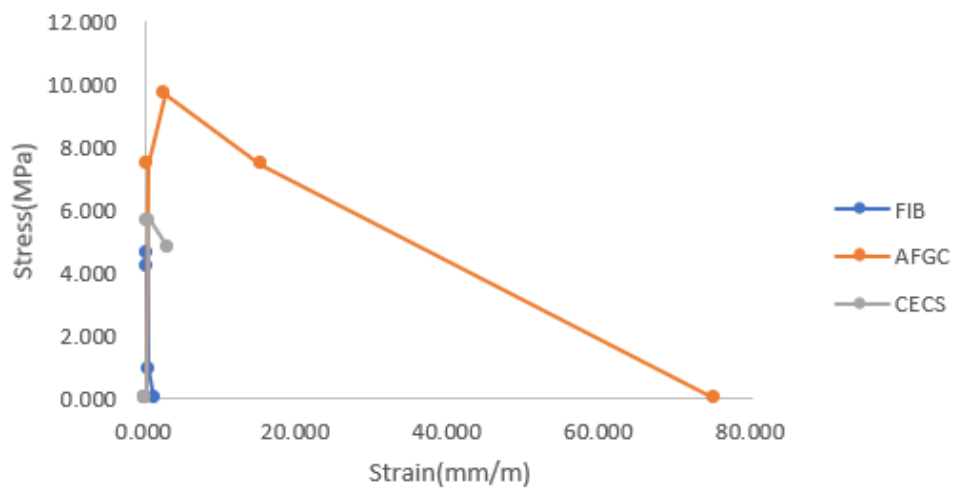
Figure 28. Stress-Strain Curves for Concrete in Compression (All Codes).



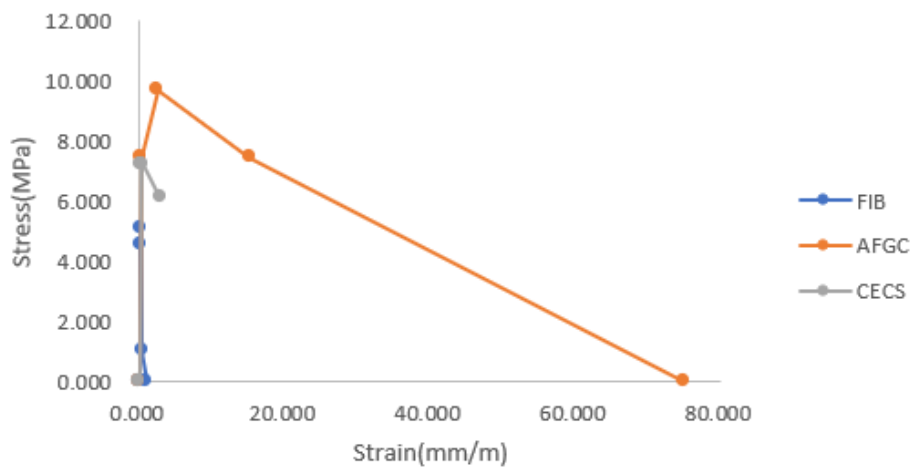
G11



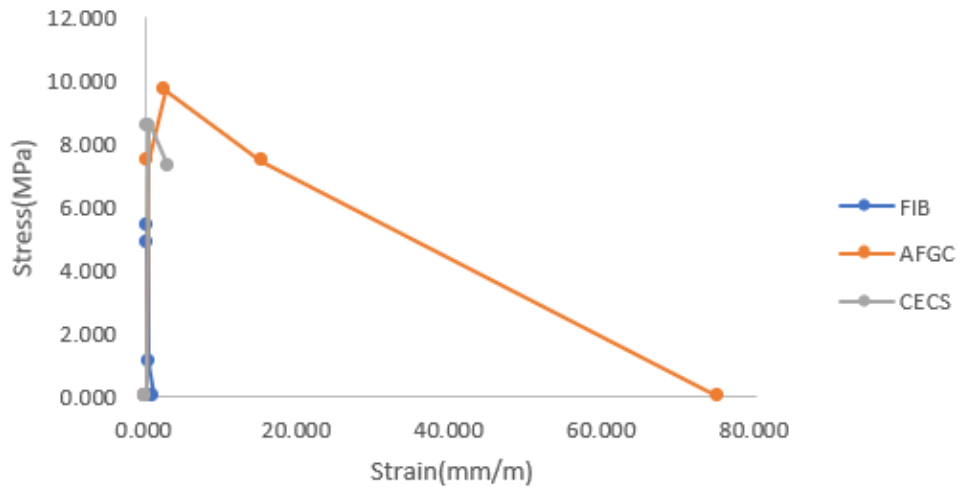
G13



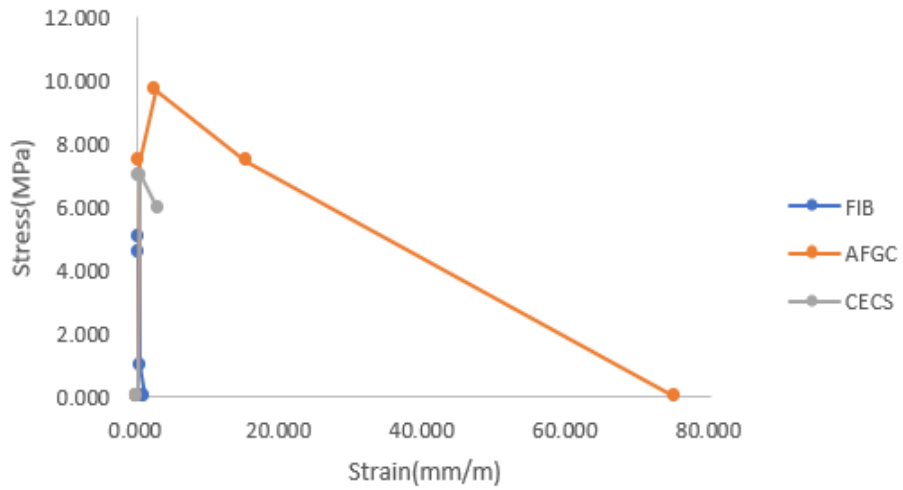
G14



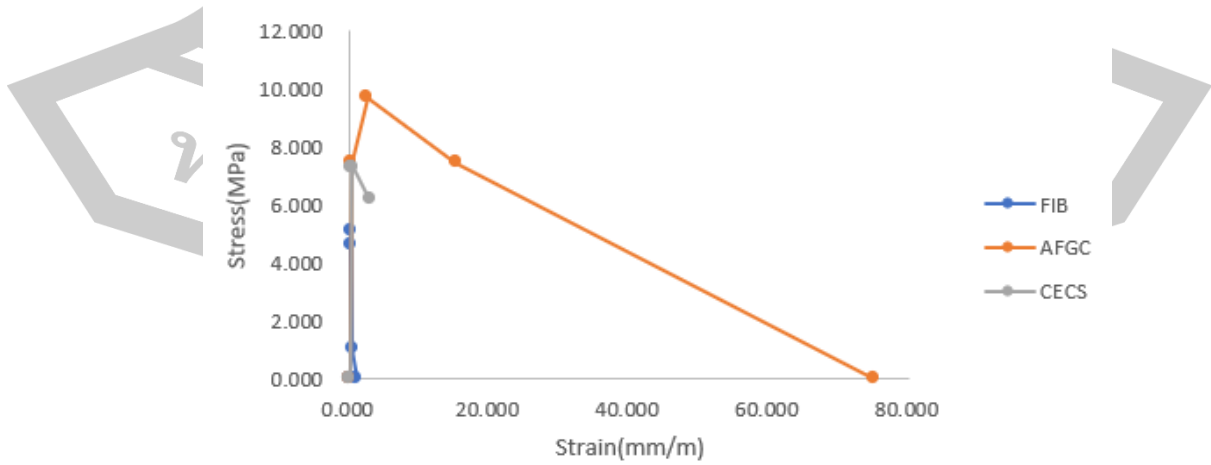
G15



G21



G22 G23 G24



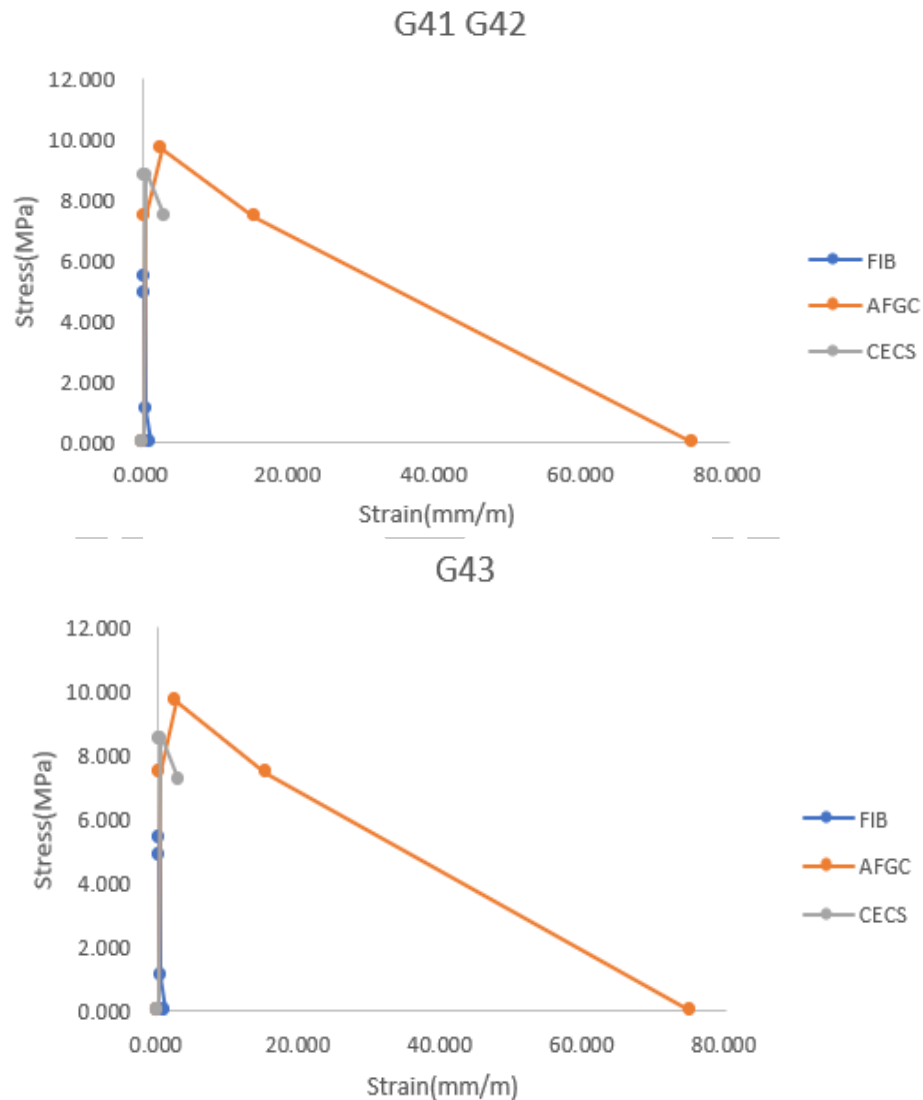


Figure 29. Stress-Strain Curves for Concrete in Tension (All Codes).

4.1.1.3 Structural Model

The deep beams studied by Yaseen [36] were tested under two symmetrically placed concentrated loads. The total length of the beams was 1200 mm. The overall cross section was 100 mm x 200 mm. All the tested specimens were simply supported. The details of the tested beams are provided in [Figure 30](#) and [Table 17](#). The tested deep beams had a span length of 1000 mm with a point load applied at the midpoint of the span.

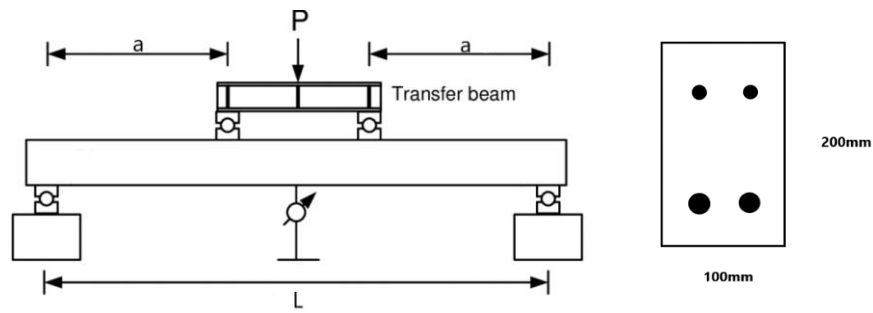


Figure 30. Details and Typical Cross Section of The Tested Beams (Yaseen [36]).

Table 17. Details of The Tested Beams (Yaseen [36]).

Beam	L (mm)	a (mm)	d (mm)	a/d	$\rho\%$
G11(NSC)	1000	334	167	2.00	6.108
G13(HSC)	1000	334	167	2.00	6.108
G14(RPC)	1000	334	167	2.00	6.108
G15(RPC)	1000	334	167	2.00	6.108
G21(RPC)	1000	167	167	1.00	6.108
G22(RPC)	1000	250	167	1.50	6.108
G23(RPC)	1000	418	167	2.50	6.108
G24(RPC)	1000	500	167	3.00	6.108
G41(RPC)	1000	334	167	2.00	1.35
G42(RPC)	1000	334	167	2.00	2.4
G43(RPC)	1000	334	167	2.00	3.76

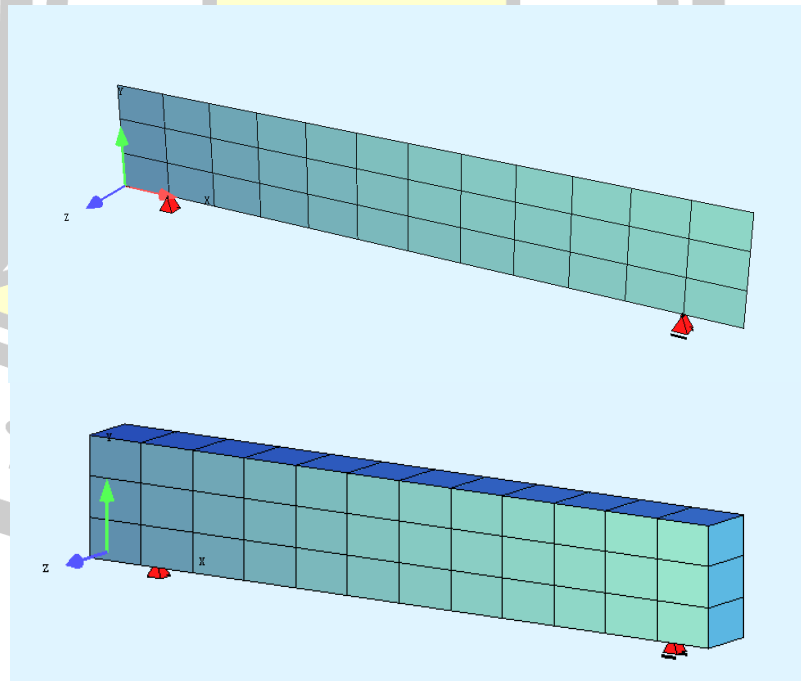


Figure 31. Typical FE Model of The Beams.

Figure 31 depicts the typical FE model employed in this study. The models used four-node shell or QUAD elements displaying plate structural behavior according to the Reissner-Mindlin theory. The QUAD elements integrated a layer material model to aid in cracked concrete analysis and contained. Discrete Kirchhoff conditions as well as an optional penalty term to consider shear deformation. The nonlinear analysis was executed through an incremental solution technique founded on the modified Newton Raphson method.

4.1.1.4 Numerical Results

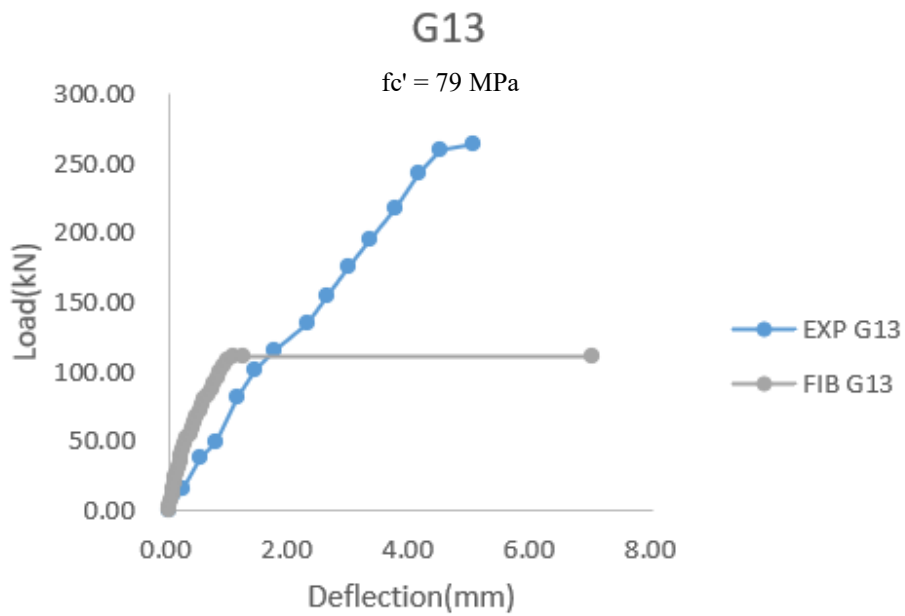
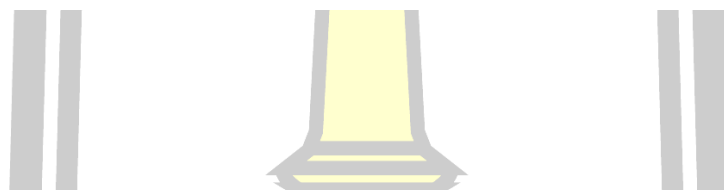
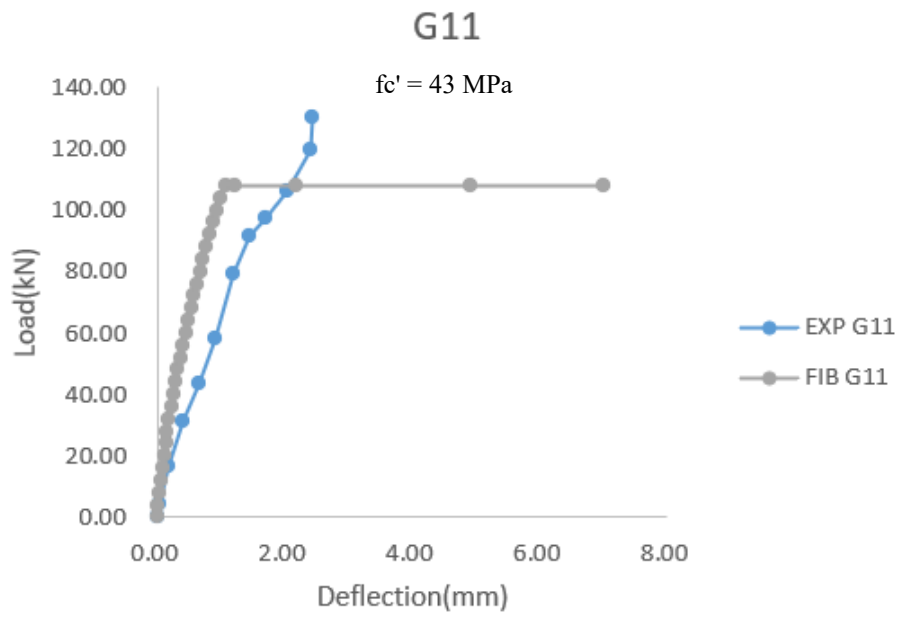
Load-Deflection Response

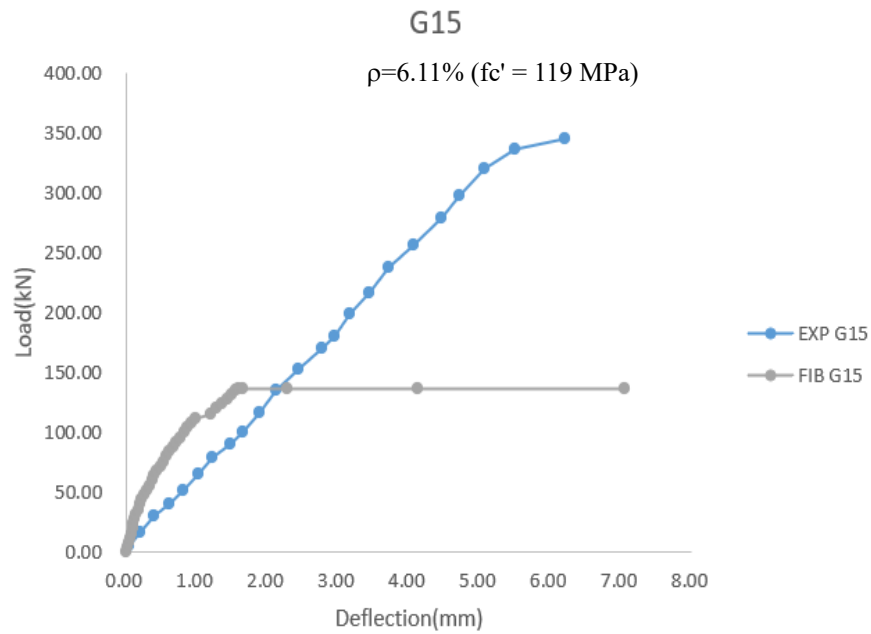
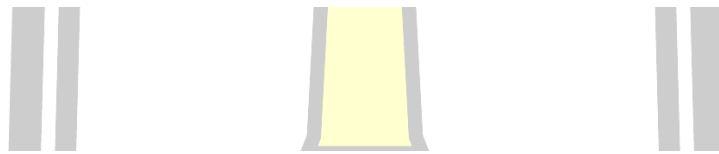
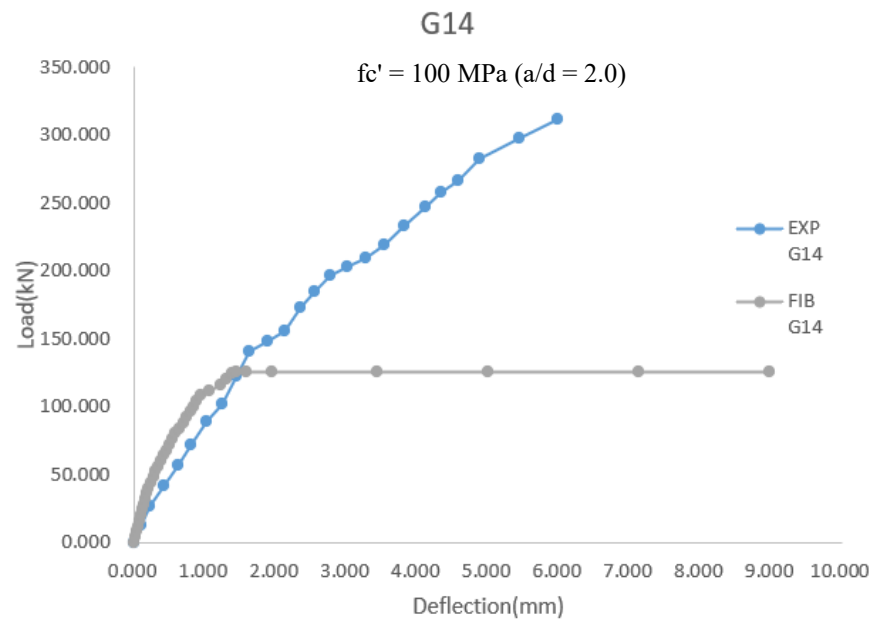
Figure 32 presents the comparison between the numerical curves and the experimental results based on the *fib* model code 2010. Figure 33 presents the comparison between the numerical curves and the experimental results based on AFGC code. Figure 34 presents the comparison between the numerical curves and the experimental results based on CECS code. Figure 35 presents the comparison between the numerical curves and the experimental results based on all codes. Table 18 shows the peak loads from FEA compared to the values from the test results.

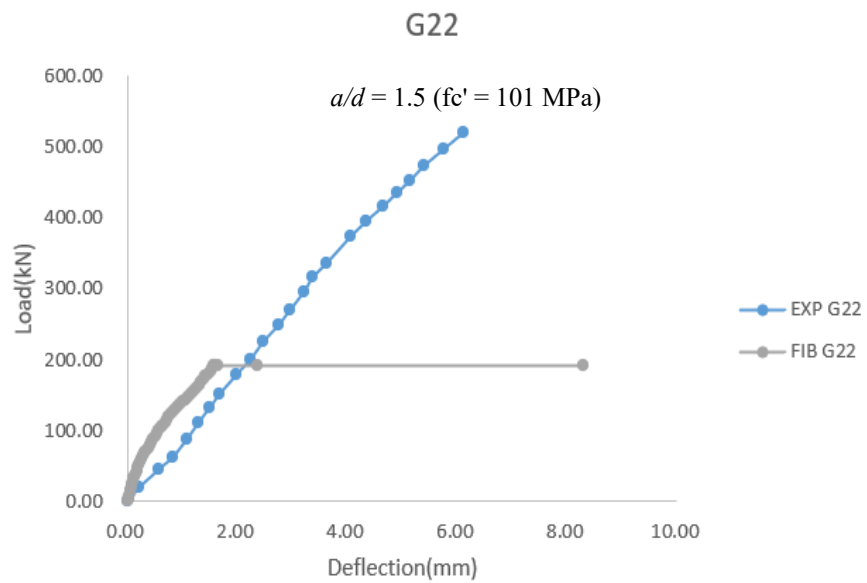
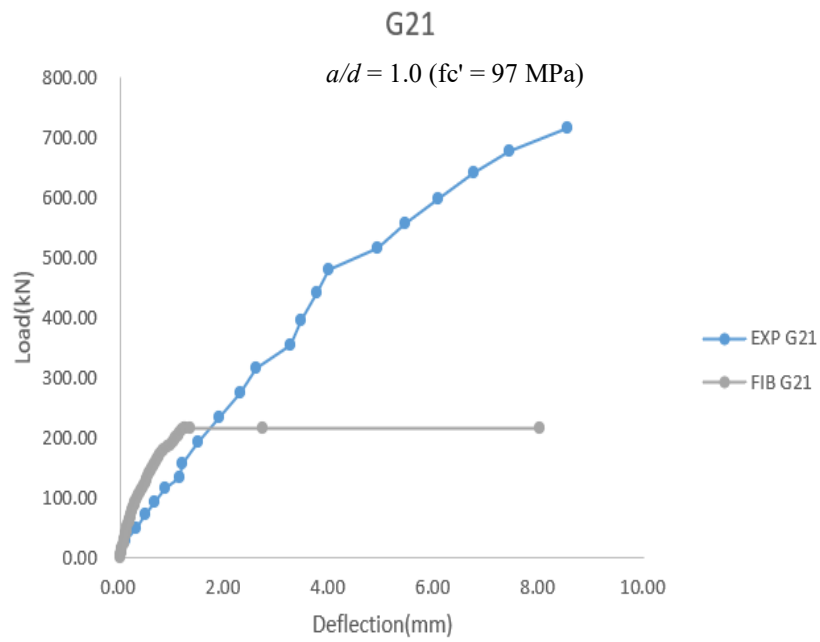
From Table 18, when only HSC and RPC deep beams are considered (except G24), it can be observed that the predicted peak loads from the FEA with AFGC code and CECS codes are closer to the test values compared to the predicted values with the *fib* code. While for NSC deep beam, the *fib* code can predict the peak load well. This implies that the *fib* code is suitable for NSC but not for RPC and even for HSC. For G24, Yaseen [36] also observed a bad prediction with this beam therefore the test result itself might not be good and used for reference. When the predictions of G24 and G11 and G13 are excluded, the mean value of the FEA value to experimental value ratio for the AFGC and CECS codes becomes 1.20 and 1.17 with the corresponding coefficient of variation of 0.11 and 0.10, respectively. The predicted range of FEA value to experimental value ratio for the AFGC code model is 1.06 to 1.43 and for CECS code model is 1.02 to 1.37.

Nevertheless, from Figures 32 to 35, it can be observed that the current FE model employed in the analysis fails to capture other important characteristics such as elastic stiffness, inelastic stiffness, and post-peak behavior for all types of deep beams. This limitation stems from the inherent characteristics of the FE model itself.

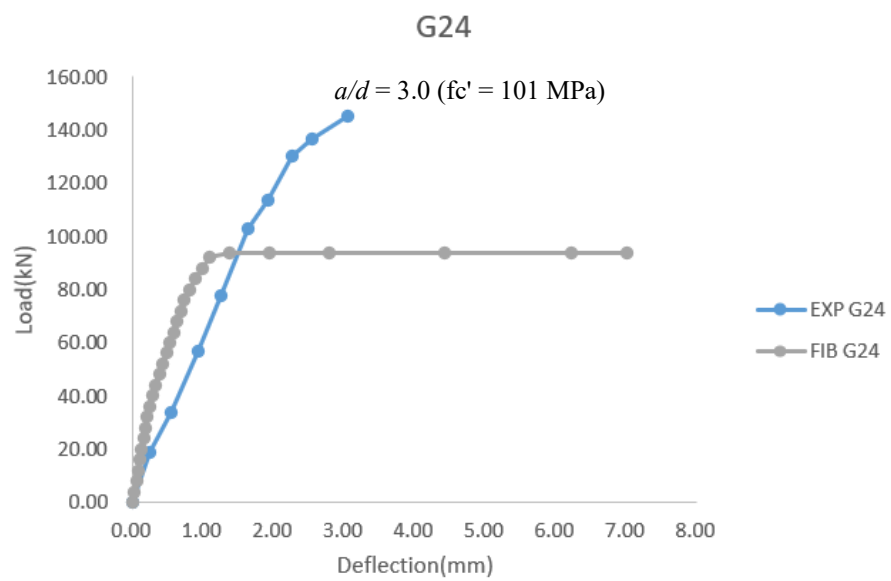
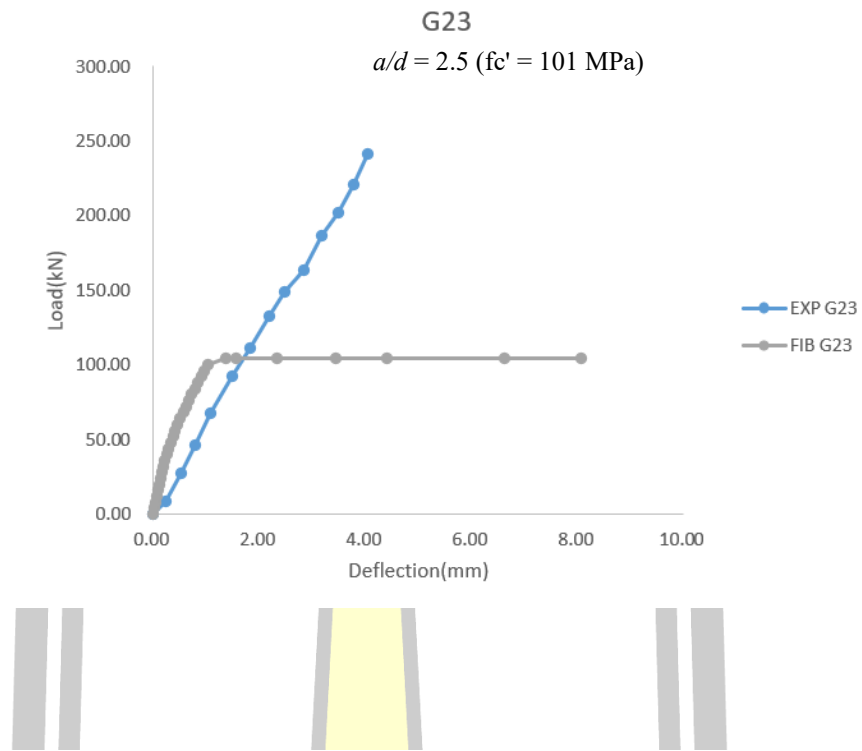


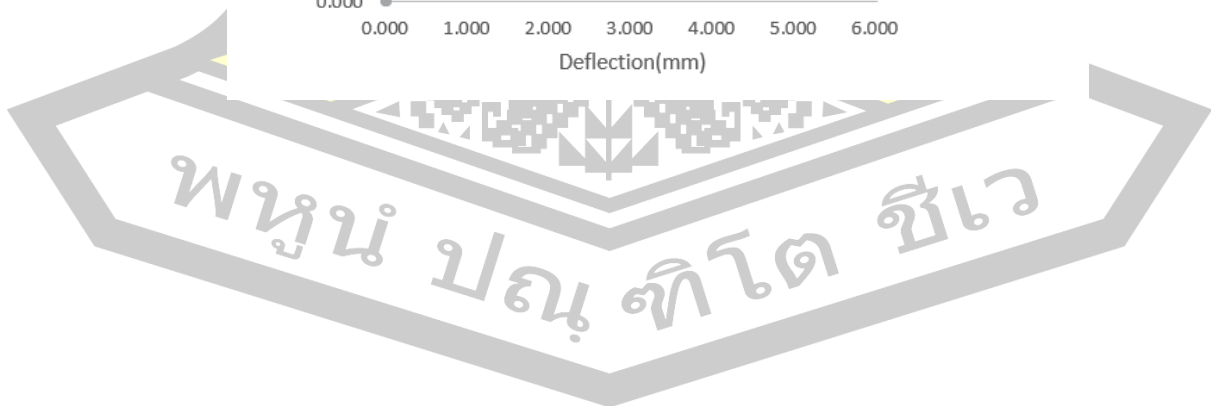
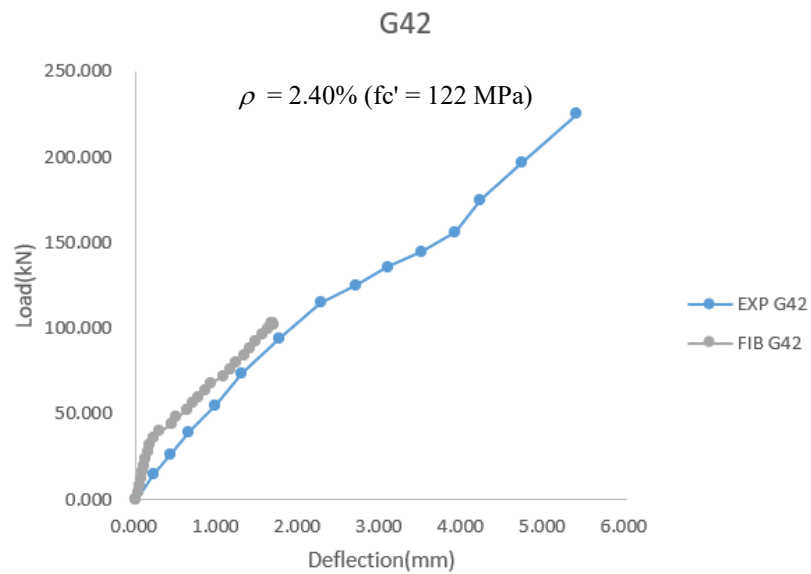
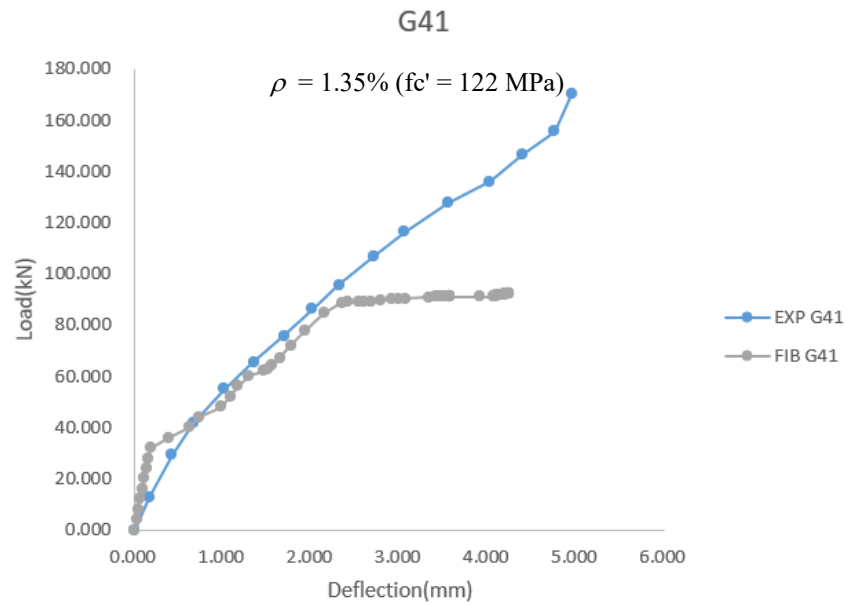






พหุบัณฑิต ชีวะ





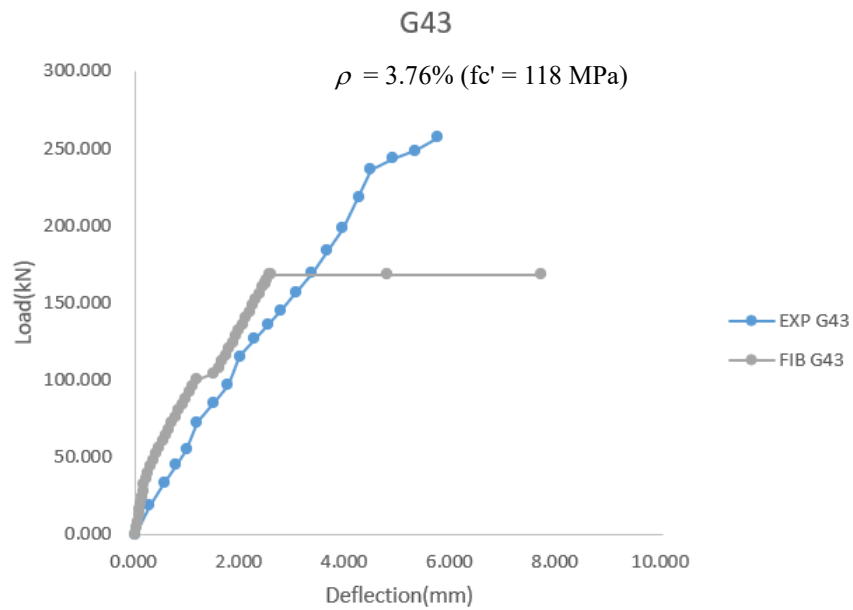
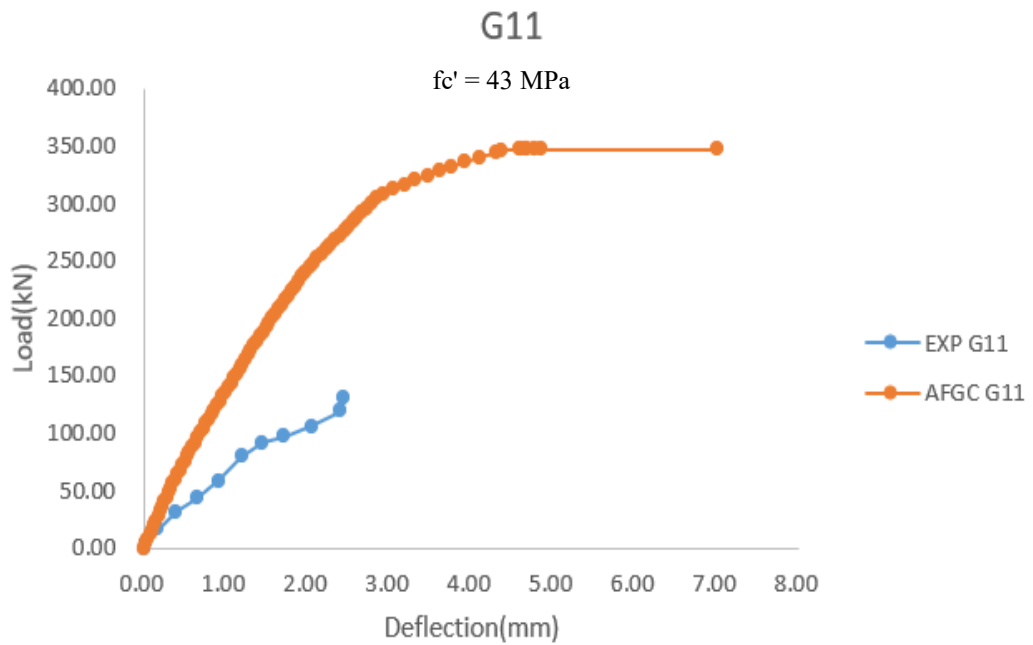
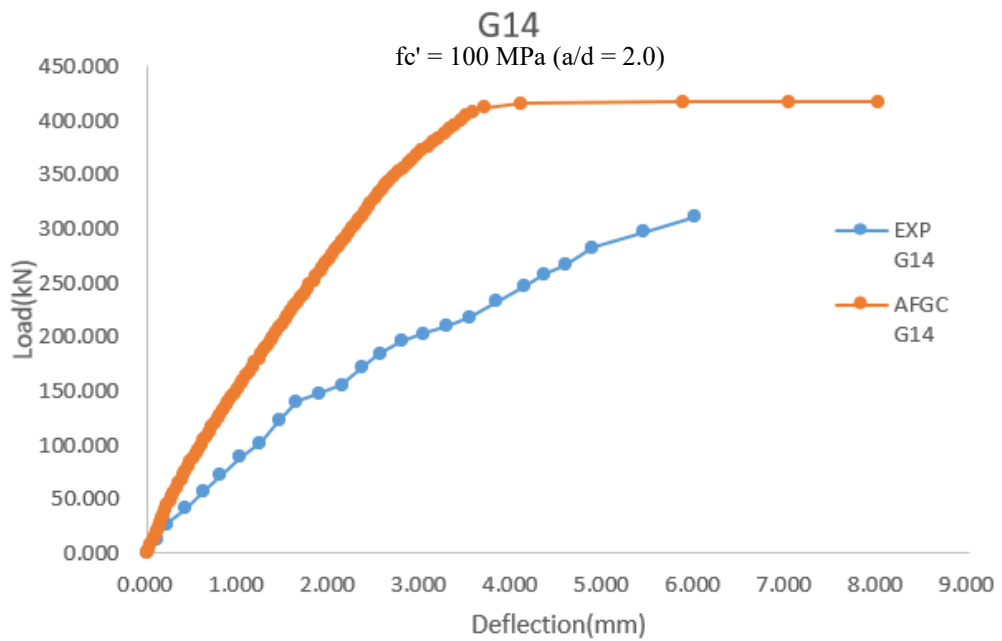
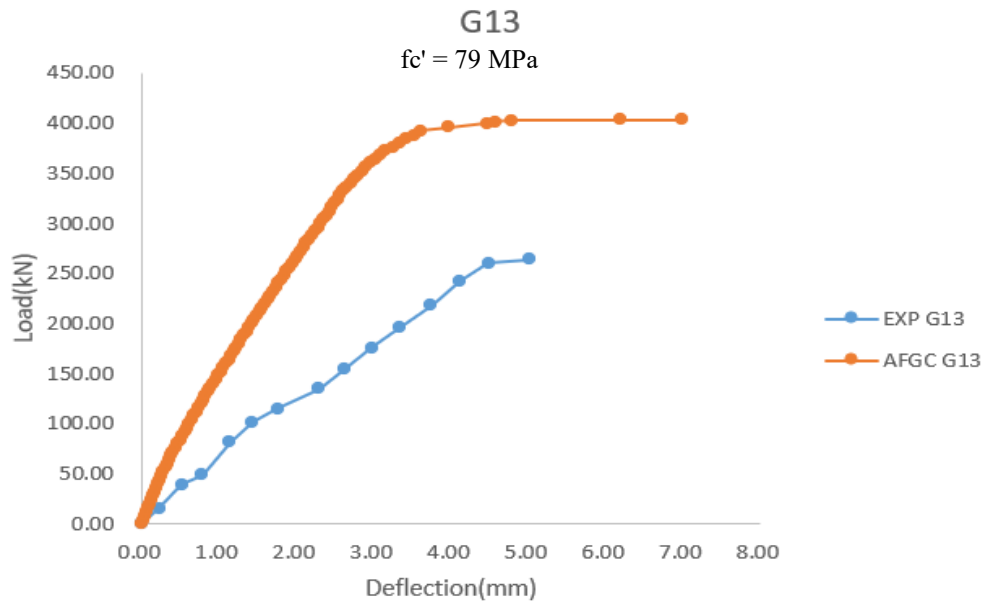


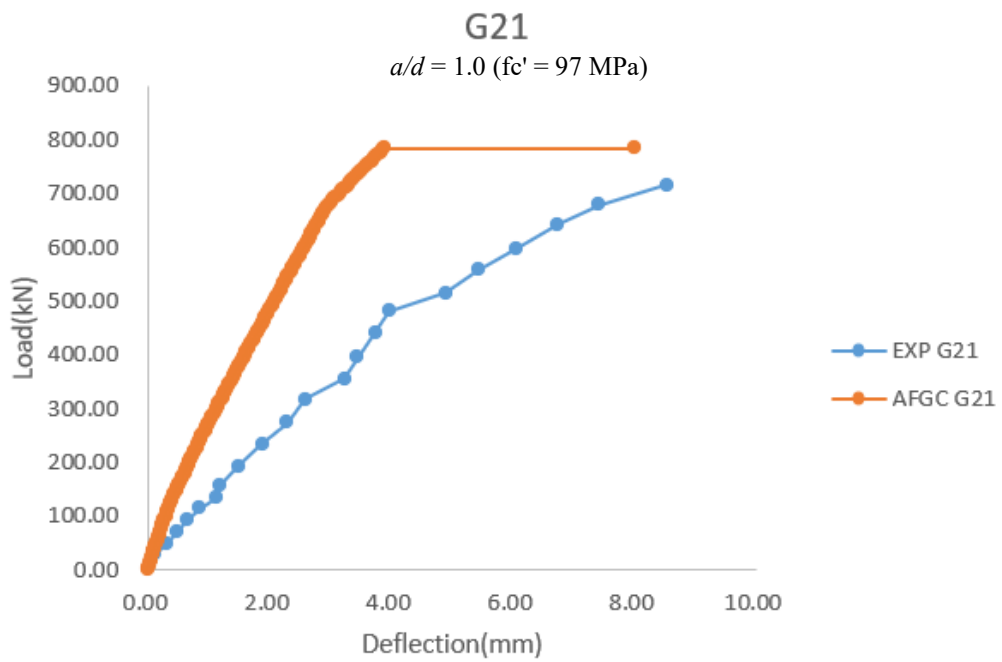
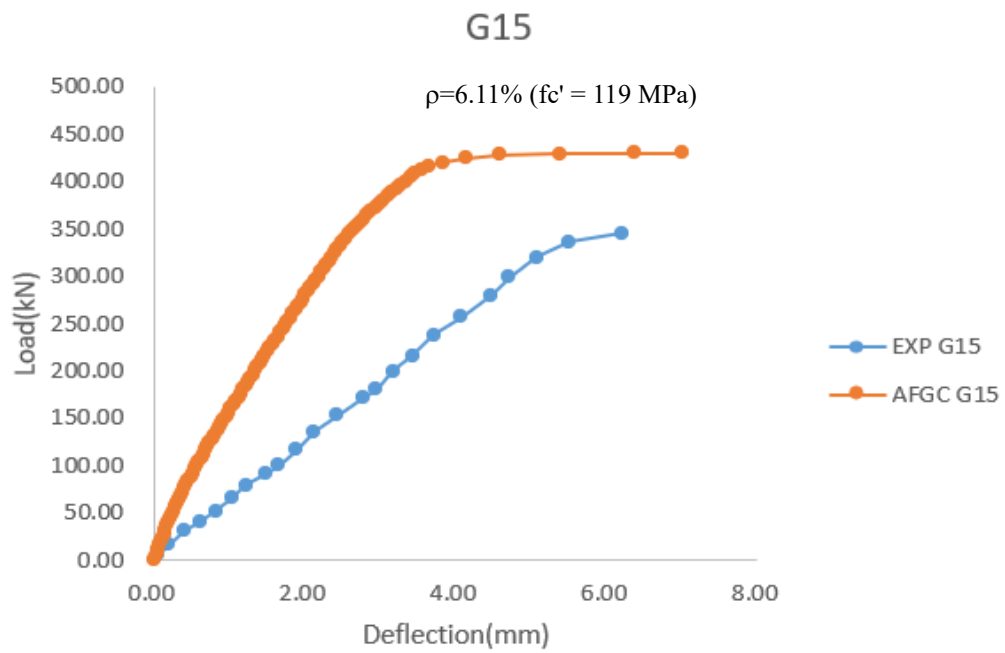
Figure 32. Load-Deflection Curves from Numerical (*fib* Model Code 2010) and Test Results of Yaseen [36].



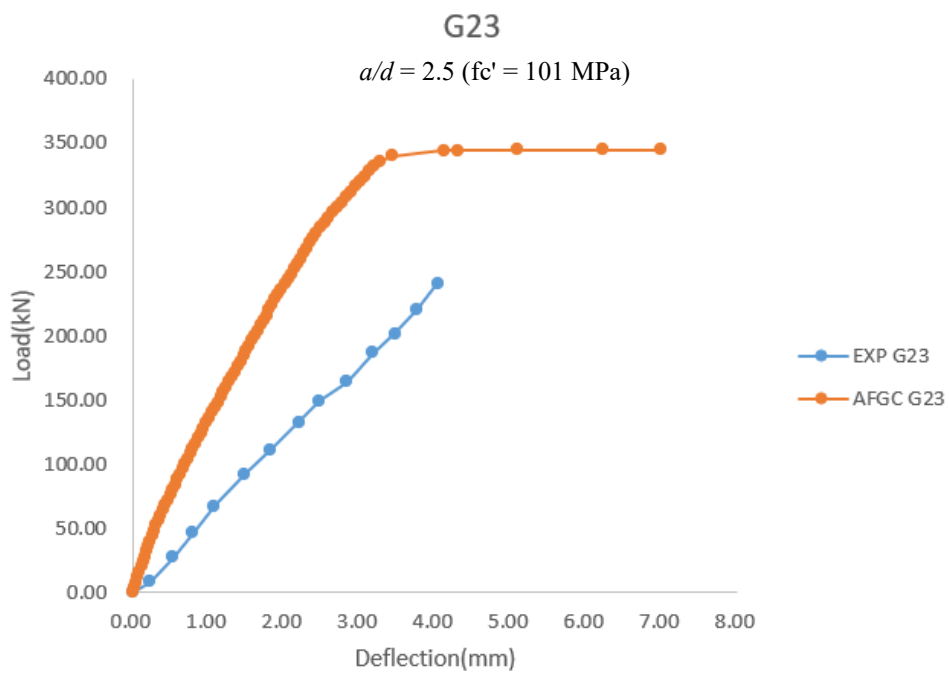
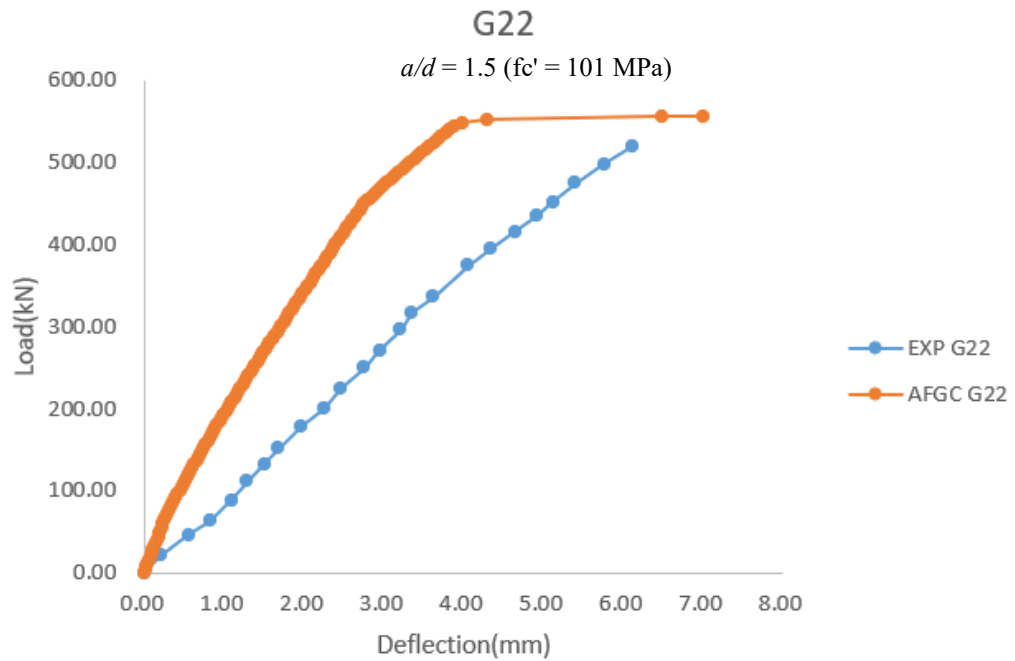
ปณ. ๓๓๓



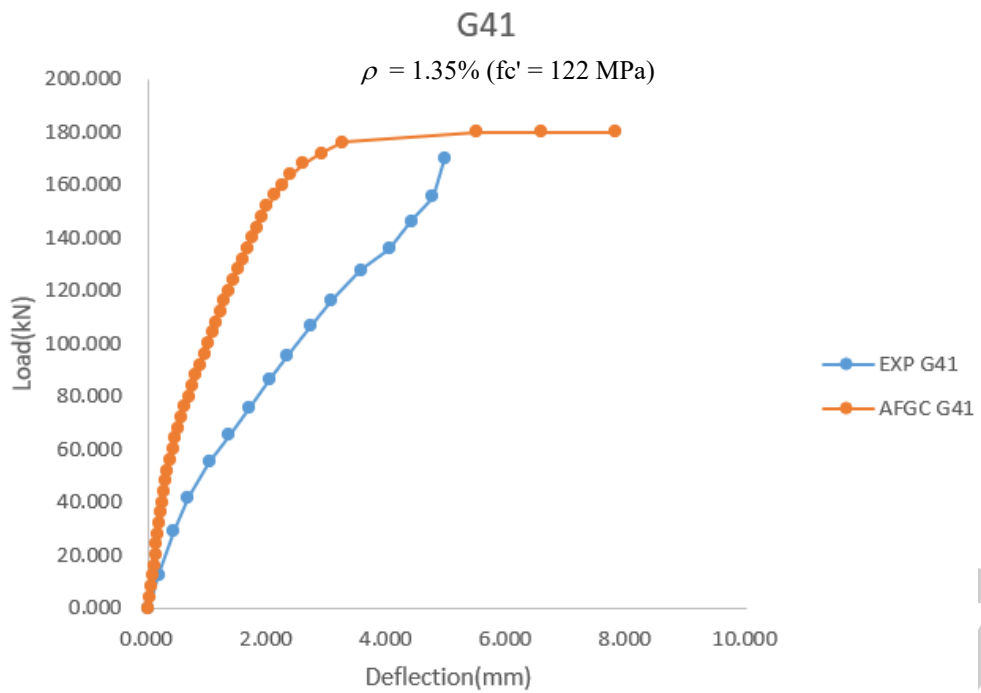
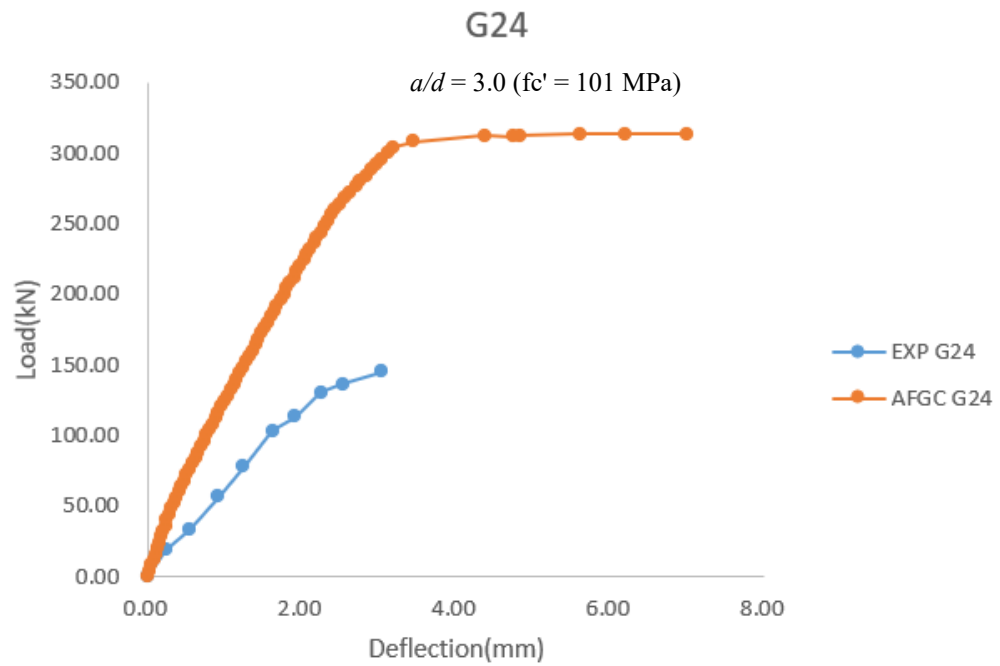
พหุ ประถมศึกษา ชีวะ



พหุ ประถมศึกษา ชีวะ



ศูนย์ ปณ. ที. โตะ ข.



คณะ ปรณุ ทิโต

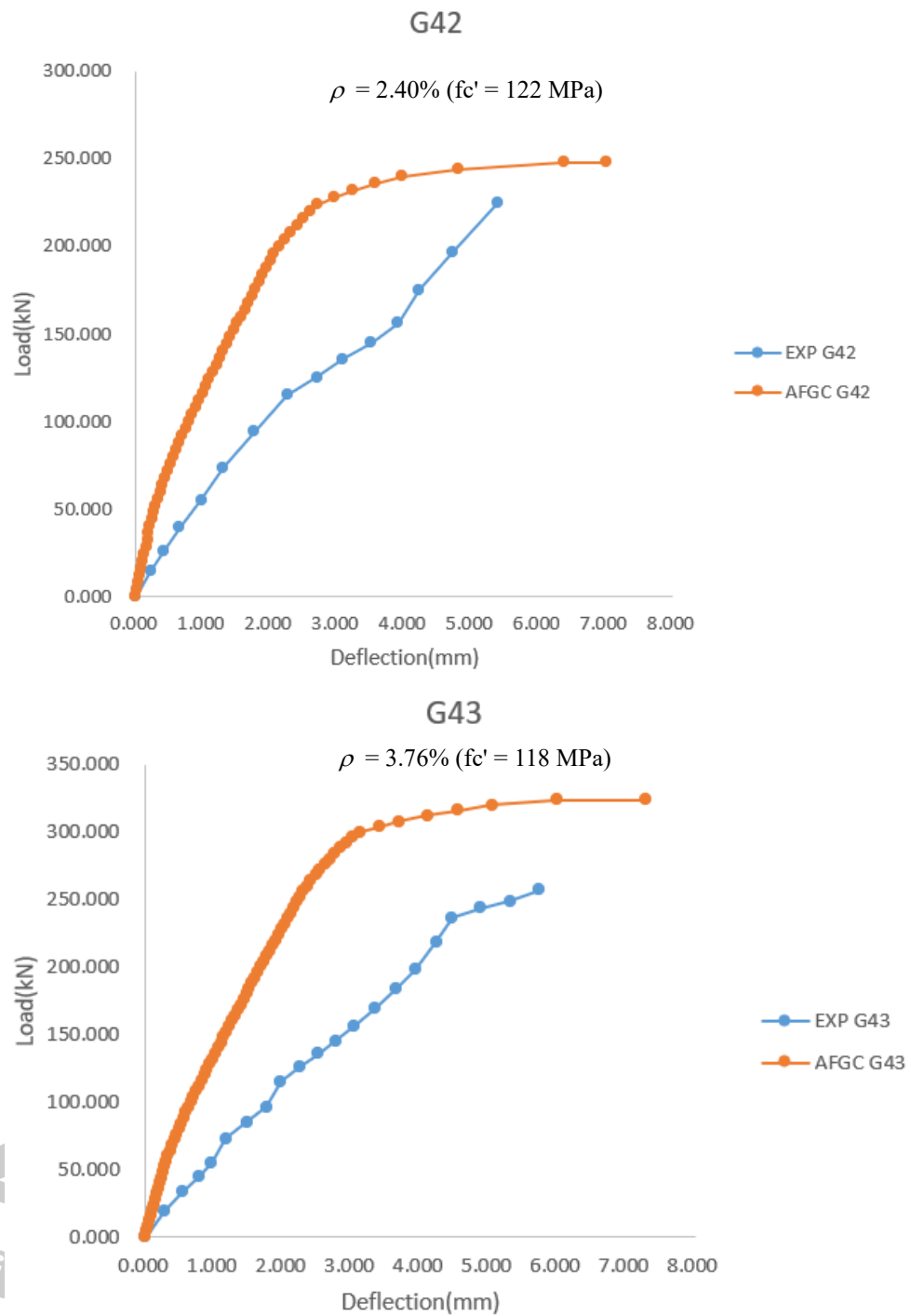
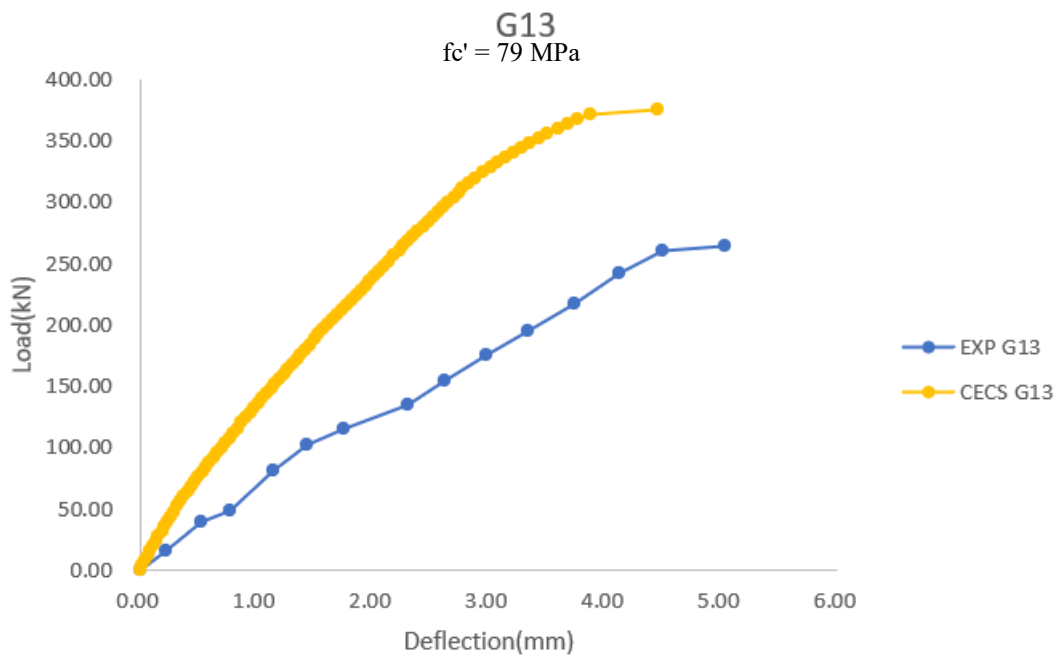
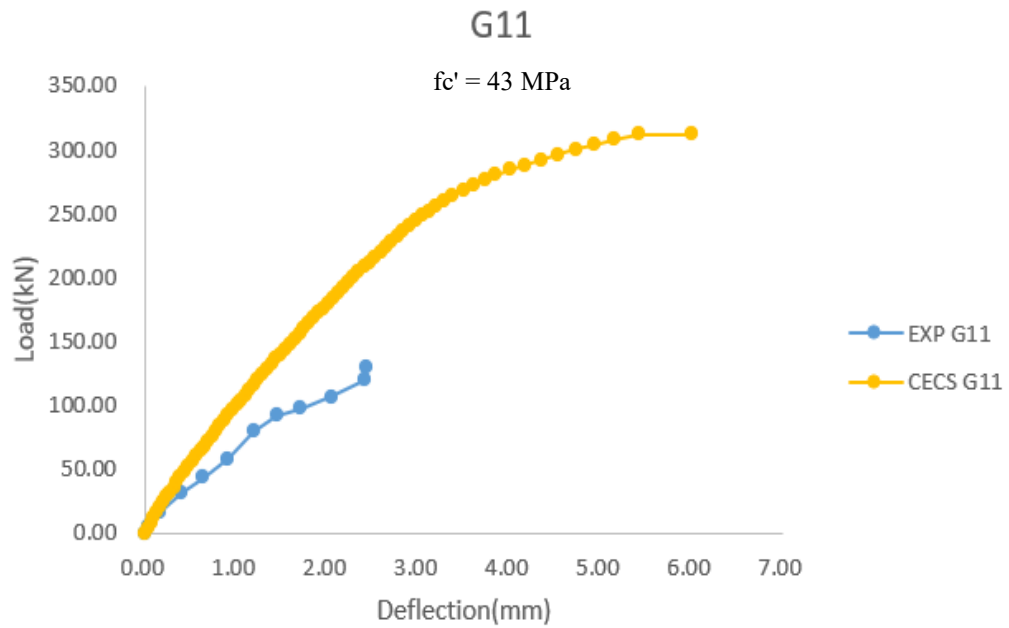
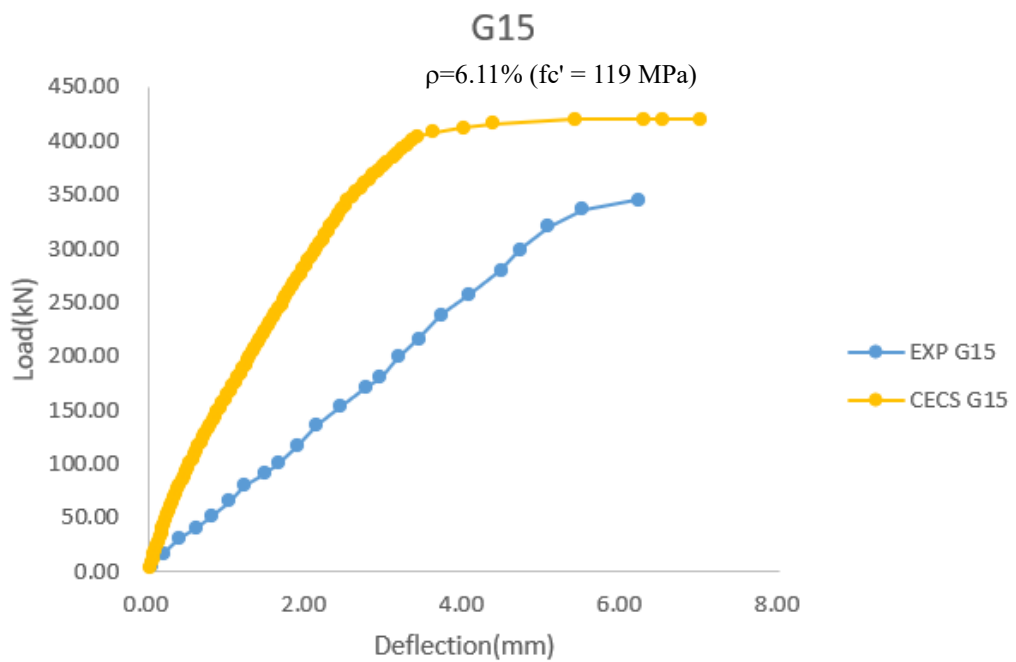
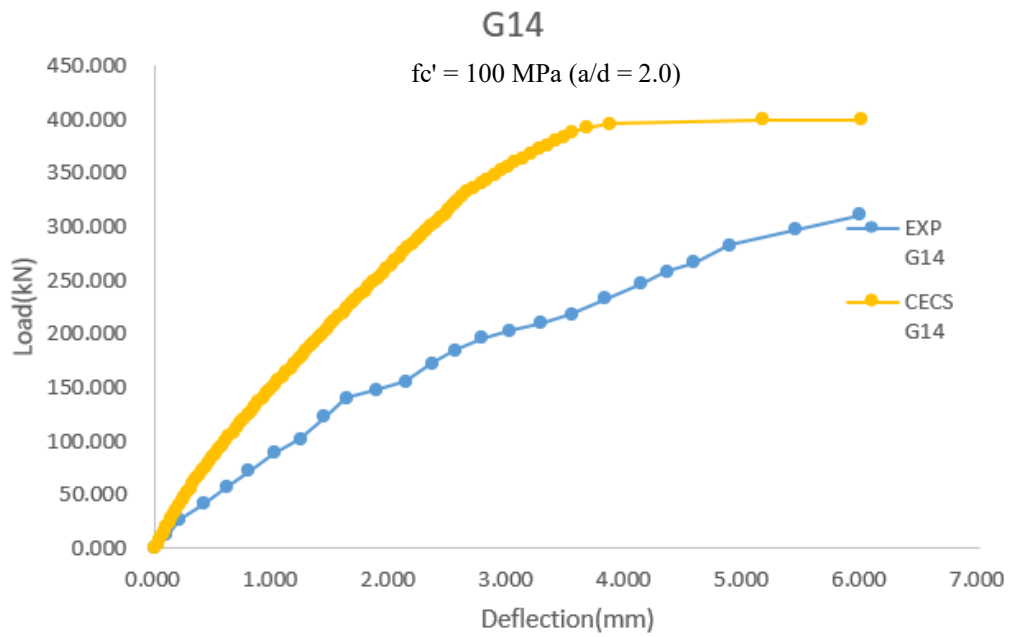


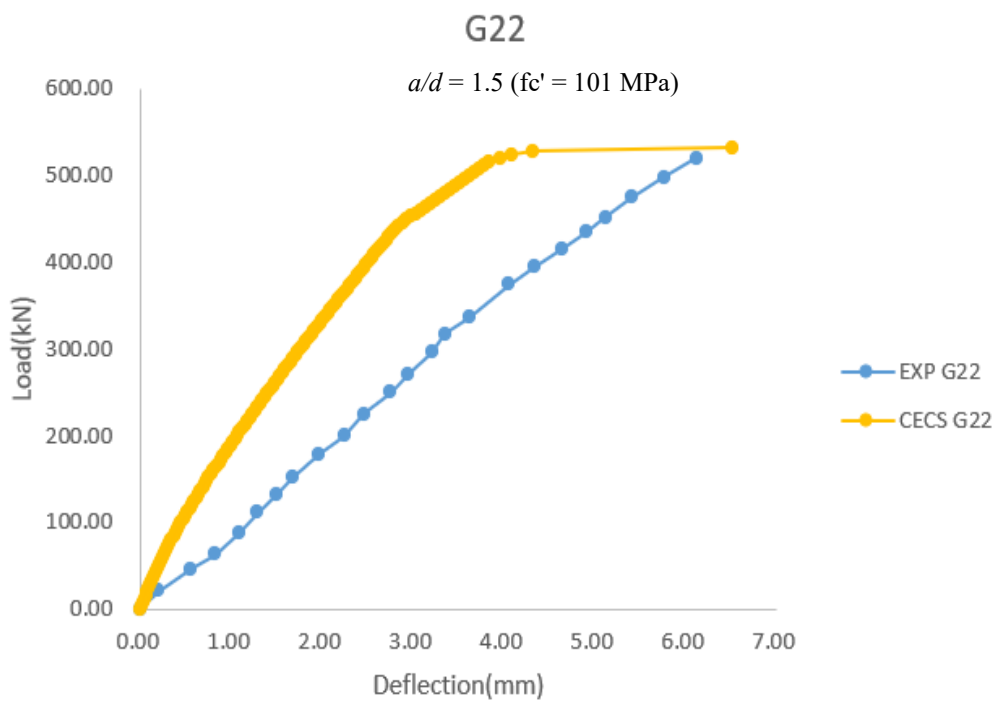
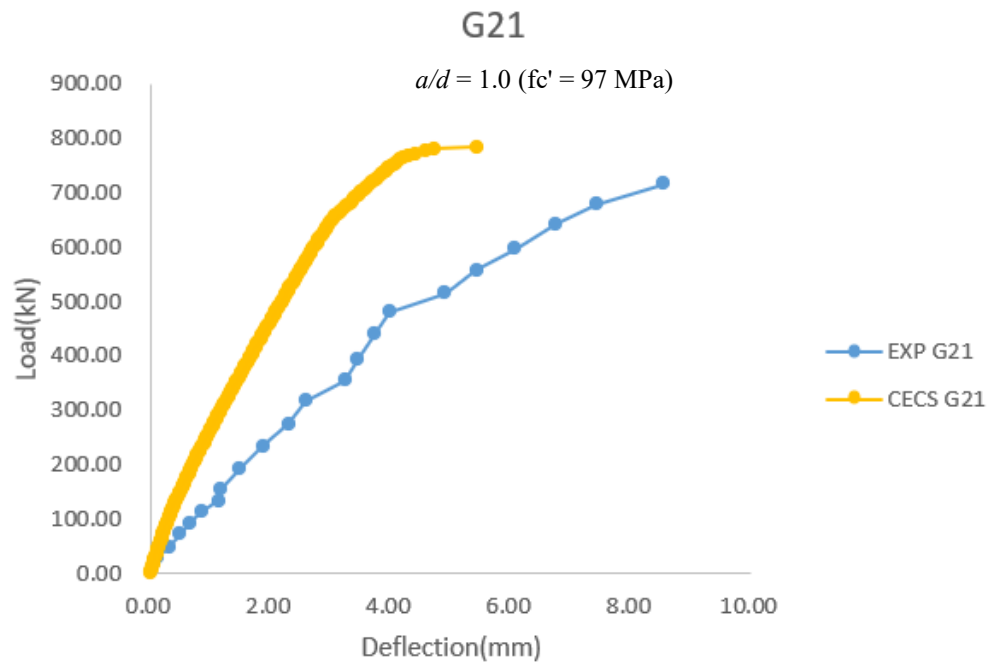
Figure 33. Load-Deflection Curves from Numerical (AFGC Code) and Test Results of Yaseen [36].



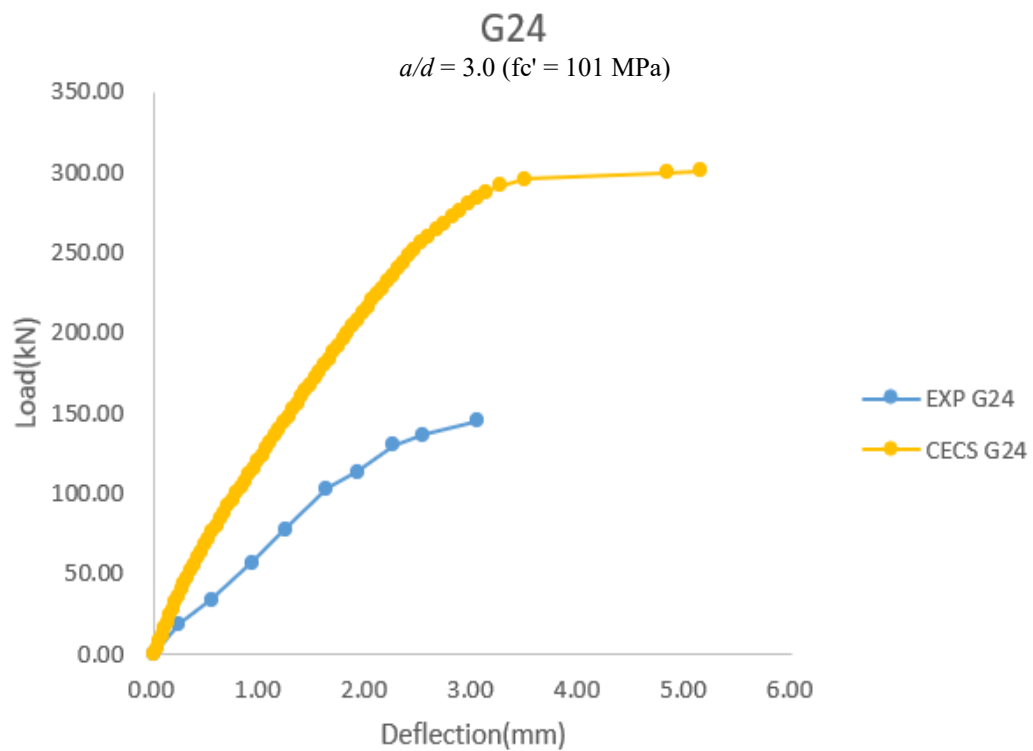
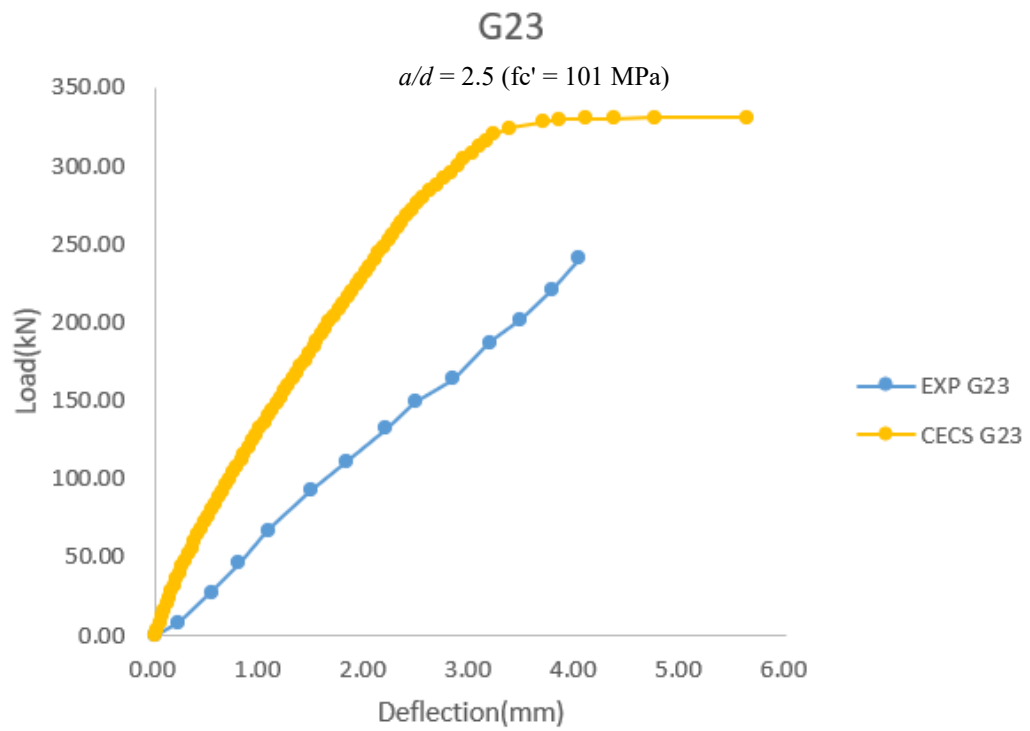
พหุ ประถมศึกษา ชีวะ

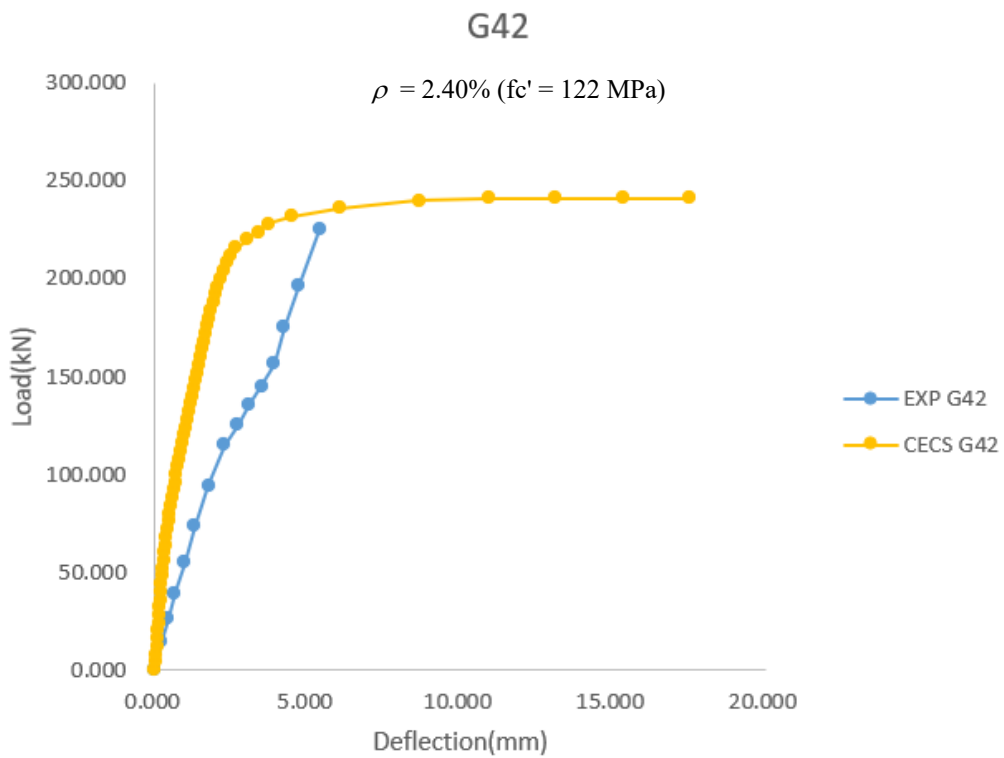
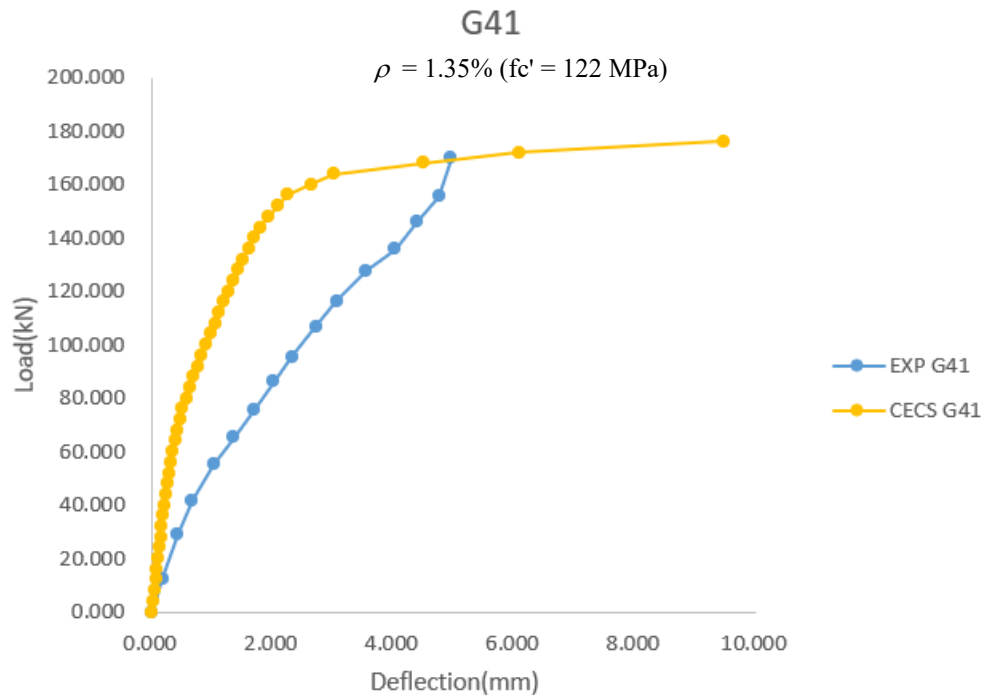


พหุ ประถมศึกษา ชีวะ



คณะ ปรณ ฑี โด ม





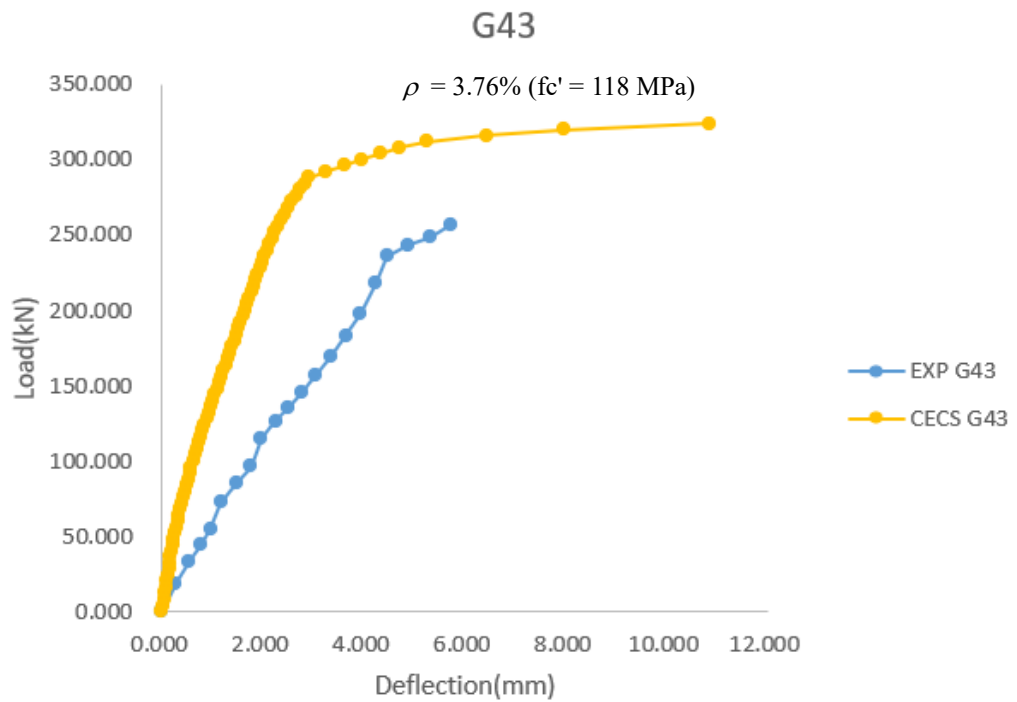
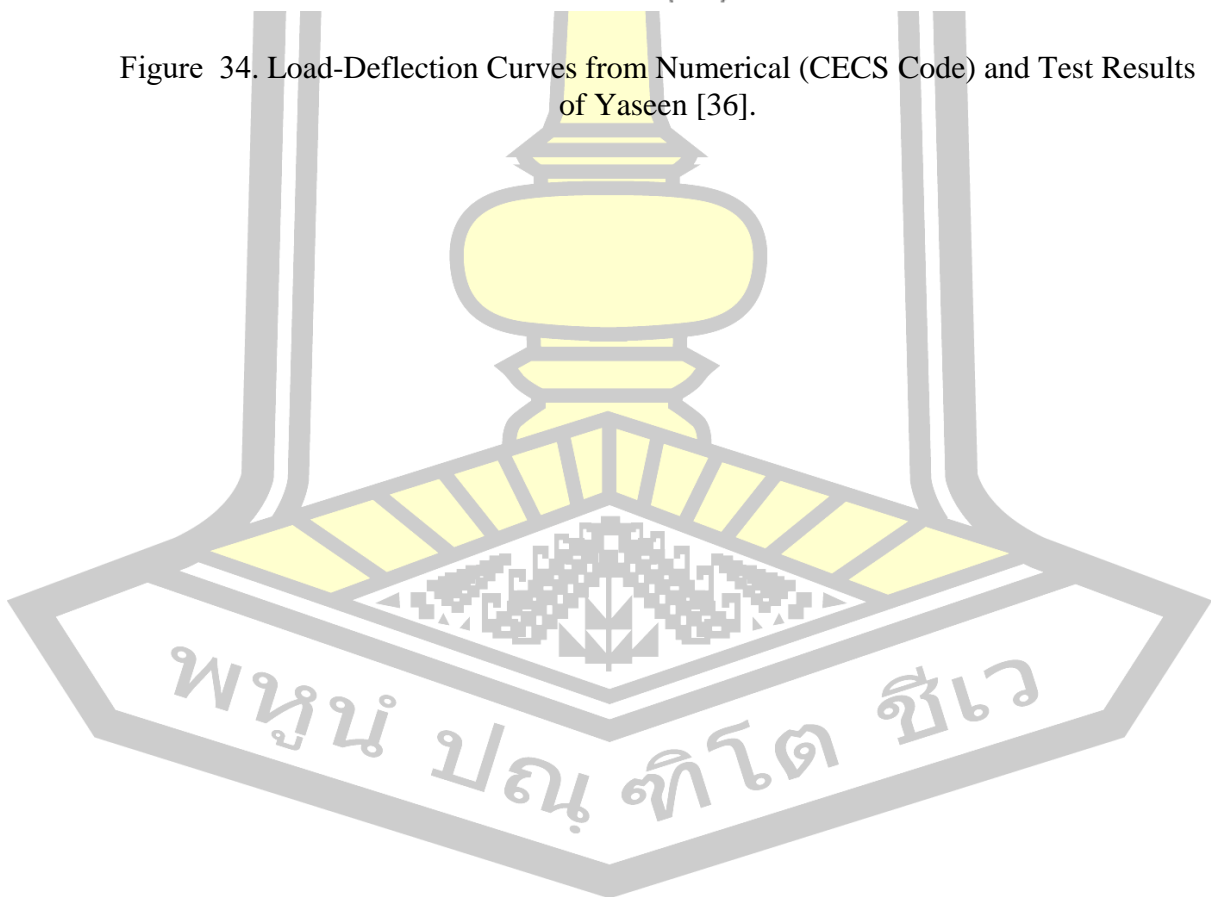
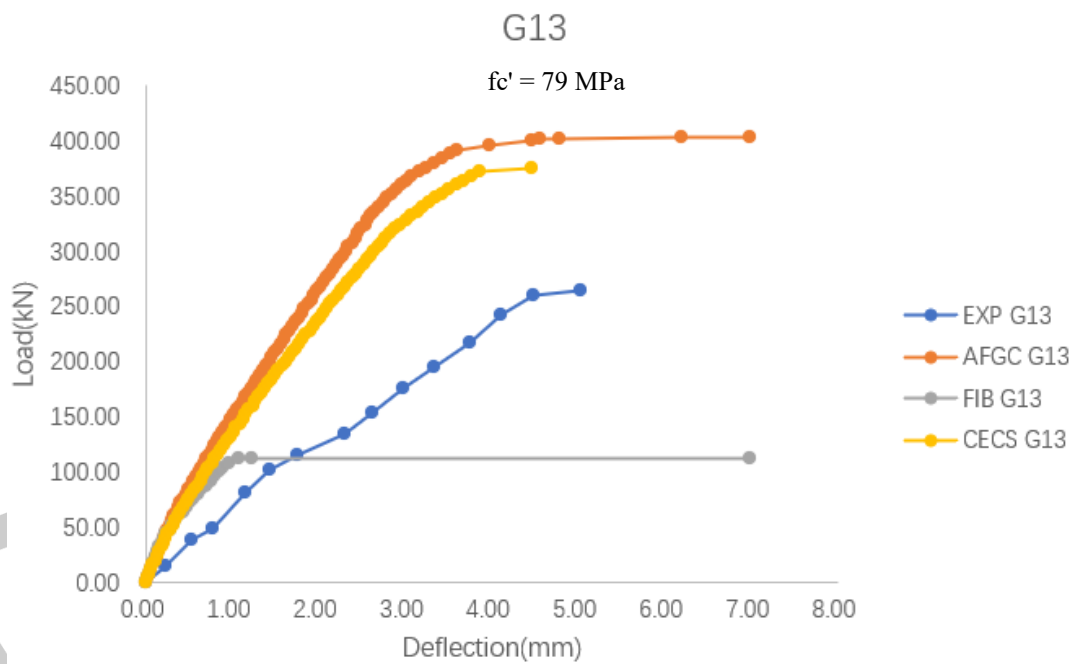
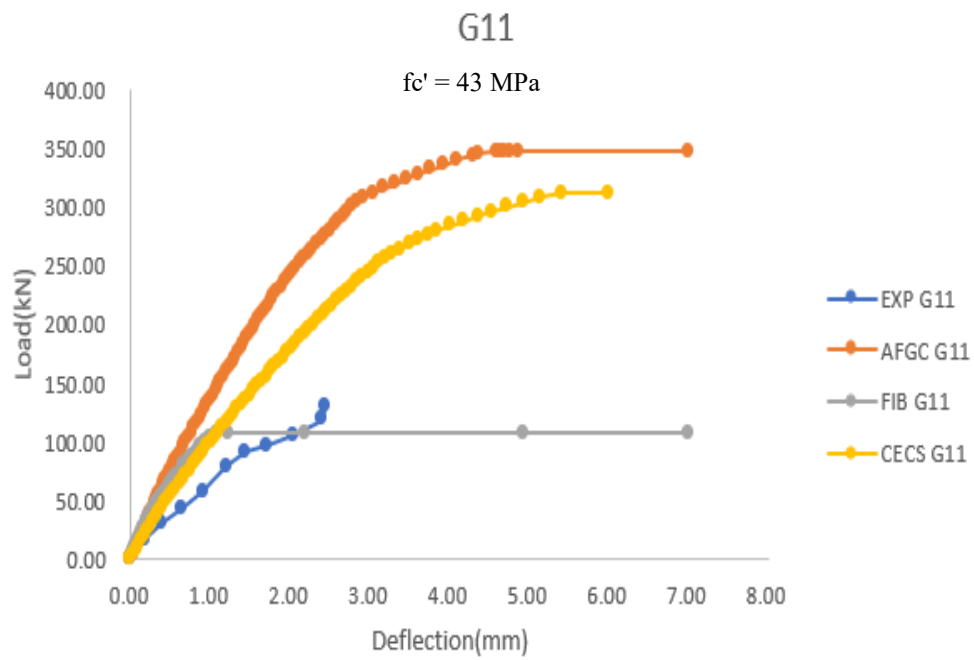
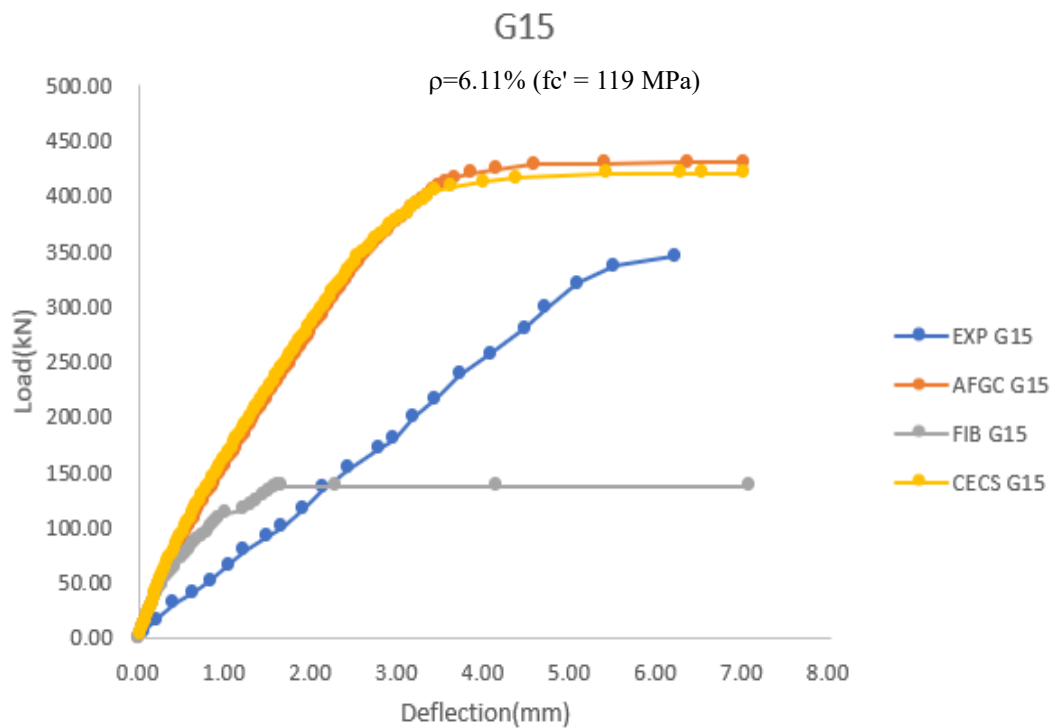
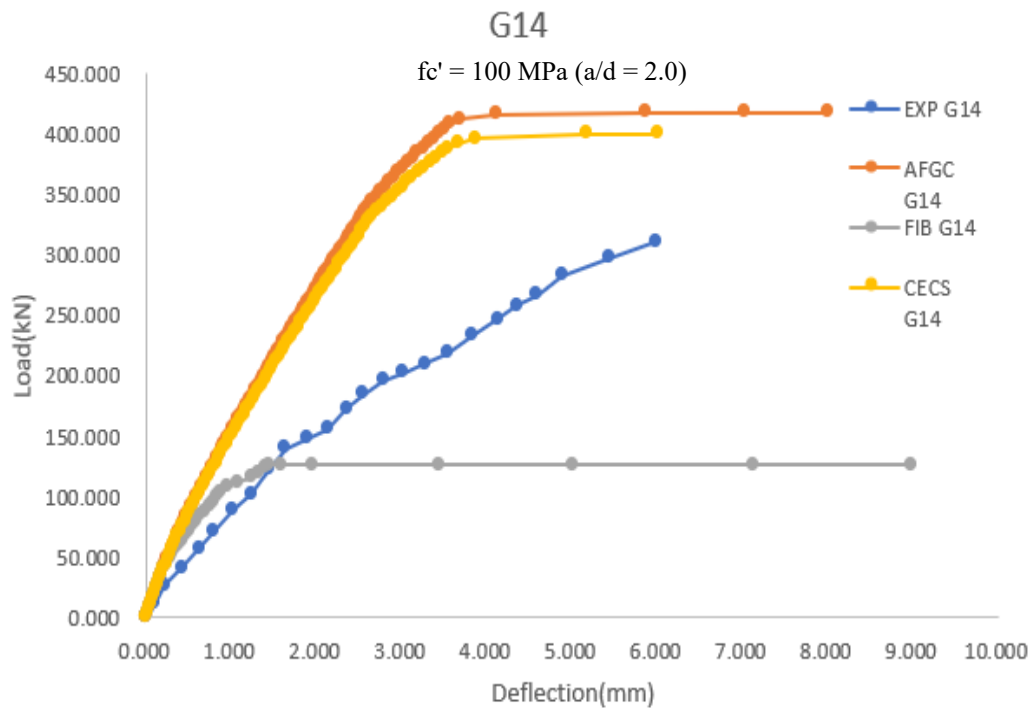


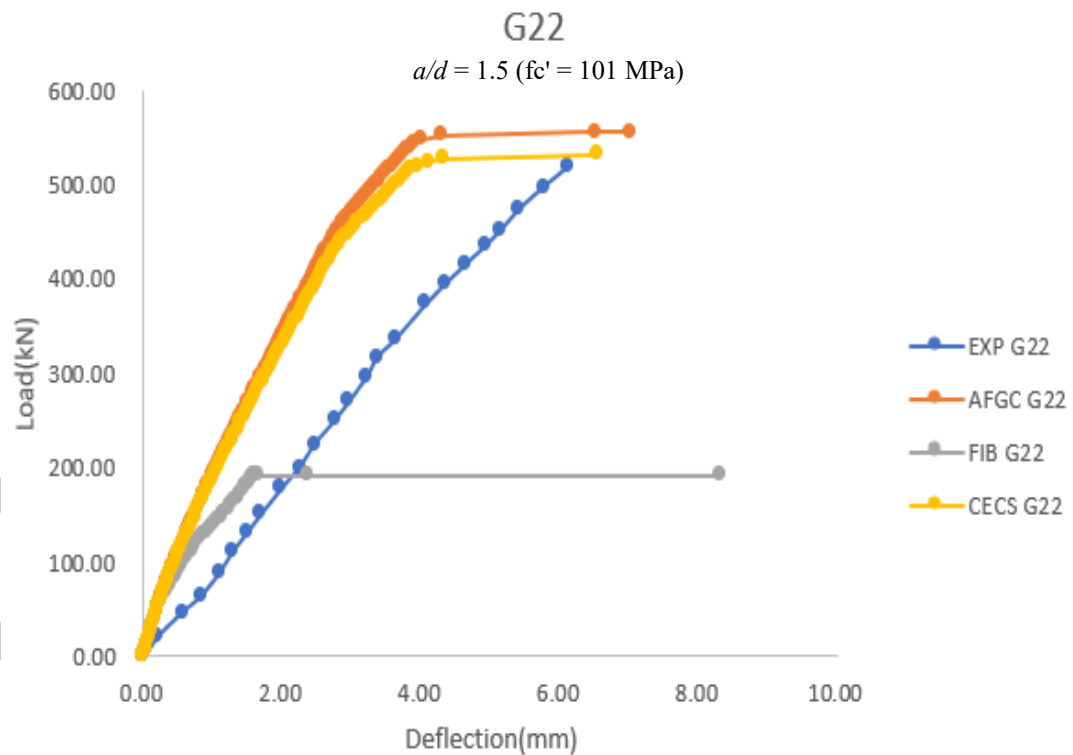
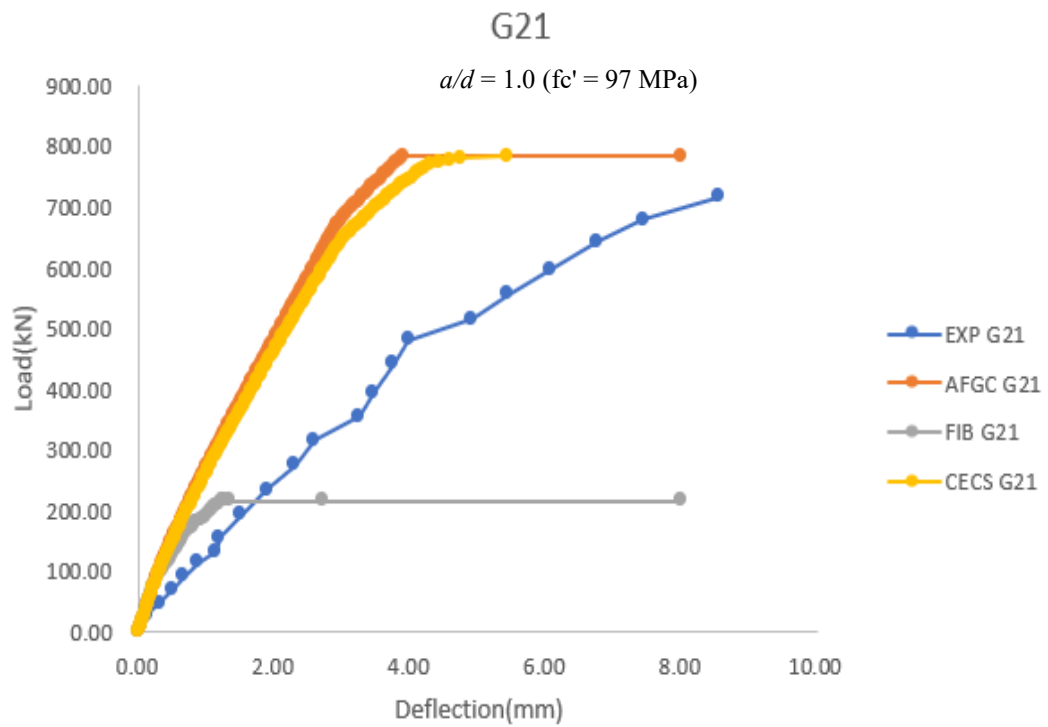
Figure 34. Load-Deflection Curves from Numerical (CECS Code) and Test Results of Yaseen [36].

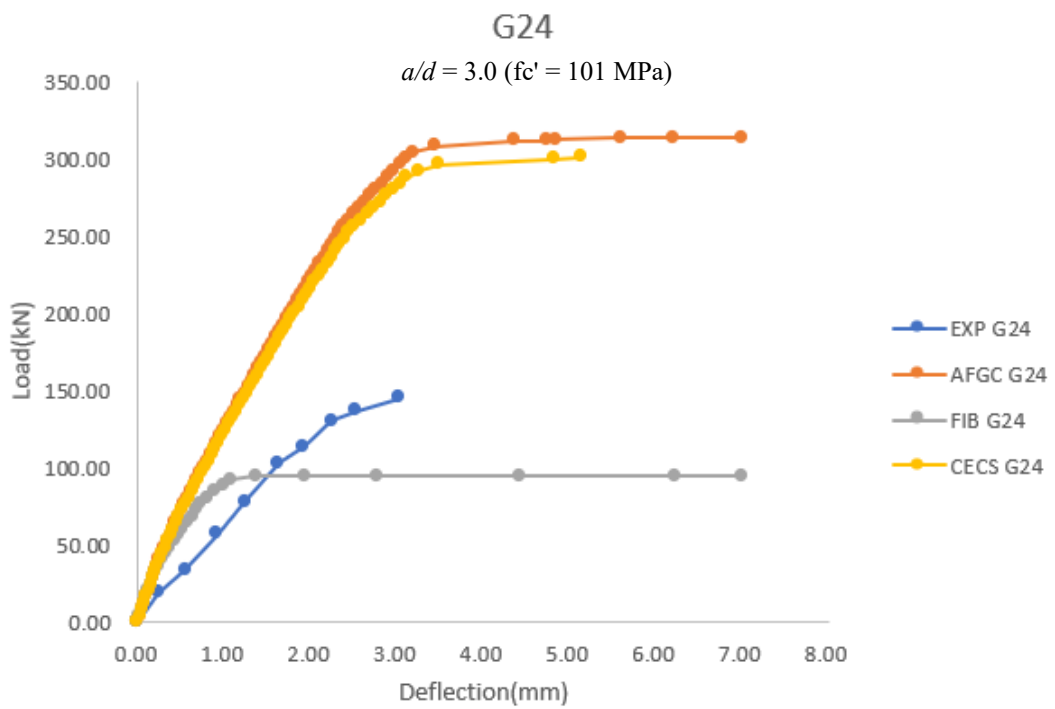
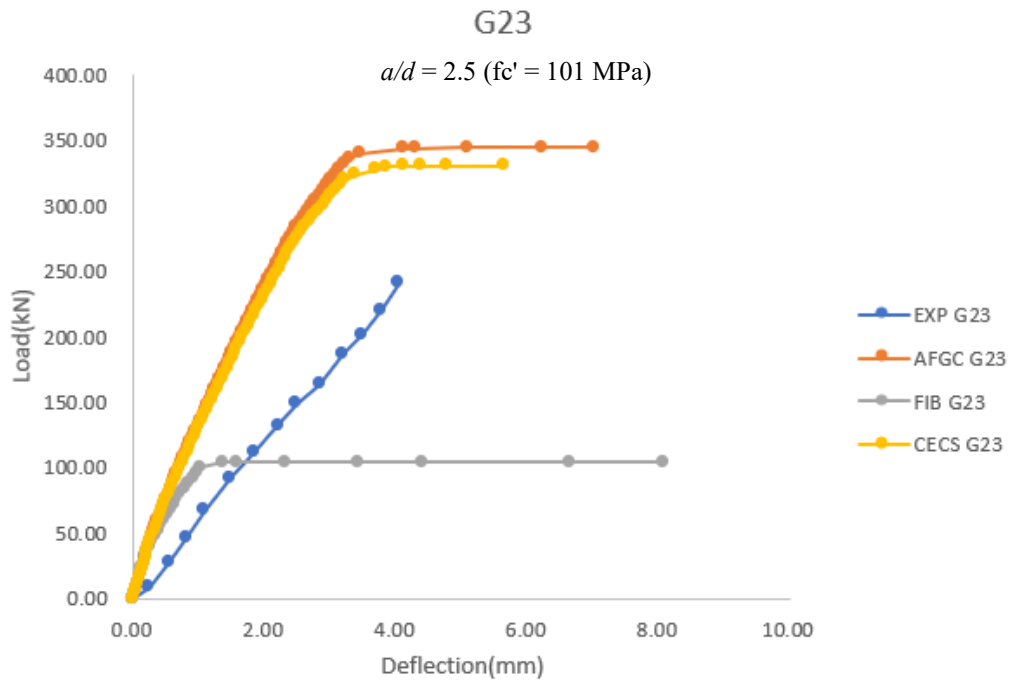




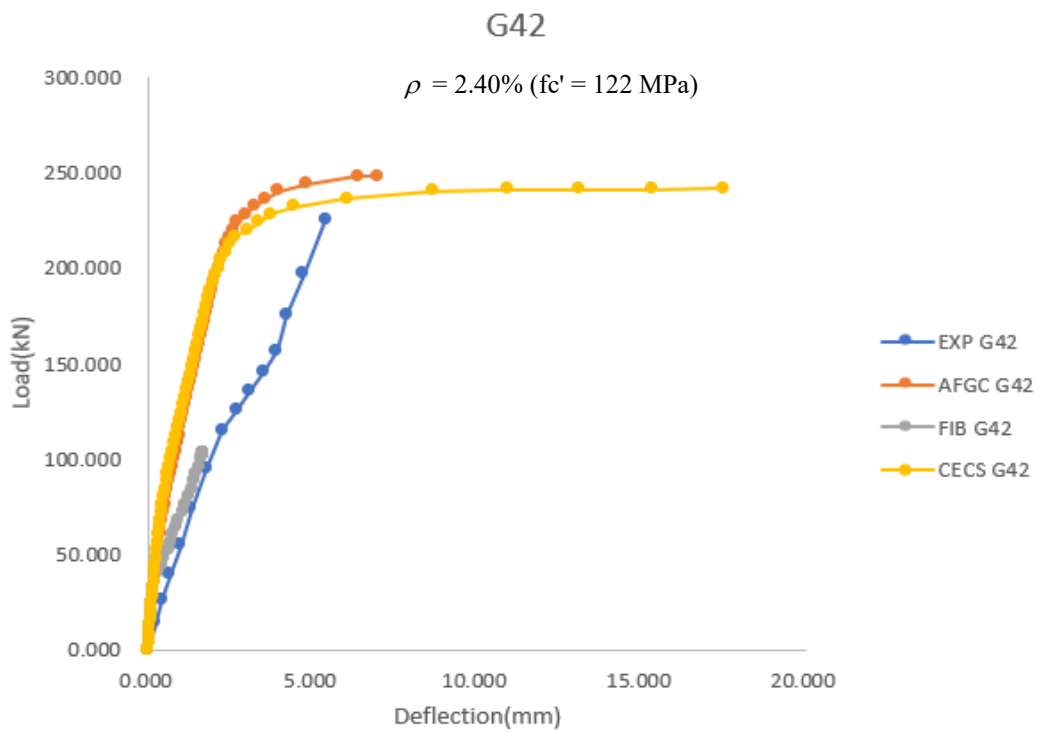
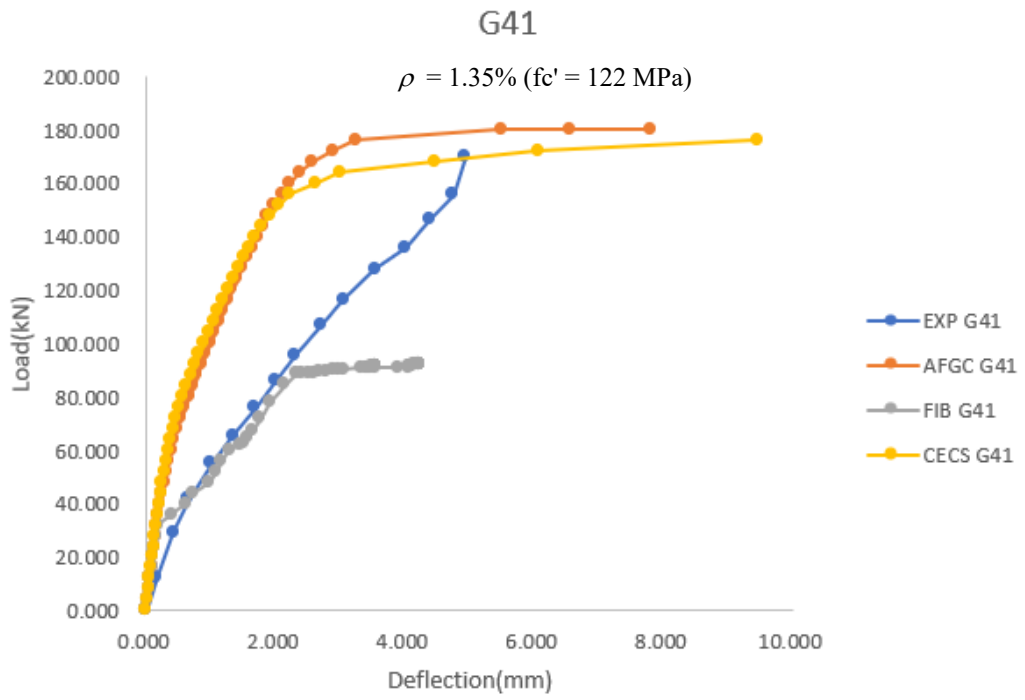
ศูนย์ ปณฺ ทัต โด ม







ม.อ. สุโขทัย



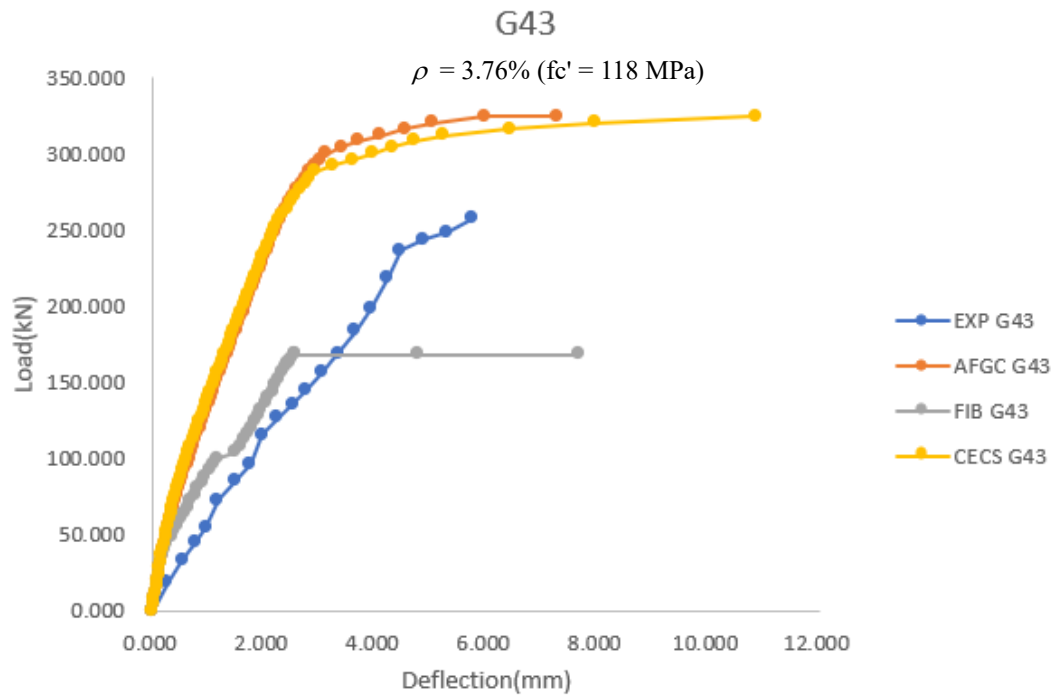


Figure 35. Load-Deflection Curves from FEA (All Codes) and Test Results of Yaseen [36].

Table 18. Peak Loads from FEA and Test Results of Yaseen [36].

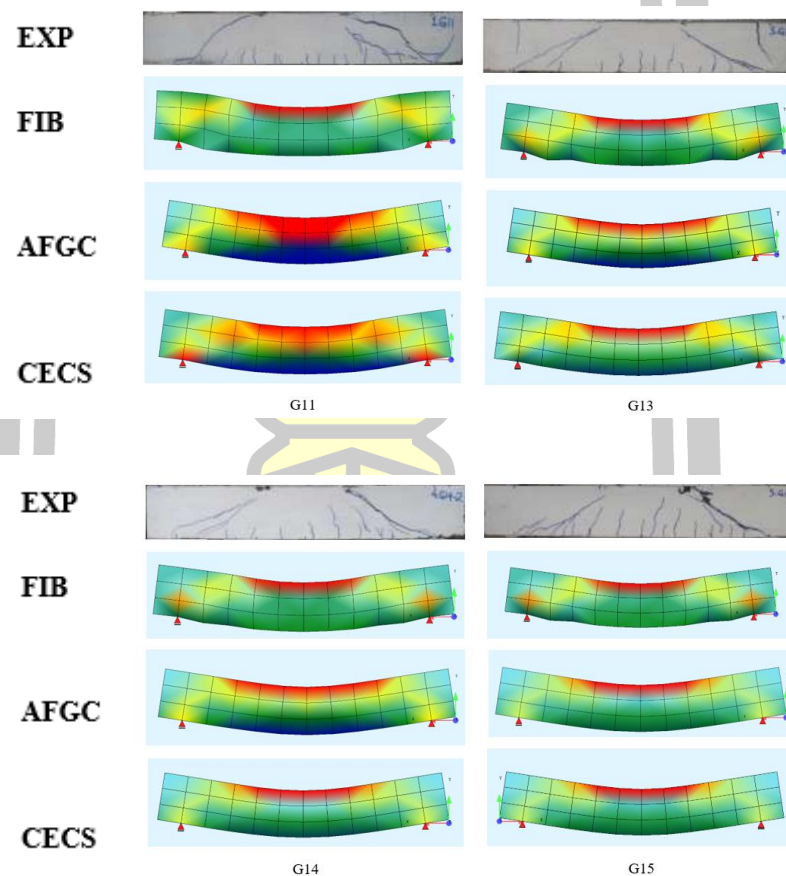
Beam	F_{EXP} (kN)	F_{FEA} (kN)			F_{FEA}/F_{EXP}		
		<i>fib</i> Code	AFGC Code	CECS Code	<i>fib</i> Code	AFGC Code	CECS Code
G11 (NSC)	130	108.03	347.33	312.00	0.83	2.67	2.40
G13 (HSC)	264	112.00	403.04	378.28	0.42	1.53	1.43
G14 (RPC)	311	126.00	417.27	400.00	0.41	1.34	1.29
G15 (RPC)	345	137.00	430.28	419.89	0.40	1.25	1.22
G21 (RPC)	716	216.50	784.00	784.00	0.30	1.10	1.10
G22 (RPC)	520	191.22	556.00	532.00	0.37	1.07	1.02
G23 (RPC)	241	104.00	344.50	330.59	0.43	1.43	1.37
G24 (RPC)	145	94.00	313.33	301.28	0.65	2.16	2.08
G41 (RPC)	170	92.00	180.00	176.00	0.54	1.06	1.04
G42 (RPC)	225	101.84	248.00	241.30	0.45	1.10	1.07
G43 (RPC)	257	168.04	324.00	324.00	0.65	1.26	1.26
Mean value					0.50	1.45	1.39
Mean value excluding G11 & G13& G24					-	1.20	1.17
Coefficient of variation					0.30	0.34	0.31
Coefficient of variation excluding G11 & G13& G24					-	0.11	0.10

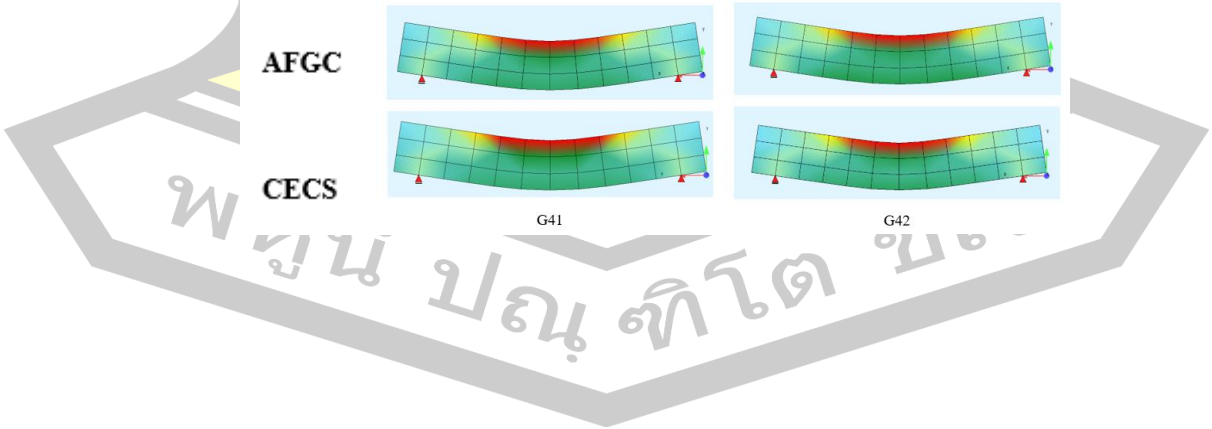
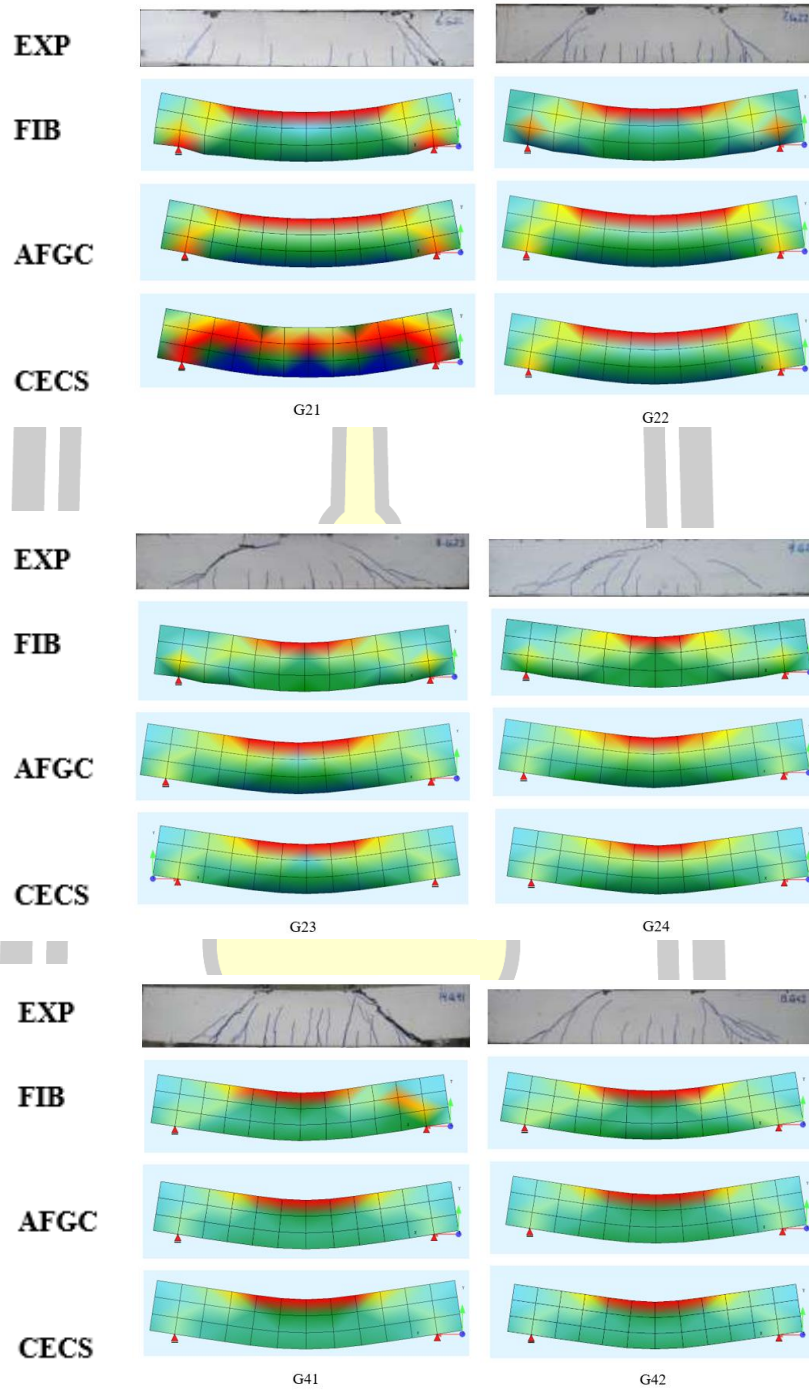
Cracking and Failure Mode

Figure 36 depicts the cracking and failure of all beams. The experimental findings show that all the beams failed due to diagonal crack. The stress distribution from the FEA seems to match the experimental results. Cracks generally formed at regions where tensile stresses exceeded the specified strength in the concrete beams. The experimental results revealed two types of cracks [39]:

1) Flexural cracks resulting from flexural tensile stresses in the cross-sectional region of the beam below the neutral axis for positive bending.

2) Shear cracks form as diagonal cracks begin at the last flexural crack and gradually turn into increasingly inclined cracks under shear loading. These cracks do not immediately lead to failure as they encounter resistance while moving into the compression zone, becoming flatter and eventually stopping at a certain point. The tension crack gradually extends at a flat slope until sudden failure occurs due to the inclined or principal tensile stresses in the combined bending and shear region.





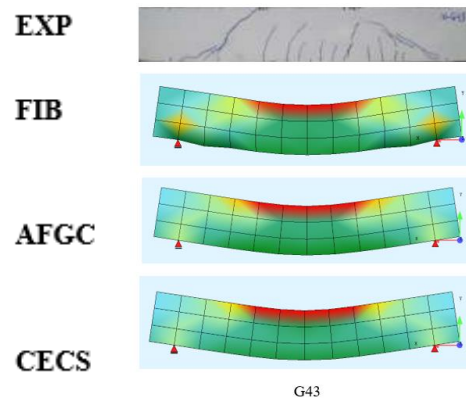


Figure 36. Crack Patterns from FEA (All Codes) and Test Results of Yaseen [36].

The crack width corresponding to the peak load of each beam was also obtained from the FEA as listed in Table 19. It can be observed that both AFGC and CECS codes seem to give a similar crack width for each beam but the *fib* code give a lower crack width due to the lower peak load.

Table 19. Crack Width at Peak Load from FEA Results of Yaseen [36].

Beam	Crack width (mm)		
	<i>fib</i> Code	AFGC Code	CECS Code
G11(NSC)	0.03	0.10	0.10
G13(HSC)	0.03	0.10	0.10
G14(RPC)	0.04	0.09	0.10
G15(RPC)	0.04	0.09	0.09
G21(RPC)	0.03	0.09	0.09
G22(RPC)	0.04	0.09	0.09
G23(RPC)	0.03	0.09	0.09
G24(RPC)	0.03	0.09	0.09
G41(RPC)	0.15	0.15	0.15
G42(RPC)	0.08	0.07	0.15
G43(RPC)	0.09	0.11	0.15

4.1.1.5 Conclusions

In conclusion, the validity of the stress-strain model of concrete, as per the *fib* model code 2010 and AFGC code and CECS code, was evaluated in simulating the behavior

of RPC deep beam in comparison to NSC and HSC deep beams. Based on the study results, the following conclusions can be drawn:

1. The *fib* model code 2010 demonstrates the capability to good predict the loading capacity of NSC deep beams. However, it significantly underestimates the loading capacity of RPC deep beams, providing conservative predictions.

2. The AFGC code model and CECS code model demonstrates the capability to good predict the loading capacity of HSC deep beams about 1.45 times. But both of them significantly overestimates the loading capacity of HSC deep beam.

3. The AFGC code model and CECS code model demonstrates the capability to accurately predict the loading capacity of RPC deep beams. But both of them can't estimate the loading capacity of NSC deep beams.

4.1.2 RPC Deep Beams Tested by Yousef et al. [37]

4.1.2.1 Stress-Strain Curves of Rebar

All RPC deep beams tested by Yousef et al. [37] that were investigated in this study used the two types of rebar with the properties listed in Table 20. The stress-strain points were calculated using the concept described in Section 3.1.4. Figure 37 shows the obtained curve. The model incorporated the Poisson's ratio values of 0.3 for steel rebar.

Table 20. Parameters for Stress-Strain Models of Steel Rebar.

Rebar diameter	Parameter	Value
18(mm)	f_y (MPa)	491.2
	E_s (GPa)	200
10(mm)	f_y (MPa)	407.64
	E_s (GPa)	200

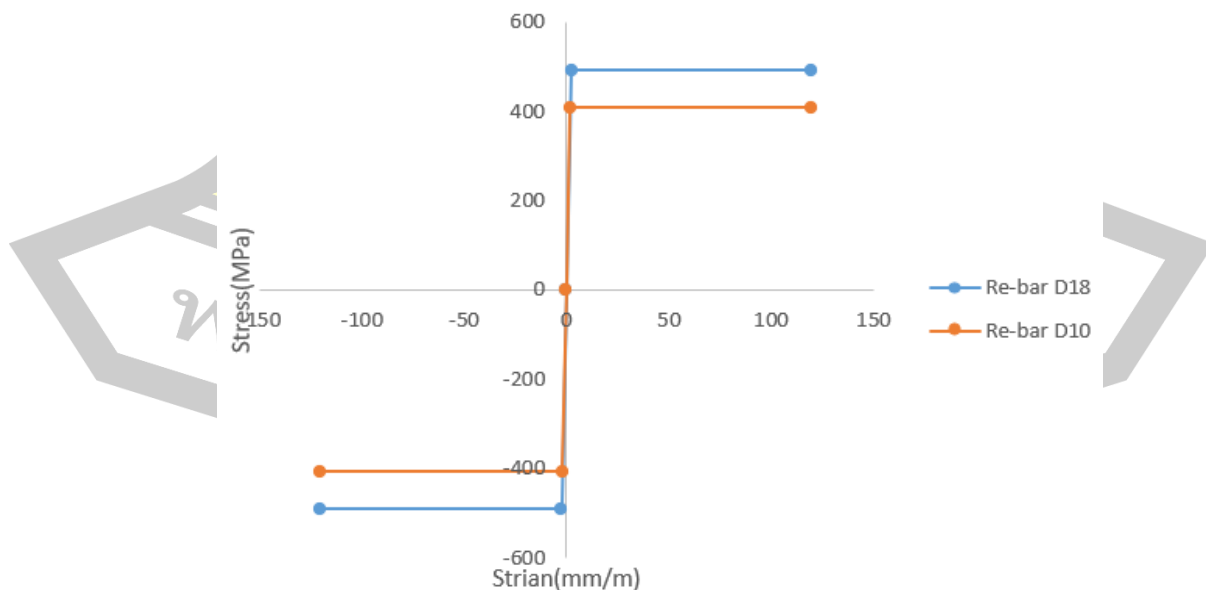


Figure 37. Stress-Strain Curves for Rebar Used in FEA.

4.1.2.1 Stress-strain curves of concrete

The concrete properties provide by Yousef et al. [37] are compressive strength. To be able to obtain the stress-stress curve some properties were determined using the equations provided by the code which are generally based on the compressive strength.

fib 2010 code

The stress-strain points for concrete in compression and tension zones were calculated using the parameters listed in Table 21 and the concept described in Section 3.1.1. It should be noted that all concrete parameters are dependent on the concrete grade, therefore, the concrete grade is C180. It is worth noting that the input required by the *fib* 2010 code is only the test value of compressive strength.

AFGC Code

The stress-strain points for concrete in compression and tension zones were calculated using the parameters listed in Table 21 and the concept described in Section 3.1.2. In AFGC code, the load factor for RPC under tension γ_{bf} take 1.3 and the Poisson's ratio ν take 0.19 and the concrete tensile strength (f_t) take 9.7 MPa. The test values of concrete compressive strength were used in the model. However, the code does not provide the equation to calculate the concrete elastic modulus, therefore, the values obtained from the *fib* code were also used in the models using the AFGC code.

CECS Code

The stress-strain points for concrete in compression and tension zones were calculated using the parameters listed in Table 21 and the concept described in Section 3.1.3. In CECS code, the key parameters needed are the concrete compressive strength, the steel fiber volume ratio, the steel fiber length, and the equivalent diameter of steel fiber. The Poisson's ratio ν take 0.2 as suggested by the code. It should be noted that the rest parameters can be determined from the compressive strength using the equations or the values in the table provided by the code, anyway, the obtained values are very close to each other. The values in Table 21 are obtained from the table provided by the code.

Table 21. Parameters for Stress-Strain Models of Concrete.

Code	Parameters	Value
FIB	<i>Compression</i>	
	f'_c (MPa)	188.1
	E_c (GPa)	57.18
	k	1.82
	$e_{c,lim}$ (mm/m)	3.5
	e_{cl} (mm/m)	1.44

Code	Parameters	Value
	<i>Tension</i>	
	f_t (MPa)	6.33
	e_{tl} (mm/m)	0.224
AFGC	<i>Compression</i>	
	f'_c (MPa)	188.1
	E_c (GPa)	51.25
	ϵ_{bc} (mm/m)	3.67
	ϵ_u (mm/m)	5.20
	<i>Tension</i>	
	f_t (MPa)	9.7
	ϵ_e (mm/m)	1.27
	$\epsilon_{u1\%}$ (mm/m)	15.15
	ϵ_{lim} (mm/m)	23.44
CECS	<i>Compression</i>	
	f'_c (MPa)	188.1
	ϵ_0 (mm/m)	2.94
	ϵ_{cu} (mm/m)	3.94
	<i>Tension</i>	
	λ	3.6
	f_t (MPa)	9.35
	E_c (GPa)	49.22
	ϵ_{t0} (mm/m)	0.19
	ϵ_{tp} (mm/m)	1.00
	ϵ_{tu} (mm/m)	2.79

The obtained stress-strain curves in compression and tension for concrete are illustrated in [Figure 38](#). The stress-strain points were directly inputted into the program.

พหุ ประถมศึกษา

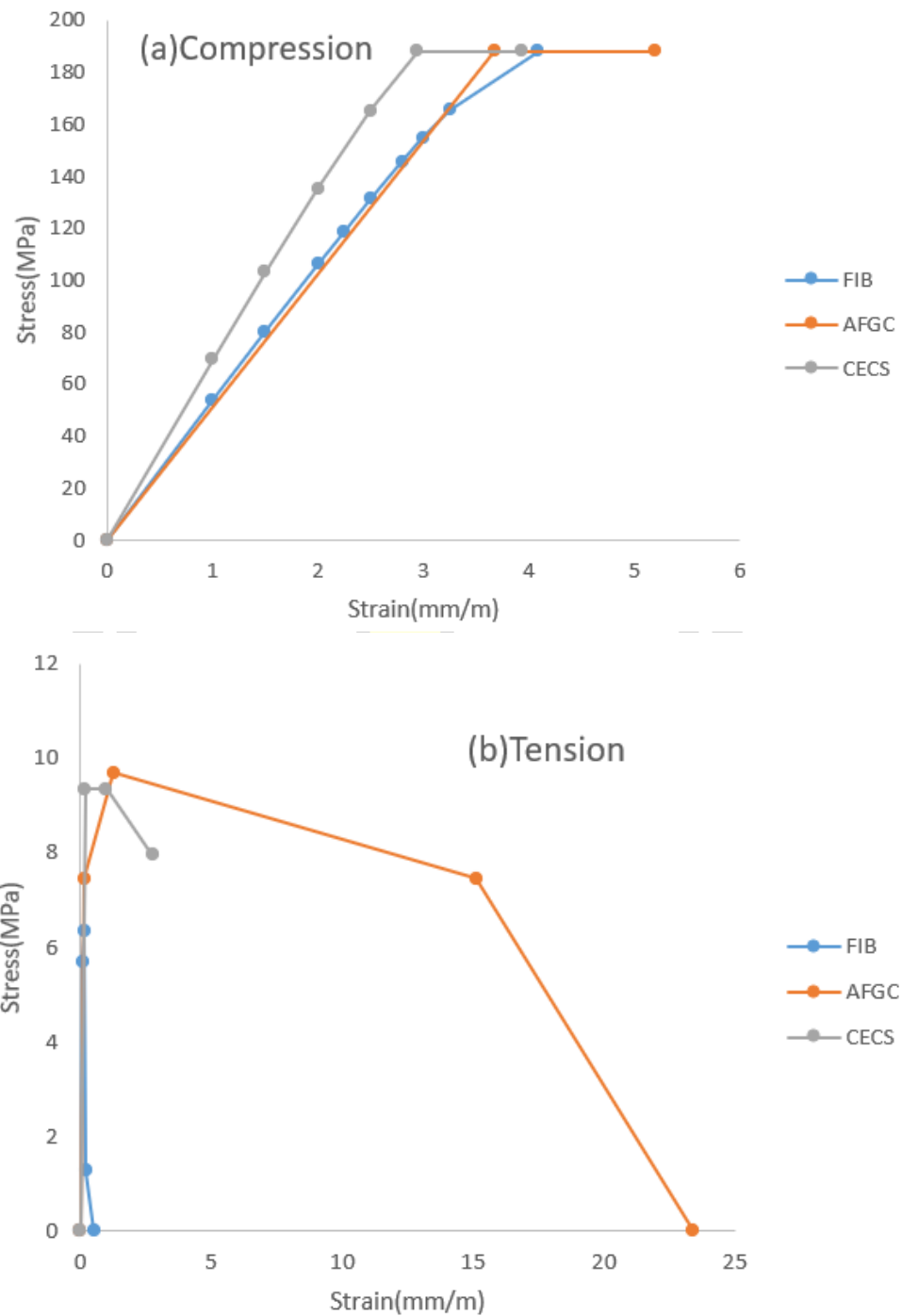


Figure 38. Stress-Strain Curves for Concrete Used in FEA (All Codes).

4.1.2.2 Structural Model

The deep beams studied by Yousef et al. [37] were tested under two symmetrically placed concentrated loads. The total length of the beams is 1000 mm with a point load applied at the midpoint of the span. The overall cross section was 80 mm x 400 mm.

Figure 39 shows details and typical cross section of tested beams. Table 22 shows details of tested beams.

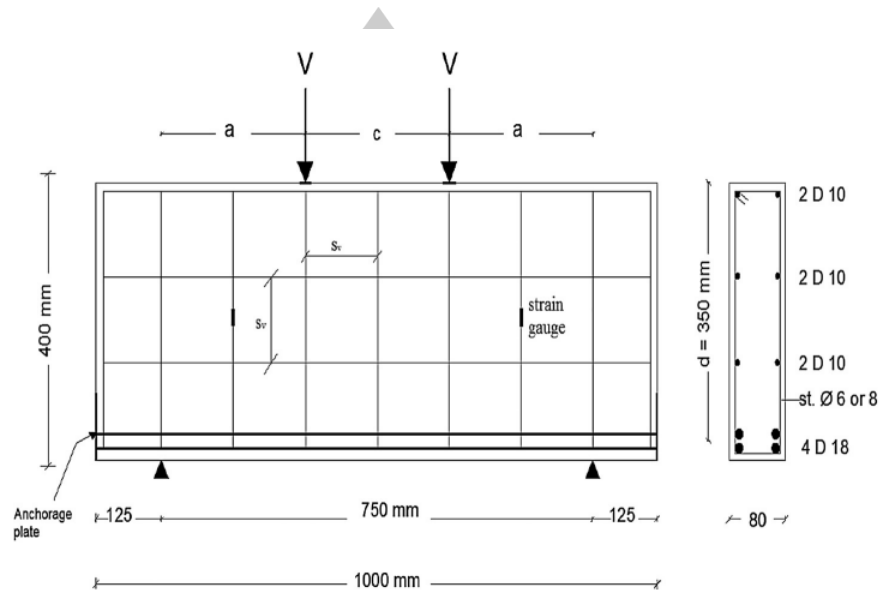


Figure 39. Details and Typical Cross Section of The Tested Beams (Yousef et al. [37]).

Table 22. Details of The Tested Beams (Yousef et al. [37]).

Beam designation	l(mm)	a(mm)	d(mm)	a/d	Stirrups (vertical reinforcement)	
					s_v (mm)	d_v (mm)
DBSU2(RPC)	750	275	350	0.79	150	8
DBSU4(RPC)	750	330	350	0.94	150	8

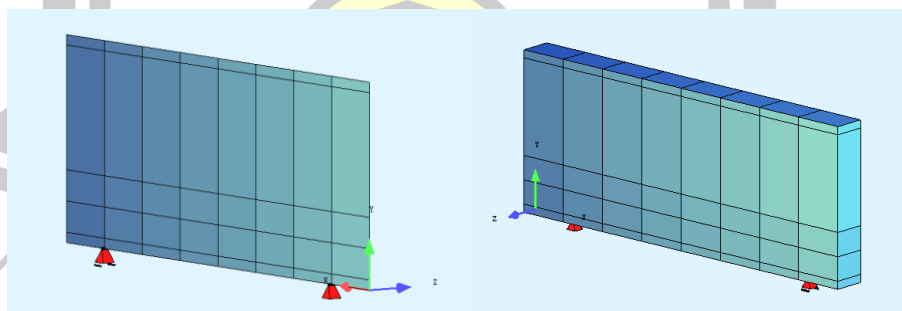


Figure 40. Typical FE Model of The Beams.

Figure 40 depicts the typical FE model employed in this study. The models used four-node shell or QUAD elements displaying plate structural behavior according to the Reissner-Mindlin theory. The QUAD elements integrated a layer material model to aid in cracked concrete analysis and contained. Discrete Kirchhoff conditions as well as an optional penalty term to consider shear deformation. The nonlinear analysis was

executed through an incremental solution technique founded on the modified Newton Raphson method.

4.1.2.3 Numerical Results

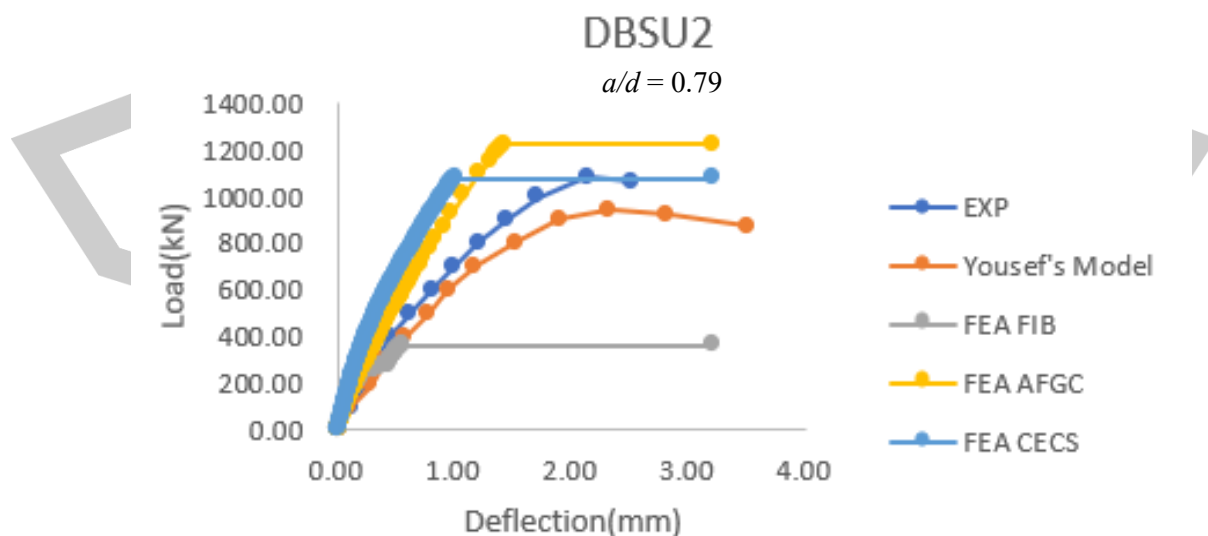
Load-Deflection Response

Figure 41 presents the comparison between the numerical curves and the experimental results. Table 23 shows the peak loads from FEA compared to the values from the test results.

From Table 23, it can be observed that the predicted peak loads from the FEA with AFGC code and CECS codes are closer to the test values compared to the predicted values with the *fib* code. The beam (DBSU2) can be good predicted with the FEA value to experimental value ratio 1.00 and 0.85 for AFGC code model and CECS code model, respectively. And The beam (DBSU4) can also be good predicted with the FEA value to experimental value ratio 0.86 and 0.97 for AFGC code model and CECS code model, respectively. The mean value for AFGC code model and CECS code model is 0.99 and 0.98, respectively. And the corresponding coefficient of variation is 0.13 and 0.01, respectively. However, the predicted of *fib* code model only get about 0.37 times of the experimental results which means that *fib* code model is not suitable for RPC applications.

In this paper, the authors also used ABAQUS program to simulate the experimental results. In this program, concrete is modeled using a three-dimensional reinforced concrete element named SOLID C3D8R element, which is capable of cracking in tension and crushing in compression. The main and web reinforcement are modeled using a bar element (T2D3) within the concrete solid 65 element. The bar element is assumed to be smeared within the concrete solid element. The concrete constitutive model in the paper also gives good simulation results.

Nevertheless, from Figures 41, it can be observed that the current FE model employed in the analysis fails to capture other important characteristics such as elastic stiffness, inelastic stiffness, and post-peak behavior for all types of deep beams. This limitation stems from the inherent characteristics of the FE model itself.



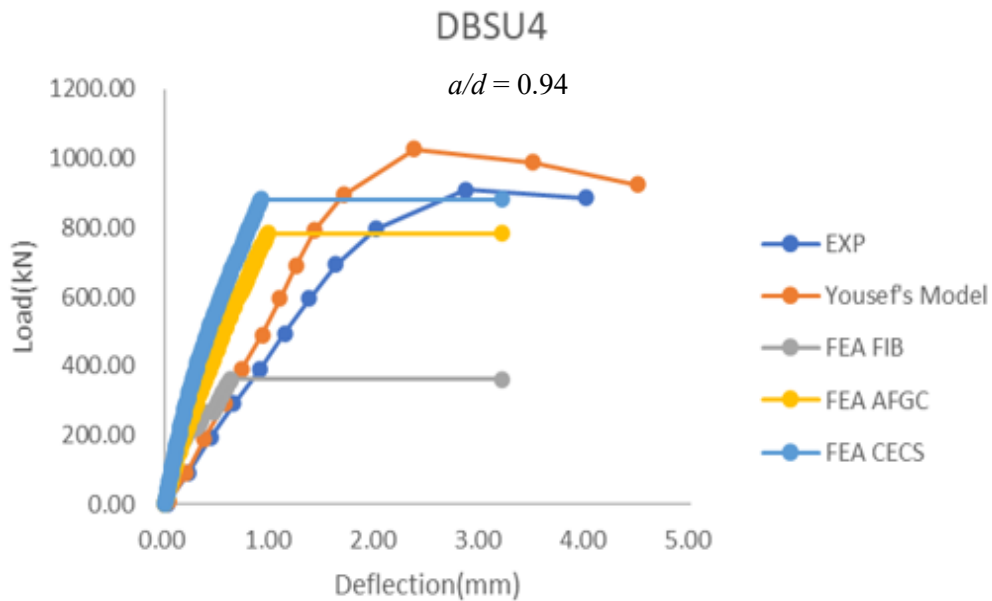


Figure 41. Load-Deflection Curves from FEA (All Codes) and Test Results of Yousef et al. [37].

Table 23. Peak Loads from FEA and Test Results of Yousef et al. [37].

Beam	F_{EXP} (kN)	F_{FEA} (kN)			
		<i>fib</i> Code	AFGC Code	CECS Code	Yousef's Model
DBSU2(RPC)	1082.62	364	1220.67	1078	919.94
DBSU4(RPC)	909.26	361	784	882	988.22
Beam		F_{FEA}/F_{EXP} (kN)			
		<i>fib</i> Code	AFGC Code	CECS Code	Yousef's Model
DBSU2(RPC)		0.34	1.13	1.00	0.85
DBSU4(RPC)		0.4	0.86	0.97	1.09
Mean value		0.37	0.99	0.98	0.97
Coefficient of variation		0.08	0.13	0.01	0.12

Cracking and Failure Mode

Figure 42 depicts the cracking and failure of all beams. In the experimental results, all beams are shear compression failure [39]. The stress distribution from the FEA seems to match the experimental results.

The vertical compressive stress caused by the load minimizes the likelihood of additional tension cracks, while the compressive stress above the reaction location prevents bond splitting and diagonal cracking along the steel. In shorter shear spans, a high shear may initiate a 45° crack across the neutral axis before a flexural crack emerges. A crack of this sort concentrates the shear resistance in a small area and creates

rising stress levels. This tends to be self-perpetuating until halted by the load or reaction. Regardless of the cause, a compression failure eventually occurs next to the load.

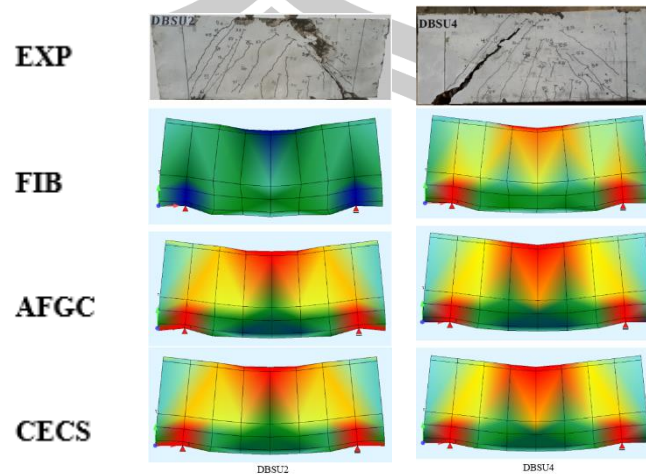


Figure 42. Crack Patterns from FEA (All Codes) and Test Results of Yousef et al. [37].

The crack width corresponding to the peak load of each beam was also obtained from the FEA as listed in Table 24. It can be observed that both AFGC and CECS codes seem to give a similar crack width for each beam but the *fib* code give a lower crack width due to the lower peak load.

Table 24. Crack Width at Peak Load from FEA Results of Yousef et al. [37].

Beam	Crack width (mm)		
	<i>fib</i> Code	AFGC Code	CECS Code
DBSU2	0.55	1.43	1.00
DBSU4	0.63	0.98	0.92

4.1.2.4 Conclusions

In conclusion, the validity of the stress-strain model of concrete, as per the *fib* model code 2010 and AFGC code and CECS code, was evaluated in simulating the behavior of RPC deep beam in comparison to NSC and HSC deep beams. Based on the study results, the following conclusions can be drawn:

1. The *fib* model code 2010 demonstrates the capability to good predict the loading capacity of NSC deep beams about 0.37 times. However, it significantly underestimates the loading capacity of RPC deep beam, providing conservative predictions.

2. The AFGC code model and CECS code model demonstrates the capability to accurately predict the loading capacity of RPC deep beams with an error margin of less than 3%. But both of them can't estimate the loading capacity of NSC deep beams.

4.1.3 RPC Deep Beams Tested by Li et al. [38]

All RPC deep beams tested by Li et al. [38] that were investigated in this study used the same type of rebar with the properties listed in Table 25. The stress-strain points were calculated using the concept described in Section 3.1.4. Figure 43 shows the obtained curve. The model incorporated the Poisson's ratio values of 0.3 for steel rebar.

Table 25. Parameters for Stress-Strain Models of Steel Rebar.

Parameter	Value
f_y (MPa)	500
E_s (GPa)	200

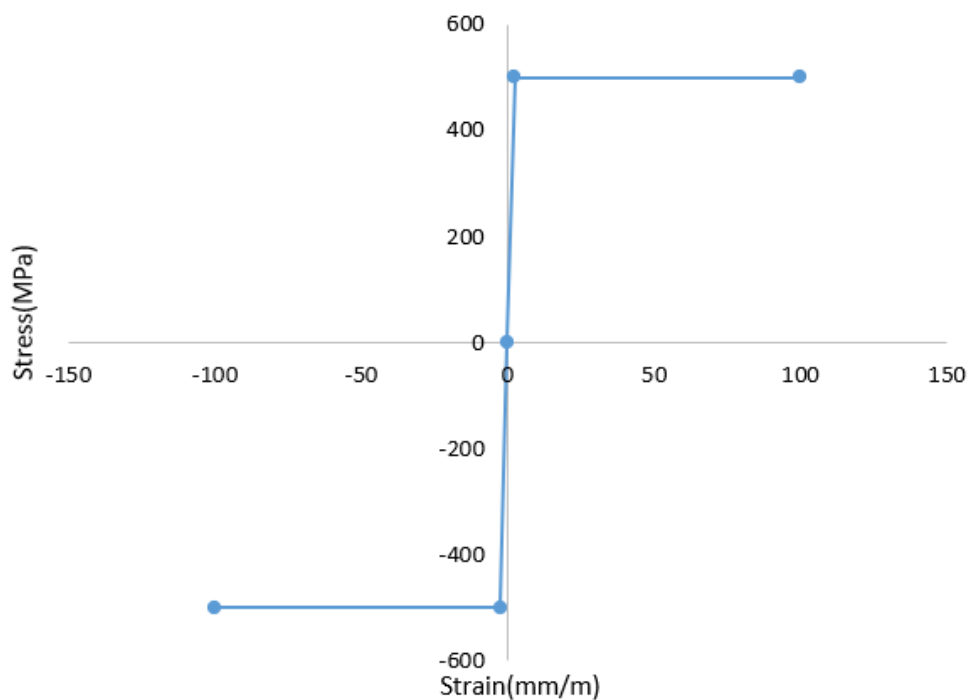


Figure 43. Stress-Strain Curves for Rebar Used in FEA.

4.1.3.1 Stress-strain curves of concrete

The concrete properties provide by Li et al. [38] are compressive strength. To be able to obtain the stress-stress curve some properties were determined using the equations provided by the code which are generally based on the compressive strength.

fib 2010 code

The stress-strain points for concrete in compression and tension zones were calculated using the parameters listed in Table 26 and the concept described in Section 3.1.1. It should be noted that all concrete parameters are dependent on the concrete grade, therefore, the concrete grade is C120. It is worth noting that the input required by the *fib* 2010 code is only the test value of compressive strength.

AFGC Code

The stress-strain points for concrete in compression and tension zones were calculated using the parameters listed in Table 26 and the concept described in Section 3.1.2. In AFGC code, the load factor for RPC under tension γ_{bf} take 1.3 and the Poisson's ratio ν take 0.19 and the concrete tensile strength (f_t) take 9.7 MPa. The test values of concrete compressive strength were used in the model. However, the code does not provide the equation to calculate the concrete elastic modulus, therefore, the values obtained from the *fib* code were also used in the models using the AFGC code.

CECS Code

The stress-strain points for concrete in compression and tension zones were calculated using the parameters listed in Table 26 and the concept described in Section 3.1.3. In CECS code, the key parameters needed are the concrete compressive strength, the steel fiber volume ratio, the steel fiber length, and the equivalent diameter of steel fiber. The Poisson's ratio ν take 0.2 as suggested by the code. It should be noted that the rest parameters can be determined from the compressive strength using the equations or the values in the table provided by the code, anyway, the obtained values are very close to each other. The values in Table 26 are obtained from the table provided by the code.

The obtained stress-strain curves in compression and tension for concrete are illustrated in Figure 44. The stress-strain points were directly inputted into the program.

Table 26. Parameters for Stress-Strain Models of Concrete.

Code	Parameters	Value
FIB	<i>Compression</i>	
	f'_c (MPa)	117.2
	E_c (GPa)	48.8
	k	1.18
	$e_{c,lim}$ (mm/m)	3.0
	e_{cI} (mm/m)	2.75
	<i>Tension</i>	
	f_t (MPa)	5.39
	e_{tI} (mm/m)	1.08

Code	Parameters	Value
AFGC	<i>Compression</i>	
	f'_c (MPa)	117.2
	E_c (MPa)	42.9
	ϵ_{bc} (mm/m)	2.73
	ϵ_u (mm/m)	5.20
	<i>Tension</i>	
	f_t (MPa)	9.7
	ϵ_e (mm/m)	1.97
	$\epsilon_{u1\%}$ (mm/m)	15.17
	ϵ_{lim} (mm/m)	19.50
CECS	<i>Compression</i>	
	f'_c (MPa)	117.2
	ϵ_0 (mm/m)	2.59
	ϵ_{cu} (mm/m)	4.15
	<i>Tension</i>	
	λ	1.3
	f_t (MPa)	6.7
	E_c (MPa)	42.59
	ϵ_{t0} (mm/m)	0.16
	ϵ_{tp} (mm/m)	1.89
ϵ_{tu} (mm/m)	3.88	



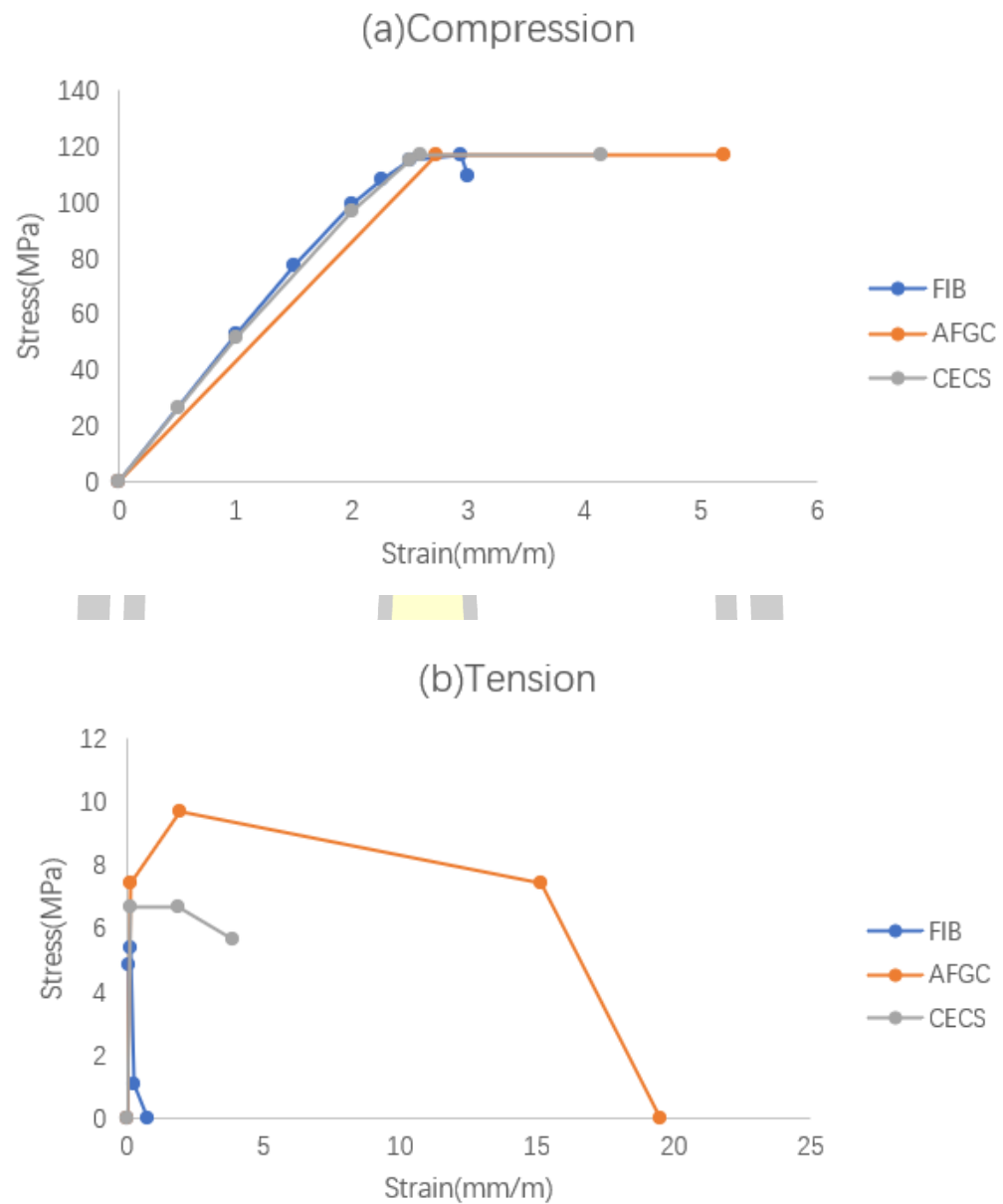


Figure 44. Stress-Strain Curves for Concrete Used in FEA (All Codes).

4.1.3.2 Structural Model

The deep beams studied by Li et al. [38]. The RPC deep beams with high-strength steel bars are designed, and their section sizes are all $B \times h = 150\text{mm} \times 250\text{mm}$, beam length is 2200mm and beam span is 2000mm. The static loading method is adopted in this test, and two equivalent and synchronous concentrated forces are obtained by distributing the symmetrical position of the steel beam on the test beam. See Figure 45 for details. Parameters of each test beam are shown in Table 27.



Figure 45. Loading Device Diagram (Li et al. [38]).

Table 27. Main Design Parameters of The Test Beams (Li et al. [38]).

Specimen number	Shear span ratio λ	Longitudinal reinforcement	Longitudinal reinforcement ratio (%)	Effective height of concrete section(mm)
L1-1(RPC)	1.51	4D25	6.58	205
L1-2(RPC)	2.26	4D25	6.58	205
L1-3(RPC)	3.02	4D25	6.58	205
L2-1(RPC)	2.26	3D25	4.43	221.5
L2-2(RPC)	2.26	5D25	8.04	199

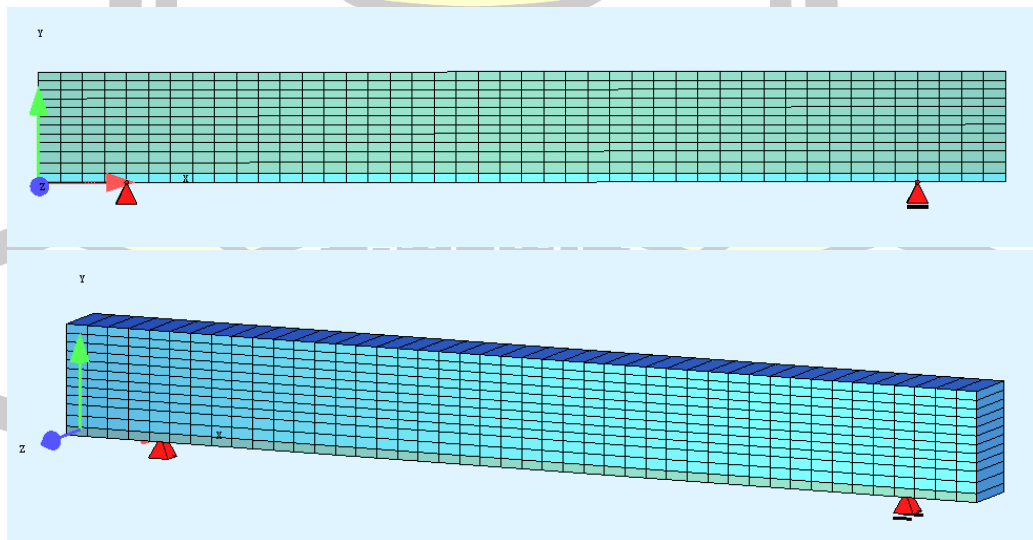


Figure 46. Typical FE Model of The Beams.

Figure 46 depicts the typical FE model employed in this study. The models used four-node shell or QUAD elements displaying plate structural behavior according to the

Reissner-Mindlin theory. The QUAD elements integrated a layer material model to aid in cracked concrete analysis and contained. Discrete Kirchhoff conditions as well as an optional penalty term to consider shear deformation. The nonlinear analysis was executed through an incremental solution technique founded on the modified Newton Raphson method.

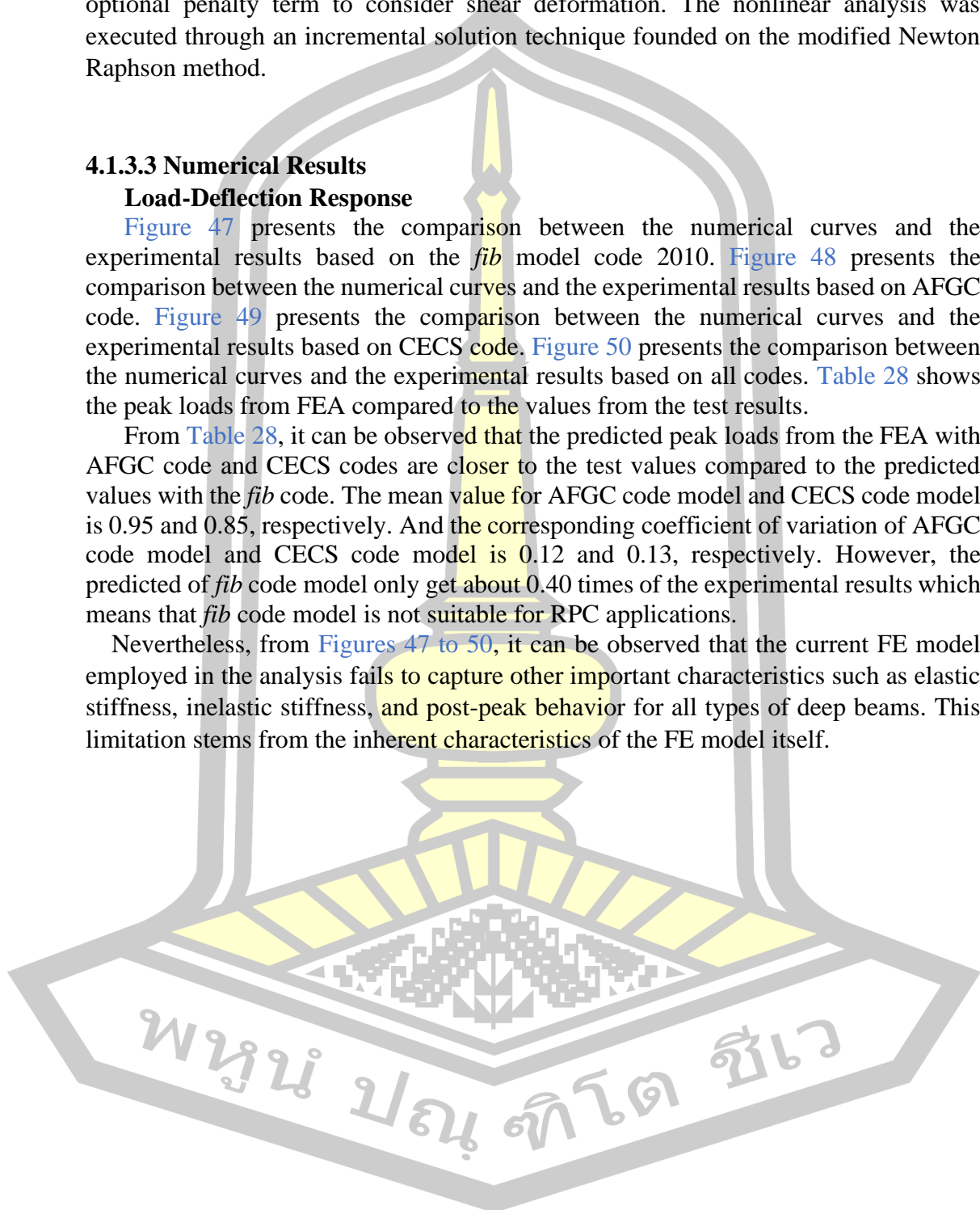
4.1.3.3 Numerical Results

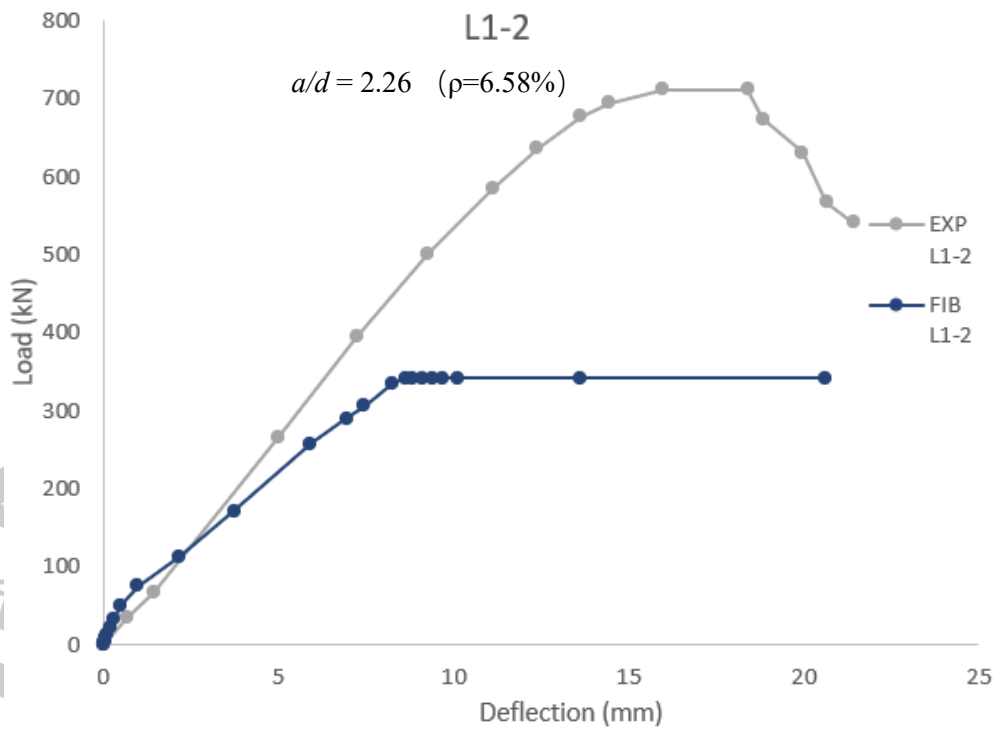
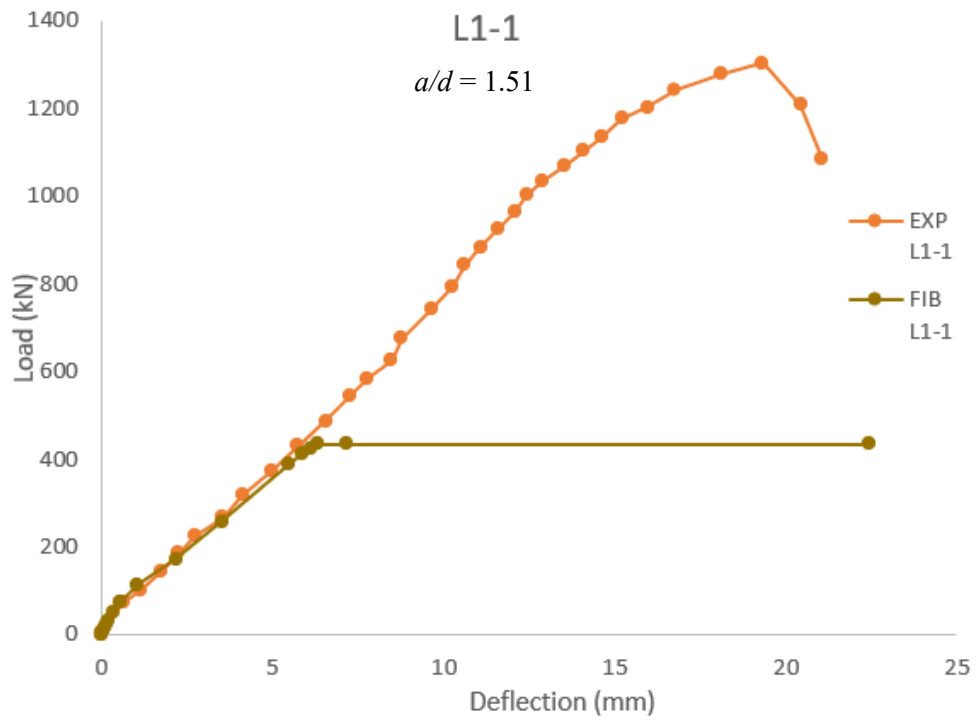
Load-Deflection Response

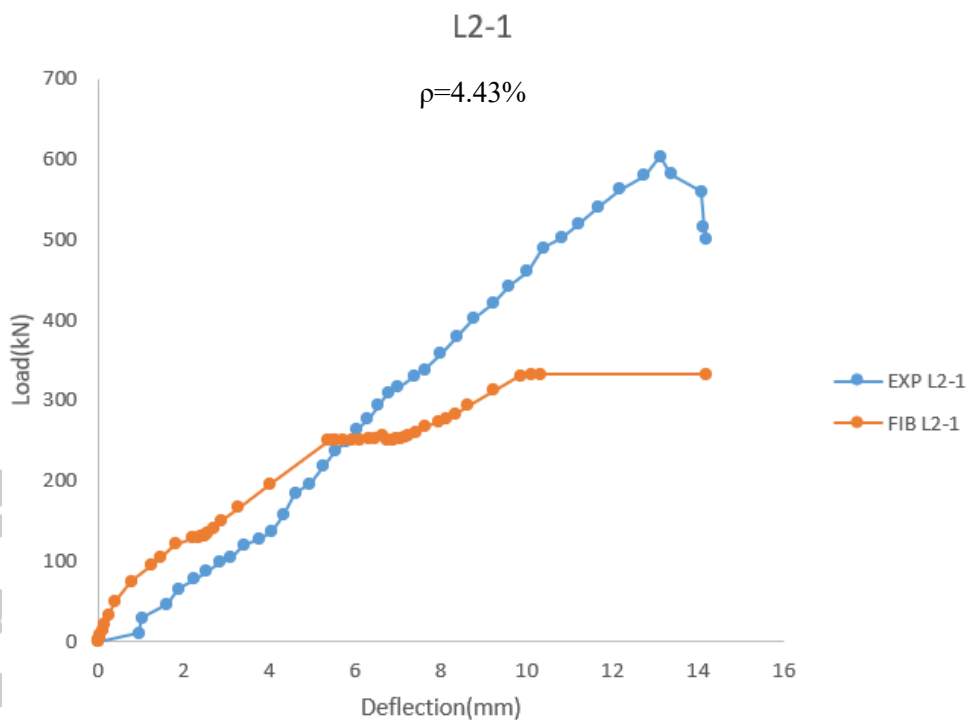
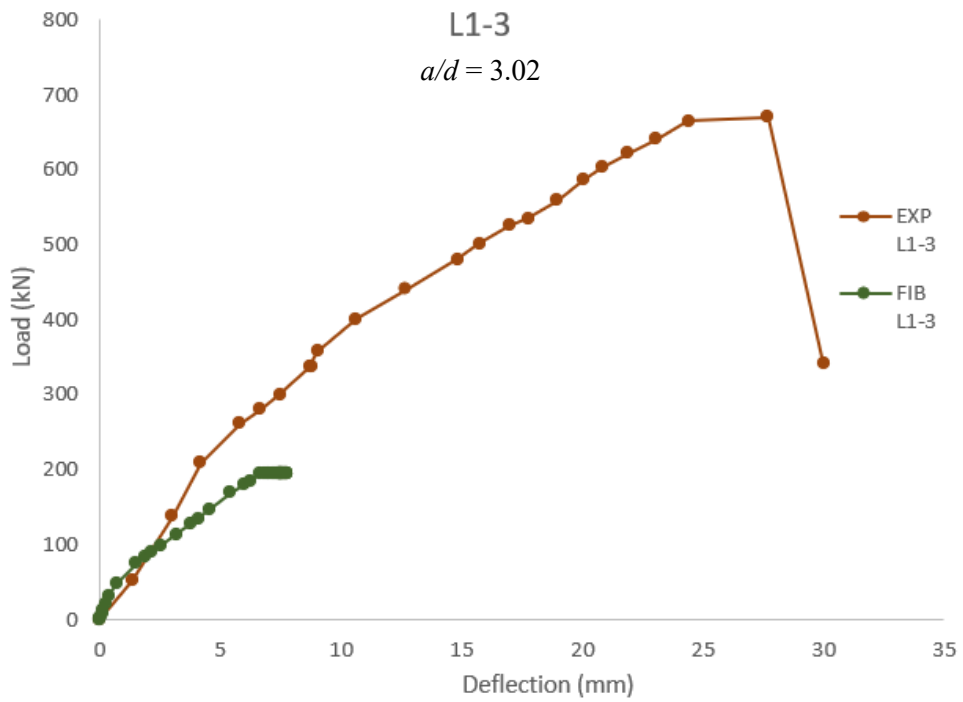
Figure 47 presents the comparison between the numerical curves and the experimental results based on the *fib* model code 2010. Figure 48 presents the comparison between the numerical curves and the experimental results based on AFGC code. Figure 49 presents the comparison between the numerical curves and the experimental results based on CECS code. Figure 50 presents the comparison between the numerical curves and the experimental results based on all codes. Table 28 shows the peak loads from FEA compared to the values from the test results.

From Table 28, it can be observed that the predicted peak loads from the FEA with AFGC code and CECS codes are closer to the test values compared to the predicted values with the *fib* code. The mean value for AFGC code model and CECS code model is 0.95 and 0.85, respectively. And the corresponding coefficient of variation of AFGC code model and CECS code model is 0.12 and 0.13, respectively. However, the predicted of *fib* code model only get about 0.40 times of the experimental results which means that *fib* code model is not suitable for RPC applications.

Nevertheless, from Figures 47 to 50, it can be observed that the current FE model employed in the analysis fails to capture other important characteristics such as elastic stiffness, inelastic stiffness, and post-peak behavior for all types of deep beams. This limitation stems from the inherent characteristics of the FE model itself.







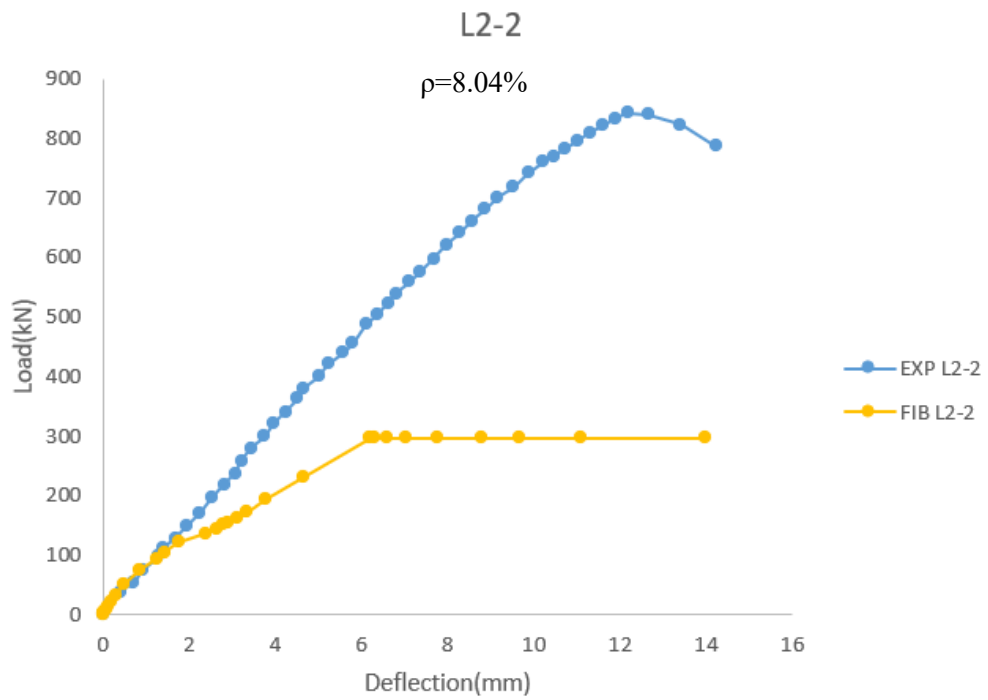
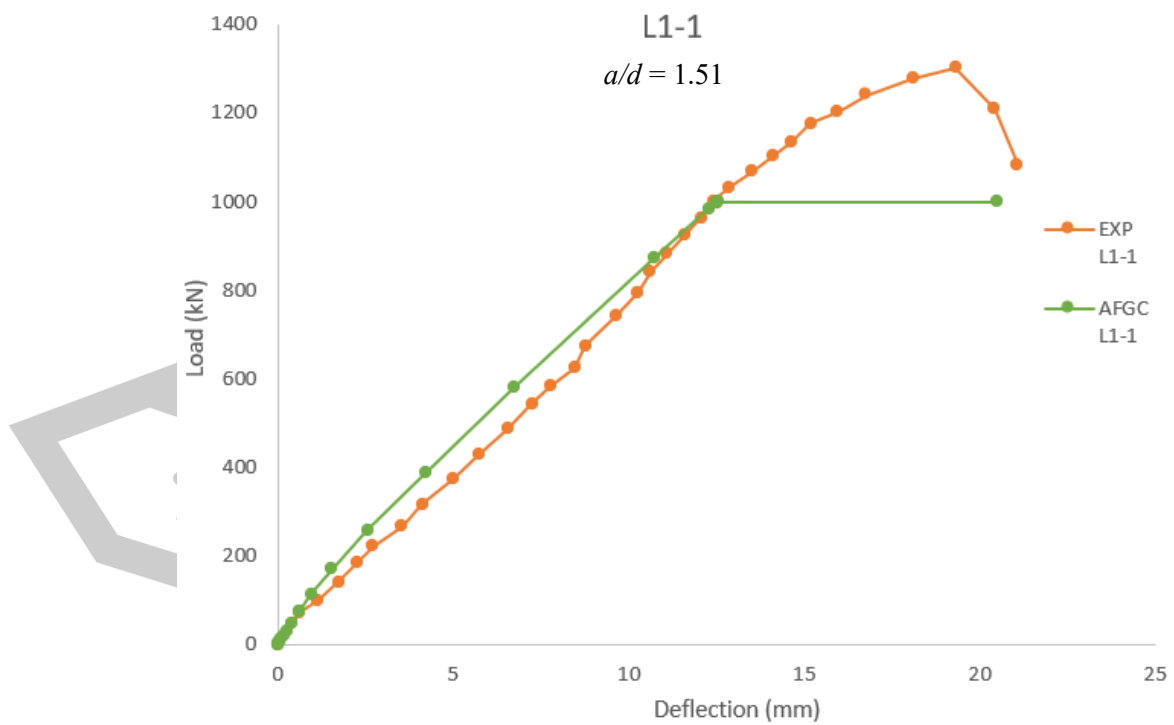
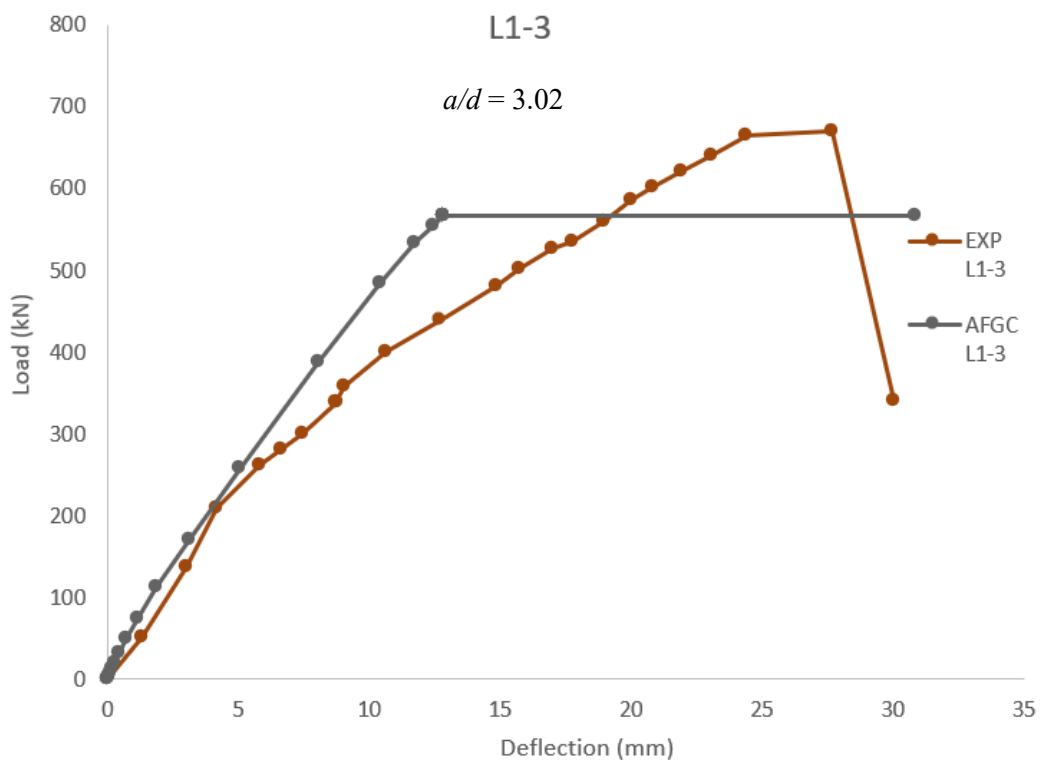
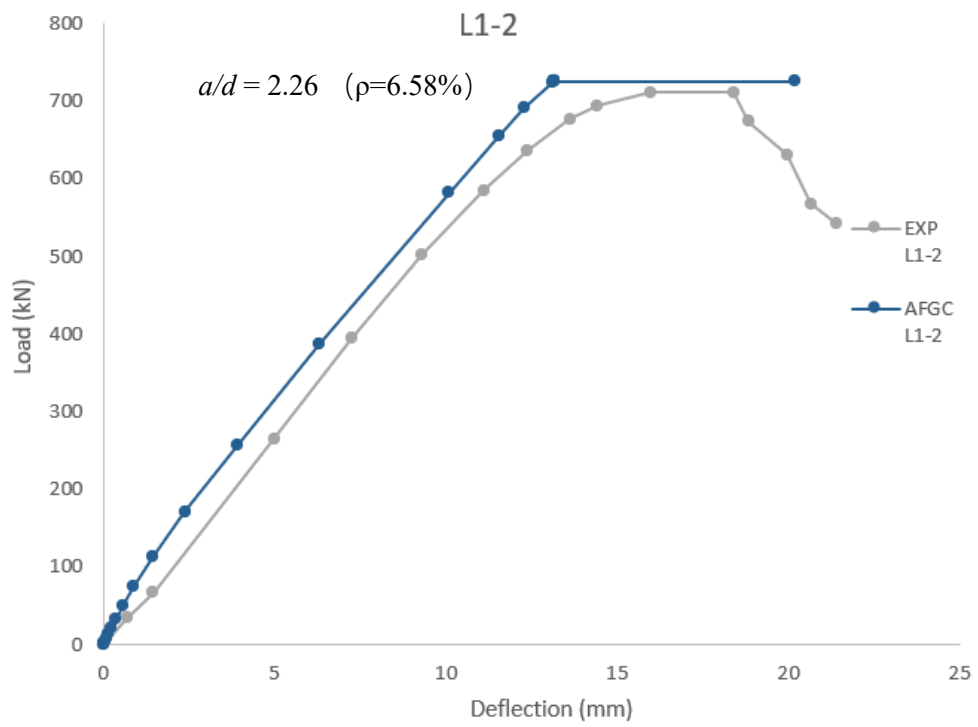


Figure 47. Load-Deflection Curves from Numerical (*fib* Model Code 2010) and Test Results of Li et al. [38].





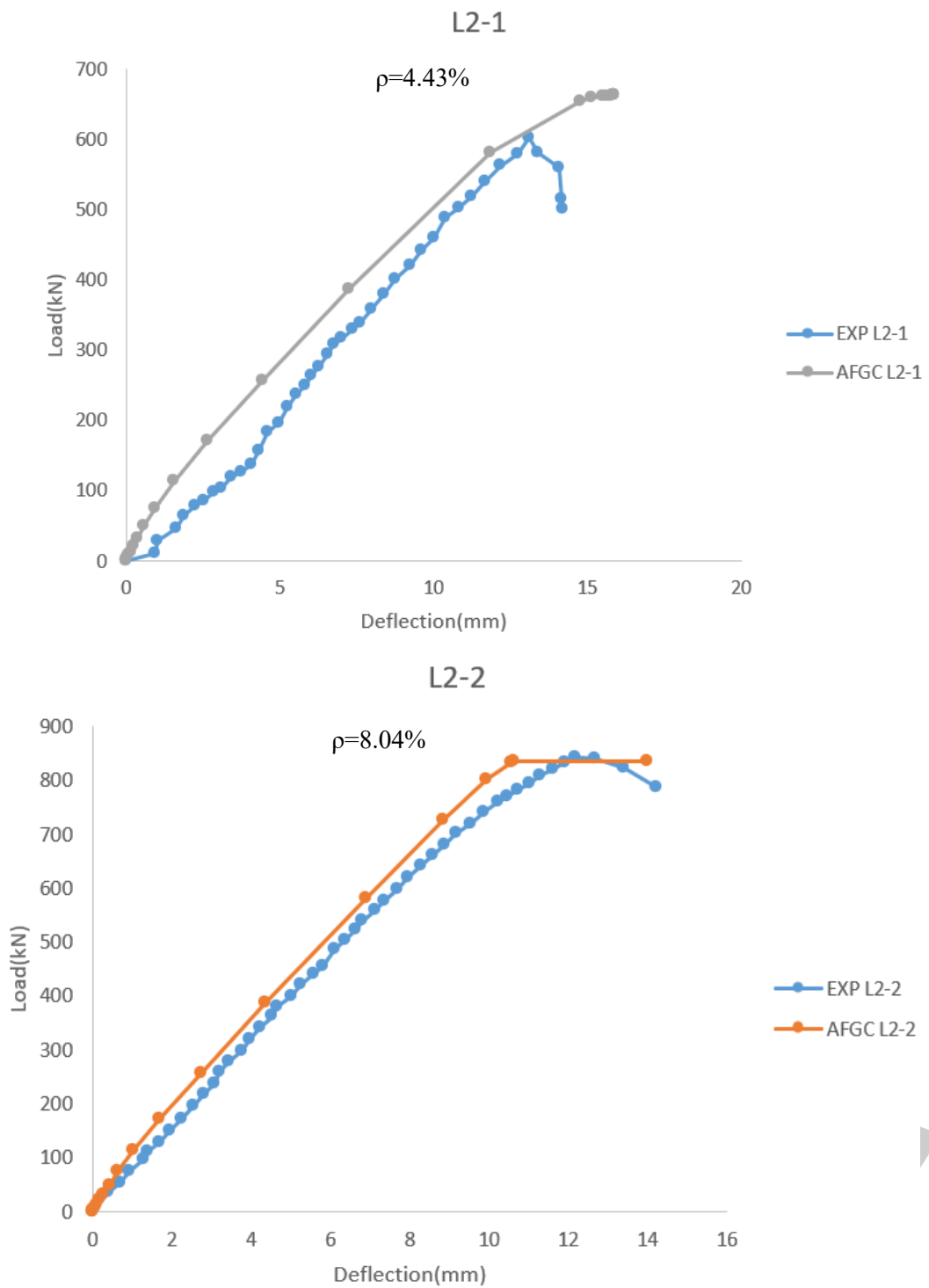
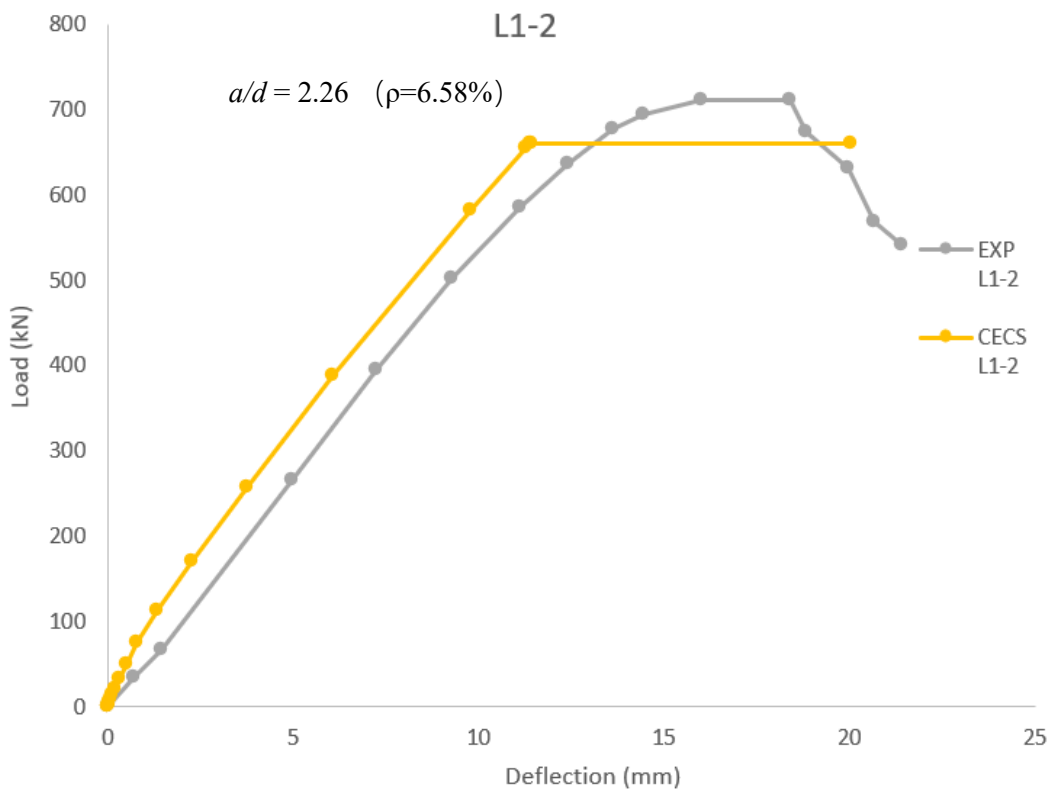
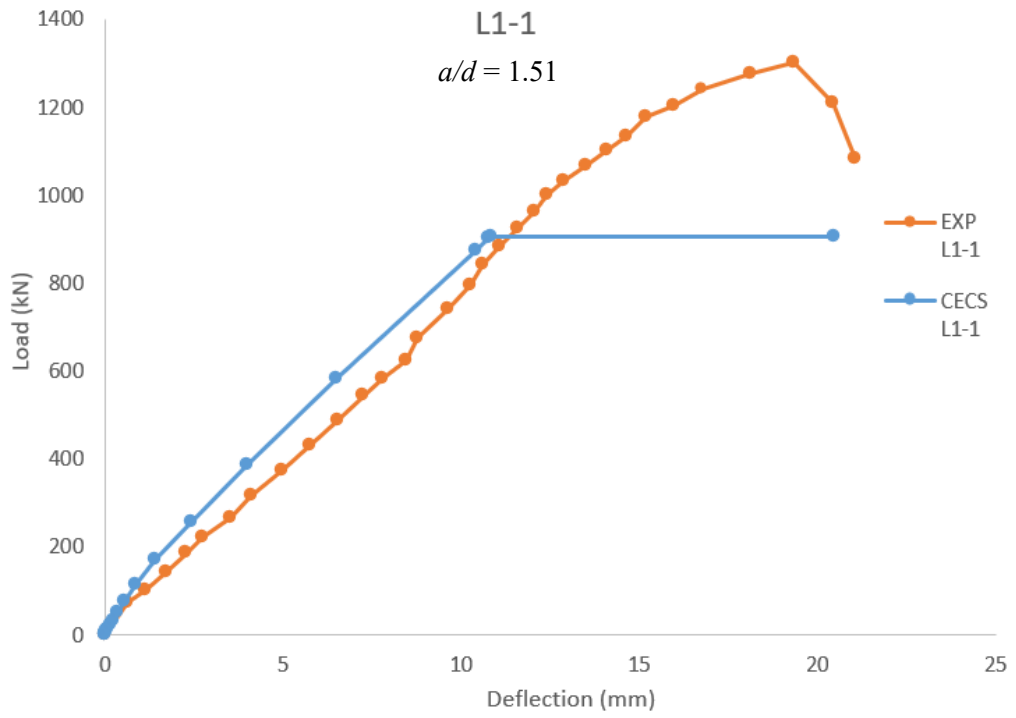
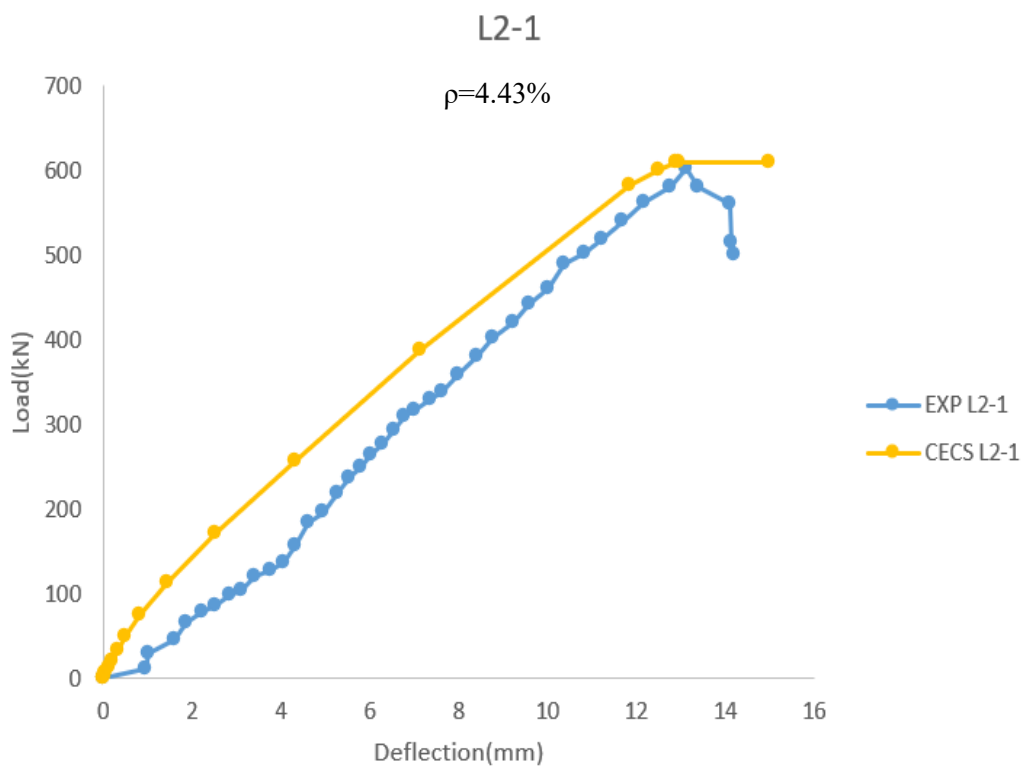
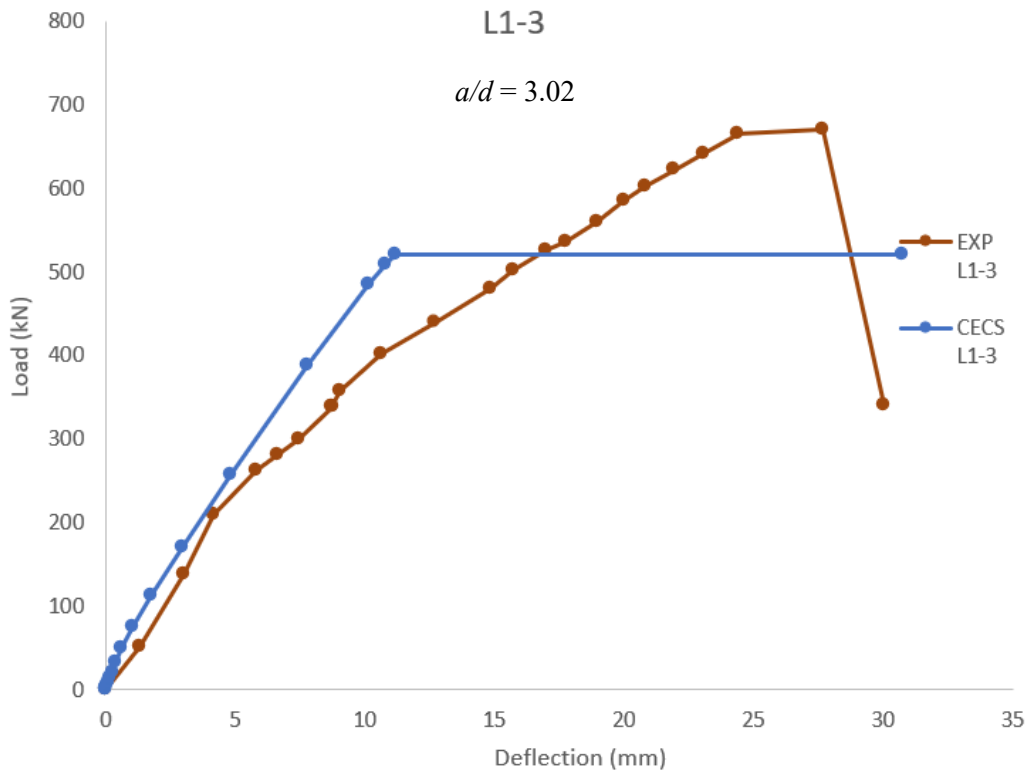


Figure 48. Load-Deflection Curves from Numerical (AFGC Code) and Test Results of Li et al. [38].





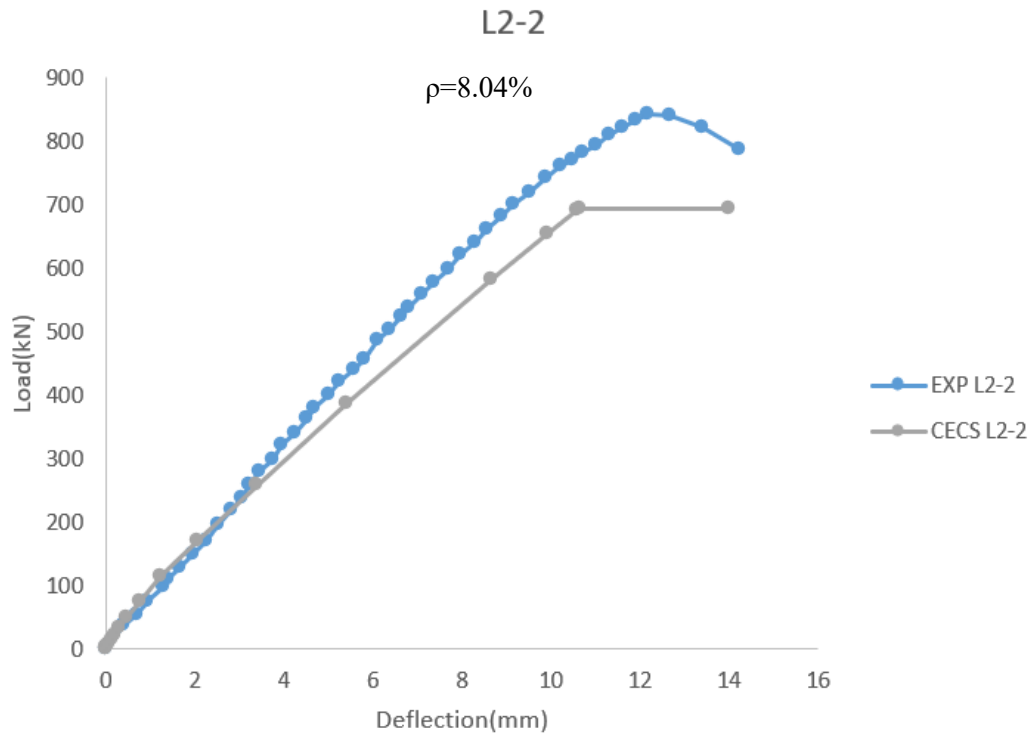
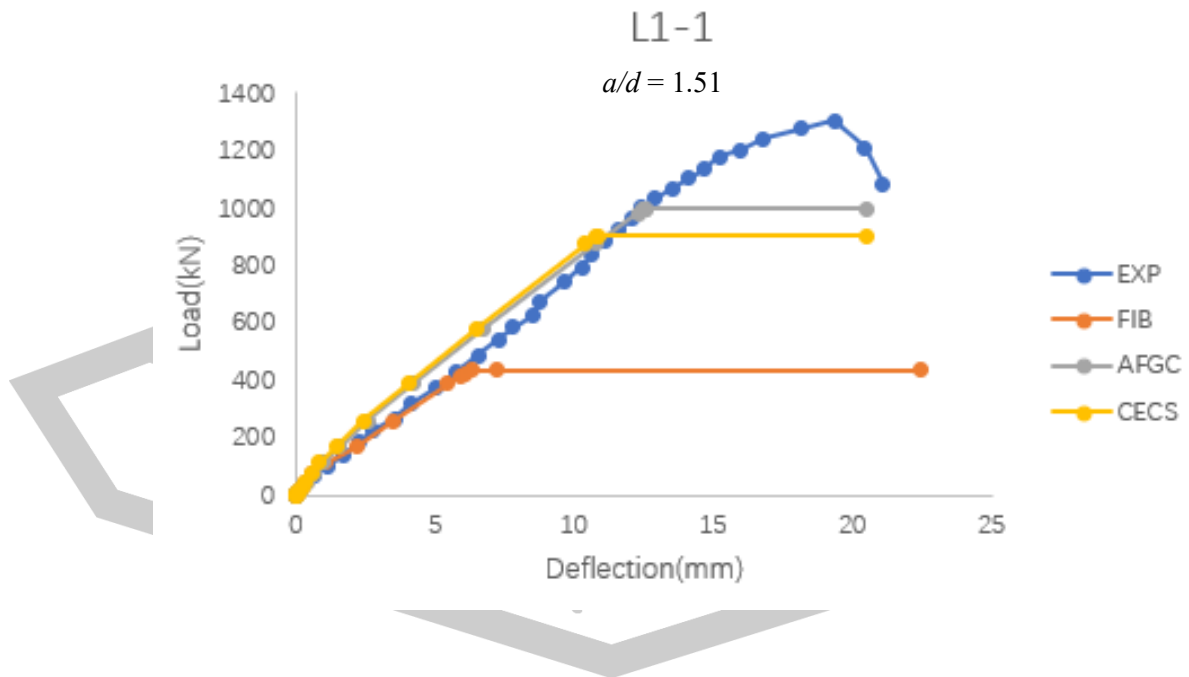
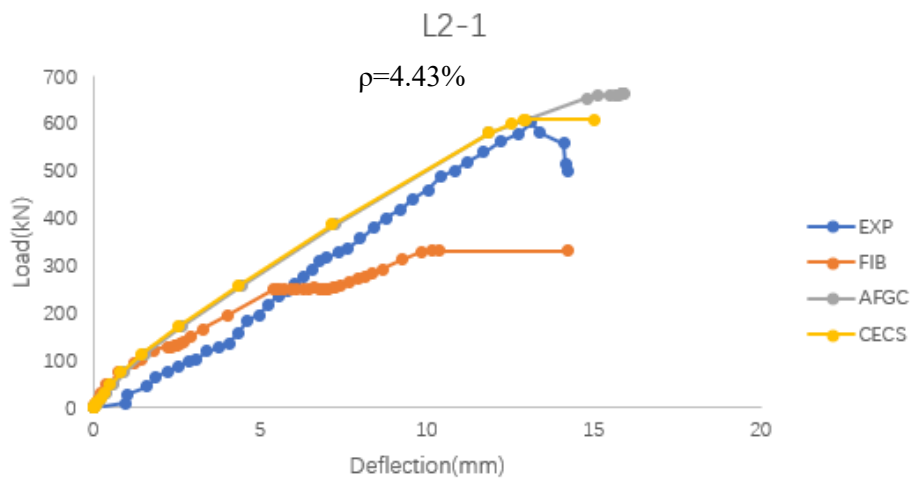
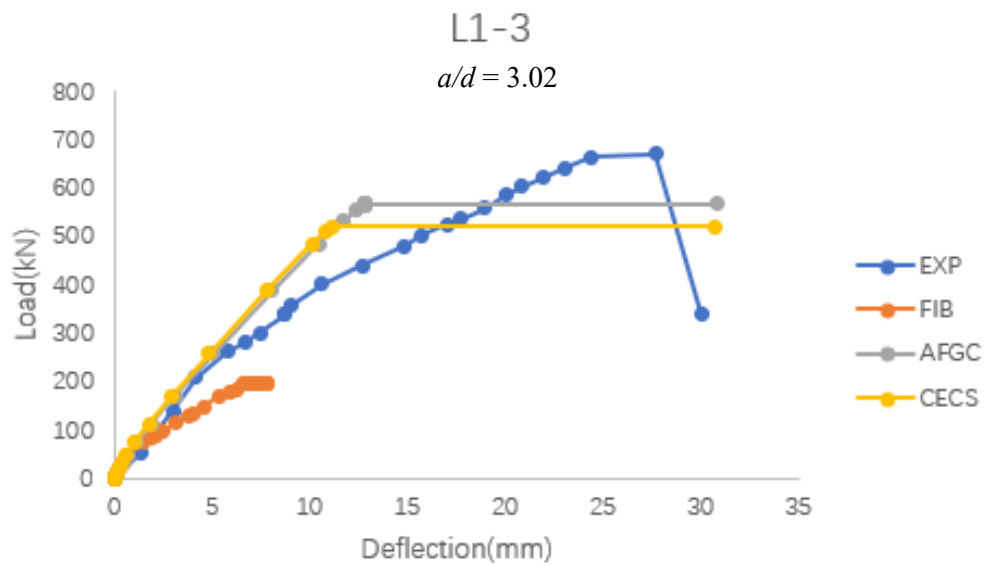
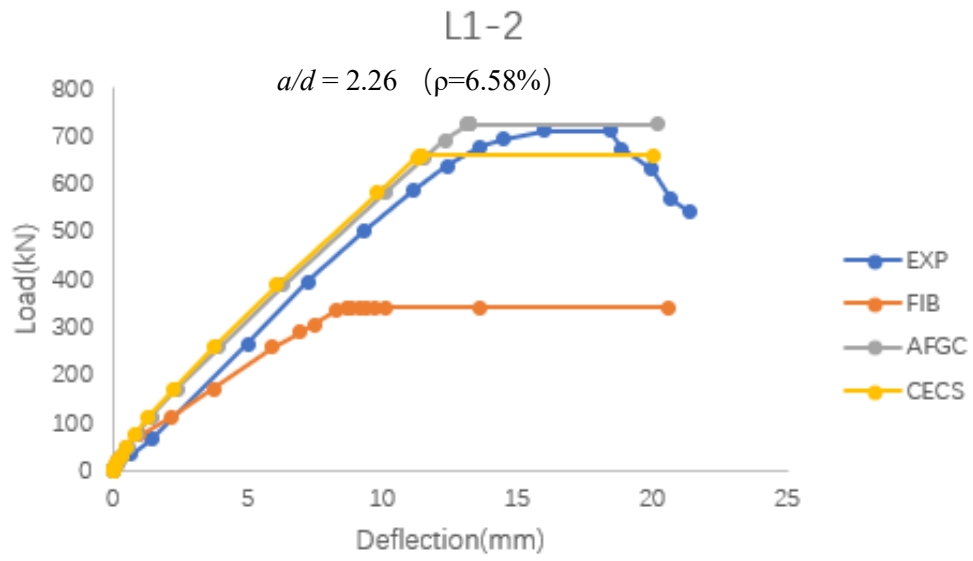


Figure 49. Load-Deflection Curves from Numerical (CECS Code) and Test Results of Li et al. [38].





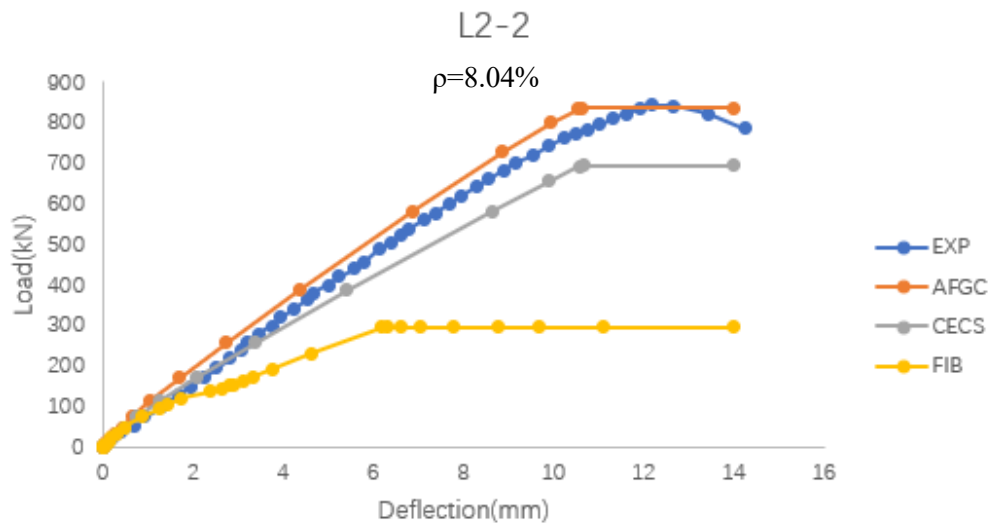


Figure 50. Load-Deflection Curves from FEA (All Codes) and Test Results of Li et al. [38].

Table 28. Peak Loads from FEA and Test Results of Li et al. [38].

Beam	F_{EXP} (kN)	F_{FEA} (kN)			F_{FEA}/F_{EXP}		
		<i>fib</i> Code	AFGC Code	CECS Code	<i>fib</i> Code	AFGC Code	CECS Code
L1-1(RPC)	1302.69	434.68	999.00	904.58	0.33	0.77	0.69
L1-2(RPC)	711.52	341.91	725.70	659.69	0.48	1.02	0.93
L1-3(RPC)	669.75	194.37	566.60	521.04	0.29	0.85	0.78
L2-1(RPC)	501.22	332.21	662.86	610.25	0.55	1.09	1.01
L2-2(RPC)	786.87	296.00	835.70	693.39	0.35	0.99	0.83
Mean value					0.40	0.95	0.85
Coefficient of variation					0.24	0.12	0.13

Cracking and Failure Mode

Figure 51 depicts the cracking and failure of all beams. The experimental findings show that all the beams failed due to diagonal crack. The stress distribution from the FEA seems to match the experimental results. Cracks generally formed at regions where tensile stresses exceeded the specified strength in the concrete beams. The experimental results revealed two types of cracks [39]:

1) Flexural cracks resulting from flexural tensile stresses in the cross-sectional region of the beam below the neutral axis for positive bending.

2) Shear cracks form as diagonal cracks begin at the last flexural crack and gradually turn into increasingly inclined cracks under shear loading. These cracks do not immediately lead to failure as they encounter resistance while moving into the compression zone, becoming flatter and eventually stopping at a certain point. The

tension crack gradually extends at a flat slope until sudden failure occurs due to the inclined or principal tensile stresses in the combined bending and shear region.

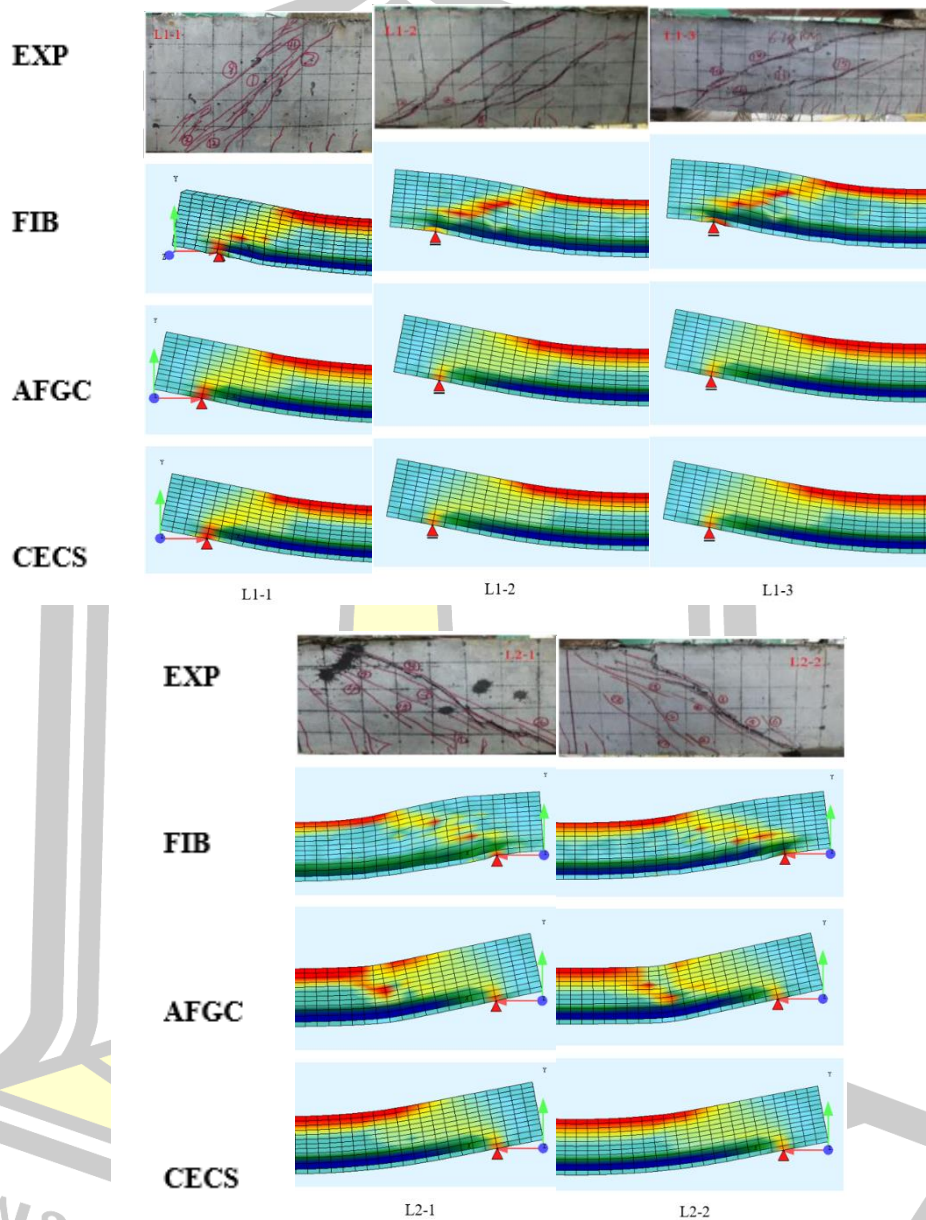


Figure 51. Crack Patterns from FEA (All Codes) and Test Results of Li et al. [38].

The crack width corresponding to the peak load of each beam was also obtained from the FEA as listed in Table 29. It can be observed that both AFGC and CECS codes seem to give a similar crack width for each beam but the *fib* code give a lower crack width due to the lower peak load.

Table 29. Crack Width at Peak Load from FEA Results of Li et al. [38].

Beam	Crack width (mm)		
	<i>fib</i> Code	AFGC Code	CECS Code
L1-1	0.11	0.60	0.69
L1-2	0.14	0.62	0.48
L1-3	0.12	0.55	0.57
L2-1	0.19	0.28	0.63
L2-2	0.14	0.28	0.49

4.1.3.4 Conclusions

In conclusion, the validity of the stress-strain model of concrete, as per the *fib* model code 2010 and AFGC code and CECS code, was evaluated in simulating the behavior of RPC deep beam in comparison to NSC and HSC deep beams. Based on the study results, the following conclusions can be drawn:

1. The *fib* model code 2010 demonstrates the capability to good predict the loading capacity of NSC deep beams about 0.40 times. However, it significantly underestimates the loading capacity of RPC deep beam, providing conservative predictions.

2. The AFGC code model and CECS code model demonstrates the capability to accurately predict the loading capacity of RPC deep beams. But both of them can't estimate the loading capacity of NSC deep beams.

4.1.4 Main Parameter Effects on FEA Load-Deflection Curve

In this study, different main parameters affecting deep beam behavior were investigated and varied including concrete compressive strength (f'_c), shear span-to-effective depth ratio (a/d), main reinforcement ratio (ρ). Thus, the validity of the stress-strain model of concrete, as per the *fib* model code 2010 and AFGC code and CECS code, was evaluated in simulating the behavior of RPC deep beam under the different parameters.

The Load-Deflection Curves from FEA (All codes) and Test Results with different concrete compressive strength and shear span-to-effective depth ratio and main reinforcement ratio are shown in Figure 52 and Figure 53 and Figure 54, respectively.

From Figure 52 to Figure 54, we can draw the following conclusions:

- 1) When the concrete compressive strength increases, the load capacity of the RPC deep beams also increases. The trend of finite element analysis results is consistent with the experimental results and the finite element analysis results can capture structural behavior of RPC deep beams.
- 2) When the shear span-to-effective depth ratio increases, the load capacity of the RPC deep beams also decreases. The trend of finite element analysis results is

consistent with the experimental results and the finite element analysis results can capture structural behavior of RPC deep beams

- 3) When the main reinforcement ratio increases, the load capacity of the RPC deep beams also increases. The trend of finite element analysis results is consistent with the experimental results and the finite element analysis results can capture structural behavior of RPC deep beams.
- 4) The AFGC and CECS code models are more adequate for capturing the unique characteristics and performance of RPC deep beams. While, the *fib* model code 2010 is not adequate for capturing the unique characteristics and performance of RPC deep beams.

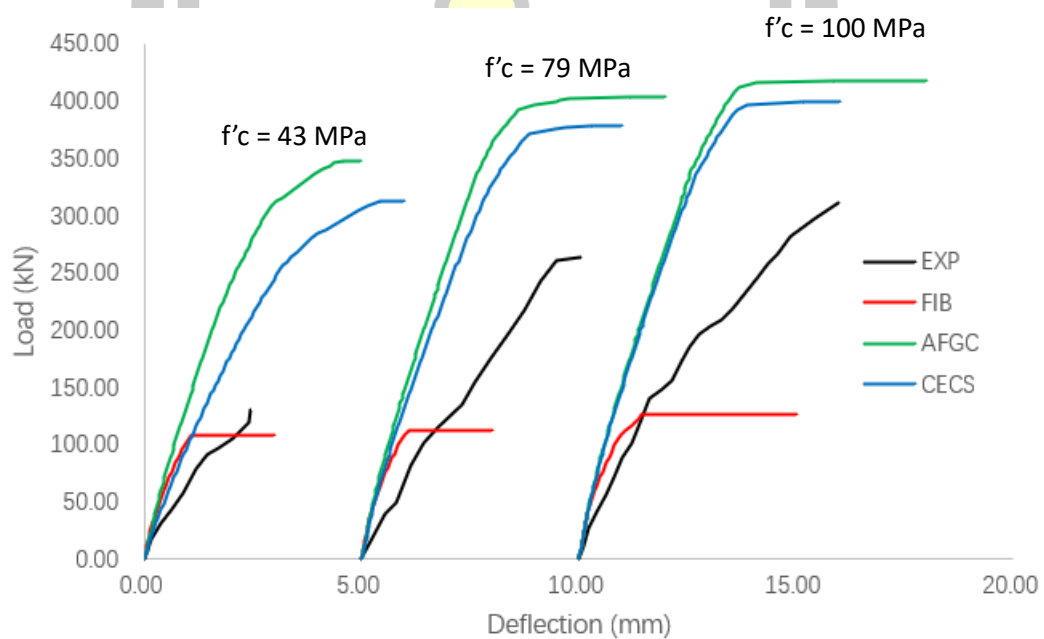


Figure 52. Concrete Compressive Strength Effects on FEA Load-Deflection Curves (All Codes).

พหุ ประถมศึกษา

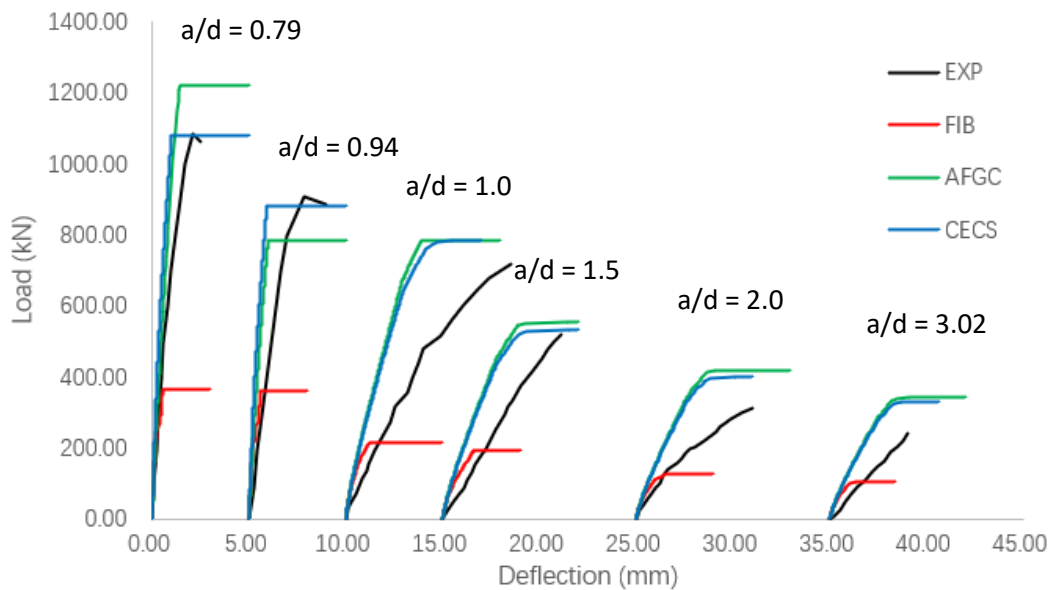


Figure 53. Shear Span-to-Effective Depth Ratio Effects on FEA Load-Deflection Curves (All Codes).

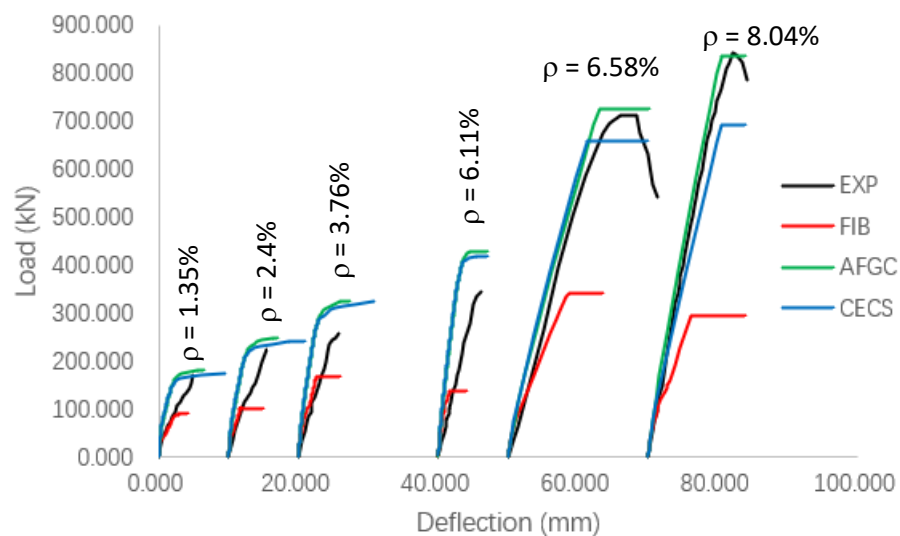


Figure 54. Main Reinforcement Ratio Effects on FEA Load-Deflection Curves (All Codes).

4.2 Shear Strength Prediction Using Strut-and-Tie Model

The strut-and-tie models (STM) according to ACI 318-11 [3], EN 1992-1-1 [35], and NF P 18-710 (AFGC) [33] codes are adopted to predict the shear strength (V) of the tested deep beams. The details are as follows:

4.2.1 Parameters of Deep Beams for STM

According to the details of STM for deep beams given in Section 3.2 and Figure 21, the parameters used for the STM are listed in Table 30.

Table 30. Parameters of Deep Beams Using Strut-and-Tie Model.

Beam	a/d	a (mm)	h (mm)	d (mm)	b (mm)	l_b (mm)	l_a (mm)	f_c (MPa)	f_y (MPa)
G11(NSC)	2.0	334	200	167	100	50	50	43	416
G13(HSC)	2.0	334	200	167	100	50	50	79	416
G14(RPC)	2.0	334	200	167	100	50	50	100	416
G15(RPC)	2.0	334	200	167	100	50	50	119	416
G21(RPC)	1.0	167	200	167	100	50	50	97	416
G22(RPC)	1.5	250	200	167	100	50	50	101	416
G41(RPC)	2.0	334	200	167	100	50	50	122	416
G42(RPC)	2.0	334	200	167	100	50	50	122	416
G43(RPC)	2.0	334	200	167	100	50	50	118	416
DBSU2(RPC)	0.79	276.5	400	350	80	50	50	172.9	491.2
DBSU4(RPC)	0.94	329	400	350	80	50	50	172.9	491.2
L1-1(RPC)	1.5	307.5	250	205	150	50	50	117.2	500

It is obvious that for each beam using different STM codes, the calculation of the ties is the same, the difference in the calculation is the compressive strengths of the struts and of nodal zones. However, the lesser value (the effective compressive strength) will be used for both. The calculated effective compressive strength of struts and nodal zones under different codes is shown in Table 31.

Table 31. The Calculated Effective Compressive Strength of Struts and Nodal Zones for Different Codes.

Beam	a/d	f_c (MPa)	f_{ce} (MPa)		
			ACI Code	EN Code	AFGC Code
G11(NSC)	2.0	43	29.24	36.62	19.87
G13(HSC)	2.0	79	53.72	55.58	24.62
G14(RPC)	2.0	100	68.00	61.71	25.27
G15(RPC)	2.0	119	80.92	64.13	24.78
G21(RPC)	1.0	97	65.96	61.06	25.26
G22(RPC)	1.5	101	68.68	61.91	25.27
G41(RPC)	2.0	122	82.96	64.24	24.62
G42(RPC)	2.0	122	82.96	64.24	24.62
G43(RPC)	2.0	118	80.24	64.08	24.83
DBSU2(RPC)	0.79	172.9	117.57	54.84	18.71
DBSU4(RPC)	0.94	172.9	117.57	54.84	18.71
L1-1(RPC)	1.5	117.2	79.70	64.03	24.87

4.2.2 Calculated and Experimental Shear Strengths

The calculated shear strengths based on different codes are compared with the test results as shown in Table 32.

For RPC deep beams (excluding G11 and G13), it can be observed that with $a/d < 1.0$ (DBSU2 and DBSU4), ACI code can give a good prediction while EN and AFGC codes give lower or conservative shear strength with safety of factor at least = $1/0.60=1.67$ and $=1/0.78=1.28$, respectively. When $a/d = 1.0$ (G21), ACI, EN, and AFGC codes give a conservative shear strength with safety of factor of 1.19, 1.30, and 1.61, respectively. When $a/d > 1.0$ (G14, G15, G41, G42, G43, and L1-1), all codes seem to give more conservative shear strengths.

For HSC deep beam with $a/d > 1.0$ (G13), ACI and EN codes gave an overestimated shear strength, while AFGC code gave an underestimated or conservative shear strength.

For NSC deep beam with $a/d > 1.0$ (G11), all codes gave an overestimated shear strength.

Table 32. Comparison of Calculated and Experimental Shear Strengths of Deep Beams.

Beam	a/d	V_{EXP} (kN)	V_{ACI} (kN)	V_{EN} (kN)	V_{AFGC} (kN)	V_{ACI}/V_{EXP}	V_{EN}/V_{EXP}	V_{AFGC}/V_{EXP}
G11(NSC)	2	65	73.62	92.20	71.08	1.13	1.42	1.09
G13(HSC)	2	132	135.26	139.93	106.62	1.02	1.06	0.81
G14(RPC)	2	155.5	163.85	155.38	124.76	1.05	1.00	0.80
G15(RPC)	2	172.5	163.85	161.48	140.11	0.95	0.94	0.81
G21(RPC)	1	358	299.17	276.93	220.23	0.84	0.77	0.62
G22(RPC)	1.5	260	218.91	205.20	165.33	0.84	0.79	0.64
G41(RPC)	2	85	37.75	37.75	37.75	0.44	0.44	0.44
G42(RPC)	2	112.5	67.11	67.11	67.11	0.60	0.60	0.60
G43(RPC)	2	128.5	104.87	104.87	104.87	0.82	0.82	0.82
DBSU2(RPC)	0.79	530	542.48	293.52	382.05	1.02	0.55	0.72
DBSU4(RPC)	0.94	455	455.91	274.34	357.08	1.00	0.60	0.78
L1-1(RPC)	1.5	656	479.78	385.48	331.60	0.73	0.59	0.51
Mean value						0.87	0.80	0.72
Standard deviation						0.19	0.26	0.17
Coefficient of variation						0.22	0.33	0.23

4.2.3 Conclusions for Shear Strength Predictions

In conclusion, the validities of the strut-and-tie models, as per ACI code and EN code and AFGC codes, were evaluated in predicting the shear strength of RPC deep

beams in comparison to NSC and HSC deep beams. Based on the study results, the following conclusions can be drawn:

- 1) For RPC deep beams, when $a/d < 1.0$, ACI code can give a very good prediction while EN and AFGC codes give conservative shear strength; When $a/d \geq 1.0$, all codes give conservative shear strength.
- 2) For HSC deep beam with $a/d > 1.0$, ACI and EN codes give overestimated shear strength, while AFGC code give conservative shear strength.
- 3) For NSC deep beam with $a/d > 1.0$, all codes give overestimated shear strength.

4.3 Comparison of the FEA and STMs Peak Loads

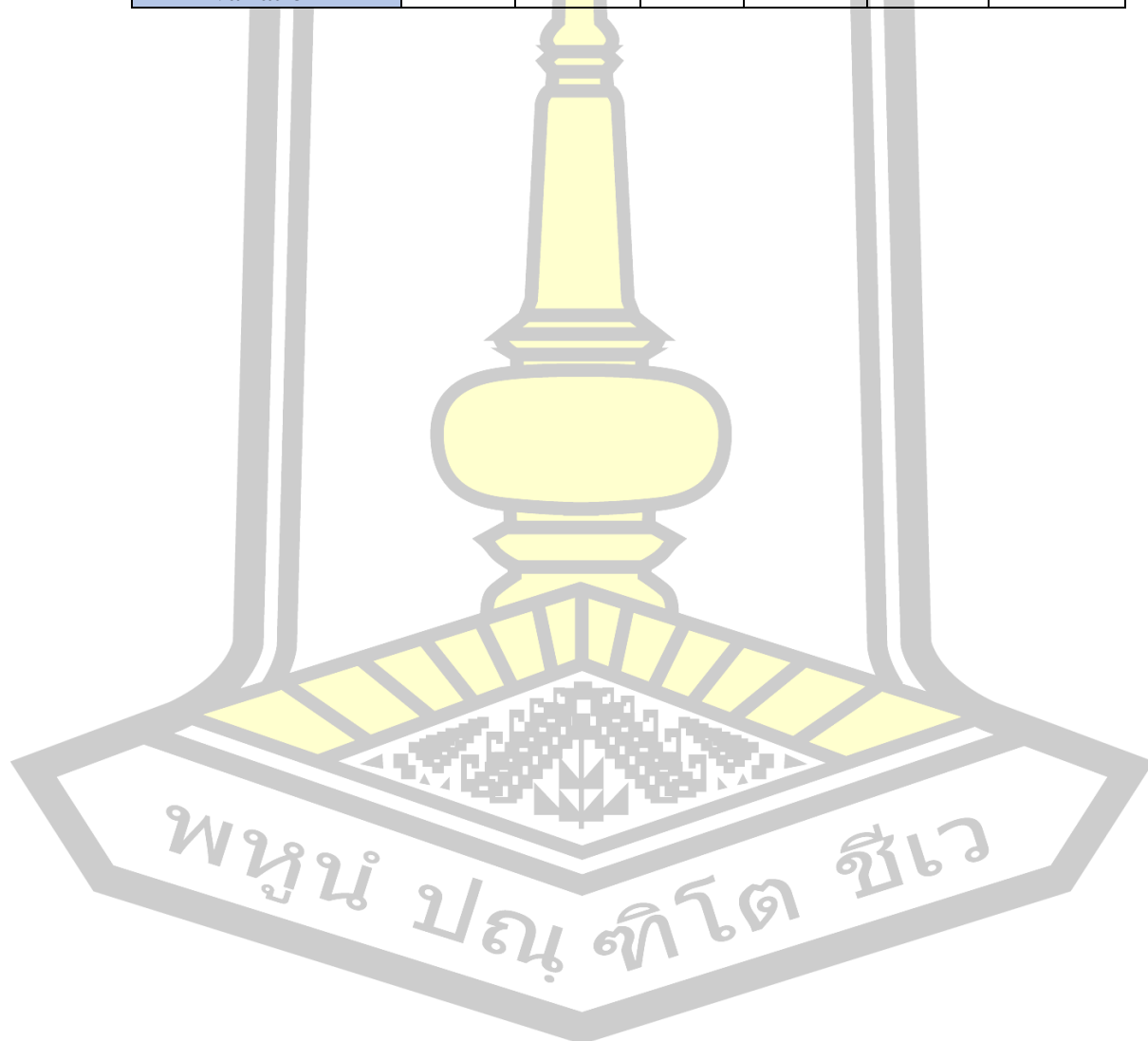
The peak loads of RPC deep beams obtained from FEA and STMs as [Table 33](#) shows. From [Table 33](#), we can draw the following conclusions:

- 1) The *fib* model code 2010 is not adequate for capturing the unique characteristics and performance of RPC deep beams. The peak loads of finite element results based on the *fib* model code 2010 are only 0.42 times of experimental results with the coefficient of variation is 0.24. The *fib* model code 2010 significantly underestimates the loading capacity of RPC deep beam, providing conservative predictions.
- 2) The AFGC and CECS code models are very adequate for capturing the unique characteristics and performance of RPC deep beams. The peak loads of finite element results based on AFGC code are 1.09 times of experimental results with the coefficient of variation is 0.15. And the peak loads of finite element results based on CECS code are 1.07 times of experimental results with the coefficient of variation is 0.15.
- 3) For strut-and-tie models, the prediction of peak loads based on ACI code are 0.83 times of experimental results with the coefficient of variation is 0.22. The prediction of peak loads based on EN code are 0.71 times of experimental results with the coefficient of variation is 0.24. The prediction of peak loads based on AFGC code are 0.67 times of experimental results with the coefficient of variation is 0.19. The accuracy of the prediction of peak loads based on the three codes: ACI code > EN code > AFGC code.

Table 33. The Peak Loads Obtained from FEA and STMs.

Deep Beam	F_{FEA}/F_{EXP}			V_{STM}/V_{EXP}		
	<i>fib</i> Code	AFGC Code	CECS Code	ACI Code	EN Code	AFGC Code
G14 (RPC)	0.41	1.34	1.29	1.05	1.00	0.80
G15 (RPC)	0.40	1.25	1.22	0.95	0.94	0.81
G21 (RPC)	0.30	1.10	1.10	0.84	0.77	0.62
G22 (RPC)	0.37	1.07	1.02	0.84	0.79	0.64
G41 (RPC)	0.54	1.06	1.04	0.44	0.44	0.44

Deep Beam	F_{FEA}/F_{EXP}			V_{STM}/V_{EXP}		
	<i>fib</i> Code	AFGC Code	CECS Code	ACI Code	EN Code	AFGC Code
G42 (RPC)	0.45	1.10	1.07	0.60	0.60	0.60
G43 (RPC)	0.65	1.26	1.26	0.82	0.82	0.82
DBSU2 (RPC)	0.34	1.13	1.00	1.02	0.55	0.72
DBSU4 (RPC)	0.40	0.86	0.97	1.00	0.60	0.78
L1-1 (RPC)	0.33	0.77	0.69	0.73	0.59	0.51
Mean value	0.42	1.09	1.07	0.83	0.71	0.67
Standard deviation	0.10	0.17	0.16	0.19	0.17	0.13
Coefficient of variation	0.24	0.15	0.15	0.22	0.24	0.19



Chapter 5

Conclusions and Recommendations

In this study, the nonlinear structural behavior of RPC deep beams has been studied numerically using SOFiSTiK finite element code with the strain-strain models provided by the *fib* model code 2010 [32], NF P 18-710 (AFGC) [33], and CECS 2020 [34]. For comparison and validation purposes, some test results with different parameters in terms of compressive strength (f'_c), shear span-to-effective depth ratio (a/d), tensile reinforcement ratio (ρ) available in literature were used. The strut-and-tie models (STM) according to ACI 318-11 [3], EN 1992-1-1 [35], and NF P 18-710 (AFGC) [33] have also been utilized to predict shear strength of RPC deep beams. Based on the research conducted, the following primary conclusions were drawn:

5.1 FEA with Material Models Provided by Standard Codes

The findings highlight the critical need for a suitable stress-strain model specific for RPC in order to accurately simulate the behavior RPC deep beams. Using the existing models can be concluded that:

- 1) The *fib* model code 2010 is not adequate for capturing the unique characteristics and performance of RPC deep beams.
- 2) The AFGC and CECS code models are more adequate for capturing the unique characteristics and performance of RPC deep beams.

All in all, each model code has its own advantages and disadvantages:

- 1) The *fib* model code 2010 requires only one input parameter for concrete, i.e. f'_c , while the rest of the parameters can be estimated from f'_c .
- 2) The AFGC code requires 3 input parameters for concrete including f'_c , concrete elastic modulus, and concrete tensile strength.
- 3) The CECS code requires 3 input parameters for concrete including f'_c , concrete elastic modulus, and concrete tensile strength.

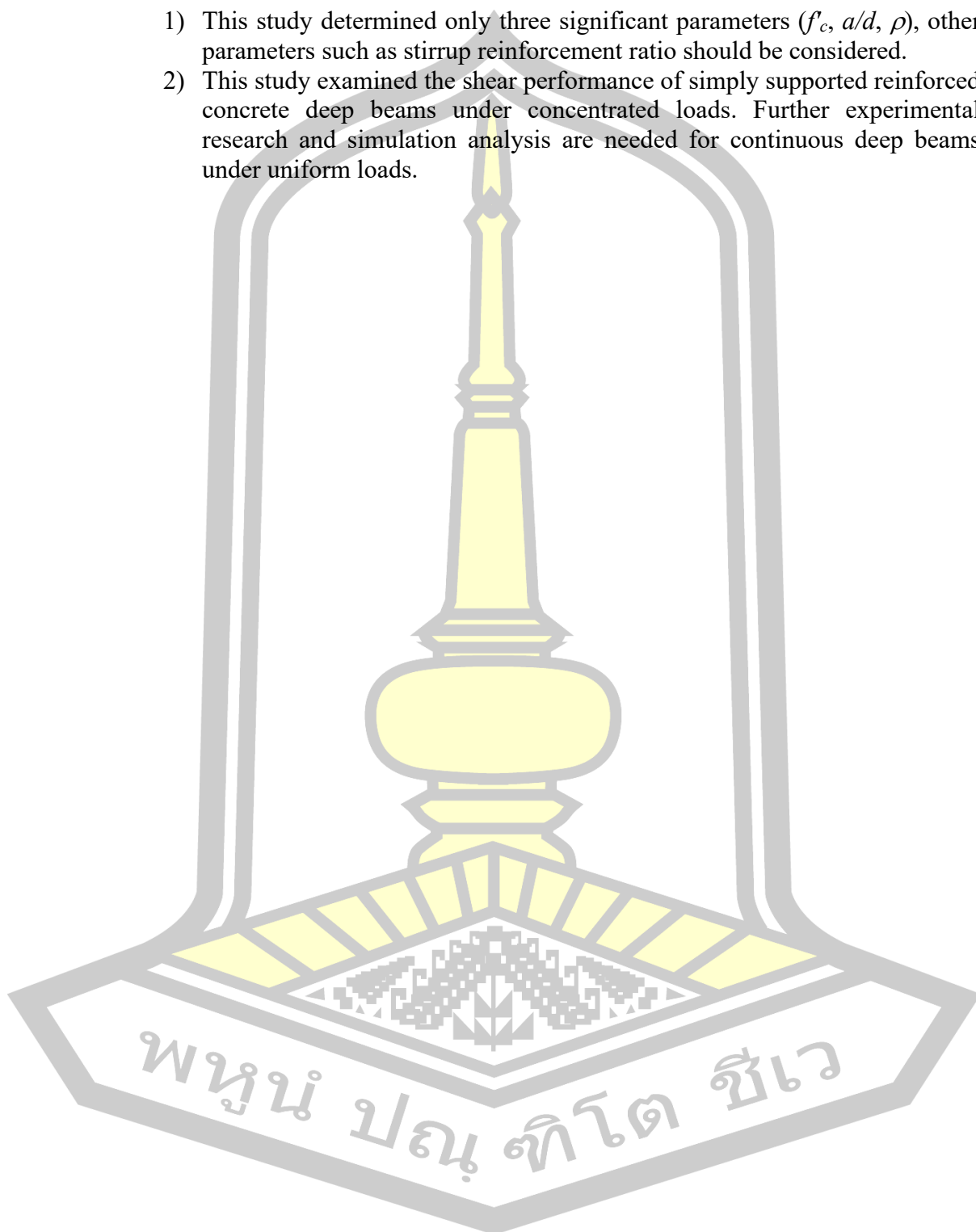
5.2 STM and Shear Strength Prediction

The findings highlight the critical need for a suitable STM specific for RPC in order to accurately predict the shear strength of RPC deep beams. Using the existing models can be concluded that:

- 1) For RPC deep beams, when $a/d < 1.0$, ACI code can give a very good prediction while EN and AFGC codes give conservative shear strength. When $a/d \geq 1.0$, all codes give conservative shear strength.
- 2) For HSC deep beam with $a/d > 1.0$, ACI and EN codes give overestimated shear strength, while AFGC code give conservative shear strength.
- 3) For NSC deep beam with $a/d > 1.0$, all codes give overestimated shear strength.

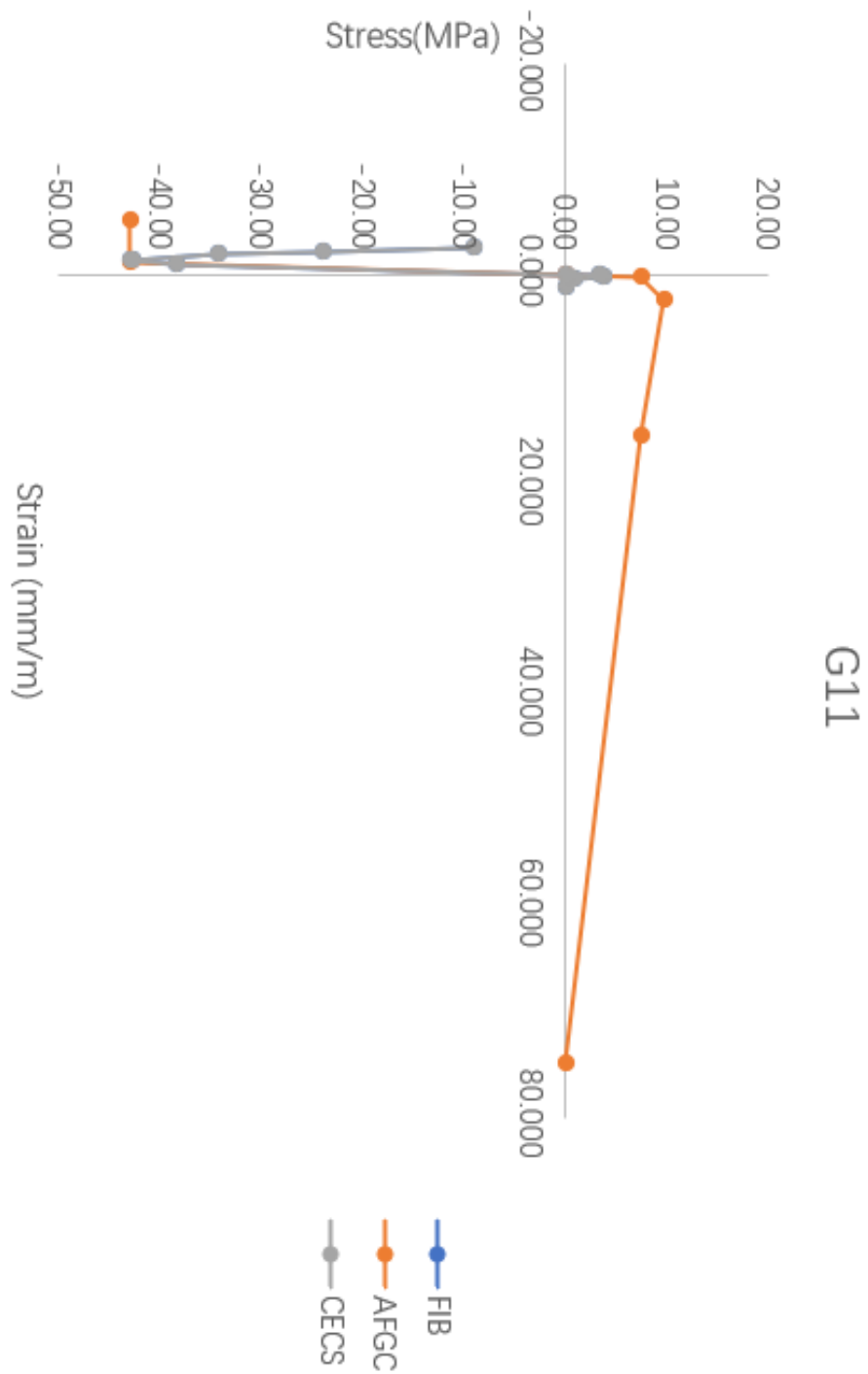
5.3 Recommendations for Future Research

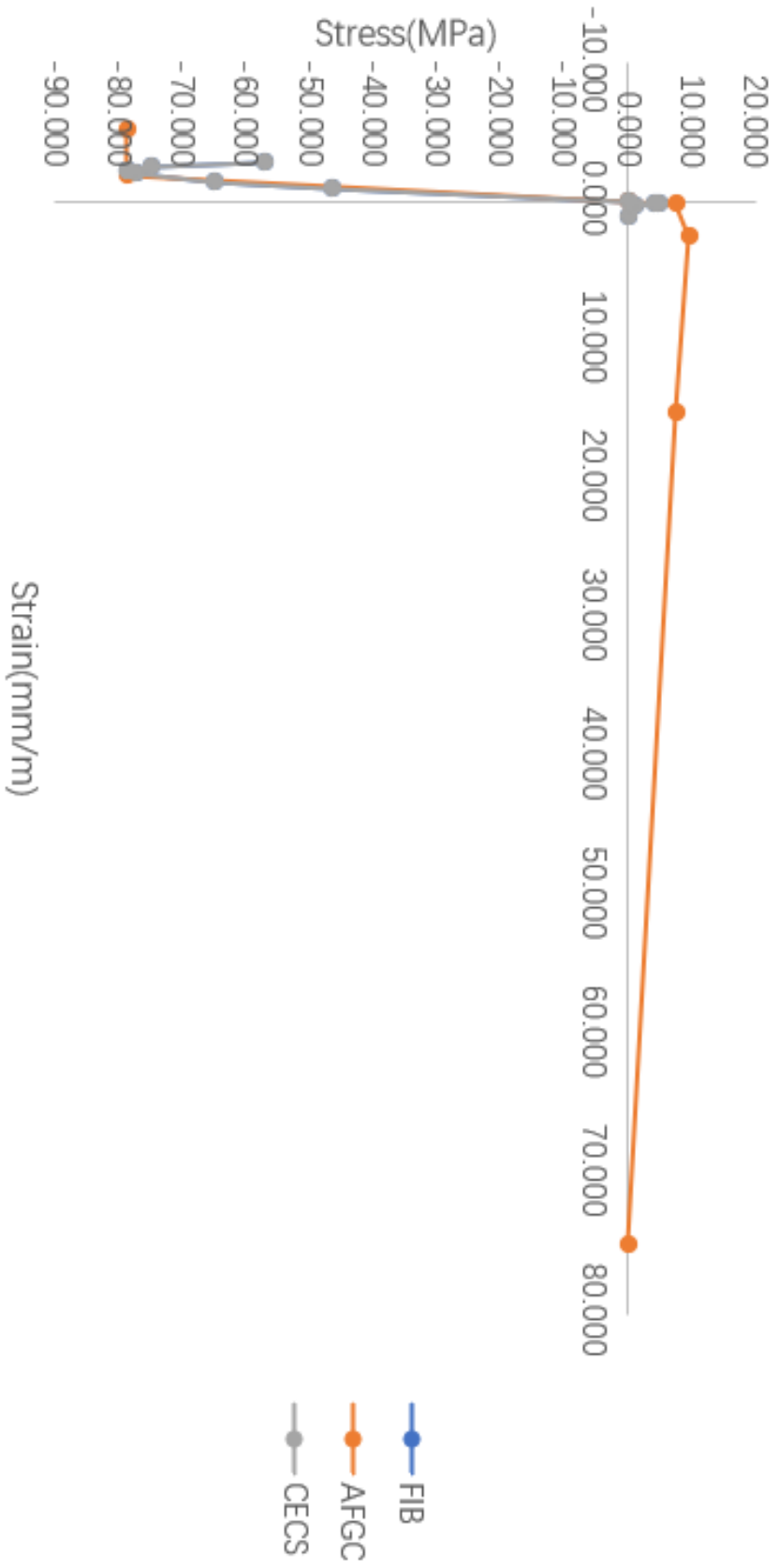
- 1) This study determined only three significant parameters (f_c , a/d , ρ), other parameters such as stirrup reinforcement ratio should be considered.
- 2) This study examined the shear performance of simply supported reinforced concrete deep beams under concentrated loads. Further experimental research and simulation analysis are needed for continuous deep beams under uniform loads.



APPENDIX A

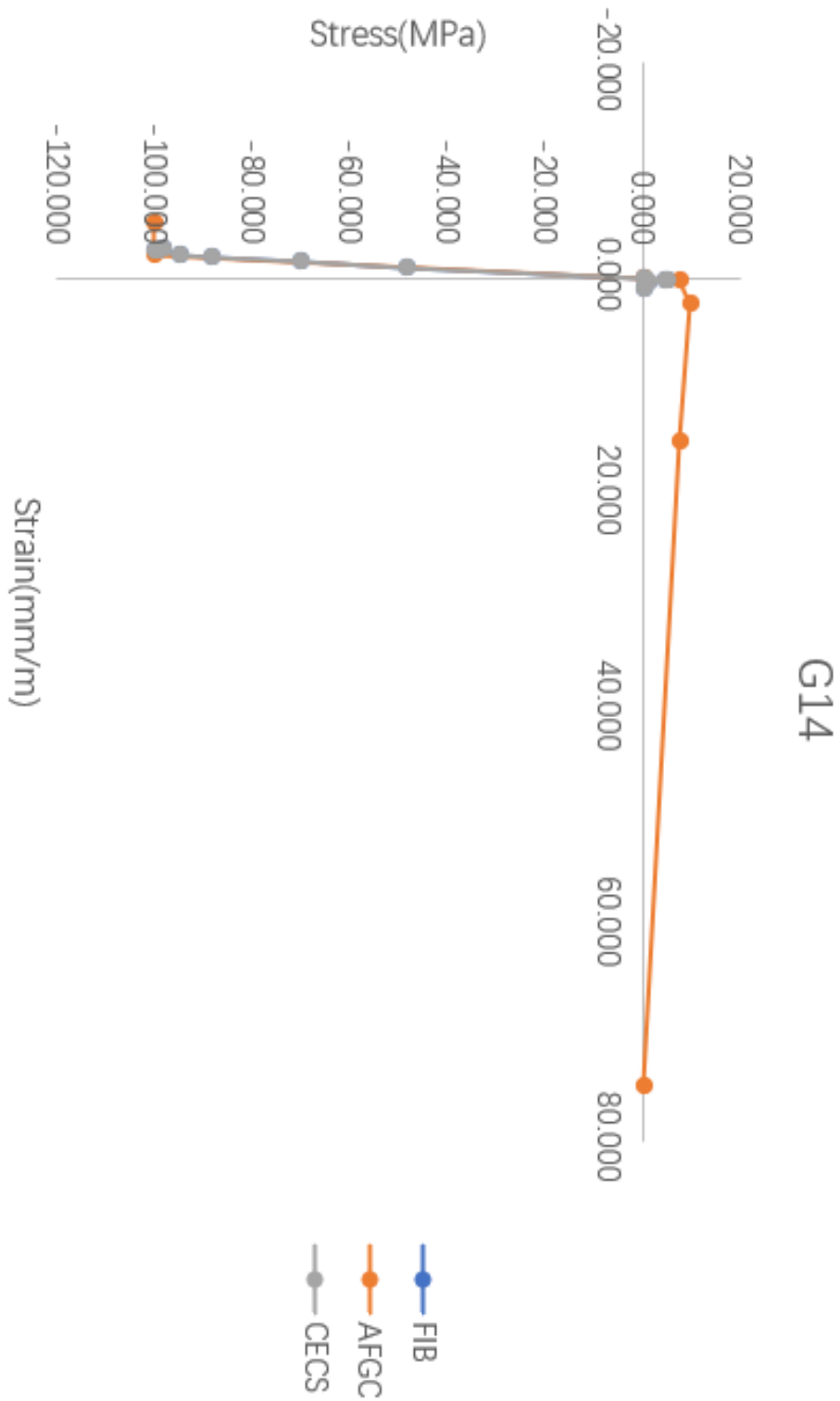
A.1 Stress-Strain Curves of Concrete in Tension and Compression Zones for Deep Beam Tested by Yaseen [36]

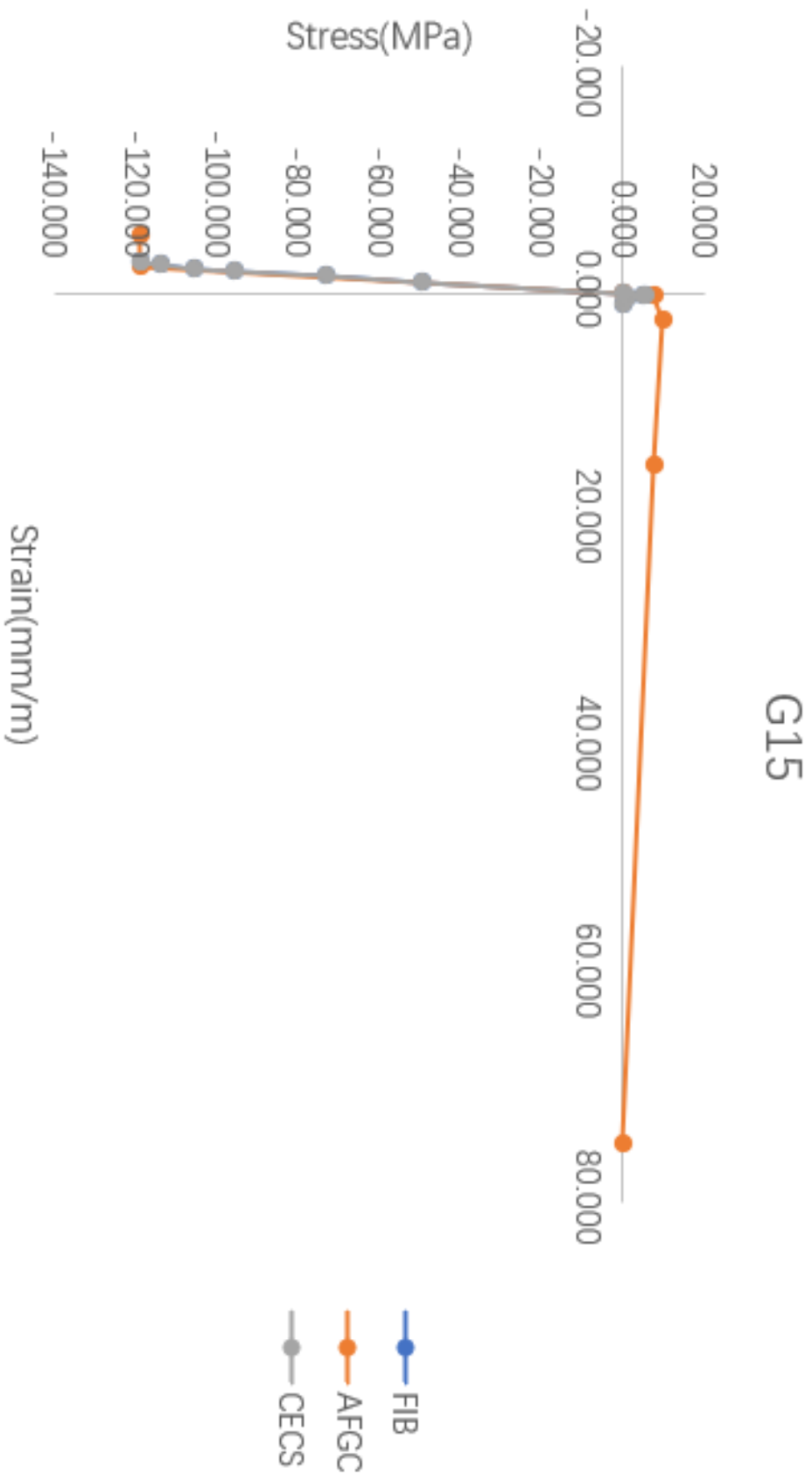


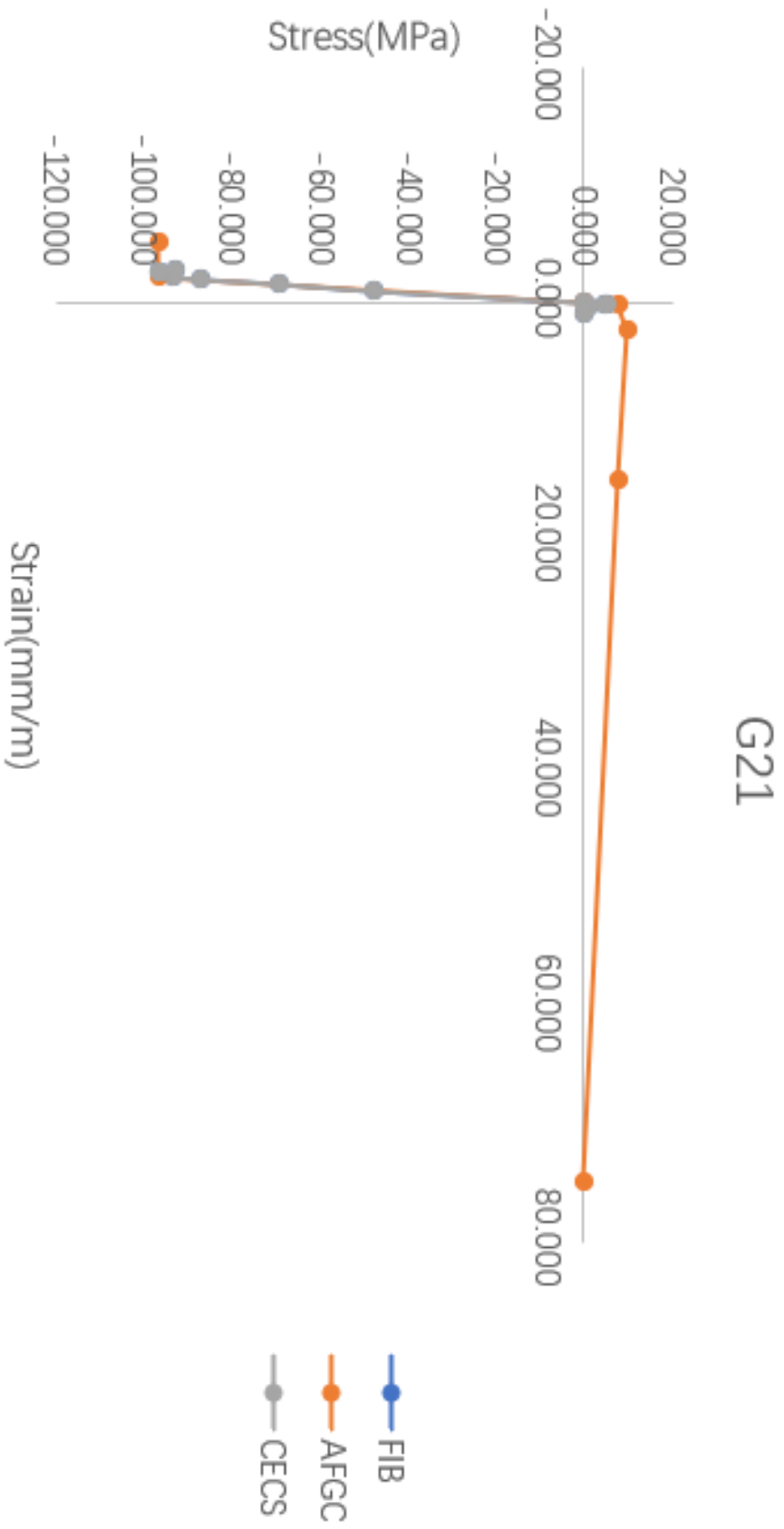


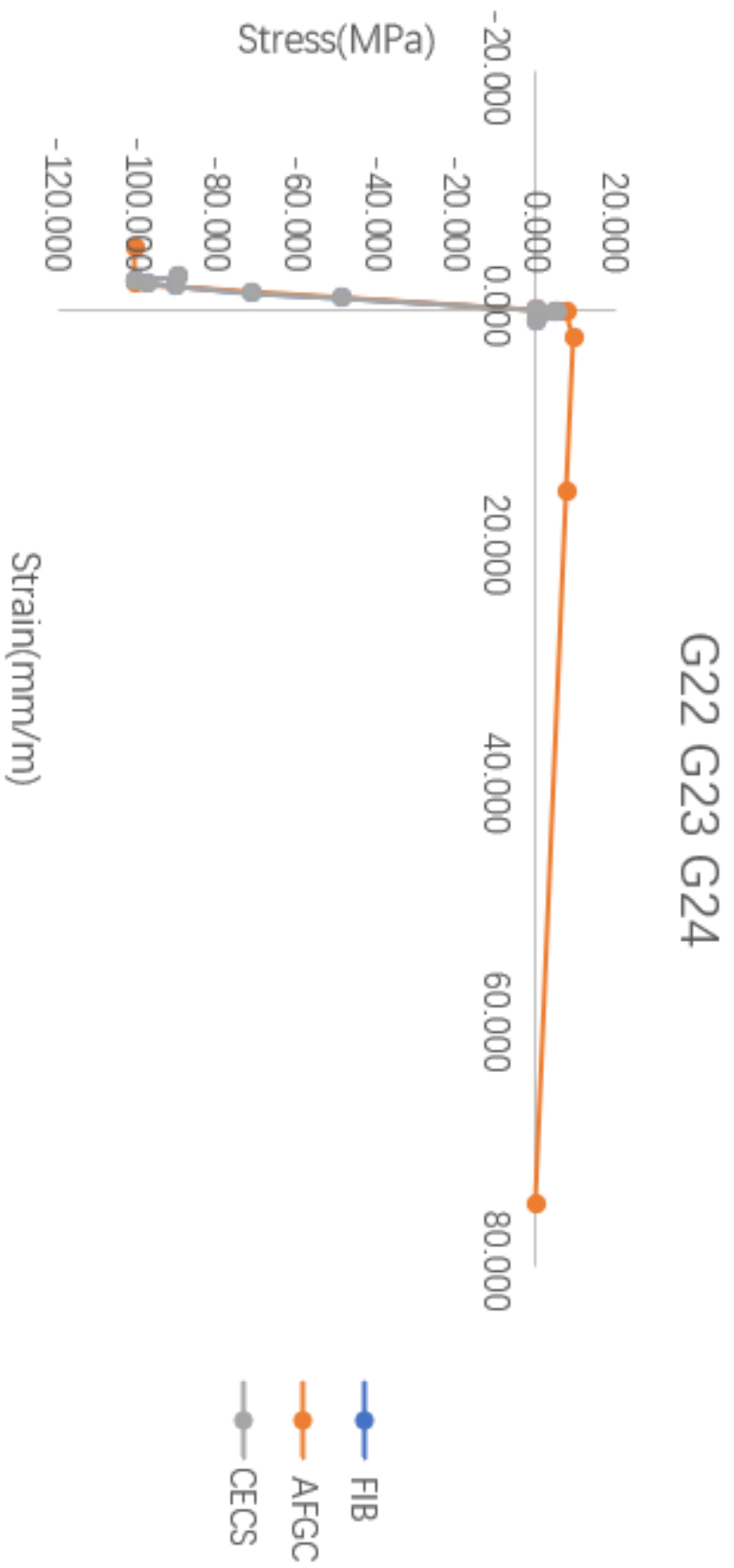
G13

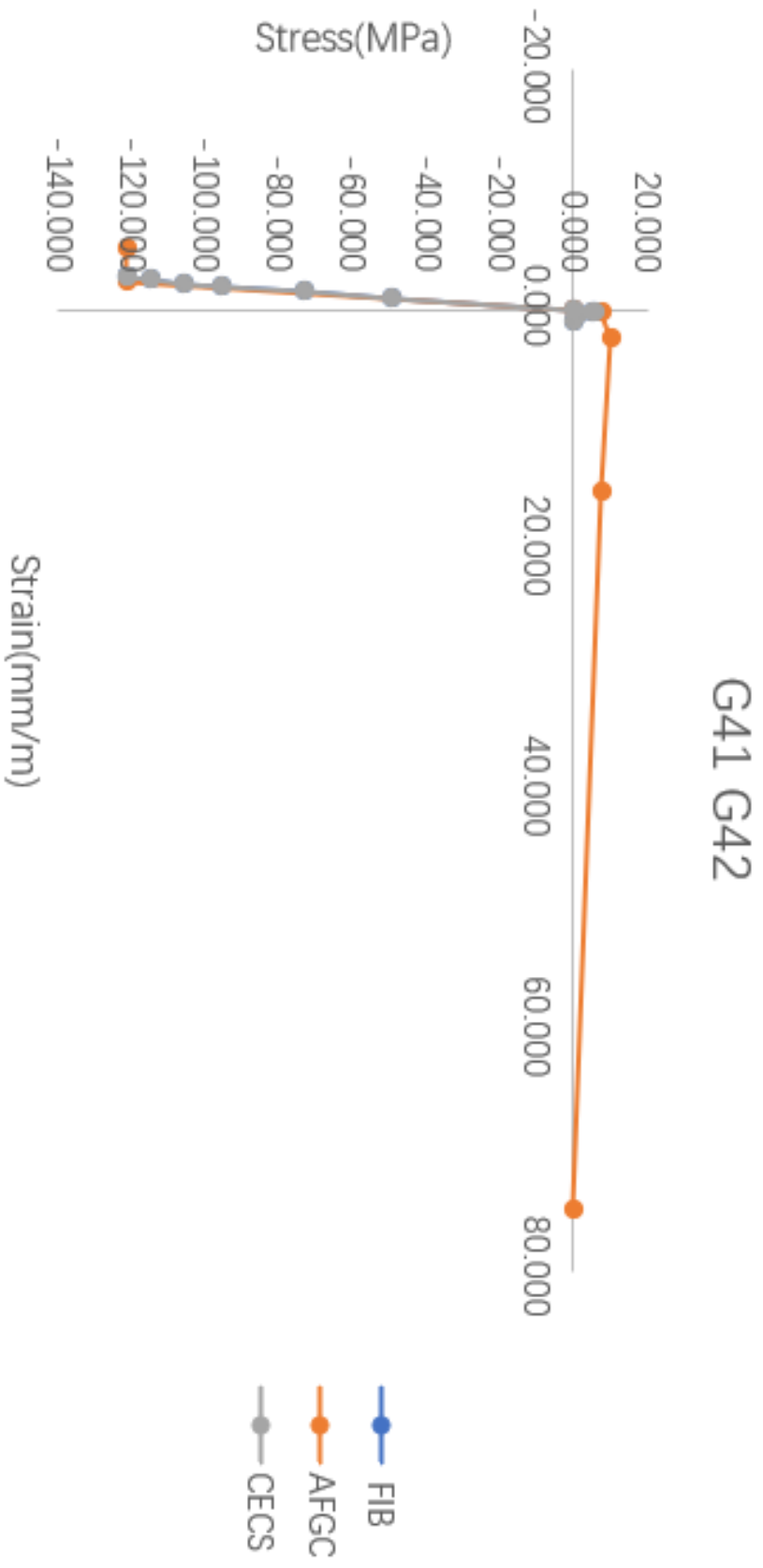


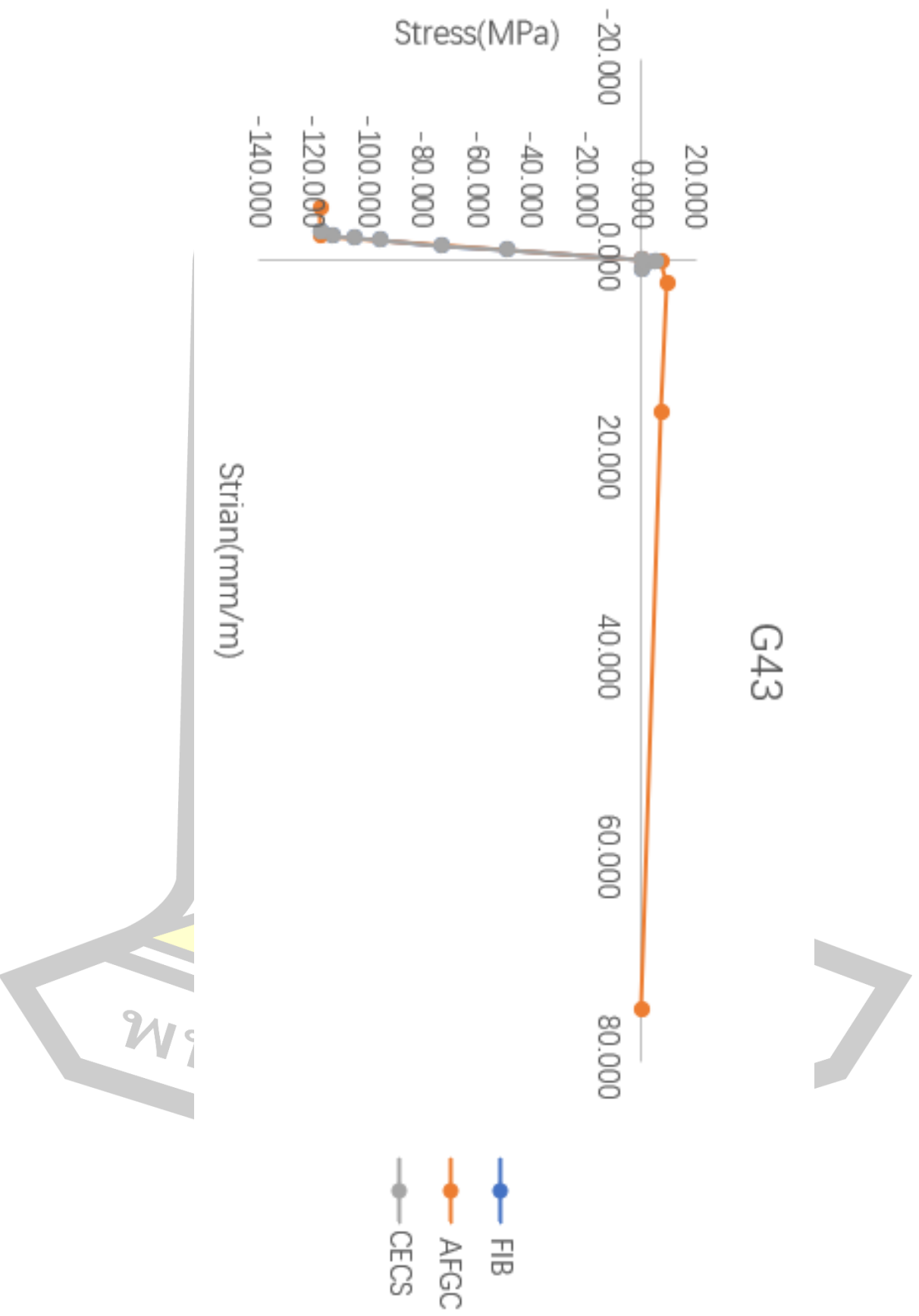




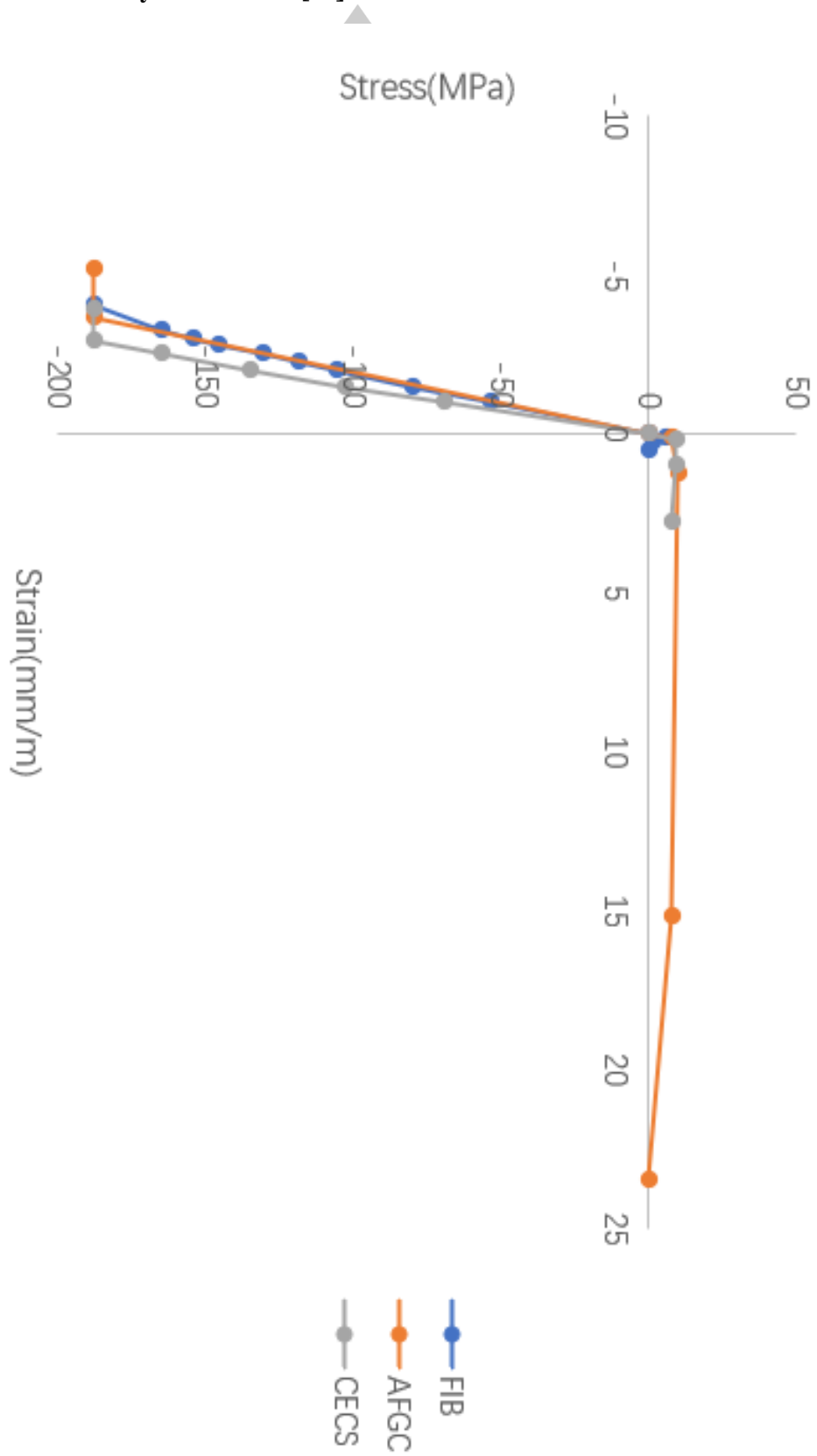




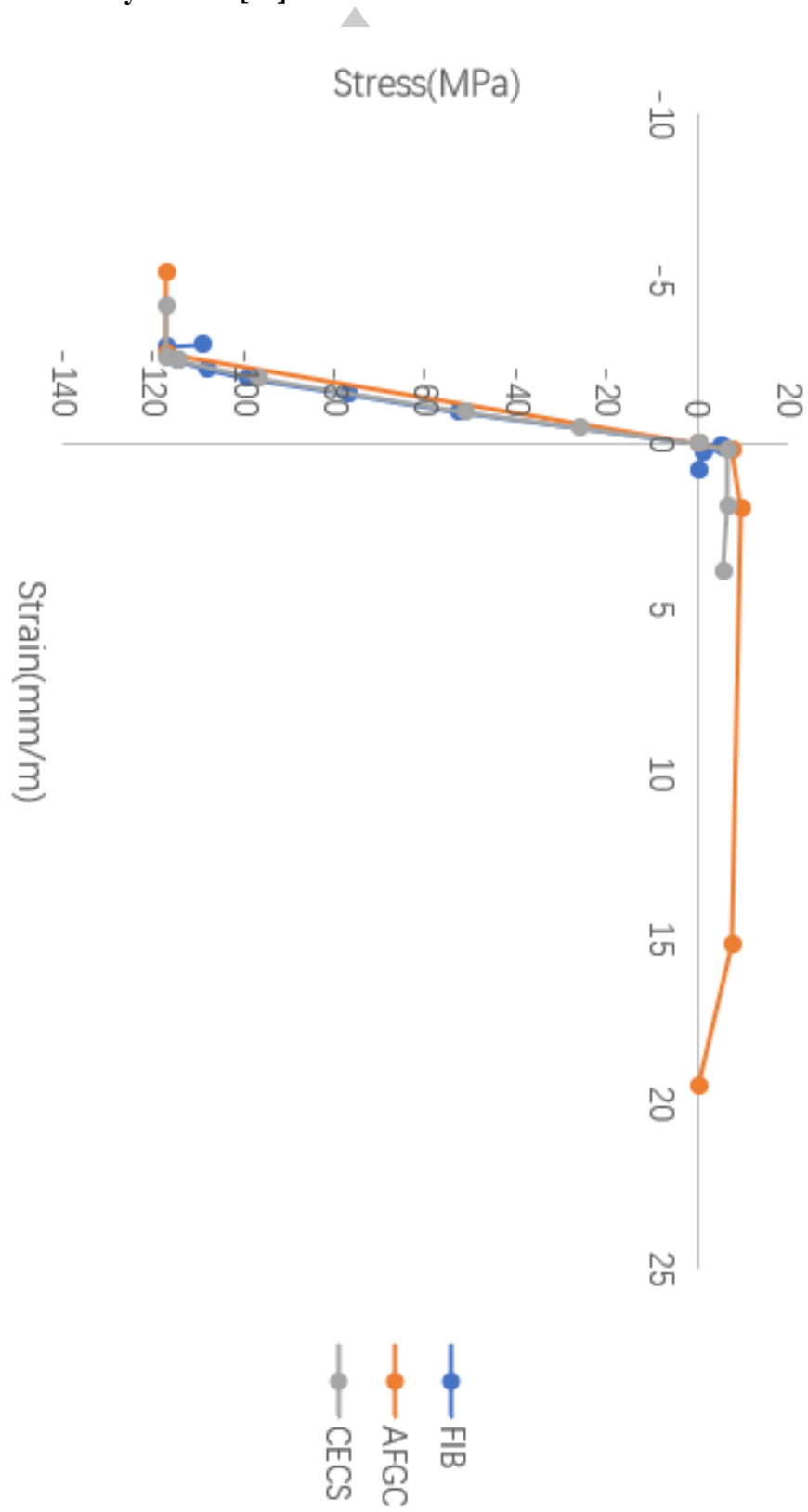




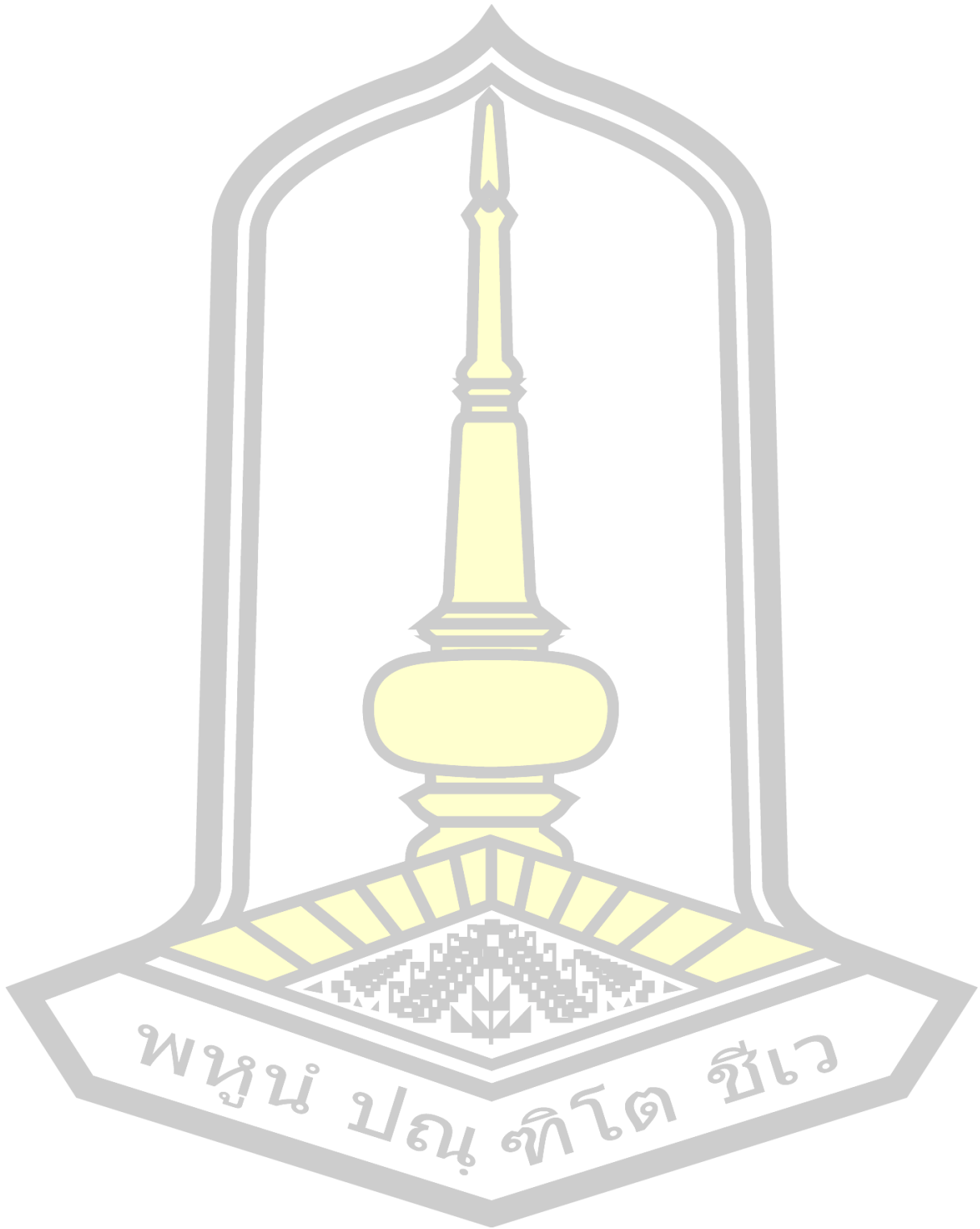
A.2 Stress-Strain Curves of Concrete in Tension and Compression Zones for Deep Beam Tested by Yousef et al. [37]



A.3 Stress-Strain Curves of Concrete in Tension and Compression Zones for Deep Beam Tested by Li et al. [38]



REFERENCES

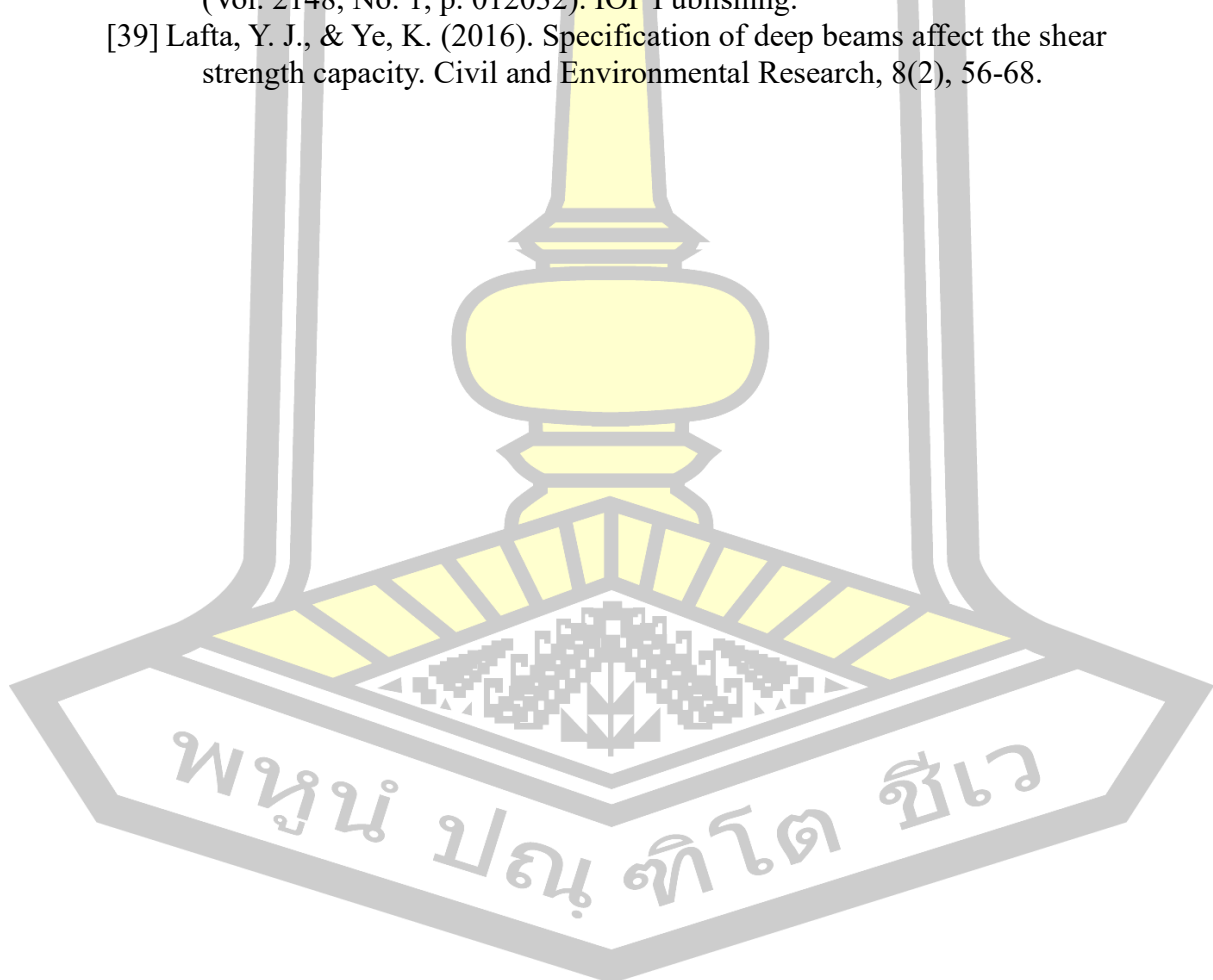


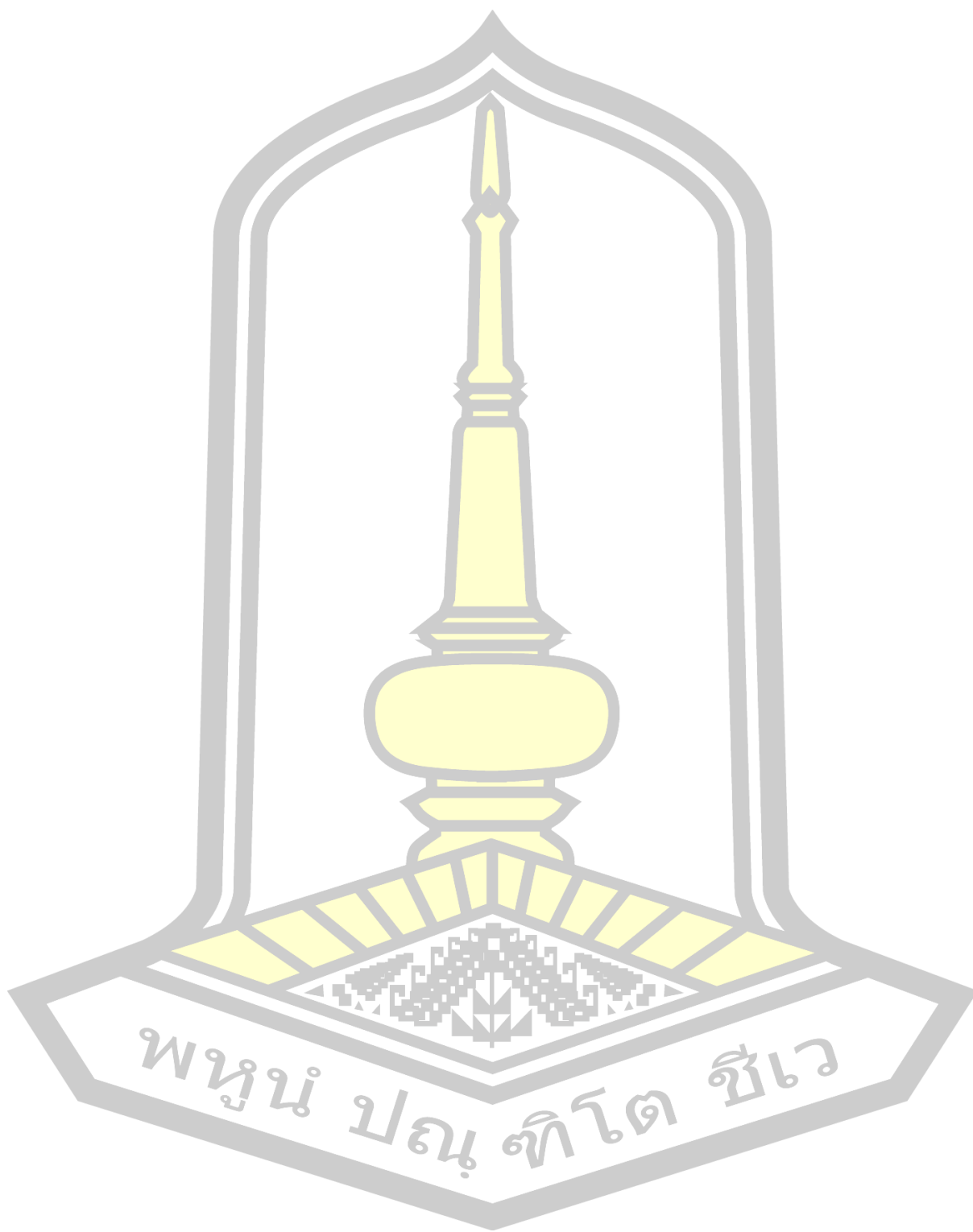
- [1] Li, J., Wu, Z., Shi, C., Yuan, Q. and Zhang, Z. (2020). "Durability of ultra-high performance concrete—A review." *Construction and Building Materials*, 255, 119296.
- [2] Birrcher, D.B. (2009). *Design of reinforced concrete deep beams for strength and serviceability*, The University of Texas at Austin.
- [3] ACI Committee. (2011). "Building code requirements for structural concrete (ACI 318-11) and commentary." American Concrete Institute.
- [4] Fatehi Makki, R., Talib Jassem, A. and Abd Al-Latef Jassem, H. (2019). "Behavior of reactive-powder concrete deep beams with CFRP-strengthened openings." *Practice Periodical on Structural Design and Construction*, 24(4), 04019016.
- [5] Fahmi, H.M., AlShaarba, I.A. and Ahmed, A.S. (2013). "Behavior of reactive powder concrete deep beams." *AL-Mansour Journal*, 12(20), 22-44.
- [6] Makki, R.F., Jassem, A.T. and Jassem, H. (2018). "Non-linear analysis of Reactive Powder Concrete (RPC) deep beams with openings strengthened by CFRP." *Al-Qadisiyah Journal for Engineering Sciences*, 11(2), 176-196.
- [7] Hassan, H.F. (2015). "Behavior of hybrid deep beams containing ultra high performance and conventional concretes." *Engineering and Technology Journal*, 33(1), 30-50.
- [8] Hasan, M.J. and Al-Shamaa, M.F.K. (2018). "Effect bubbles on the behavior of reinforced reactive powder concrete deep beams." *International Journal of Civil Engineering and Technology*, 9(12), 592-602.
- [9] Seo, S.-Y., Yoon, S.-J. and Lee, W.-J. (2004). "Structural Behaviour of R/C Deep Beam with Headed Longitudinal Reinforcements." *13th World Conference on Earthquake Engineering, Vancouver, BC, Canada*.
- [10] Fu, C.C. *THE STRUT-AND-TIE MODEL OF CONCRETE STRUCTURES*. 2001 [cited September 25, 2022; Available from: <https://cpb-us-e1.wpmucdn.com/blog.umd.edu/dist/f/392/files/2016/08/stm-oj2izh.pdf>].
- [11] Richard, P. and Cheyrezy, M. (1995). "Composition of reactive powder concretes." *Cement and concrete research*, 25(7), 1501-1511.
- [12] The Constructor. *Reactive Powder Concrete - Composition and Advantages*. 2022 [cited September 25, 2022; Available from: <https://theconstructor.org/concrete/reactive-powder-concrete-composition-advantages/1266/>].
- [13] Wikipedia contributors. *Finite element method*. 2022 August 5, 2022 08:14 UTC [cited 2022 September 20, 2022 09:14 UTC]; Available from: https://en.wikipedia.org/w/index.php?title=Finite_element_method&oldid=1102479146.
- [14] Cook, R.D., Malkus, D.S., Plesha, M.E. and Witt, R.J. (1989). "Concepts and Applications of Finite Element Analysis, John Willey and Sons." *New York*.
- [15] SOFiSTiK AG. *FEM - Finite Elemente Methode Software for civil engineers*. 2022 [cited September 20, 2022; Available from: <https://www.sofistik.com/products/finite-elements/sofistik-fem-packages>].
- [16] SOFiSTiK AG. (2018). *VERiFiCATiON MANUAL: Mechanical Benchmarks*, SOFiSTiK AG.
- [17] Team, m. *Strut-and-Tie Model: Part 1 - Basics*. 2022 [cited September 20, 2022; Available from:]

<https://www.midasbridge.com/en/blog/bridgeinsight/strut-and-tie-model-part-1-basics>.

- [18] MacGregor, J.G., Wight, J.K., Teng, S. and Irawan, P. (1997). *Reinforced concrete: Mechanics and design*, Prentice Hall New Jersey.
- [19] Muhaison, S.K., Abd, W.K. and Alwan, M.K. (2018). "Behaviour of Reactive Powder Rectangular Deep Beam with Shear Zone Opening Subjected to Repeated Load." *Journal of Engineering and Sustainable Development*, 22(1), 77-94.
- [20] Yang, I.H., Joh, C. and Kim, B.-S. (2010). "Structural behavior of ultra high performance concrete beams subjected to bending." *Engineering structures*, 32(11), 3478-3487.
- [21] Adeline, R., Behloul, M. and Bernier, G. (1996). "High ductile beams without passive reinforcement." *4th International Symposium on Utilization of High-Strength/High Performance Concrete, Paris, France*, 29-31.
- [22] Yoo, D.-Y. and Yoon, Y.-S. (2015). "Structural performance of ultra-high-performance concrete beams with different steel fibers." *Engineering Structures*, 102, 409-423.
- [23] Spasojevic, A., Redaelli, D., Fernández Ruiz, M. and Muttoni, A. (2008). "Influence of tensile properties of UHPFRC on size effect in bending." *Ultra High Performance Concrete (UHPC), Second International Symposium on Ultra High Performance Concrete*, 303-310.
- [24] Bărbos, G.A. (2016). "Long-term behavior of ultra-high performance concrete (UHPC) bended beams." *Procedia Technology*, 22, 203-210.
- [25] Alkaysi, M. and El-Tawil, S. (2017). "Factors affecting bond development between Ultra High Performance Concrete (UHPC) and steel bar reinforcement." *Construction and building materials*, 144, 412-422.
- [26] Hasgul, U., Turker, K., Birol, T. and Yavas, A. (2018). "Flexural behavior of ultra - high - performance fiber reinforced concrete beams with low and high reinforcement ratios." *Structural Concrete*, 19(6), 1577-1590.
- [27] SOFiSTiK FEM Software. (2022). "Analysis Program." SOFiSTiK AG, berschleissheim.
- [28] Dominique, C. and Stefan, M. *Implementation of Ductal as a Material inside SOFiSTiK*. [cited 2022 August, 1; Available from: https://sofistik-sonar.ams3.digitaloceanspaces.com/pub/infoline/SOFiSTiK-Seminar/2010/v04_ductal.pdf].
- [29] Nyomboi, T., Matsuda, H., Demizu, A. and Makino, K. (2010). "Experimental and analytical study on shear capacity in steel fiber and stirrup RC beam." *Journal of Structural Engineering*, 56A, 13-22.
- [30] SOFiSTiK AG. (2018). *ASE Manual: General Static Analysis of Finite Element Structures*, SOFiSTiK AG.
- [31] SOFiSTiK AG. (2018). *BEMESS Manual: Design of Plates and Shells*, SOFiSTiK AG.
- [32] Kordina, K., Mancini, G., Schäfer, K., Schießl, A., & Zilch, K. (2010). fib Bulletin 54. Structural Concrete Textbook on behaviour, design and performance Second edition Volume 4. In Bulletin - FIB. <https://doi.org/10.35789/fib.bull.0055>.

- [33] NF P18-710 (2016). National addition to Eurocode 2 – Design of concrete structures: specific rules for ultra-high performance fibre-reinforced concrete (UHPFRC). Saint-Denis Cedex: AFNOR.
- [34] CECS 2020 (2020). Technical specification for ultra-high performance concrete structures, China Association for Engineering Construction Standardization. <http://www.cecs.org.cn/uploads/soft/200529/1-200529154K8.pdf>.
- [35] EN 1992-1-1 (2004) Design of concrete structures—Part 1-1: General rules and rules for buildings. CEN, Brussels.
- [36] Abdulhaleq Yaseen, S. (2016). An experimental study on the shear strength of high-performance reinforced concrete deep beams without stirrups. *Engineering and Technology Journal*, 34(11), 2123-2139.
- [37] Yousef, A. M., Tahwia, A. M., & Marami, N. A. (2018). Minimum shear reinforcement for ultra-high performance fiber reinforced concrete deep beams. *Construction and Building Materials*, 184, 177-185.
- [38] Li, Y., Yang, H., & Liu, C. (2022). Experimental Study on Shear Behavior of Reactive Powder Concrete Beam. In *Journal of Physics: Conference Series* (Vol. 2148, No. 1, p. 012032). IOP Publishing.
- [39] Lafta, Y. J., & Ye, K. (2016). Specification of deep beams affect the shear strength capacity. *Civil and Environmental Research*, 8(2), 56-68.





พญูน์ ปณฺ ทิตฺ สีเว

BIOGRAPHY

NAME Bin Wang

DATE OF BIRTH 1992/01/22

PLACE OF BIRTH SHANXI

ADDRESS China Railway Building, Donghai Road, Yantian District, Shenzhen, Guangdong Province

EDUCATION 2011-2015 Bachelor of Engineering, Civil Engineering, Shanxi Agricultural University
2021-2023 Master of Engineering, Civil Engineering, Mahasarakham University

